STUDIES ON BETANIN NATURAL DYE INCORPORATED ZnO COMPOSITES AT NANO AND MICRO SCALE FOR PHOTONIC DEVICE APPLICATIONS

Aparna Thankappan

International School of Photonics
Cochin University of Science and Technology
Cochin- 682022, Kerala,India

Ph. D. Thesis submitted to
Cochin University of Science and Technology
in partial fulfillment of the requirements for the
Degree of Doctor of Philosophy

February 2015

Studies on betanin natural dye incorporated ZnO composites at nano and micro scale for photonic device applications
Ph. D Thesis in the field of nanophotonics

Author:
Aparna Thankappan
Research Fellow, International School of Photonics
Cochin University of Science and Technology
Kochi-22,India
Email: aparna.subhash@gmail.com

Research Advisors:
Dr. V P N Nampoori
Emeritus Professor, International School of Photonics
Cochin University of Science and Technology
Kochi-22,India
Email: vpnnampoori@cusat.ac.in

Dr. Sheenu Thomas
Associate Professor, International School of Photonics
Cochin University of Science and Technology
Kochi-22,India
Email:st@cusat.ac.in

International School of Photonics
Cochin University of Science and Technology
Kochi-22,India
URL:www.photonics.cusat.edu

February 2015

Front cover: SEM images of low dimensional structures of ZnO
Cover design: Pramod K.S

CERTIFICATE

Certified that the work presented in the thesis entitled "**Studies on betanin natural dye incorporated ZnO composites at nano and micro scale for photonic device applications**" is based on the original work done by Ms. Aparna Thankappan under our guidance and supervision at the International School of Photonics, Cochin University of Science and Technology, Kochi-22, India and has not been included in any other thesis submitted previously for the award of any degree.

Certified that relevant corrections and modifications suggested by the audience during the pre-synopsis seminar has been incorporated in this thesis.

Kochi 682022	Prof. V P N Nampoori	Dr. Sheenu Thomas
10.02.2015	(Supervising Guide)	(Co-guide)

DECLARATION

Certified that the work presented in the thesis entitled "**Studies on betanin natural dye incorporated ZnO composites at nano and micro scale for photonic device applications**" is based on the original work done by me under the guidance of Dr. V. P. N Nampoori, Emeritus Professor, International School of Photonics, Cochin University of Science and Technology, Kochi-22, India and the co-guidance of Dr. Sheenu Thomas, Associate Professor, International School of Photonics, Cochin University of Science and Technology, Kochi-22, India and it has not been included in any other thesis submitted previously for award of any degree.

Kochi 682022 Aparna Thankappan
10.02.2015

Dedicated to the caring hands

Contents

Acknowledgment

I am grateful to the God for all his blessings in my life which made me what I am today.

I would like to take this opportunity to acknowledge and extend my sincere gratitude for those who help me to make this Ph.D. thesis possible.

The first person who helped me to walk in the field of research is my supervisor and guide Prof.V.P.N Nampoori, Emeritus professor, ISP. I take this opportunity to express my sincere thanks to him for his personal encouragement, stimulating discussions and able guidance right from the beginning to date as a consequence of which the present study reached fruition.

I also thank my co-guide Dr Sheenu Thomas, Prof. P. Radhakrishnan, Prof. C. P Girijavallabhan and Dr.M Kailasnath for their constant support. Thanks to all other teachers of ISP.

I wish to thank the reviewers of my articles, their critical comments helps to improve the quality of the research work.

Special acknowledgment is also given to IUCND for the financial support. Thanks to all staffs of ISP.

I would like to thank to my colleagues especially Mathew, Santhi Ani Joseph, Divya, Sister Anju, Sabitha, Indu, Lins, Bejoy and Misha. I also remember Bobby sir, Pradeep Chandran, Libeesh sir, Linesh , Sreeja, Rajeena, Sreelekha , Tintu, Suneetha , Nithyaja, Hrudhya, Jaison, Musfir, Manju, Roopa, Jessy, Ajeena, Aleena and all my friends of the photonics family. Their support, encouragement and friendship made my Ph. D. study a journey of happiness. It gives me immense pleasure to thank to every individual who directly or indirectly helped me in my research work.

I am indebted to the love, care, prayers and blessings of my parents, brother, husband and parents in-law. I also remember my sweet babies kunjatta and kichu.

Aparna Thankappan

Preface

Green energy and Green technology are the most of the quoted terms in the context of modern science and technology. Technology which is close to nature is the necessity of the modern world which is haunted by global warming and climatic alterations. Proper utilization of solar energy is one of the goals of Green Energy Movement.

The present thesis deals with the work carried out in the field of nanotechnology and its possible use in various applications (employing natural dyes) like solar cells. Unlike artificial dyes, the natural dyes are available, easy to prepare, low in cost, non-toxic, environmentally friendly and fully biodegradable.

Looking to the 21^{st} century, the nano/micro sciences will be a chief contributor to scientific and technological developments. As nanotechnology progresses and complex nanosystems are fabricated, a growing impetus is being given to the development of multi-functional and size-dependent materials. The control of the morphology, from the nano to the micrometer scales, associated with the incorporation of several functionalities can yield entirely new smart hybrid materials. They are special class of materials which provide a new method for the improvement of the environmental stability of the material with interesting optical properties and opening a land of opportunities for applications in the field of photonics. Zinc oxide (ZnO) is one such multipurpose material that has been explored for applications in sensing, environmental monitoring, and bio-medical systems and communications technology. Understanding the growth mechanism and tailoring their morphology is essential for the use of ZnO crystals as nano/micro electromechanical systems and also as building blocks of other nanosystems.

One approach to the design of technologically important class of oxide materials is the incorporation of the natural organic molecules to modify inorganic nano/microstructures. In this instance, the inorganic oxide contributes to the enlarged functionality by incorporation, as one component in a hierarchical structure where there is a synergistic interaction between organic material and the inorganic oxide. These organic- inorganic frameworks are particularly attractive from several perspectives such as they possess a remarkable chemical and structural diversity. The ability to connect the functionalities to the material expands the scope of the science significantly.

Both the design and characterization of nonlinear optical (NLO) materials have attracted very much in order to discover and develop materials possessing large nonlinearities and satisfying various technological requirements for photonic device applications. Various nonlinear optical spectroscopy, including wave mixing, Z scan and transmission methods, have been developed to measure the third-order nonlinearity of a material. The Z-scan method has become a standard tool for measurement of the nonlinear absorption and nonlinear refractive index coefficients of various NLO materials because of its simplicity, its high sensitivity, and its indication of the sign and type of nonlinearity immediately after the measurement is finished.

Detailing the chief merits of nano/micro composites as photonic media are included in this thesis. Several optical and solar cell applications where the nano/micro structures play a critical role are presented. The focus is on the optical characterization of nanocomposites for the photonic device applications including optical limiting, optical switching and solar cell applications. The interactions of biomolecules with the ZnO low dimensional structures provide new opportunities for the development of photonic devices. The natural dye reinforcements with the biodegradable polymers have a high potential for the design of environmentally friendly 'green materials' for the future applications. These hybrid materials can provide promising applications in optics, electronics, ionics, mechanics, membranes, functional and protective coatings, catalysis, sensors and biology. Finally, we focus on the device performance i.e. dye sensitized solar cells (DSSCs) that represent a cheap and clean technology that harnesses solar energy efficiently. DSSC with various photo-anodes were fabricated using betanin natural dye from red beets. Results at this date show that betanin dyes are efficient sensitizer in DSSC applications and are environmentally and economically superior to standard ruthenium-based dyes currently used in DSSC. Following is the chapter wise description of the thesis.

Chapter 1 gives an over view of the morphology engineering of ZnO structures, properties and applications to Photonics especially dye sensitized solar cells (DSSC). This chapter discusses the opportunity of natural dye as a photonic material along with their applications. The importance of hybrid/composite materials and the basics of nonlinear optics are also mentioned in this chapter.

The purpose of **chapter 2** is to provide an overview of the experimental techniques that were applied to investigate the crystal samples and characterization of ZnO films. Within the individual sections the fundamental principles and details of experimental techniques are briefly explained. The films discussed in this work were grown by tape casting method and by two step

solution method. Various analyzing tools were used to investigate the electrical, optical and structural properties of the films. The surface morphology was characterized as well. In order to test the device performance, current-voltage measurement was used.

Studies on the low dimensional structures of ZnO have been carried out extensively over the last decade not only for their remarkable chemical and physical properties, but also for their current and future diverse technological applications. The **chapter 3** gives a comprehensive overview of the progress that has been made in the context of ZnO low dimensional structures via wet chemical method. We will cover several growth experiments under different conditions such as time, precursor concentration and temperature to rationally get control over the morphologies of the nanostructures. Morphological control techniques in this system will contribute to the development of the future oxide devices. Their linear optical properties are also studied.

In **chapter 4**, we report a methodical study on the third order optical non linearity of anisotropic growth of ZnO crystals embedded in polymeric matrices and nanowires on the glass substrate with the use of pre-existing textured ZnO, ZnS and TiO_2 seeds employing Z-scan method with Nd: YAG laser (532 nm, 7 ns, 10 Hz). The controlled morphologies of ZnO including dumb bell (DB) microrods, nanoflakes, nanoplates and microrods are prepared by low temperature wet chemical method. The studies show that the optical non linearity of ZnO crystals is highly dependent on the structural geometry. Our study offers better insights into the third-order nonlinear optical characteristics of ZnO crystals and reveals the great potential for applications in nonlinear photonic devices.

Chapter 5 deals with the solvent effect on the third order optical non linearity of betanin natural dye extracted from red beet root using a Q-switched Nd: YAG laser at 532 nm. The third order non linearity of these samples are dominated by non linear absorption ,which leads to strong optical limiting and their strength is influenced by the solvent used, suggesting that betanin natural dyes are promising candidates for the development of photonic non linear optic devices.

Chapter 6 contains the intensity dependent nonlinear absorption properties of bio-inspired hybrid materials (betanin-ZnO) embedded in polymeric matrices employing the Z-scan technique using an Nd: YAG laser. We observed a change over in the sign of nonlinearity due to the interplay of exciton bleaching and optical limiting mechanisms. Light confinement effect and ship-in-a bottle effect play crucial roles. Theoretical analysis has been performed

using a model based on nonlinear absorption coefficient and saturation intensity. The result of the present study gives an additional mechanism for the gain enhancement in dye doped ZnO matrix.

Performance of DSSC based on betanin natural dye from red beets with various nanostructured photo-anodes on transparent conducting glass has been investigated in **chapter 7**. Moreover, the influences of various electrolytes have been studied. Cell efficiency of 2.99% and overall photon to current conversion efficiency of (IPCE) 20% were achieved using ZnO photoanode with iodide based electrolyte in acetonitrile (ACN) solution. To enhance solar harvesting in organic solar cells, uniform sized metal nanoparticles (gold (Au) of $\approx$8 nm) synthesized by microwave irradiation method were incorporated into the device consisting of ZnO. Enhanced power conversion efficiency of 1.71% was achieved in ZnO/Au nanocomposite compared to the 0.868% efficiency of the bare ZnO DSSC with ferrocene based electrolyte. We also report heterojunction DSSC using ZnO composites synthesized through a simple facile two step solution growth method using pre-existing textured ZnO, ZnS, CdS and TiO_2 seeds and also a ZnO DSSC decorated with highly conducting and chemically stable titanium nitride (TiN) nanoparticles (NPs). Effects of their incorporation on the cell performance are studied.

The summary and conclusions based on the present work are given in **chapter 8**. A brief report on the future prospects and the possibility of the extension of the present work are also included in this chapter.

Following section is the list of publications arising out of the work presented in the thesis. Copies of some of the selected papers are included as an appendix at the end of the thesis.

List of Publications

A. Journal Publications:

- Aparna Thankappan, Misha Hari, S Mathew, Santhi Ani Joseph and V.P.N Nampoori "Structural and optical properties of zinc oxide micro rods synthesized by low temperature hydrothermal route " AIP Conf. Proc. of Optics: Phenomena, Materials ,Devices and Characterization, 1391, 514-516 (2011).
- Aparna Thankappan, Misha Hari, S. Mathew, Santhi Ani Joseph, Erni Rolf,Debajeet Bora, Artur Brau and V.P.N. Nampoori "Synthesis of monocrystalline zinc oxide microrods by wet chemical method for light confinement applications" Physica E 44 , 2118-2123 (2012).
- Aparna Thankappan,Sheenu Thomas and V. P. N. Nampoori "Effect of betanin natural dye extracted from red beet root on the non linear optical properties ZnO nanoplates embedded in polymeric matrices" J. Appl. Phys., 112, 123104 (2012).
- Aparna Thankappan, Divya S. Sheenu Thomas and V.P.N. Nampoori "Optical characterization of ZnO nanoplates embedded in polymeric matrices for optical limiting applications" Opt Laser Technol 52, 37-42 (2013).
- Aparna Thankappan, Sheenu Thomas and V.P.N. Nampoori "Solvent effect on the third order optical nonlinearity and optical limiting ability of betanin natural dye extracted from red beet root" Opt. Mater., 35, 2332-2337 (2013).
- Aparna Thankappan, Sheenu Thomas, and V. P. N. Nampoori "Tuning the face orientation of ZnO nano/microcrystals by a wet chemical method" Chin. Opt. Lett. 11, 10,101801(2013).
- Aparna Thankappan, Sheenu Thomas and VPN Nampoori "Optical limiting performance of ZnO nanoflakes and nanoplates embedded in PVA matrix" QScience Connect ,33, 10,5339 (2013).
- Aparna Thankappan, Sheenu Thomas and V.P.N. Nampoori "Novel composites based on polymer micro-rods for photonic device applications" Opt Laser Technol 58, 2014, 63-70 (2014).
- Aparna Thankappan, C.L. Linslal,S.Divya, P.V. Sabitha, Sheenu Thomas, and V.P.N. Nampoori "Optical nonlinear investigations on morphology controlled growth of ZnO crystals" Opt. Laser Technol. 64 ,133-139 (2014).

- S. Divya,Aparna Thankappan, C. P. G. Vallabhan, V. P. N. Nampoori, P. Radhakrishnan, and A. Mujeeb "Electrolyte/photoanode engineered performance of TiO_2 based dye sensitised solar cells" J. Appl. Phys.,115, 064501 (2014).
- Ani Augustine Jose, Pranam Prakash, Aparna Thankappan, Sheenu Thomas, and V.P.N Nampoori "Study of regulation of anthocyanin production from confederate rose by spectroscopic method and their nonlinear optical characterization" I.J.S.N.,4 , 2,294-298 (2013).
- Arindam Sarkar, Aparna Thankappan, and V.P.N. Nampoori "Effect of silver nanoparticles on fluorescence and nonlinear properties of naturally occurring betacyanin dye" Opt. Mater. 39 ,211-217 (2015).
- Aparna Thankappan, Divya S, Anju.K. Augustine, Girijavallaban C.P, Radhakrishnan P, Sheenu Thomas, and V.P.N. Nampoori "Highly efficient betanin dye based ZnO and ZnO/Au Schottky barrier DSSC" Thin solid films (accepted).
- Aparna Thankappan, S.Divya,C.P. Girijavallaban, P. Radhakrishnan, Sheenu Thomas, and V.P.N. Nampoori"Enhanced performance of ZnO based dye-sensitized solar cell decorated with TiN nanoparticles" Laser Phy. Lett. (under reveiw).

B. Conference Publications:

- Aparna Thankappan, S Mathew, Misha Hari,and Santhi Ani Joseph "Structural and optical properties of ZnO micro spheres with nano petal like structure synthesized by low temperature chemical bath deposition method" The Third International Conference on Frontiers in Nanoscience and Technology,Cochin Nano-2011,Cochin,14-17 Aug 2011.
- Aparna Thankappan, Santhi Ani Joseph, and V.P.N Nampoori "Enhancement of UV emission of ZnO microrods on changing the excitation wavelength", National Symposium on Nanoscience and Technology, NanosTech 2011, Muvattupuzha, Kerala,1-2 September 2011.
- Aparna Thankappan, Sheenu Thomas,and V.P.N. Nampoori "Morphology impact on the onlinear optical properties of ZnO crystals embedded in polymeric matrices", National laser symposium ,NLS-22, Manipal, Karnataka, 8-11 January 2014.
- Arindam Sarkar, Aparna Thankappan and V.P.N Nampoori "Nonlinear studies of Betacyanin dyes in the presence of Silver Nano particles", National laser symposium ,NLS-22, Manipal, Karnataka, 8-11 January 2014.

- Aparna Thankappan, Sheenu Thomas, and V.P.N. Nampoori "Optical limiting performance of betanin natural dye", National conference on advanced materials and applications,NCMA 2013,Tiruchirappalli, Tamilnadu, 4-5 April 2013.
- Aparna Thankappan, Divya S, Sheenu Thomas,and V.P.N. Nampoori optical characterization of ZnO nanoplates stabilized with PVA for optical limiting applications , The first national conference on trends and applications in laser technology and optoelectronics, TALTO 2013,Gurgaon, India, 4 April 2013.
- Aparna Thankappan, Sheenu Thomas, and V.P.N. Nampoori "Optical limiting performance of ZnO nano flakes and nano plates stabilized in PVA matrix", International conference on nanomaterials: science, technology and applications, ICNM'13, Chennai,1-5 December 2013.
- Aparna Thankappan, Divya S, Sabitha P. V, Anju.K. Augustine, C.P. Girijavallaban, P. Radhakrishnan, Sheenu Thomas, and V.P.N. Nampoori "Performance comparison of betanin sensitized heterojunction dye-sensitized solar cells", Second International Conference on Nanostructured Materials and Nanocomposites, ICNM 2014, Kottyam, Kerala 19-21 December 2014.

List of Figures

List of Tables

List of Abbreviations

LED	Light emitting diodes
PVA	Poly vinyl alcohol
APMOCVD	Atomic pressure metal organic chemical vapour deposition
UV	Ultra-violet
DSSC	Dye sensitized solar cell
NLO	Nonlinear optics
SHG	Second harmonic generation
EO	Electro optic
SA	Saturable absorption
TPA	Two photon absorption
MPA	Multi photon absorption
RSA	Reverse saturable absorption
OL	Optical limiting
ESA	Excited state absorption
FCA	Free carrier absorption
CNT	Carbon nanotube
MOCVD	Metal organic chemical vapour deposition
MBE	Molecular beam epitaxy
1D	One dimensional
SEM	Scanning electron microscopy
TEM	Transmission electron microscopy
FWHM	Full width half maximum
VIS	Visible
PL	Photoluminescence
OA	Open aperture
CA	Closed aperture
ITO	Indium tin oxide
TCO	Transparent conducting oxide
FF	Fill factor
IPCE	Incident photon conversion efficiency
HMTA	Hexamethylenetetramine
DB	Dumb bell
TTIP	Titanium tetra-isopropoxide
TEA	Tri ethanol amine
HOMO	Highest occupied molecular orbital
LUMO	Lowest occupied molecular orbital
ISC	Inter-system crossing
WE	Working electrode

CE	Counter electrode
TBP	Tert-butylpyridine
ACN	Acetonitrile

"Every great dream begins with a dreamer. Always remember, you have within you the strength, the patience, and the passion to reach for the stars to change the world." : ***Harriet Tubman***

Chapter 1

Introduction: Principles and Basic Literature Survey

1.1 Abstract:

This chapter is an over view of the morphology engineering of zinc oxide (ZnO) structures, properties and device applications to photonics especially dye sensitized solar cells (DSSC).This chapter also discusses the possibility of natural dye as a photonic material along with their applications. The importance of hybrid materials and the basics of nonlinear optics are also mentioned in this chapter.

1.2 Background

The world's growing awareness towards health and safety stresses the need for monitoring all aspects of the environment in real time. This awareness has led to the intense study towards the development of the environmentally safe devices. With the rapid development of the science and technology into the nanoscale regime, one needs to synthesize low dimensional structures, to address their peculiar physical, chemical and optical properties related to their dimensionality with an emphasis to explore their possible applications. The combination of different synthesis techniques and materials of nanometre dimensions, nanoparticles decoration has been used to enhance the properties of the photonic devices. Wide band-gap semiconductor nanostructures are of particular interests which allows the possibility to tune the optoelectronic prop-

erties of devices working from infrared to ultraviolet range [1].

Although ZnO crystals may not be worth much for their appearance, it is their other belongings that make them useful. These crystals can be used in light emitting diodes (LEDs), solar cells and other optical devices, electronic devices, as well as biological and gas sensors [2-4]. It is often the case that their suitability for a certain purpose is deeply dependent upon its overall shape. However, only a certain face of the crystal is active. Thus, the tailored growth of inorganic crystals with high aspect ratios has been a long standing goal for material scientists [5]. In this thesis the controlled growth of one particular inorganic crystal, ZnO was investigated. ZnO was chosen as it has wide band gap (3.37 eV) and a large exciton binding energy (60 meV) and exhibits potential applications in many areas such as laser diodes, solar cells, gas sensors, optoelectronic devices depending upon its shape [6-7].

1.2.1 Material properties of ZnO

ZnO, a representative of II-VI semiconductor compounds, has a unique position due to its piezoelectric and transparent conducting properties [8-11] and has high electrical conductivity and optical transmittance in the visible region. These properties make it a perfect candidate for applications like transparent conducting electrodes in flat panel displays and window layers in solar cells. ZnO has very good thermal properties like high melting point, high thermal capacity and conductivity and a low coefficient of thermal expansion which makes it suitable for use as a ceramic [12-14]. Apart from this, bio-safe characteristics of ZnO make it smart for the biomedical applications. Some of the properties of ZnO [1-12]are shown in table 1.1.

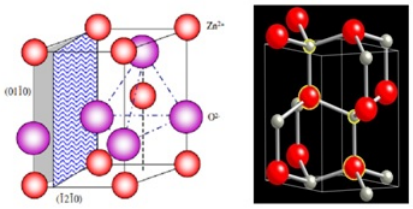

Figure 1.1: The structure of Würtzite ZnO

The hexagonal Würtzite, the cubic zinc blende and the cubic rock salt are the three crystal forms of ZnO. Natural ZnO exclusively forms hexagonal crystals with a Würtzite structure (Figure 1.1), and it is most commonly used as it has the highest stability under normal working conditions having a point group

Table 1.1: Important properties of ZnO

Property	Value
Molecular formula	ZnO
Molar mass	81.4084 g/mol
Density	5.606 g/cm^3
Melting point	1975^{o}C
Boiling point	2360^{o}C
Refractive index	2.0041
Relative dielectric constant	8.66
Energy gap	3.37 eV
Exciton binding energy	60 meV
Electron mobility (at 300 K)	200 cm^2/V.sec
Hole mobility (at 300 K)	5-50 cm^2/V.sec
Thermal conductivity	0.6-1.2 Wcm^{-1}K^{-1}
Specific heat capacity	Cp=40.3 J mol^{-1}K^{-1}
Lattice constants	a_0 = 0.32469 A^0 c_0 = 0.52069 A^0

of C_{6v}(6mm). The three native faces of ZnO crystal are: the Zn-terminated (0001) plane, the O-Terminated (000$\bar{1}$) plane and the six equivalent non-polar (10$\bar{1}$0) planes.

1.2.2 Morphology engineering of ZnO structures

Engineering of the crystal's morphology and microstructure has initiated great research interest and is essential for the development of future devices, since their physical properties depend on their dimensions and crystallographic structure. It has attracted increasing interest due to its potential applications in electronics [13], photonics [15], sensors [16], transistors [17], field emission displays [18], etc. It is one of the most gifted materials for the fabrication of short-wavelength optoelectronic devices [19]. ZnO possesses one of the richest family of nanostructures: nanorods, nanopillars, nanowires, nanotowers, nanotree, nanopropellers, nanobelts, nanobridges etc have been widely reported in literature[20]. However, such interesting morphologies of ZnO nanostructures complicate their functionality, i.e. hamper their practical applications, while the controllable growth of ordered and uniform ZnO nanostructure is highly desirable and may enable their possible applications in various devices.

In 2002, Jun Zhang et al.[21] reported nanosized ZnO with a diversity of well-defined morphologies, such as flower, snowflake, prism, prickly sphere,

and rod like samples and has been successfully fabricated by a simple solution approach by mixing 0.5 mol/L $ZnAc_2$ and 5 mol/L NaOH solutions, while Zn $(NH_3)_4{}^{2+}$ precursor was prepared by mixing 0.5 mol/L $ZnAc_2$ and fresh ammonia. It was found that the variations in solvent, precursor, reaction temperature and time, and solution basicity have significant effects on ZnO morphology. In 2004, Hui Zhang, Deren Yang et al.[22] developed different shapes of ZnO microcrystals by a capping-molecule-assisted hydrothermal process. The flowerlike, disk like, and dumbbell-like ZnO microcrystals of hexagonal phase high crystal quality had been obtained respectively using ammonia, citric acid and poly vinyl alcohol (PVA) as the capping molecules. Yoshitake Masuda et al [23] proposed an aqueous solution system to synthesize crystalline ZnO particles and to evaluate morphology control of ZnO particles. Their crystalline particles having long hexagonal cylinder shape, short hexagonal cylinder shape, rounded hexagonal cylinder shape, rounded ellipse shape, pointed ellipse or multi-needle shapes were homogeneously nucleated and precipitated in aqueous solutions at 50^0C by varying [NH3]/[Zn] ratio from 2-6. Researchers Seungho Cho et al.[24] had developed morphology-controlled growth of ZnO nano- and microstructures by microwave irradiation and a subsequent ageing process at 90^0C for 15 min. In 2010, S.L.Yang et.al.[25] reported morphology-controlled growth of tetrapod ZnO nanostructures by reaction of high-purity Zn granules with oxygen using an arc discharge method.

V.Khranovskyy et al [26]reported the atmospheric pressure metal organic chemical vapour deposition (APMOCVD) growth of ZnO nanostructures of diverse morphology within temperature range 200-500^0C using zinc acetyl acetonate as a single source precursor. They reported the distinctive feature, i.e. the nanostructures morphology changes systematically with the temperature, driven by ZnO crystal planes anisotropy and obeying the crystal growth theory. Within the temperature range 200-500^0C ,applying the varying precursors pressure ,the nanostructures undergo the evolution of their shape from the polycrystalline blocks of nanocrystals to the ordered textured array of the nanorods. In 2012, Wenzhong Wang et al [27] developed methods to synthesize using environmentally friendly NaCl non aqueous ionic liquid route ZnO nanostructures including nanowires and nanoplates.

1.2.3 Properties and device applications of ZnO

In this section we describe the physical properties of ZnO and relate them to current applications in electronic and optoelectronic devices. ZnO is a promising material for semiconductor device applications; it has a direct and wide band gap in the near UV-spectral region and a large free-exciton binding energy [28,29]. The wide band gap energy enables applications in optoelectronics

in the blue/UV region including light emitting diodes, photo detectors and laser diodes. The ZnO crystals are almost always n-type, this n-type conductivity makes it suitable for applications in field emission displays and vacuum fluorescent displays. The high thermal conductivity of ZnO translates into the high efficiency of heat removal during device operation, and this property makes ZnO useful as an additive [30]. ZnO crystals exhibit second and third order nonlinear optical behaviour, which is suitable for the integrated nonlinear optical devices.

Commercially available ZnO varistors ,made of semiconducting polycrystalline films,have high nonlinear resistance i.e. high non-ohmic currentvoltage characteristics which is attributed to the grain boundaries. The conductivity of ZnO thin films is very sensitive to the exposure of the surface to various gases and this strong sensitivity makes ZnO useful as a sensor [31]. In piezoelectric materials, an applied voltage can generate a deformation in the crystal and vice versa and are generally used as sensors, transducers and actuators. The low symmetry of the wurtzite crystal structure along with a large electromechanical coupling in ZnO gives rise to strong piezoelectric and pyroelectric properties. Semiconductor device fabrication processes greatly benefit from the amenability to low-temperature wet chemical etching which adds great flexibility in the processing, designing and integration of electronic and optoelectronic devices. In addition to the above mentioned properties, ZnO has also attracted consideration due to the possibility of making thin film transistors on flexible substrates with high electron mobilities compared to the amorphous silicon [32]. ZnO is regarded as a promising alternative to TiO_2 for transparent conductive electrode application in solar cell, since it has similar band gap and electron affinity values to those of TiO_2 and it is also an environment friendly oxide semiconductor.

1.3 Natural dye as a photonic material

A vast array of dyes obtained from natural sources such as plants, insects/animals and microbes have been examined in recent past for their use in various applications. Investigation into new natural dye sources have greatly aided in widening the scope of natural dyes in various traditional and advanced application disciplines. The majority of natural dyes are vegetable dyes. Plant dyes may contain several compounds and their proportions vary with the nature of soil and the climate. Historically, natural dyes were used in textile industry, and by the mid-1800s chemists began producing synthetic dye substitutes for them. By the early part of this century only a few percentage of dyes were extracted from plants. Lately there has been increasing attention in natural dyes, as the public becomes aware of ecological and environmental problems

related to toxic from the complex world of synthetic dye process.

1.3.1 Advantages of natural dyes

- Natural dyes are more eco-friendly than the synthetic dyes
- Natural dyes are free from carcinogenic components
- Depth of some natural dyes are enhanced with age
- Most of them are known as antioxidants
- The colours of dyes depend on the source of the dye and the mordants
- High diversity of rich and complex natural dye colours
- Different colours go well together and rarely clash
- Beauty of the results when using natural dyes
- Excitement of unexpected results
- Satisfaction of growing your own dye plants and produce your own colours
- Self-sufficiency if growing your own plants for plant dyes
- Non dependence on non-renewable materials
- Allowing endless experimentation
- Allowing the replication of ancient techniques
- Aromatic smell when simmering the plants

1.3.2 Disadvantages of natural dyes

- Require large quantities in comparison to chemical dyes
- Longer time required for natural dyeing.
- There is still a dependency on chemicals or mordant for bonding the colour to the fabric.
- Need of huge amount of water.
- Availability of natural dyes are limited
- Difficult to reproduce shades
- As the natural dyes are extracted from plants mostly, they are dependent on growing seasons
- Even though natural dyes produce bright colours and different shades but tend to fade faster than the synthetic dyes.
- Consistency is a problem as no two dye lots are identical due to the impurities in them

1.3.3 Betalain plant pigments

In the plant world, pigments play a vital role in the survivability of species and they have been extensively investigated as sensitizers for the DSSC. Pigments have properties allowing them to power photosynthesis, protect from oxidative stress, or attract pollinators with their colour. These pigments vary not only in colour, but structure and function. There are four types of natural plants pigments: chlorophyll, carotenoids, anthocyanins, and betalains [33]. Chlorophyll is active in photosynthesis, absorbing mostly yellow and blue light and facilitating the transfer of energy from sunlight to a plant [34]. Carotenoids often act as an accessory pigment to chlorophyll in the fruit or roots of plants, capable of both participating in photosynthesis and dissipating excess energy from the sun through oxidation [35]. The anthocyanins are water soluble flavonoids responsible for the red and blue colours of many fruits and leaves.They are not involved in photosynthesis and may serve as antioxidants, photo protective agents and osmotic regulators [36,37]. Betalains and anthocyanins are mutually exclusive in their natural occurrence; it is interesting that the two have never been found in any of the same plants [38,39]. Betalains are water-soluble nitrogen-containing pigments, which comprise the red-violet betacyanins and the yellow-orange betaxanthins. The betalain is relatively stable over broad pH range from 3 to 7 [40] and have several applications in food such as deserts, dry mixes and dairy, comprise the red-purple betacyanins, betanin (I) and betanidin (II), with maximum absorptivity at λ_{max} about 535 nm, and the yellow betaxanthins with λ_{max} near 480 nm [41]. The structure of indicaxanthin (III), a common betaxanthins found in beet root, is shown in figure 1.2. Betanin, the red-purple pigment distributed in beets, is the 5-O–glucoside of betanidin.

Betalains accumulate in flowers,fruits and occasionally in vegetative tissues of plants belonging to most families of the Caryophyllales [42] but have also been found in some higher fungi, for example in the fly agaric(Amanita muscaria). Even though the functions of betalains in plant flower and fruit colouration are obvious, their role in fungi is unknown. There is growing interest in the use of natural pigments for food colouring, since synthetic dyes are becoming more and more critically assessed by the consumer. In food processing, betalains are less commonly used than anthocyanins and carotenoids, although these water-soluble pigments, stable between pH 3 and 7, are well suited for colouring low acid food. The most important source of betanin is the red beet root.

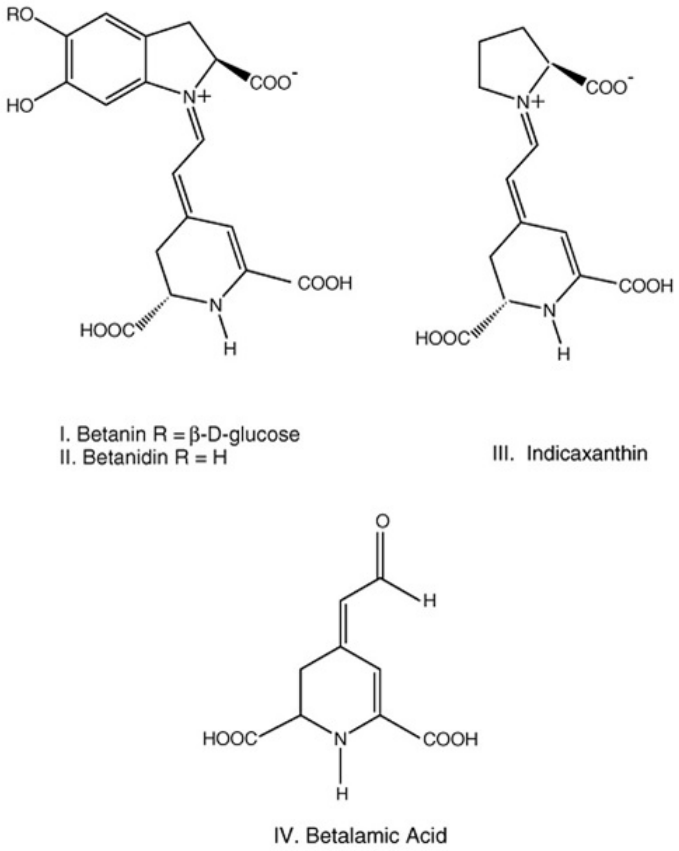

Figure 1.2: Structure of betalain pigments

1.3.4 Applications of natural dye in different fields

While the usage of natural dyes is growing in food industry and in modern medicine, there is also an interest in nanophotonics applications in the field of nonlinear optics as well as green photosensitising media in dye sensitised solar cell technology. Some of the applications of natural dyes are depicted in figure1.3.

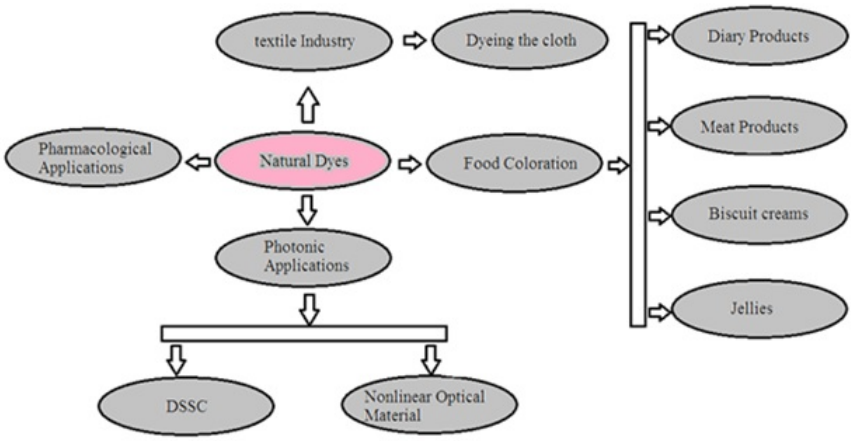

Figure 1.3: Various applications of natural dye

1.4 Hybrid materials

Organic-inorganic hybrid materials represent the natural interface between two worlds of chemistry each with major contributions to the field of material science. The art of combining dissimilar components to yield a smart natural material is not new, in fact it goes way back to ancient construction materials like Adobe, which was used to build houses and was made from the mixture of clay (inorganic) and straw (organic)[43]. Nevertheless, the modern concept of hybrid materials is away from the concept of a mixture of these components. The organic-inorganic composites can be broadly defined as nanocomposites that found a compromise between different properties or functions such as mechanics, density, permeability, and colour. The structure-function relationship of organic-inorganic hybrid structure exhibits an interface where there is a synergistic interaction between the organic and inorganic components. It has influence on the bio-mineralization, hydrogen bonding, and hydrophilic-hydrophobic interactions. Based on the bonding, chemical nature between organic inorganic interface, the hybrid materials can be classified as class I and class II. In class I, organic and inorganic components are embedded and only weak bonds (hydrogen, van der Waals or ionic bonds) give the cohesion to the whole structure and in class II materials, the two phases are linked together through strong chemical bonds (covalent or iono-covalent bonds).

The Maya blue pigment is a beautiful example of an old man-made class I hybrid material for which conception was the fruit of an ancient serendipitous

Figure 1.4: Examples of Mayan paintings where Maya blue was used

discovery which is a composite of organic and inorganic constituents, primarily indigo dyes derived from the leaves of plants combined with a natural clay. Ancient Maya fresco paintings are characterized by bright blue colours that had been miraculously preserved (Figure 1.4).[44]. Indeed Maya blue is an extremely resistant pigment, not only resisting biodegradation, but showing also extraordinary stability when exposed to acids, alkalis and organic solvents [44,45].

1.4.1 Optical nonlinear composites

The ability to control the structure at the nanoscale opens new horizons and vast opportunities to create new materials with superior performance. Nanocomposite materials show great promise as they can provide the necessary stability and processability for the applications in optical switching, waveguides and optical fibers.

Nanomaterials are an exciting subject in the field of both fundamental study and applied science. Recent research has progressed to nanocomposite materials with various structures and functions. Among the corporative candidates for constructing nanocomposites, polymers are the best choice, as they have many complementary functions such as elasticity, viscosity and plasticity that inorganic nanocrystals lack. Photonic nano/micro composite are generally constructed by embedding an optically functional guest materials at nano/micro scale into an optically transparent host matrix. The schematic representation of optical composite is shown in figure 1.5.

The assembly of nanoparticles in matrices is of major interest in several optical and sensor applications [46]especially those which require large area

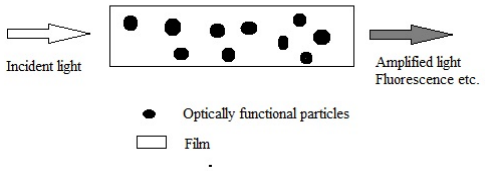

Figure 1.5: Schematic of optical composite

coating. Polymeric materials are the perfect choice for such an integrated platform due to their lightweight and often ductile nature. They generally have a low-cost room-temperature fabrication process. However, they have some drawbacks, such as low modulus and strength compared to metal and ceramics. Polymers can be synthesized with customer-defined optical characteristics such as selective transparency bands in different spectral ranges, variable refractive indices, low birefringence, etc. The common approach to such materials includes casting of films using the mixture of nanoparticles and polymer; in these physical mixtures, polymers and nanoparticles are connected through static interaction, van der Waals forces or Lewis acid base interactions, and inbuilt growth inside the solid matrix in which bonding between polymers and nanostructured materials occurs chemically [47].

Polymer matrices reinforced with micro and nanoparticles possess properties superior to those of the starting materials and can enhance their properties of the polymers due to the strong interfacial adhesion or interaction between the organic polymer and the inorganic particles. They exhibit high optical damage threshold, micro-hardness, good thermal stability, etc and enable the transformation of radiations over a wide spectral range with better efficiency than polymers and dyes separately [48]. ZnO has wide band gap with large refractive index and exciton binding energy, high catalysis activity, effective antibacterial and bactericide function and intensive ultraviolet and infrared absorption which make these particles of particular interest. Composites based on this can be widely utilized in coatings, rubbers, plastics, sealants, fibres and other applications [49].

Thus nano/micro composite provide a new method to enhance the processability and stability of materials with interesting optical properties. Organic dye-polymer nanocomposites have been generating significant research attention by way of their high degree of compatibility, easy mode of preparation, flexibility in molecular design strategy, versatility and diverse functionality. The

interactions of biomolecules with the ZnO low dimensional structures provide new opportunities for the development of photonic devices. The composites have wide applications ranging from solid-state amplifier films to transparent magnets. On the whole, their opportunities and rewards appear to be great , and hence there is an excellent worldwide interest in these materials. Materials

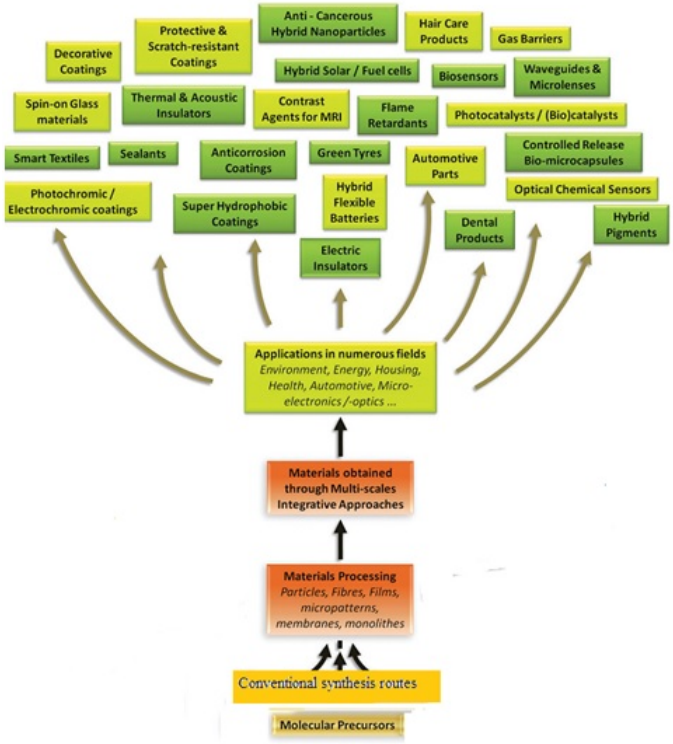

Figure 1.6: Applications of advanced hybrid organic-inorganic nanomaterials (nanocomposites): from laboratory to market

with large optical nonlinearity are key elements in many areas of photonics and optical technology such as all-optical switching (optical computer) devices, three dimensional fluorescence imaging, and optical limiting. However, most of the synthesized materials require elaborate preparation procedures and safety measures, use or generation of hazardous materials, costly materials, as well as fragile or chemically unstable structures beyond certain threshold irradiance. Therefore, we suggest natural dye extracts as environment friendly, safe, and inexpensive materials, as well as having high chemical stability during optical

excitations with coherent light sources. The natural pigments from plants have been extensively investigated as sensitizers for the DSSC.Besides anthocyanins, chlorophylls, and carotenoids, betalains are the most common pigments in the plant kingdom. Though the former have inherent limitations as sensitizers owing to weak absorption of green wavelengths, the absorption spectra of the latter have more favourable overlap with the solar spectrum.

Without any doubt, hybrid materials will soon generate smart micro-optical and photonic materials and play a major role in the development of advanced functional materials. Some of the applications of hybrid organicinorganic nanomaterials (nanocomposites): from laboratory to market [50] is shown in figure 1.6.

1.5 Nonlinear optics

Nonlinear optics (NLO) is the study of field induced modification of the optical properties of a material system. The observation of nonlinear effects requires the application of laser beam. Observation of second harmonic generation (SHG) by Franken et al.(1961) marked the beginning of the field of NLO[51], shortly after the demonstration of the first working laser by Maiman in 1960. They propagated a ruby laser beam ($6942A^0$) through a quartz crystal and observed ultraviolet radiation (3471 A^0) from the crystal. It should be noted that some nonlinear effects were discovered prior to the invention of the laser. The observation of saturation effects in the luminescence of the dye molecules reported by G.N. Lewis et al.(1941) is an example for this[51,52]. Numerous NLO phenomena have been discovered since 1961.

In nonlinear optics, the optical response, the polarization P(t), can be described as a power series in the field strength E(t) as

$$P(t) = \epsilon_0[\chi^{(1)}E^1(t) + \chi^{(2)}E^2(t) + \chi^{(3)}E^3(t) + ... = P(1)t + P(2)t + P(3)t + ... \tag{1.1}$$

The quantities $\chi^{(2)}$ and $\chi^{(3)}$ are known as the second and third-order nonlinear optical susceptibilities, respectively. SHG can occur only in non centrosymmetric crystals i.e, in crystals that do not display inversion symmetry. On the other hand, third-order nonlinear optical interactions can occur for both centro-symmetric and non centro symmetric media.

The studies of nonlinear processes in photonic materials are crucial in the context of their technological applications, especially in areas such as passive optical power limiting, optical switching, design of logic gates, frequency conversion and electro optic (EO) applications especially in EO modulators and

such materials are capable of processing information with the speed of light. In the last three decades there has been increasing awareness of organic materials due to their large nonlinear optical responses. This enhancement is due to the existence of conjugated electron systems and hydrogen bonding of organic molecules. They generate NLO material with large hyper-polarisability which is obtained from the charge transfer mechanism of molecular structure.

The organic-inorganic composites offer tremendous opportunities in material engineering to produce suitable materials with wonderfully tailored physical properties. Sufficient attention has not been paid towards the proper utilization of their capabilities in photonic device applications. Thus, there exists a pressing need to develop novel optical materials, for which a deep insight into the optical processes is essential.

The goal of this thesis is to develop the nonlinear optical materials with large optical nonlinearity and to simultaneously satisfy growing technological and economical requirements. Such a progress in nonlinear optical materials requires an in-depth knowledge of material's nonlinear polarization mechanisms, and of their relation to the material structure. The interaction of intense light with matter leads to the stimulated emission and absorption, complicated energy transitions from molecular systems and the generation of free carriers in solids. These phenomena are manifested optically in a reduced or increased absorption.

1.5.1 Saturable absorption

Saturable absorption (SA) is a significant deterioration of absorptive properties of the optically nonlinear material with increase in the incident light intensity. Such a material is also referred to as a saturable absorber. The following factors may contribute to the absorption drop, the excited states of the material having longer life time and the excited state absorption being much smaller than the ground state absorption. Indeed the ground state will be rapidly depleted and will not be repopulated at high input pulse . This will lead to a drop in the absorption as the excited state absorption cannot match the same level of absorption as the ground state absorption produces. At sufficiently high incident light intensity, atoms in the ground state of a saturable absorber material become excited into an upper energy state at such a rate that there is insufficient time for them to decay back to the ground state before the ground state becomes depleted, and the absorption subsequently saturates. Materials which show saturable absorption properties can be used as saturable absorber in mode locking to generate ultra-short laser pulses i.e they are useful in laser cavities (passive mode locking).

1.5.2 Two/multi photon absorption

Two photon absorption (TPA) is a nonlinear absorption process in which two photons are absorbed simultaneously by the atom, ion or molecule and an electron is promoted from the ground state to excited state. The total energy of the transition is equal to the sum of the two photon energies[53].The schematic representation of a two photon excitation up-conversion process is shown in figure 1.7.

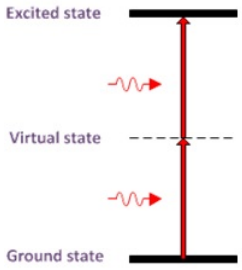

Figure 1.7: Energy scheme of a two photon excitation up-conversion process

The equation describing the intensity attenuation of a light beam passing through a material undergoing single photon and two photon absorption is given by

$$\frac{dI}{dz} = -\alpha I - \beta I^2 \tag{1.2}$$

where α and β are constants. The constant β is for two photon absorption and is related to third order susceptibility.

Multi photon absorption (MPA) is another important nonlinear process in which the material simultaneously absorbs n photons (n$\geq$2) of identical or different frequencies in order to excite an electron from one state to higher electronic state. The typical MPA processes are TPA and 3PA (three photon absorption) which belong to the third and fifth nonlinear process, respectively. MPA is several orders of magnitude weaker than linear absorption and its strength of absorption depends on higher order of light intensity.MPA is essential in a wide range of applications such as multi-photon excitation microscopy, multi-photon micro-fabrication and lithography, photodynamic therapy, optical limiting and optical data storage.

1.5.3 Reverse saturable absorption

A class of nonlinear absorbers in which the excited state absorption is large compared to the ground state absorption can undergo a process called reverse saturable absorption (RSA).In contrast with saturable absorption,RSA can result in large absorption by the nonlinear absorber at high incident laser energies and low absorption at low laser energies. However, transparency at low input energy, but high absorption at high input energy can be attained with multi-photon absorbers (MPA) in which two or more photons are absorbed simultaneously.

1.5.4 Excited state absorption and free carrier absorption

In the case of molecules or polymers, there is a possibility of one-photon assisted excited electrons being further photo-excited to another higher excited state i.e. the electron at the low lying excited state (S_1) completely relaxes to the ground state ,it may experience absorption that promotes it to state S_2. This nonlinear process is known as Excited state absorption (ESA). Free carrier absorption (FCA) occurs when a material absorbs a photon and the generated carrier is excited from a filled state to an unoccupied state (in the same band).

1.5.5 Kerr effect

When an intense laser beam passes through a material, the electric field of the beam can induce a change in the refractive index of the material that is proportional to the intensity of the beam. This nonlinear effect is known as Kerr effect. The total refractive index (n) of the material is given by

$$n = n_0 + n_2 I \tag{1.3}$$

The change in the refractive index can be positive or negative. If change in the refractive index is positive, the Kerr effect combined with diffraction can lead to self-focusing of the laser beam since the centre of the beam will have higher intensity and a higher refractive index change than the edge of the beam. The index changes are equivalent to having a positive gradient index lens. If it is negative, self-defocusing can occur.

1.5.6 Optical limiting

Optical limiting is a NLO process in which the transmittance of a material decreases with increased incident fluences. Optical limiters are one of the important types of devices used to control the amplitude of high intensity optical pulses and have a linear transmittance at low input intensities, but above the threshold intensity its transmittance becomes constant. The ideal behaviour

of such a device is shown in figure 1.8. One of the main potential applications of these devices is sensor and eye protection and can also be used for pulse shaping and smoothing and pulse compression.

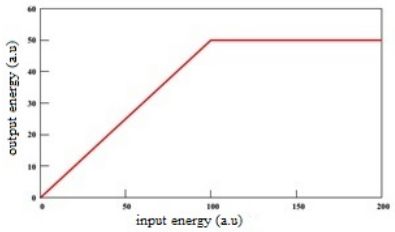

Figure 1.8: An ideal optical limiter

Some of the mechanisms responsible for optical limiting are RSA, nonlinear refraction (due to molecular reorientation, electronic Kerr effect, excitation of free carriers, photo refraction, optically induced heating in the material, induced scattering (optically induced heating or plasma generation in the medium),thermal blooming and MPA.

1.5.7 Nonlinear refraction

Nonlinear refraction is a consequence of various phenomena that may take place in the material such as self focusing or defocusing of light away from the sensor. Another nonlinear refraction related mechanism is molecular reorientation in which a strong electric field applied to a system which contains anisotropic molecules tends to align the induced dipole moments of the molecules along the direction of the field leading to the change in the refractive index. The photorefractive effect is another phenomenon related to the intensity dependent refractive index which describes a modulation in the refractive index due to spatial variation of the intensity formed by the interference of two coherent incident beams. One effect of the photorefractive mechanism is beam fanning, which is the coupling between the initially weak scattered beam in a crystal and the incident beam.

Thermal nonlinearities arise from the absorption of radiation which leads to heating of the material. As a consequence of this the local density changes and this in turn will modify the index of refraction of the material. In the case of nonlinear scattering, the formation of small scattering centers in the device can be achieved by thermally induced local density changes .Or, by using a heterogeneous material whose components have matching refractive indices for low input intensities, while for higher power the indices become mismatched,

and therefore nonlinear scattering occurs and the increased scattering at higher intensity directly limits the transmitted intensity.

1.6 Motivation for ZnO based dye sensitized solar cells

Dye sensitized solar cells (DSSCs) have received a tremendous amount of attention since the first report of a 7% efficient cell in 1991by O'Regan and Gratzel. Since the first major jump in efficiency in 1991, advances have been made in relation to many different facets of the cell. Confirmed recorded efficiencies are now 12.3% by the combination of co-sensitization of porphyrin dyes and a cobalt-complex redox mediator [54] and low-cost production methods are enabling manufacturing of DSSC products for a variety of markets.

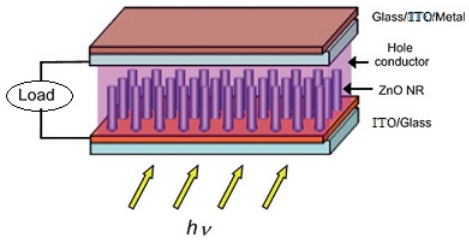

Figure 1.9: Schematic representation of a DSSC applying ZnO nanowires as the electron transport material

DSSCs can be fabricated from low-cost oxide nanoparticles and organic dye using roll-to-roll processing without the use of expensive vacuum processing or high temperature which is required for single crystal or thin film solar cell production. Over the past two decades, the amount of work has literally grown exponentially. A typical DSSC consists of a redox electrolyte sandwiched between a working electrode (WE) and a counter electrode (CE) (figure 1.9). Platinum film is widely used in fabricating a high performance DSSC since it has good catalytic activity. The semiconductor film is sensitized with a monolayer of dye molecules; photoexcitation takes place in the dye molecules, and fast electron transfer through the electrolyte to the platinum counter electrode.

The spatial separation between the light-harvesting compound (Dye) and the charge carrier material in DSSC seems to be the key to their higher efficiency and longer lifetime [55,56]. Despite the fact that TiO_2 is the most used

semiconductor oxide in DSSCs, ZnO is being intensely investigated because of its similarities with the former, i.e. it is a wide band gap semiconductor oxide (3.37 eV) with a conduction band edge located at approximately the same level as TiO_2.

The basic operating principle for solar cell consists of absorption, separation and collection. Thus, absorption occurs in the first step of the reactions occurring in DSSC. Under illumination, sensitizer D absorbs a photon which leads to excited sensitizer state D*. Photo excitation of this sensitizer is then followed by the electron injection into the conduction band of the semiconductor. This takes the sensitizer to an oxidized state D^+. With the electron donation from the electrolyte, containing a redox couple, the original state of the dye is restored. Iodide/triiodide couple is the preferred and effective redox couple used. Iodide regenerates the sensitizer, and gets itself regenerated by the reduction of triiodide at the counter electrode. This way the circuit gets completed by transfer of electron via the external load. The following reactions summarize the working in a lucid manner:

$$D_{absorbed} + h\nu \rightarrow D^*_{absorbed} \tag{1.4}$$

$$D^*_{absorbed} \rightarrow D^+_{absorbed} + e^-_{injected} \tag{1.5}$$

$$I_3^- + 2e^-_{cathode} \rightarrow 3I^-_{cathode} \tag{1.6}$$

$$D^+_{absorbed} + \frac{3}{2}I^- \rightarrow D_{absorbed} + \frac{1}{2}I_3^- \tag{1.7}$$

Sensitizer is in the form of a dye, mostly metal complex dyes. Although a lot of dyes have been tested and investigated including natural dyes, Ruthenium complexes have proved to be the most effective consistently. Fruit dyes like mulberry and others have also been tested for DSSC. Fill factor values of 0.40 to 0.61 have been achieved on dye sensitization of dye extracts from mulberry, chaste tree fruit and cabbage palm fruit most effective consistently [57]. ZnO has been proven to be efficient photocatalyst than TiO_2 when sunlight is the light source [58]. The longer electron lifetimes observed for ZnO means lower charge recombination which is beneficial for solar cell performance. An important advantage of ZnO over TiO_2 is that it can be synthesized applying a wide range of synthesis techniques; to obtain a great variety of different morphologies and nanostructured electrodes, especially vertically-aligned nanostructures. The highest efficiency solar cells applying ZnO have only reached 6-7% [59] which is less than the 11.3% obtained with the best DSSC applying TiO_2 [60]. Thus it is important to have carefully control parameters, such as

dye or polymer concentration, pH or sensitization with time, in order to improve solar cell efficiency.

In DSSC, some authors have reported that, contrary to TiO_2, low dye absorption time is required for higher solar cell efficiency [61-63] which indicates some basic differences in surface chemistry between these two oxides. Keis et.al reported the difference between dye-sensitization on TiO_2 and ZnO[62,64]. In TiO_2 there is strong adsorption of the carboxyl groups to the surface which favors monolayer growth and usually 20-24 h immersion time is needed. In ZnO, however, the sensitization process follows more complicated steps: diffusion of the dye, adsorption on the ZnO surface, dissolution of Zn surface atoms and formation of [Dye-Zn^{2+}]complex [65]. Moreover, the acidity of the -COOH binding groups from the dye affects the chemical stability of the ZnO, which dissolves and precipitates as a [Dye-Zn^{2+}] complex, which is responsible for the poor electron injection from the dye [55].

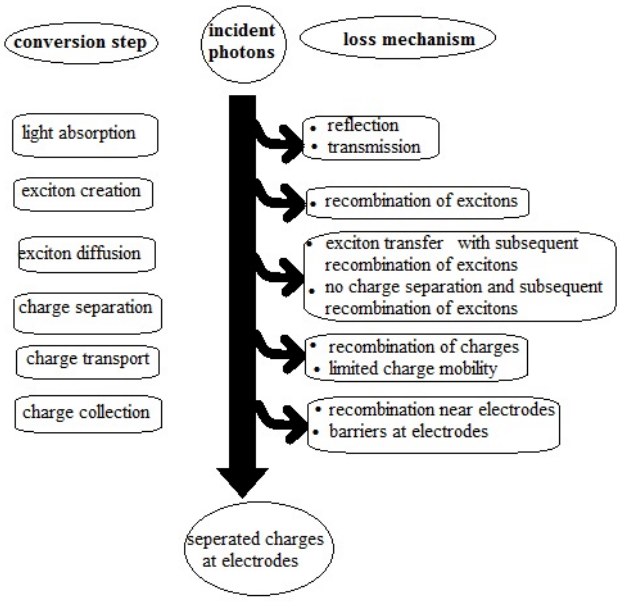

Figure 1.10: Survey of the specific conversion steps and loss mechanisms in an organic solar cell

In addition, some groups report that the use of vertical nanostructures may not be optimal for light-harvesting because some photons can fall on the gap of adjacent nanorods and the light loss could be significant. In vertically-aligned

ZnO branched nanorods the improvement could be double: higher surface area and increased interaction with light, maintaining good electron transport [66]. The survey of the specific conversion steps and loss mechanisms in an organic solar cell are illustrated in figure 1.10.

1.6.1 Advantages of DSSC

- DSSC have a good depth in their nanostructure and hence absorb the photons well in the sunlight. Furthermore the dyes used in the cells are efficient in converting the absorbed photons into electrons.
- Though the efficiency of DSSCs is less than many of the best thin-film cells, the price-to-performance ratio obtained through these solar cells is superior to others.
- Due to the reduced manufacturing costs, DSSCs are less expensive when compared to other semiconductor cells. They do not require any apparatus and can be printed on any flexible surface.
- DSSCs also work in cloudy weather and low-light conditions without much impact on efficiency, while the other traditional cells would fail at illumination below a certain range. DSSCs have a very low cut off. This makes them suitable for running small devices indoors.
- They contain primarily nontoxic, earth-abundant materials, with the exception of very small amounts of Pt and Ru.
- DSSCs are mechanically robust. They are made of lightweight materials and require no special protection from rains or trees or any other harsh objects. This makes them easy to use and maintain.
- As the temperature rises, some electrons in semiconductors are pushed to conduction band mechanically. Hence the silicon cells require protection by covering in a glass box. Such cells get heated easily and hence the efficiency is greatly reduced due to internal temperature. This situation is eliminated in the DSSCs. Because DSSCs are made of only a thin layer of plastic, heat radiates away easily to reduce the internal temperature. This lowering of temperature, in turn, helps in increasing the efficiency of the solar cells.

1.6.2 Recent advances in DSSC and Future trends

Engineers are trying to design novel photoelectric cells that are more durable, efficient and economical using mathematical modelling and nanotechnology and they are evaluating solar panels to streamline the electron transfer process inside the solar panel so that it efficiently converts radiation to electricity.

Presently, DSSCs convert about 11-12% of the sunlight striking them, into electricity. The researchers are trying to improve the efficiency and make it comparable with silicon-based solar panels.[66]

The performance of modern DSSCs is becoming more and more competitive. The researchers anticipate that adding carbon nanotubes (CNT) and titanium nitride (TiN) as counter electrode will enhance the overall charge collection efficiency of the solar cell considerably. The next portion of the research is aimed at replacing the electrolyte solution and sensitizer and separating the electrodes with a more efficient polymer material. The researchers believe that this will also increase the efficiency of the solar cell. In an effort to increase surface area and at the same time the interface between the semiconductor oxide and the corresponding organic semiconductor (Dye or conducting polymer), vertical nanostructures, such as branched nanorods or nanosheets, seem to be promising candidates for high efficiency DSSC .The best ZnO DSSC performance now reaches 7.2% efficiency, when applying vertical nanostructures made of porous single crystal ZnO. Another possible design improvement is to progress the devices with more junctions with innovative concepts. Finally, a promising research trend, is the possibility of developing DSSCs as all-solid-state devices with high efficiencies, avoiding the application of problematic liquid electrolytes, and applying solution processing techniques for fabrication.

1.7 Aim and motivation of the research

ZnO and their complexes are studied widely owing to their potential applications in the field of photonics. Studies on the growth mechanism and structural characterisation have already been carried out and reported, but the morphological dependence on the NLO behaviour of ZnO has not been dealt with in detail. The main aim of this thesis is to explore the possibility to synthesise controlled morphologies of ZnO with suitable properties via simple wet chemical method. In the present work we concentrate on the NLO behaviour of ZnO crystals with different morphology and try to establish ZnO-natural dye complexes as a photonic material. The use of betanin natural dye and their complex with ZnO as a photonic material are reported for the first time. In particular, our efforts have been devoted to test the performances of betanin dye sensitized solar cell (DSSC) especially ZnO complexes with CdS, ZnS, TiO_2, Au and TiN.

1.8 New findings in a nut shell

- We have investigated morphological effect on the nonlinear properties of ZnO at low dimensional structures.
- We have also studied the possibility of betanin natural dye for environment friendly and inexpensive photonic device applications having high photochemical stability under laser excitations.
- The photochemical performance of nanosheet based DSSC exhibit better efficiency under low-light conditions.
- The efficiency has been enhanced with the incorporation of gold (Au) and titanium nitride (TiN) nanoparticles

1.9 References

[1] J.L Costa-Kramer, N.Garcya, P.G.Mochales, P.ASerena, M.I Marques and A.Correia "Conductance quantizationin nanowires formed between micro and macroscopic metallic electrode" phys.Rev.B, 55, 5416 (1997)

[2] Xia Y. N, Yang, P. D, Sun Y. G, Wu Y. Y, Mayers B, Gates B, Yin Y. D, Kim F, Yan Y. Q, "One-dimensional nanostructures: Synthesis, characterization, and applications". Adv. Mater, 15 ,5, 353-389 (2003)

[3] Pearton S. J., Abernathy C. R, Overberg M. E, Thaler G. T, Norton D. P, Theodoropoulou N, Hebard A. F, Park Y. D, Ren F, Kim J, Boatner L. A, "Wide band gap ferromagnetic semiconductors and oxides". J. Appl. Phys., 93 ,1, 1-13 (2003)

[4] Diebold U, "The surface science of titanium dioxide". Surf. Sci. Rep., 48,5-8, 53-229 (2003).

[5] Nathan Johann Nicholas "Control of ZnO Crystal Morphology through Face Specific Adsorption" Ph.D Thesis ,The University of Melbourne Victoria, Australia (2011)

[6] Wang Z. L,"Zinc oxide nanostructures: growth, properties and applications". J. Phys.: Condens. Matter ,16,25, 829-858 (2004).

[7] Schmidt-Mende L, MacManus-Driscoll J. L, "ZnO - nanostructures, defects, and devices". Mater. Today, 10,5, 40-48 (2007).

[8] Sreetama Dutta and Bichitra N Ganguly "Characterization of ZnO nanoparticles grown in presence of Folic acid template", J. Nano biotechnology, 1-10, 29 (2012)

[9] Zhiyong Fan and Jia G. Lu, "Zinc Oxide Nanostructures: Synthesis and Properties", J. Nanosci. Nanotechnol., 5, 10, 561- 1573 (2005).

[10] S Baruah and J Dutta , "Hydrothermal growth of ZnO nanostructures", Sci. Technol. Adv. Mater. ,10,1 (2009)

[11] Hernandezbattez A, Gonzalez R, Viesca J, Fernandez J, Diazfernandez J, MacHado A, Chou R, Riba J, "CuO, ZrO_2 and ZnO nanoparticles as antiwear additive in oil lubricants", Wear ,265,422-428 (2008).

[12] T.A Polley, W.B Carter, D.B Poker, "Deposition of Zinc oxide thin films by combustion CVD", Thin Solid Films. 357, 132- 136 (1999).

[13] Ü.Özgr, Ya. I Alivov, C. Liu, A. Teke, M. A. Reshchikov, S. Doan, V. Avrutin, S. J. Cho, and H. Morko, "A comprehensive review of ZnO materials and devices", J. Appl. Phys.. 98, 041301,(2005).

[14] B. Wang, E. Shi, W. Zhong, C. Xia, W. Li, Z. Yin, "Growth habits and mechanism of ZnO", Micro Cryst. Hydrotherm. Cond. ,25,2, 223 (1997)

[15] V. Khranovskyy, G. R. Yazdi, G. Lashkarev, A. Ulyashin, and R. Yakimova, "Investigation of ZnO as a perspective material for photonics" Phys. Stat. Sol. (a) 205, 144 (2008)

[16] V. Khranovskyy, J. Eriksson, A. Lloyd-Spetz, L. Hultman and Rositza-Yakimova, "Effect of oxygen exposure on the electrical conductivity and gas sensitivity of nanostructured ZnO films" Thin Solid Films 517, 2073-2078 (2009)

[17] A. Evtukh, V. Litovchenko, M. Semenenko, V. Karpyna, G. Lashka-rev, V. Lazorenko, V. Khranovskyy, L. Kopylova, Yu. Piryatinskyy, "Peculiarities of electron field emission from ZnO nanocrystals and nanostructured films" Superlattices Microstruct., 42,451-460 (2007)

[18] V. A. Karpyna, A. A. Evtukh, M. O. Semenenko, V. I. Lazorenko, G. V. Lashkarev, V. D. Khranovskyy, R. Yakimova, D. A. Fedorchenko, "Electron field emission from ZnO self-organized nanostructures and doped ZnO:Ga nanostructured films" Microelectron. J.40, 229-231(2009)

[19] M. Willander, O. Nur, Q. X. Zhao, L. L. Yang, M. Lorenz, B. Q. Cao, J. Z. Perez, C. Czekalla, G. Zimmermann, M. Grundmann, A. Bakin, A. Behrends, M. Al-Suleiman, A. El-Shaer, A. CheMofor, B. Postels, A.Waag, N. Boukos, A. Travlos, H. S. Kwack, J. Guinard and D. Le Si Dang, "Zinc oxide nanorod based photonic devices: recent progress in growth, light emitting diodes and lasers " Nanotechnology 20, 332001 (2009)

[20] A. Djurisic, A. Ng, X. Chen,"ZnO nanostructures for optoelectronics: Material properties and device applications" Prog.Quant.Elect. 34 , 191-259 (2010)

[21] Jun Zhang, Lingdong Sun, Jialu Yin, Huilan Su, Chunsheng Liao, and Chunhua Yan "Control of ZnO Morphology via a Simple Solution Route" Chem. Mater.,14,4172-4177 (2002)

[22] Hui Zhang, Deren Yang, Dongshen Li, Xiangyang Ma, Shenzhong Li, and DuanlinQue "Controllable Growth of ZnO Microcrystals by a Capping-Molecule-Assisted Hydrothermal Process " Cryst. Growth Des., 5, 2 (2005)

[23] Yoshitake Masuda, Naoto Kinoshita, KunihitoKoumoto "Morphology control of ZnO crystalline particles in aqueous solution " Electrochim. Acta 53,171-174 (2007)

[24] Seungho Cho, Seung-Ho Jung, and Kun-Hong Lee "Morphology-Controlled Growth of ZnO Nanostructures Using Microwave Irradiation: from Basic to Complex Structures" J. Phys. Chem. C, 112, 12769-12776 (2008)

[25] S.L. Yang R.S. Gao B. Yang P.L. Niu R.H. Yu "Morphology-controlled growth of tetrapod ZnO nanostructures by direct arc discharge" Appl.Phys A , 99, 9-13 (2010)

[26] V. Khranovskyy and R. Yakimova "Morphology engineering of ZnO nanostructures", Physica. B, 407, 10, 1533-1537 (2012)

[27] Wenzhong Wang,Lijuan Wang, Lei Liu, Chen He, Jian Tan and Yujie Liang "Morphology-controlled synthesis and growth mechanism of ZnO nanostructures via the NaCl nonaqueous ionic liquid route" Cryst Eng Comm, 14, 4997-5004 (2012)

[28] Reynolds D C, Look D C and Jogai B "Optically pumped ultraviolet lasing from ZnO" Solid StateCommun.99,873-875 (1996)

[29] Anderson Janotti and Chris G Van de Walle "Fundamentals of zinc oxide as a semiconductor "Rep. Prog. Phys.,72, 126501 ,29 (2009)

[30] Florescu D I, Mourokh L G, Pollak F H, Look D C,Cantwell G and Li X "High spatial resolution thermal conductivity of bulk ZnO (0001)"J. Appl. Phys.91,890 (2002)

[31] Nanto H, Sokooshi H and Usuda T S "Smell sensor using zinc oxide thin films prepared by magnetron sputtering "Solid-State Sensors and Actuators 148948,596 - 599 (1991)

[32] Nomura K, Hiromichi O, Takagi A, Kamiya T, Hirano M and Hosono H "Room-temperature fabrication of transparent flexible thin-film transistors using amorphous oxide semiconductors " Nature, 432,488-492 (2004)

[33] Y. Tanaka, N. Sasaki, A. Ohmiya,“ Biosynthesis of plant pigments: anthocyanins, etalains and carotenoids ”, Plant Jl 54, 733-749 (2008).

[34] J. Fajer, “Chlorophyll chemistry before and after crystals of photosynthetic reaction centers” Photosynth. Res. 80 ,165-172 (2004).

[35] M. Mimuro, T. Katoh. “Carotenoids in photosynthesis: absorption, transfer and dissipation of light energy ”Pure & Appl. Chern. 63,123-130 (1991).

[36] F. C. Stintzing, R. Carle “Functional properties of anthocyanins and betalains in plants, food, and in human nutrition ”Trends Food sci Tech 15, 19-38 (2004).

[37] D.W. Lee, K.S. Gould “Why leaves turn red” Am. Sci. 90, 524 (2002)

[38] J. S. Clement, and T. J. Mabry, “Pigment evolution in the Caryophyllales : a systematic overview ”. Bot. Acta 109, 360-367 (1996).

[39] D. A. Moreno, C. Garc a-Viguera, J. I. Gil, A. Gil-Izquierdo “Betalains in the era of global agri-food science, technology and nutritional health ” Phytochem Rev. 7, 261-280(2008)

[40] Jackman, R.L. & Smith, J.L. Anthocyanins and betalains. In: Natural food colourants (edited by G.F. Hendry & J.D. Houghton).pp. 244309. London: Blackie Academic & Professional.(1996)

[41] Dongshe Zhang , Suzanne M. Laniera, Jonathan A. Downing ,Jason L. Avent , June Lumc, Jeanne L. McHalea “Betalain pigments for dye-sensitized solar cells” J. Photochem. Photobiol., A: Chem 195, 72-80(2008)

[42] Steglich, W., Strack, D., Betalains. In The Alkaloids, Chemistry and Pharmacology. Academic Press, London,1-62 (Brossi, A. (Ed.)) (1990)

[43] Gomez-Romero P, “Hybrid Organic-Inorganic Materials. In Search of Synergic Activity” Adv.Mat,13,163(2001)

[44] Yacaman m.J, Rendon L, Arenas J S. “Maya blue paint: an ancient nanostructured material” Science 273,5272,223(1996)

[45] Clement Sanchez, Beatriz Julian, Philippe Belleville and Michael Popall “Applications of hybrid organic-inorganic nanocomposites” J. Mater. Chem.,15, 3559-3592(2005)

[46] Shatabdiporel, shashisingh, S. Sreeharsha, D. Narayanarao, and T. P. Radhakrishnan “Nanoparticle-embedded polymer: in situ synthesis, Free-standing films with highly monodisperse Silver nanoparticles and optical limiting ” Chem. Mater. 17, 9-12(2005)

[47] Huan-Ming Xiongi, Zi Dong Wang, DaPengLiu, Jie-Sheng Chen, Yong-Gang Wang and Yong YaoXia " Bonding polyether onto ZnO nanoparticles: An effective method for preparing polymer nanocomposites with tunable Luminescence and stable conductivity "Adv.Fung. Mater.,15,1751-1756(2005).

[48] A.A Ishchenko "Photonics and molecular design of dye-doped polymers for modern light-sensitive materials "Pure Appl. Chem. 80 ,1525-1538(2008).

[49] J. Lee, D. Bhattacharyya, A.J. Easteal, J.B. Metson "Properties of nano-ZnO/poly(vinyl alcohol)/poly(ethylene oxide)composite thin films" Curr Appl. Phys. 8 , 42-47(2008)

[50] Cle'ment Sanchez, Philippe Belleville, Michael Popalld and Lionel Nicole "Applications of advanced hybrid organicinorganic nanomaterials: from laboratory to market Applications of advanced hybrid organicinorganic nanomaterials: from laboratory to market". Chem. Soc. Rev.,40, 696-753(2011)

[51] Robert W Boyd " Nonlinear Optics" third edition , Academic Press, Orlando, (2008).

[52] http://www.simphotek.com

[53] Yella, A.et al. "Porphyrin-Sensitized Solar Cells with Cobalt (II/III)-Based Redox Electrolyte Exceed 12 Percent Efficiency". Science, 334: 629-634 (2011)

[54] H. J. Snaith, S. M. Zakeeruddin, L. Schmidt-Mende, C. Klein and M. Gratzel, "Ion-Coordinating Sensitizer in Solid-State Hybrid Solar Cells "Angew. Chem., Int. Ed., 44,39, 6413-6417 (2005).

[55] X. Wang, J. Song and Z. L. Wang "Nanowire and nanobelt arrays of zinc oxide from synthesis to properties and to novel devices "J. Mater. Chem., 17, 711 (2007).

[56] B. R Saunders and M. L Turner, "Nanoparticle-polymer photovoltaic cells" Adv. Colloid Interface Sci., 138,1-23(2008)

[57] Md Ahsan Habib, Md Tusan Shahadat, Newaz Mohammed Bahadur, Iqbal M I Ismail and Abu Jafar Mahmood "Synthesis and characterization of ZnO-TiO_2 nanocomposites and their application as photocatalysts " Int. Nano Lett , 3,5(2013)

[58] Y. Chiba, A. Islam, Y. Watanabe, R. Komiya, N. Koide and L. Han "Dye-Sensitized Solar Cells with Conversion Efficiency of 11.1%" Jpn. J. Appl. Phys., 45,25, 638-640 (2006).

[59] J.J. Wu, G.R.Chen, H.H.Yang, C.H.Ku and J.Y.Lai, "Effects of dye adsorption on the electron transport properties in ZnO-nanowire dye-sensitized solar cells "Appl. Phys. Lett., 90, 213109 (2007).

[60] T. P. Chou, Q. Zhang and G. Cao "Effects of Dye Loading Conditions on the Energy Conversion Efficiency of ZnO and TiO_2 Dye-Sensitized Solar Cells"J. Phys. Chem. C, 111, 18804-18811 (2007).

[61] S. Sakthivel, B. Neppolian, M. V. Shankar, B. Arabindoo, M. Palanichamy and V. Murugesan "Solar photocatalytic degradation of azo dye: comparison of photocatalytic efficiency of ZnO and TiO_2 " Sol. Enery Mater. Sol. Cells,77, 65-82 (2003).

[62] K. Keis, C. Bauer, G. Boschloo, A. Hagfeldt, K. Westermark, H. Rensmo and H. Siegbahn "Nanostructured ZnO electrodes for dye-sensitized solar cell applications " J. Photochem. Photobiol., A, 148, 57-64 (2002).

[63] R. A. J. Janssen, J. C. Hummelen and N. S. Sariciftci, "Polymer-fullerene bulk heterojunction solar cells" Mater. Res. Bull., 30, 1, 33-36(2005)

[64] J. M. Kroon, N. J. Bakker, H. J. P. Smit, P. Liska, K. R. Thampi, P. Wang, S. M. Zakeeruddin, M. Gratẗzel, A. Hinsch, S. Hore, U. Wuŕfel, R. Sastrawan, J. R. Durrant, E. Palomares, H. Pettersson, T. Gruszecki, J. Walter, K. Skupien and G. E. Tulloch, "Nanocrystalline dye-sensitized solar cells having maximum performance "Prog. Photovoltaics, 15,1- 18 (2007).

[65] J. Boucle, P. Ravirajan and J. Nelson, "Hybrid polymermetal oxide thin films for photovoltaic applications "J. Mater. Chem., 17, 3141-3153(2007)

[66] http://www. Dye-Sensitized Solar Panel Research Drexel University

Chapter 2

Experimental Details : Tools for Material preparation and Characterization

2.1 Abstract:

The purpose of this chapter is to provide an overview of the experimental techniques that were employed to investigate the characterization in colloidal ZnO and films.The fundamental principles and details of experimental techniques are briefly explained in this section.The films discussed in this work were grown by tape casting method and by two step solution method. Various analyzing tools were used to investigate the electrical, optical, structural properties of the films.The surface morphology was characterized as well. In order to test the device performance, current-voltage measurement was used.

2.2 Synthesis of ZnO

ZnO in the form of low dimensional nanostructures are synthesized by a wide range of techniques, such as wet chemical methods [1-3], physical vapor deposition [4-16], metalorganic chemical vapor deposition (MOCVD) [17-23], molecular beam epitaxy (MBE) [24-27], pulsed laser deposition [28,29], sputtering [30-32],flux methods [33], electro-spinning [34-39], and top-down approaches by etching [40]. Among those techniques, physical vapor deposition and flux

methods usually require high temperature, and it is easy to incorporate catalysts or impurities into the ZnO nanostructures. Therefore, they are less likely to be able to integrate with flexible organic substrates for future foldable and portable electronics. MOCVD and MBE can give high quality ZnO nanowire arrays, but are usually limited by the poor sample uniformity, low product yield and restrictions in choices of substrate. Moreover, cost for the experiment were usually very high, and hence they are less widely adopted. Pulsed laser deposition, sputtering and top down approaches have less controllability and repeatability compared with other techniques. Electrospinning gives polycrystalline films. Comparatively, wet chemical methods are attractive for several reasons viz,

- They are low cost.
- Less hazardous .
- Capable of easy scaling up [41,42].
- Growth occurs at a relatively low temperature, compatible with flexible organic substrates.
- There is no need for the use of metal catalysts.
- It can be integrated with well-developed silicon technologies [43].
- There are a variety of parameters that can tuned to effectively control the morphologies and properties of the final products [44,45].

Wet chemical methods have been demonstrated as a very powerful and versatile technique for growing low dimensional nanostructure of ZnO. Various wet chemical techniques such as sol-gel, hydrothermal, solvothermal method, polyol, microwave heating, spray pyrolysis etc have been used for the synthesis of nanocrystalline powders.

The most accepted mechanism of one dimensional (1D) structures synthesis suggests a two-step process, i.e. nucleation and then successive growth of the particles. Nucleation is the initial formation of a crystal by the spontaneous clustering of the dissolved constituents and act as nucleation centers (also known as seeds) and their successive growth there after. Under most practical conditions seeds and their growth occur simultaneously and sometimes aggregation of nanoparticles and impurities (if present), is the additional nucleation center play a crucial role in the formation pathway. The experimental methods for the synthesis of low dimensional structures are explained in the following chapters.

2.3 Film preparation

The ZnO/Polyvinyl alcohol (PVA) composite were prepared by tape casting method (Plasto Mek, delta.0.2kW, 230V, 1 phase). PVA is a water soluble polymer. The colloid solutions of ZnO and PVA were mixed in different proportions using a magnetic stirrer. The mixture was carefully tape casted on the glass side. The films were then allowed to dry by keeping in an oven and so the free standing films of thickness in the range of 80-110μm were developed.

2.4 Characterization techniques

2.4.1 Scanning electron microscopy

Scanning electron microscopy (SEM) is a powerful tool to characterize a wide range of specimens at the nanometer to micrometer length scales. One of the most amazing aspects of SEM is the apparent ease with which SEM images of three-dimensional objects can be interpreted by any observer[46-48]. SEM analysis is said to be a non-destructive analysis as the bombardment of electrons do not cause any damage to the samples [46]. The surface imaging of ZnO samples are studied using scanning electron microscope (JSM6390, JEOL/EO, USA).

2.4.2 Transmission electron microscopy

Transmission Electron Microscopy (TEM) is another analytical tool to study crystal morphology, structure, crystal orientation, chemical composition, precipitates and dislocations, etc. TEMs strong cards are its high lateral spatial resolution and its capability to provide both image and diffraction information from a single sample[49,50].

2.4.3 X-Ray diffraction

X-ray diffraction is a powerful tool for determining the crystal properties of a sample including structure, quality and chemical composition of bulk materials, thin films and powders. As the physical properties of solid depend on atomic arrangements of materials, determination of the crystal structure is an essential part of the structural and chemical characterization of materials. X-ray patterns are used to establish the atomic arrangements of the materials as the lattice parameter, d (spacing between different planes) is of the order of x-ray wavelength. Further, X-ray diffraction method can be used to distinguish crystalline materials from amorphous materials. From X-ray diffraction pattern we can obtain the following information:-

- To judge formation of a particular material system.
- Unit cell structure, lattice parameters, and miller indices.
- Types of phases present in the material.
- Estimation of crystalline/amorphous content in the sample.
- Evaluation of the average crystalline size from the width of the peak in a particular phase pattern. Large crystal size gives rise to sharp peaks, while the peak width increases with decreasing crystal size.
- An analysis of structural distortion arising as a result of variation in d-spacing caused by the strain, thermal distortion.

The peaks in the XRD spectra directly relate to the spacing of the atomic planes through Braggs law,

$$2dsin(\Theta) = n\lambda \tag{2.1}$$

where d is the perpendicular spacing between the h, k, l lattice planes in a crystal (d-spacing), is the reflected angle of the X-ray , n is an integer equivalent to the order of the diffraction peak, and λ is the wavelength of the incident X-ray. For a hexagonal crystal structure, the relationship between d_{hkl} and the lattice parameters a and c plane is given by,

$$\frac{1}{d^2} = \frac{4}{3}(\frac{h^2 + hk + k^2}{a^2}) + \frac{l^2}{c^2} \tag{2.2}$$

where a and c are the lengths of the slides of the primitive cell and h, k, l are the Miller indices. The grain size can be estimated from the Scherrer equation

$$D = k\lambda/\beta cos(\theta) \tag{2.3}$$

Where D mean dimension of the crystallite size,λ is wave length of X-ray,k is a constant (=0.9) β is Full width half maximum (FWHM) in radian, θ is Bragg angle[51-53].

2.4.4 UV-VIS spectroscopy

The optical methods for characterizing samples in this thesis include optical absorption spectroscopy and photoluminescence. UV-VIS spectroscopy which utilizes the ultraviolet (UV) and visible (VIS) range of electromagnetic radiation. It is frequently referred to as electronic spectroscopy which implies that these relatively high energy photons disturb the electron distribution within the molecule.

The promotion of electron from the low energy state E_1(usually ground state) to higher energy E_2 is possible if the molecule absorbs the electromagnetic radiation of the corresponding wavelength $\lambda=\frac{ch}{(E_2-E_1)}$(c is the speed of light and h is the Planck constant).The electron at the higher energy is then said to be excited. Excited states have very small life times (femtoseconds to microseconds), because the higher energy state is unstable and the extra energy is lost through the relaxation processes such as emission of light or the relaxation to some other states. The typical energy difference between the ground and the first excited sates of many molecules corresponds to electromagnetic waves of the ultra-violet (UV) and visible regions of the electromagnetic spectrum.

When light travels through the sample of thickness Δx, its intensity diminishes by an amount proportional to the initial intensity I_0 and the thickness of the slice

$$I_1 = I_0 - \alpha I_0 \Delta x \tag{2.4}$$

This can be rewritten as

$$\frac{I_1 - I_0}{\Delta x} = -\alpha I_0 \tag{2.5}$$

Or

$$\frac{dI}{dx} = -\alpha I_0 \tag{2.6}$$

which is the differential equation with solution of

$$I(x) = I_0 exp[-\alpha x] \quad (Lambert - Beerlaw) \tag{2.7}$$

The UV-VIS spectrometer usually measures the absorbance

$$A(\lambda) = -log\frac{I}{I_0} \tag{2.8}$$

An absorption spectrum show the wavelength at which the sample can absorb light and provides information about the electronic states of the molecule, hence absorption spectroscopy carried out in UV-visible spectral region is sometimes called electronic spectroscopy. It is employed as an analytical chemistry tool to determine the presence of a particular substance in a sample and, in many cases, to quantify the amount of the substance present. The schematic representation of transition probabilities of a molecule is shown in figure 2.1[54].

The main transitions between the electronic states are:

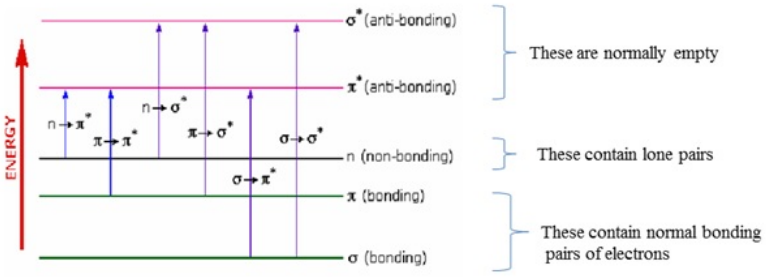

Figure 2.1: The transition probabilities of a molecule

- n, $\sigma \rightarrow \sigma^*$transitions : Saturated compounds with substituents having lone-pairs such as water, ammonia, hydrogen disulphide may only display σ- σ^* and n-σ^* transitions.
- $\pi \rightarrow \pi^*$transitions : For molecules that possess bonds like alkenes, alkynes, aromatics, acryl compounds or nitriles, light can promote electrons from a $\pi \rightarrow \pi^*$(a bonding molecular orbital to a anti-bonding molecular orbital) which is usually strong (high extinction coefficient).
- n$\rightarrow \pi^*$transitions : Even lone pairs that exist on oxygen and nitrogen atoms may be stimulated from their nonbonding molecular orbital (n) to a anti-bonding molecular orbital within a molecule. This is called an n$\rightarrow \pi^*$transition and requires less energy compared to a $\pi \rightarrow \pi^*$transition within the same chromophore. However, this transition has less probability.

2.4.5 Photoluminescence

Photoluminescence (PL) is an important tool for the characterization of surfaces and is the spontaneous emission of light from a material under optical excitation. PL is simple, versatile, and nondestructive. When light of sufficient energy is incident on a sample material, photons are absorbed and electronic excitations are created. Finally, these excitations relax and the electrons return to the ground state. If it is a radiative relaxation, the emitted light is called PL .This light can be collected and examined to yield a wealth of information about the photo excited material. The PL spectrum provides the transition energies, which can be used to determine electronic energy levels and the PL intensity gives a measure of the relative rates of radiative and non-radiative recombination. The PL spectrum depends on the nature of the optical excitation. The PL signal often depends on the density of photo excited electrons.

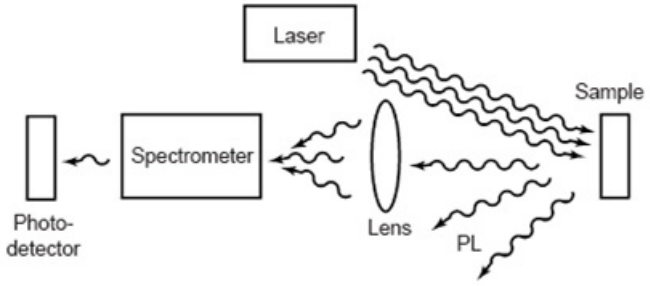

Figure 2.2: Typical experimental set-up for PL measurements

A typical PL set-up is shown in figure 2.2.

2.4.6 Nonlinear spectroscopy

In nonlinear spectroscopy multiple light-matter interactions can be used to correlate different spectral features and dissect complex spectra. The linear spectroscopy such as absorption or emission spectroscopy involve a weak light-matter interaction with one primary incident radiation field, and are typically presented through a single frequency axis and can be treated as a linear response between the incident light and the matter. The ambiguities that arise when interpreting linear spectroscopy are

- One cannot resolve couplings or spectral correlations directly.
- Linear spectra cannot uniquely interpret line broadening mechanism, or decompose heterogeneous behavior in the sample.
- It has little ability to interpret dynamics and relaxation. Nonlinear spectroscopy provides a way of resolving these scenarios as it uses multiple indepenent incident light fields or time-ordering in order to probe correlations between different spectral features.

2.4.7 Z scan technique

Nonlinear absorption can be experimentally measured by several techniques, such as two-photon excited fluorescence, nonlinear transmission and Z-scan experiment. In this section, we discuss the optical method to determine the nonlinear refraction and nonlinear absorption by Z-scan technique.

The nonlinear medium is scanned along the z-axis in the back focal region of an external lens. The whole transmittance (open aperture, OA) and the far-field on-axis transmittance (closed aperture, CA) are monitored as a function of the scan distance z. The open aperture Z-scan transmittance is insensitive to the nonlinear refraction and solely determines the nonlinear absorption, whilst the closed aperture Z-scan transmittance is coupled with both of the nonlinear effects i.e. nonlinear absorption and refraction. Actually, both the nonlinear effects are often present simultaneously in nonlinear optical materials. Nonlinear absorption is inevitably present for resonant absorption wavelength ranges as well as for transparent regions owing to multi-photon absorption when the laser beam intensity is sufficiently high. For simplicity, we only concentrate on TPA.

The interaction of intense laser pulse with the matter can induce various nonlinear effects and phenomena. The Z-scan technique devised by Sheik-Bahae et al [55] has been an extensively employed yet effective and popular technique for characterizing the optical nonlinearity of materials and outstands due to its efficacy and simplicity in determining the nonlinear optical parameters. This technique is used to measure the non-linear index n_2 i.e. the strength of Kerr nonlinearity and the non-linear absorption coefficient via the "closed" and "open" aperture methods respectively. The materials with different absorption processes such as saturable absorption (SA), reverse saturable absorption (RSA), two photon absorption (TPA) and multi photon absorption(MPA) are the promising candidates in the different applications of science and technology. For example, SA materials (the transmittance increases with the increase of optical intensity) have been used in the lasers as Q-switching elements.TPA, MPA and RSA materials (their transmittances decreases with the increase of optical intensity) have been used in two-photon microscopy and optical limiters. Therefore, it is necessary to identify their nonlinear absorption effects, and to determine their nonlinear absorption parameters, such as the saturable intensity (I_s) for saturable absorber, the TPA coefficient (β) for two-photon absorbing material. The schematic representation of Z-scan set up is shown in figure 2.3 .

In the OA Z-scan, the normalized transmittance in the far field is measured while the sample is scanned through the focal plane of a focused Gaussian beam [55]. The typical OA Z-scan curves is shown in figure 2.4. The nonlinear absorption and refraction were measured from the normalized energy transmission using Z-scan without an aperture and with an aperture respectively. If transmitted light is measured through an aperture placed in the far field with respect to focal region, the technique is called CA Z-scan.

Here, we present the results of the propagation of a Gaussian beam that is

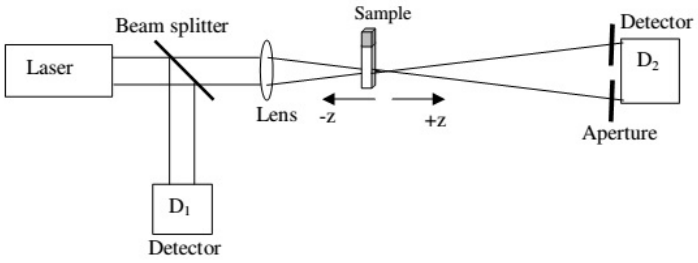

Figure 2.3: Schematic representation of experimental set up of Z-scan technique

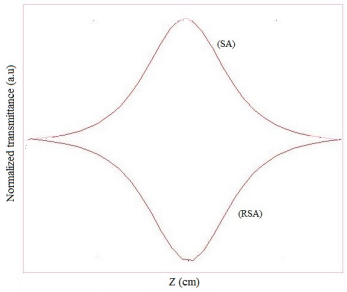

Figure 2.4: Typical OA Z-scan curves

initially focused by an external lens and is then incident on a slice of a cubically nonlinear Kerr medium. The propagating Gaussian beam induces its own lens, which is positive for a material having a positive n_2. Note that if the position of the induced lens is at the back focal plane of the external lens, the former does not affect the propagation of the beam behind the material and the situation is thus the same as the propagation of the externally focused Gaussian beam in a linear diffraction limited environment. However, if the lens-sample separation is less than the focal length of the external lens, the beam in the far field is wider than the linear diffraction-limited case. On the other hand, if the lens-sample separation is larger than the focal length, the beam width is smaller. This is the basis of the Z-scan measurement [56,57]. For a material with a positive n_2, the scanning of the sample through the back focal plane of the external lens starting from a position to the left of the focus yields far-field profiles that are initially larger and eventually smaller than the width in the linear diffraction-limited case. The opposite is true for materials with a negative n_2 [58].The curves for closed Z-scan in the case of $n_2>0$ and $n_2<0$ shows

opposite effects as depicted in figure 2.5.

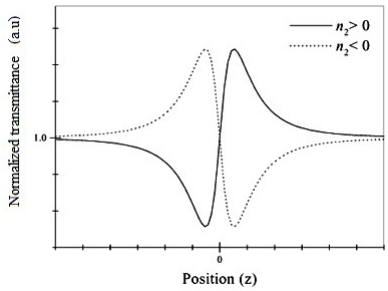

Figure 2.5: Z-scan theoretical curves of the transmittance as a function z

Consider the fundamental Gaussian electric field (TEM_{00}mode) of waist radius w_0 travelling in the z direction as

$$E(r,z) = E_0 \frac{\omega_0}{\omega(z)} exp[-(\frac{r^2}{\omega^2} + i\frac{kr^2}{2R})]exp[-i\psi(z)] = E(0,z)exp[-i\frac{kr^2}{2q}] \quad (2.9)$$

where E_0 is the amplitude of the electric field at the focus z=0, $\omega(z) = \omega_0$ $(1+ (z/z_0)^2)^{1/2}$ is the beam radius at z, w_0 is the waist radius at the focus. R(z)=z $(1+ (z/z_0)^2)$ is the radius of curvature of the wave at z, $z_0 = k\omega_0^2/2$ is the Rayleigh diffraction length of the beam $k=2\pi/\lambda$ is the wave number and is the wavelength of the laser beam [59].

Here, q denotes the complex beam parameter that covers all the information needed to specify its characteristics in the beam propagation and is defined by $1/q = 1/R - i\lambda/\pi\omega^2$. For a Kerr medium with TPA process the nonlinear refractive index and the nonlinear absorption coefficient can be written as [55,60].

$$n = n_0 + n_2 I \quad (2.10)$$

$$\alpha = \alpha_0 + \beta I \quad (2.11)$$

where n_0 and n_2 are linear and nonlinear refractive indices respectively.

$$I(r,z) = \epsilon_0 C n_0 |E(r,z)|^2/2 \quad (2.12)$$

denotes the incident Gaussian laser beam intensity , α_0 is the linear absorption coefficient and β is the two photon absorption coefficient. Solving the wave

equation that describes the propagation of a Gaussian laser beam through the medium and neglecting the transverse effect, the intensity variation for two photon absorption and the nonlinear phase shift of the beam at the exit surface of the sample are given by, [55]

$$I_e(r,z) = \frac{I(r,z)exp[-\alpha_0 L]}{1+q(r,z)} \tag{2.13}$$

$$\Delta\Phi(r,z) = \frac{kn_2}{\beta} ln[1+q(r,z)] \tag{2.14}$$

where I(r,z)=I_0exp[-$\frac{2r^2}{\omega^2}$] $\frac{\omega_0^2}{\omega^2}$ is the incident beam intensity I_0 is the on-axis intensity at the focus. q(r,z)=βI(r,z) L_{eff} is the nonlinear absorbance of the medium, L_{eff}=(1-exp[-α_0 L])/α_0 is the effective length of the sample and L is the thickness of the sample.By combining equations (2.13) and (2.14) we obtain the complex electric field at the exit surface of the sample:

$$E_e(r,z) = [\frac{I(r,z)exp[-\alpha_0 L]}{1+q(r,z)}]^{\frac{1}{2}} exp[i\Delta\phi] \tag{2.15}$$

$$= E(r,z)exp[i\Delta\phi(1+i\frac{\beta}{2kn_2})]exp[-\alpha_0 L/2] \tag{2.16}$$

According to the aberration-free approximation of a Gaussian beam, which requires the Gaussian beam profile be approximated as being parabolic, by expanding the exponential in the intensity and retaining only the quadratic term, the nonlinear phase shift, Eq. (2.14) can be approximated as:

$$\Delta\Phi(r,z) \approx -\frac{kn_2}{\beta}\frac{q_0}{1+q_0}\frac{2r^2}{\omega^2} \tag{2.17}$$

where q_0=q(0,z)=q_{00}/(1+ (z/z_0)^2) and q_{00}=β I_0 L_{eff} It is noted that eq(2.17) is always valid whether |q|$\geq$1 or not. By substituting eq.(2.17) into eq.(2.16) and employing the complex beam parameter formulation [60] we have finally obtain the closed aperture Z-scan transmittance of the far-field at the aperture plane, including both of the effects of nonlinear absorption and nonlinear refraction as follows:

$$T_{close}(z) = \frac{1}{1-\frac{4(z/z_0-\eta)\Delta\phi_0}{(1+(z/z_0)^2)^2(1+q_0)}+\frac{4(1+\eta^2)\Delta\phi^2}{(1+(z/z_0)^2)^2(1+q_0)^2}} \tag{2.18}$$

$\Delta\phi_0$=kn_2 I_0 L_{eff} is the on-axis nonlinear phase at focus and η=q_{00}/(2$\Delta\phi_0$) =β/(2kn_2) is the ratio of the imaginary part to the real part of the complex nonlinearity

When the aperture is removed, however, the Z-scan is irrelevant to beam distortion caused by nonlinear refraction and is only a function of the nonlinear absorption, as mentioned above. Hence, the nonlinear absorption coefficient can readily be determined from the open aperture Z-scan transmittance. By spatially integrating eq.(2.13) at z over all r($0 \leq r \leq \infty$) without having to include the free space propagation process, we have the CW open aperture Z-scan transmittance as:

$$T_{open}(z) = \frac{ln[1 + q_0(z)]}{q_0(z)} \tag{2.19}$$

If $q_0 < 1$ equation can be simplified as

$$T(z, S = 1) = \sum_{m=0}^{\infty} \frac{[-q_0(z, 0)]^m}{(m+1)^{(\frac{3}{2})}} \tag{2.20}$$

where m is an integer. The imaginary part of third order susceptibility (Im χ^3) determines the strength of the nonlinear absorption.

$$Im(\chi^3) = \frac{n_0^2 c^2 \beta}{240\pi^2\omega}(esu) \tag{2.21}$$

For a cubic nonlinearity, the peak and valley of the Z-scan transmittance can be calculated by solving the equation

$$\frac{dT(z, \Delta\phi_0)}{dz} = 0 \tag{2.22}$$

Solution to this equation (2.21) yields the peak valley separation as

$$\Delta z_{p-v} = 1.7 z_0 \tag{2.23}$$

Then the peak valley transmittance change is

$$\Delta T_{p-v} = 0.406\Delta\phi_0 \tag{2.24}$$

The n_2 is related to Re(χ^3) by the relation

$$Re(\chi^3) = \frac{n_0 n_2}{3\pi}(e.s.u) \tag{2.25}$$

From the real and imaginary part of χ^3 , the modulus of third order nonlinear susceptibility can be found out.

$$|\chi^3| = \sqrt{[Re(\chi^3)]^2 + [Im(\chi^3)]^2} \tag{2.26}$$

The magnitude of χ^3 is significantly affected by the molecular orientation and it determines the strength of nonlinearity of the material.

The Z-scan method has become a standard tool for measurement of the nonlinear absorption and nonlinear refractive index coefficients of various NLO materials because of its simplicity, its high sensitivity, and its indication of the sign and type of nonlinearity immediately after the measurement is finished [61]. Moreover,the same part of the sample is investigated during the entire experiment ,thus the samples imperfection induced linear and nonlinear distortions in the Z-scan curve are decreased significantly. However, there are some disadvantages associated with this method. For example, the Z-scan curve will be distorted by the misalignment, sample imperfections, and intensity fluctuation during the measurement[62] and the thickness non uniformity of the sample leads to error in the calculation of the nonlinear refractive index coefficient from the difference between the peak and valley transmittances. The curved surface of the nonlinear sample also distorts the Z-scan curve significantly.

2.5 DSSC fabrication

2.5.1 Materials and reagents for the device fabrication

Indium tin oxide (ITO, In_2O_3- SnO_2) thin films are used as transparent conducting oxides (TCOs) in flat panel displays, optoelectronic devices, and solar cells due to its low resistivity and high transmittance [63]. Highly indium-doped TCO films deposited on glass plates were purchased from sigma Aldrich (ITO 8-12 Ω /sq) and were first cleaned in a detergent solution using an ultrasonic bath for 10 min, rinsed with water and ethanol, and then dried. The photo anodes were prepared by depositing the synthesized structures on the ITO conducting glass: two edges of the ITO glass plate were covered with a layer of adhesive tape to control the thickness of the film and to mask electric contact strips. Film thickness was measured using a digimatic micrometer and was found to be 33 μm. The nanostructure paste was then spread uniformly on the substrate by sliding a glass rod along the tape spacer. The as-prepared samples were then subjected to an annealing process at 300^0C for 30 min to obtain good porosity.

The photo-electrodes were impregnated with fresh juice from red beets without further purification. Dye adsorption was carried out for 24 h at room temperature, after which the photo electrodes were removed from the dye solution and rinsed several times with water in order to remove weakly adsorbed dye molecules and finally dried in a hot plate. The platinized ITO glass was used as the counter electrode. For this, ITO conducting glass was dipped into a 10 mM chloroplatinic acid hexahydrate solution in ethanol and then annealed at 450^0C for 15 min. The counter electrode was then placed on top of the photo electrode, and filled with electrolyte by using capillary force through the sides.

Binder clips were used to hold the electrodes together. The photograph of one of the fabricated dye sensitized film and DSSC is shown in figure 2.6.

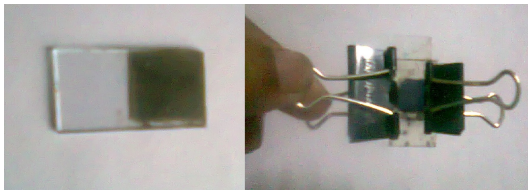

Figure 2.6: Photograph of one of the fabricated dye sensitized thin film and DSSC.

2.5.2 Basic parameters to evaluate the performance of DSSC

The performance of DSSCs is usually evaluated by the following four parameters

- Open circuit photovoltage (V_{oc}) is the cell voltage measured when the current within the cell is zero
- Short circuit photocurrent (I_{sc}) the cell photocurrent measured at zero voltage. In general, it is presented in the form of the short circuit current density (J_{sc})
- Fill factor (FF) The degree of the squared shape of the J-V curve is given by the fill factor (FF), which measures the ideal nature of the device and is defined as the ratio of the maximum power output per unit area to the product of V_{oc} and J_{sc}

$$FF = \frac{J_{maxpower} V_{maxpower}}{J_{sc} V_{oc}} \tag{2.27}$$

- Energy conversion efficiency (η)

  The solar to electric power conversion efficiency η is given by the ratio of the maximum extractable power to the incident solar power (P_{in}) given by equation

$$\eta = \frac{P_{max}}{P_{in}} = \frac{J_{max} V_{max}}{P_{in}} = \frac{J_{sc} V_{oc} FF}{P_{in}} \tag{2.28}$$

  where P_{in} is the incident power, P_{out} is the output power, FF is the fill factor, η is the efficiency, J_{sc} is the short circuit current density,

and V_{oc} is the open circuit voltage. As η is a function of I_{sc},V_{oc} and FF,enhancement of DSSC performance is achieved by optimization of these parameters and is also depend on the incident irradiation power .

2.5.3 Charcterization techniques of DSSCs

The basic characterization techniques of DSSCs are described as follows

- Photocurrent-photovoltage (I-V) measurement ,A typical I-V curve is shown in figure 2.7

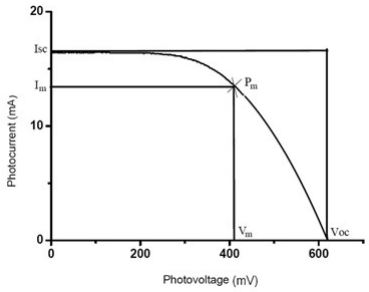

Figure 2.7: Characteristc I-V curve of a DSSC

- Incident photon to electron conversion efficiency (IPCE) measurement

  The sensitivity of a DSSC varies with the wavelength of incident radiation. IPCE measures the ratio of the number of electrons produced in the external circuit to the number of photons incident on the cell and is calculated using the formula [64]

$$IPCE(\%) = \frac{n_{electrons}(\lambda)}{n_{photons}(\lambda)} = \frac{I(\lambda)/e}{P_{in}(\lambda)/h\nu} = \frac{I(\lambda)}{P_{in}(\lambda)}.\frac{hc}{e\lambda} = \frac{1240 J_{sc}}{\lambda P_{in}} 100 \tag{2.29}$$

  Where I(λ) is the photocurrent given by the cell under monochromatic illumination at wavelength λ(nm) ,P_{in} is the input optical power at wavelength λ, e is the elementary charge ,h is the plank constant ,ν is the frequency of light ,c is the speed of light in vacuum.

Detailed experimental and working principles of DSSC are described in chapter 7.

2.6 References

[1] Laudise R. A and Ballman A. A, "Hydrothermal synthesis of zinc oxide and zinc sulfide". J. Phys. Chem.64, 688-691 (1960)

[2] Verges M. A, Mifsud A and Serna C. J, "Formation of rod- like zinc-oxide microcrystals in homogeneous solutions". J. Chem. Soc., Faraday Trans.,86, 959-963 (1990).

[3] Vayssieres L, Keis K, Lindquist S. E and Hagfeldt A, "Purpose-built anisotropic metal oxide material: 3D highly oriented microrod array of ZnO". J. Phys. Chem. B, 105, 3350-3352 (2001).

[4] Pan Z. W, Dai Z. R and Wang Z. L, "Nanobelts of semiconducting oxides ". Science, 291, 1947-1949 (2001).

[5] Huang M. H,Wu Y. Y, Feick H, Tran N, Weber E and Yang P. D, "Catalytic growth of zinc oxide nanowires by vapor transport ". Adv. Mater., 13, 113-116 (2001).

[6] Yao B. D, Chan Y. F and Wang N, "Formation of ZnO nanostructures by a simple way of thermal evaporation" Appl. Phys. Lett., 81, 757-759 (2002).

[7] Seung Chul Lyu , Ye Zhang and Cheol Jin Lee "Low-Temperature Growth of ZnO Nanowire Array by a Simple Physical Vapor-Deposition Method" Chem. Mater., 15, 17, 3294-3299 (2003)

[8] Y. C. Kong, D. P. Yu, B. Zhang, W. Fang and S. Q. Feng "Ultraviolet-emitting ZnO nanowires synthesized by a physical vapor deposition approach" Appl. Phys. Lett., 78, 407-409 (2001)

[9] Huang M. H, Mao, S, Feick H, Yan H. Q, Wu Y. Y, Kind H, Weber E, Russo R and Yang P, "Room-temperature ultraviolet nanowire nanolasers" Science, 292, 1897-1899 (2001).

[10] Huang M. H, Wu Y. Y, Feick H, Tran N, Weber E and Yang P. D, "Catalytic Growth of Zinc Oxide Nanowires by Vapor Transport " Adv. Mater.,13, 113-116 (2001).

[11] Liu R, Vertegel A. A, Bohannan E. W, Sorenson T. A and Switzer J. A, "Epitaxial electrodeposition of zinc oxide nanopillars on single-crystal gold" Chem. Mater., 13, 508,(2001).

[12] Kong Y. C, Yu D. P, Zhang B, Fang W and Feng S. Q, "Ultraviolet-emitting ZnO nanowires synthesized by a physical vapor deposition approach "Appl.Phys. Lett., 78, 4, 407-409(2001)

[13] J. Q. Hu, Quan Li, N. B. Wong, C. S. Lee and S. T. Lee, "Synthesis of Uniform Hexagonal Prismatic ZnO Whiskers", Chem. Mater. 14, 1216-1219 (2002).

[14] Wu J. J and Liu S. C "Low-temperature growth of well-aligned ZnO nanorods by chemical vapor deposition" Adv. Mater., 14, 3, 215 (2002).

[15] Park W. I, Kim D. H, Jung S.W and Yi G.C, "Metalorganic vapor-phase epitaxial growth of vertically well-aligned ZnO nanorods" Appl. Phys. Lett., 80, 4232-4234 (2002).

[16] Lisheng Wang and Xiaozhong Zhanga, Songqing Zhao, Guoyuan Zhou, Yueliang Zhou and Junjie Qi "Synthesis of well-aligned ZnO nanowires by simple physical vapor deposition on c-oriented ZnO thin films without catalysts or additives" Appl. Phys. Lett. 86, 024108 (2005)

[17] Park W. I, Yi G. C, Kim M. Y and Pennycook S. J, "ZnO Nanoneedles grown vertically on Si substrates by non-catalytic vapor-phase epitaxy". Adv. Mater., 14, 1841-1843 (2002).

[18] Park W. I, Kim D. H, Jung S. W and Yi G. C, "Metal organic vapor-phase epitaxial growth of vertically well-aligned ZnO nanorods". Appl. Phys. Lett., 80, 4232-4234 (2002).

[19] Yuan H and Zhang Y, "Preparation of well-aligned ZnO whiskers on glass substrate by atmospheric MOCVD". J. Cryst. Growth, 263, 119-124 (2004).

[20] W.I. Park,G.C. Yi,M. Kim and S.J. Pennycook "ZnO Nanoneedles Grown Vertically on Si Substrates by Non-Catalytic Vapor-Phase Epitaxy" Adv. Mater.,14, 24,1841-1843 (2002)

[21] Naoki Nishimoto , Obuliraj Senthilkumar, Takahiro Yamamae, Kasilingam Senthilkumar and Yasuhisa Fujita Growth of ZnO Thin Films by Using MOCVD with a High-Speed Rotating Disk Reactor J. Korean Phy. Soc., 53, 5,2951-2954 (2008)

[22] S. Nicolay, S. Fay and C. Ballif "Growth Model of MOCVD Polycrystalline ZnO" Cryst. Growth Des., 9, 4957-4962 (2009)

[23] Sriram Muthukumar, Haifeng Sheng, Jian and Zhong Nuri William Emanetoglu "Selective MOCVD Growth of ZnO Nanotips" IEEE Transactions on Nanotechnology, 2,1,50-54 (2003)

[24] Heo Y. W, Varadarajan V, Kaufman M, Kim K, Norton D.P, Ren F and Fleming P. H, "Site-specific growth of ZnO nanorods using catalysis-driven molecular-beam epitaxy". Appl. Phys. Lett., 81, 3046-3048 (2002).

[25] L.C. Tien, D.P. Norton , S.J. Pearton,, Hung-Ta Wang and F. Ren "Nucleation control for ZnO nanorods grown by catalyst-driven molecular beam epitaxy" Appl. Surf. Sci., 253 ,4620-4625 (2007)

[26] Y. W. Heo, D. P. Norton and S. J. Pearton "Origin of green luminescence in ZnO thin film grown by molecular-beam epitaxy" J. Appl. Phys. 98, 073502 (2005)

[27] Yefan Chen, D. M. Bagnall, Hang-jun Koh, Ki-tae Park, Kenji Hiraga, Ziqiang Zhu and Takafumi Yao "Plasma assisted molecular beam epitaxy of ZnO on c-plane sapphire: Growth and characterization" J. Appl. Phys. 84, 3912 (1998)

[28] Sun Y, Fuge G. M and Ashfold M. N. R, "Growth of aligned ZnO nanorod arrays by catalyst-free pulsed laser deposition methods"' Chem. Phys. Lett., 396, 21-26 (2004).

[29] Hong J. I, Bae J, Wang Z. L and Snyder R. L, "Room temperature, texture-controlled growth of ZnO thin films and their application for growing aligned ZnO nanowire arrays" Nanotechnology, 20, 085609,(2009).

[30] Chiou W. T, Wu W. Y and Ting J. M, "Growth of single crystal ZnO nanowires using sputter deposition". Diam. Relat. Mater., 12, 1841-1844,(2003).

[31] N. Koshizaki and T. Oyama, "Sensing characteristics of ZnO-based NOx sensor" Sens. Actuators, B 66, 119-121(2000)

[32] Liao L, Li J. C, Wang D. F, Liu C, Liu C. S, Fu Q and Fa L. X "Field emission property improvement of ZnO nanowires coated with amorphous carbon and carbon nitride films" Nanotechnology. 16, 985 (2005)

[33] Xu C. K, Xu G. D, Liu Y. K and Wang G. H,"A simple and novel route for the preparation of ZnO nanorods" Solid. State. Commun., 122, 175-179(2002)

[34] Lin D. D, Pan W and Wu H, "Morphological control of centimeter long aluminum-doped zinc oxide nanofibers prepared by Electrospinning". J. Am. Ceram. Soc., 90, 71-76 (2007).

[35] Lin D, Wu H and Pan W, "Photo switches and memories assembled by electrospinning aluminum-doped zinc oxide single nanowires". Adv. Mater., 19, 3968-3972 (2007).

[36] Sui X. M, Shao C. L and Liu Y. C, "White-light emission of polyvinyl alcohol/ZnO hybrid nanofibers prepared by Electrospinning". Appl. Phys. Lett., 87, 113115 (2005).

[37] Dandan Lin, Hui Wu, Rui Zhang and Wei Pan," Enhanced Photocatalysis of Electrospun Ag-ZnO Heterostructured Nanofibers" Chem. Mater., 21, 3479-3484 (2009)

[38] Lin D. D, Wu H and Pan W, "Photoswitches and Memories Assembled by Electrospinning Aluminum-Doped Zinc Oxide Single Nanowires " Adv. Mater., 19, 22, 3968-3972 (2007)

[39] Haiqing Liu, Jinxia Yang, Jianhe Liang, Yingxing Huang, and Chunyi Tang "ZnO Nanofiber and Nanoparticle Synthesized Through Electrospinning and Their Photocatalytic Activity Under Visible Light" J. Am. Ceram. Soc., 91, 4, 1287-1291 (2008)

[40] Wu J. J, Wen H. I, Tseng C. H and Liu S. C, "Well-aligned ZnO nanorods via hydrogen treatment of ZnO films". Adv. Funct. Mater., 14, 806-810 (2004).

[41] Zhang H, Yang D. R, Ma X. Y, Du N, Wu J. B and Que D. L, "Straight and thin ZnO nanorods: Hectogram-scale synthesis at low temperature and cathodoluminescence". J. Phys. Chem. B, 110, 827-830(2006)

[42] Chang P. C and Lu J. G, "ZnO nanowire field-effect transistors". IEEE T. Electron Dev., 55, 2977-2987 (2008)

[43] Xu S, Wei Y, Kirkham M, Liu J, Mai W, Davidovic D, Snyder R. L and Wang Z. L, "Patterned growth of vertically aligned ZnO nanowire arrays on inorganic substrates at low temperature without catalyst". J. Am. Chem. Soc., 130, 14958-14959(2008)

[44] Govender K, Boyle D. S, Kenway P. B and O'Brien P, " Understanding the factors that govern the deposition and morphology of thin films of ZnO from aqueous solution". J.Mater. Chem., 14, 2575-2591 (2004)

[45] Xu S, Adiga N, Ba S, Dasgupta T, Wu C. F. J and Wang Z. L, "Optimizing and improving the growth quality of ZnO nanowire arrays guided by statistical design of experiments". ACS Nano , 3, 1803-1812 (2009).

[46] `http://serc.carleton.edu/researcheducation/geochemsheets/SEM.html`

[47] `http://serc.carleton.edu/researcheducation/geochemsheets/SXD.html`

[48] `http://rsic.puchd.ac.in/em.html`

[49] `http://en.wikipedia.org/wiki/transmissionelectronmicroscope`

[50] `http://en.wikipedia.org/wiki/highresolutionTEM`

[51] B. D. Cullity and S. R. Stock, Elements of X-ray diffraction, Prentice Hall, New Jersey, 3 edition (2001).

[52] C. Kittel, Introduction to Solid State Physics, Wiely Eastern Limtd (1996).

[53] Siemens, Munchen, Germany, XRD analysis Manual.

[54] http\WWW.UVSspectroscopy HS 13.com

[55] Sheik-Bahae M, Said A. A, Wei T. H, Hagan D. J and Stryland E. V. "Sensitive measurement of optical nonlinearities using a single beam". IEEE J. Quantum Electron, 26, 4,760-769 (1990)

[56] M Sheik-bahae, A A Said, and E W. Van Stryland, "High-sensitivity, single-beam n_2 measurements ", Opt. Lett., 14955-957(1989).

[57] Banerjee P.P and Misra R.M "Propagation of profiled optical beams through kerr media " Microw.Opt.Technol.Lett.4,11,471 -475 (1991)

[58] Partha I Banerjee, "Nonlinear Optics Theory, Numerical Modeling, and Applications" , 270 Madison Avenue, New York 10016 (2004)

[59] Georgiy V.T kachenko, "New developments in liquid crystals" , 234, I-Tech, Vienna, Austria, (2009)

[60] Kwak C. H, Lee Y. L and Kim S. G"Analysis of asymmetric Z-scan measurement for large optical nonlinearities in an amorphous As_2S_3 thin film" . J. Opt. Soc. Am. B, 16,4, 600-604 (1999)

[61] H.Nasibov and I.Mamedbeili "Low power continuous wave laser induced optical nonlinearities in Saffron (Crocus sativus L.)" Laser Phys. 20, 12,2029-2035 (2010)

[62] Qiguang Yang, JaeTae Seo, Santiel Creekmore, Doyle Temple, Andy Mott, Namkung Min, KiPung Yoo, Sun Young Kim and Sungsoo Jung "Distortions in Z-scan spectroscopy" Appl. Phys. Lett. 82, 19 (2003)

[63] SeonMiKon, Yubin Xiao, Kyung Ha Kim, Wan In Lee and Chee Won Chung "Performance improvement of dye-sensitized solar cells by surface patterning of fluorine-doped tin oxide transparent electrodes"Thin Solid Films 519,3173-3176 (2011)

[64] Zhang D, Lanier S M, Downing J A, Avent J L, Lum J and McHale J L. "Betalain pigments for dye-sensitized solar cells" J. Photochem. Photobiol. A: Chem ,195,72-80 (2008)

Chapter 3

Synthesis and characterization of ZnO at nano/micro scales

3.1 Abstract:

Intense studies on ZnO low dimensional structures have been carried out extensively over the last decade not only for their remarkable chemical and physical properties, but also for their current and future diverse technological applications. This chapter gives a comprehensive overview of the progress that has been made in the context of ZnO low dimensional structures via wet chemical method. We will discuss several types of experiments under different conditions such as time, precursor concentration and temperature to rationally get control over the morphologies of the nanostructures. Morphological control techniques in this system will contribute to the development of the future oxide devices. Their linear optical properties are also studied.

Results of this chapter are published in

- Aparna Thankappan, Misha Hari, S. Mathew, Santhi Ani Joseph, Erni Rolf, Debajeet Bora, Artur Braun, V.P.N. Nampoori ,"Synthesis of monocrystalline zinc oxide microrods by wet chemical method for light confinement applications" Physica E 44 , 2118-2123 (2012)
- Aparna Thankappan, Sheenu Thomas, and V. P. N. Nampoori, "Tuning the face orientation of ZnO nano/microcrystals by a wet chemical method" Chinese Optics Letters 11, 10,1671-7694,(2013)

3.2 Introduction

Control over the morphology and structure of nanomaterials is essential for the development of future devices [1]. During the past few years, much effort has been invested in controlling morphology of the nanocrystals to fine tune its properties for potential applications, as the size, orientation and morphology, aspect ratio and even crystalline density can significantly influence various properties. Crystallization and morphological control of oxide particles, tubes, fibers etc. have been developed based on scientific knowledge of the solution chemistry of inorganic materials [2]. The development of morphology controlled synthesis of nanostructures remains a significant challenge [3] to answer the demand for exploring the potentials of ZnO.

As indicated earlier, among many promising optoelectronic semiconductors, ZnO is a key functional material exhibiting ultraviolet photoluminescence emission, transparent conductivity along with semiconducting, magnetic and piezoelectric properties. It has been attracting attention in both fundamental research and practical studies. Another notable feature is that ZnO is biocompatible and exhibits excellent chemical, mechanical and thermal stability [4]. As we know, ZnO is a polar crystal with hexagonal phase and high anisotropy which leads to the oriented growth along c-axis [5]. Crystal growth morphology results from the interplay of crystallographic anisotropy and growth kinetics [6]. Anisotropy is the basic property of the crystal. Anisotropic tendency during crystal growth in association with the relationship between crystal planes of solid materials and their physicochemical properties has been studied by several researchers[7]. Given the poor morphology-controlled synthesis of nanoscale metal oxides, systematic studies on the connection between crystal planes and properties are limited. Morphology-controlled syntheses can clearly demonstrate the strong excitation wavelength dependence of the fluorescence emission of ZnO crystals. The excitation wavelength-dependent features of fluorescence emission allows for tunable laser sources.

The development in ZnO area is recently moving towards nanostructures. The most promising of them are one dimensional (1D) nanostructures such as nanowires, nanotubes and nano ribbons etc. There are many techniques to synthesize these structures such as pulse laser deposition, chemical vapour deposition and electrochemical deposition. All of them require highly sophisticated and expensive instruments, high temperature and also require complex process. Keeping in view the various aspects of ZnO synthesis, we have reached the conclusion that the simplest, cheapest and most effective way to synthesize ZnO is by wet chemical method. Various wet chemical techniques such as sol-gel, hydrothermal, solvothermal method, polyol, microwave heating, spray

pyrolysis etc have been used for the synthesis of nanocrystalline powders. So far, numerous nanostructured ZnOs with different morphologies have been fabricated, such as nanowires, nanosheets, nanotubes, nanotower and nanoflowers. In addition to simple ZnO crystals, controlled growth of hierarchical ZnO crystal structures has received particular attention to support demands for more complex structures to impart greater control over material and device properties [8].

In the present work, we report on the controlled synthesis of the ZnO nano/micro crystals with different morphologies using a simple wet chemical method. Dumb bell(DB) microrod, nanoflakes, nanoplates and microrod of good crystalline nature were synthesized at growth durations (6-22 hrs) with excellent reproducibility. The influence of precursor concentration, reaction time and temperature on the size and morphology of ZnO were investigated. It was revealed from scanning electron microscopy that the morphology of ZnO can be effectively controlled as DB microrod, nanoflakes, nanoplates and microrod. X-ray diffraction measurements showed that all the samples are of a hexagonal phase structure. The room temperature photoluminescence of the as-prepared ZnO significantly depends on the crystal size, orientation and morphology, aspect ratio and crystalline density.

3.3 Experimental

All chemicals were purchased from Merck Ltd and used as received without further purification. The nutrient solution was prepared from an aqueous solution of zinc nitrate hexahydrate [$Zn(NO_3)_26H_2O$] and hexamethylenetetramine (HMTA) [$(CH_2)_6N_4$]. The hexamine solution was added to the zinc nitrate solution drop wise while stirring. The following reactions were involved in the crystal growth of ZnO [9].

$$(CH_2)_6N_4 + 6H_2O \rightarrow 6CHOH + 4NH_3 \tag{3.1}$$

$$NH_3 + H_2O \rightarrow NH_4^+ + OH^- \tag{3.2}$$

$$Zn(NO_3)_2 + H_2O \rightarrow Zn^{2+} + 2HNO_3 \tag{3.3}$$

$$2OH^- + Zn^{2+} \rightarrow ZnO(S) + H_2O \tag{3.4}$$

The reaction decomposes HMTA to formaldehyde (HCHO) and ammonia (NH_3), acting as a pH buffer by slowly decomposing to provide a gradual and controlled supply of ammonia, which can form ammonium hydroxide and support OH^- [10]. Finally OH^- anions react with Zn^{2+}cations to form ZnO .The precursor concentration, time and temperature dependant experiments were

carried out to investigate the growth processes of ZnO.

The size and morphology of ZnO samples were characterized by scanning electron microscopy (JEOL/EO, and JSM6390). The X-ray diffraction data were collected on an AXS Bruker D% diffractometer using Cu Kα-radiation (λ=0.1541nm,the operating conditions were 35m A and 40 kV at a step of 0.020^0 and step time of 29.5 s in the 2 range from 30 to 70^0. The measurement of fluorescence emission were recorded using a Cary Eclipse fluorescence spectrometer (Varian).

3.4 Results and discussions

In the following sections, the growth mechanism of ZnO crystals are elucidated by detailed analysis of our experimental results, which provides a means to achieve control over ZnO crystals and is essential for tailoring optical, electrical and magnetic properties of crystals for certain applications.

3.4.1 Factors Affecting Morphology of ZnO

Effect of growth duration

The morphology of the ZnO crystals at nano/micro scales synthesized with controlled growth rate of 6 hrs, 11 hrs, 18 hrs and 22 hrs is revealed by the scanning electron microscopic images shown in figure 3.1. All ZnO samples are of Würtzite structure (hexagonal phase, space group $P6_3mc$). In the Xray diffraction patterns of ZnO with typical morphologies shown in figure 3.2, all diffraction peaks are well assigned to hexagonal phase ZnO [reported in JCPDS card 36-1451]. No characteristic peaks of impurity phases and no diffraction peaks except that of ZnO were found, which indicates that only single phase hexagonal ZnO is present. The summarized morphologies and estimated parameters are illustrated in table 3.1. In figure 3.2, the strongest detected (h k l) peaks are at 2θ values of 31.8^0,34.6^0,36.4^0,47.6^0 ,56.7^0 ,62.9^0, corresponding to the following lattice planes: (100),(002),(101),(102),(103), respectively. The d spacing along the (100) plane is found to be 2.807 A^0. The lattice constants a and c were determined as a=0.3249nm, c=0.5206 nm by using following equation [5]

$$\frac{1}{d^2{}_{(hkl)}} = \frac{4}{3}\frac{(h^2+hk+k^2)}{a^2} + \frac{l^2}{c^2} \tag{3.5}$$

When the reaction media was heated at 80^0C for 6 hr ZnO DB microrod with an average diameter of 800 nm and length of 3μm were formed. The ZnO DB microrods preferentially grow along the [0001] direction and form similar to the sharing of two individual microrods, stabilizing between Zn [0001] planes

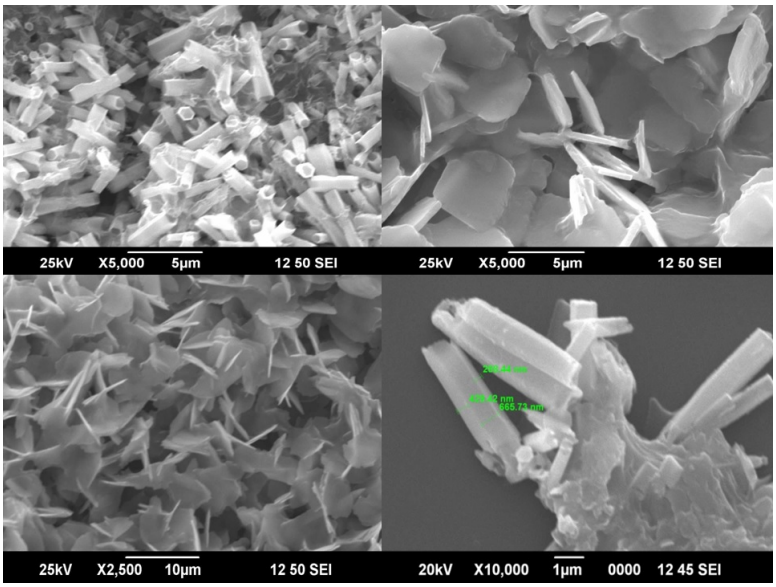

Figure 3.1: Growth time dependence of ZnO nano-crystals in $Zn(NO_3)_2$. $6H_2O$ (1 mM) and HMTA (1 mM) solutions under 80^0C (a) 6h, (b) 11h, (c) 18h and (d) 22h.

and with Zn [0001]faces masked. They also have wider size distribution than the nanoplates and nanoflakes. Wenquin and co workers [11] reported the precursor concentration dependant structure morphology of ZnO nano and micro crystals. To understand the observed behaviors of ZnO, it is necessary to study the growth mechanism. ZnO exhibits a Würzite crystal structure which is a polar molecule with [0001] polar surfaces and non-polar $[01\bar{1}0]$ faces. The non-polar surfaces are electrically neutral having a low surface energy and the polar surfaces have a high surface energy, which is the main factor for the differentiation of the growth rate along both the polar and non-polar directions [12]. The length and width of the synthesized ZnO crystals would be directly affected by the growth rate in the [0001] polar face and the [0110] non-polar faces respectively. When the heating time is prolonged for 11 hr, the crystal growth along [0001] direction decreases, leading to the formation of nanoflakes. The DB ZnO microrods were changed into flake shaped crystals, due to the sequential dissolution of the polar O $[001\bar{1}]$ and non-polar $[01\bar{1}0]$ ones [13]. When heated for 18 hr, the ZnO nanoplates with uniform size were fabricated in large scale and for 22hrs, microrods are observed. The surface reconstruction may favor a particular crystalline structure or surface orientation of a crystalline structure. The

Table 3.1: Crystalline dimensions of DB microrods, nano flakes, nano plates and microrods

	Avg.diameter (μm)	Avg.thickness/ length(μm)
DB microrods	0.8	3.0
Nanoflakes	4.0	0.35
Nanoplates	4.0	0.2
Microrods	0.8	5.0

ZnO microrods are assumed to be formed by stacking the nanoplates. It seems that both DB micro rods and hexagonal microrods have same average diameter.

The schematic representation of ZnO structures is depicted in figure 3.3. Here we believe that the growth time plays a key role for anisotropic growth of well-defined ZnO morphologies.

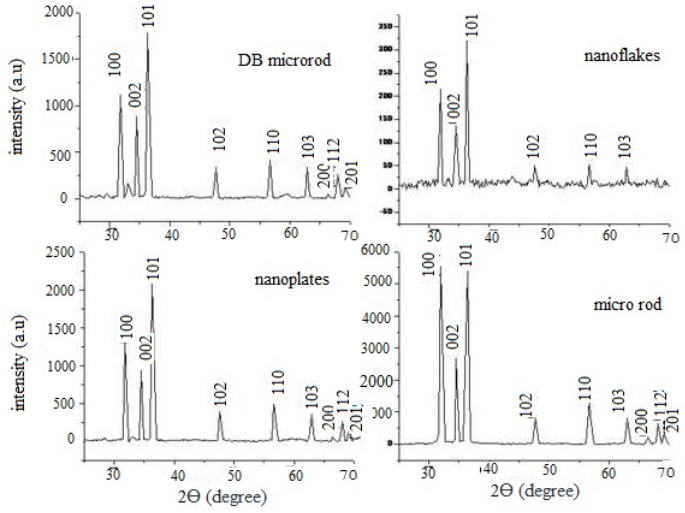

Figure 3.2: X-ray diffraction pattern of (a) ZnO DB microrods (b) nanoflakes (c) nanoplates and (d) microrods

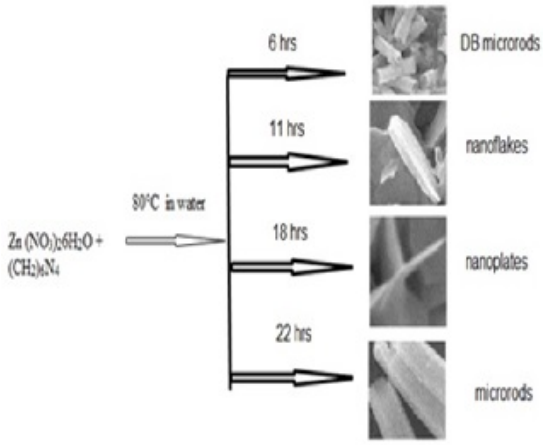

Figure 3.3: Schematic representation of face orientation of ZnO nano structures

Effect of hexamethylenetetramine (HMTA) concentration

Further, we observe that variation of the molar concentration of the HMTA precursor solutions, in the ratio with zinc nitrate is 1:0.5, 1:1 and 1:1.5. The objective of this work was to determine the role of HMTA on the DB microrod growth since the role of HMTA is still under debate. HMTA is a nonionic cyclic tertiary amine that can act as a Lewis base to metal ions and has been shown to be a bidentate ligand capable of bridging two zinc (II) ions in solution. HMTA is also known to hydrolyze, producing formaldehyde and ammonia in the pH and temperature range of the ZnO rod reaction [14]. The role of HMTA in the synthesis procedure is to control the release of the hydroxide ion during reaction and thereby tailor the aspect ratio. Therefore the concentration of OH- anions is the dominant factor in the growth process of ZnO nanorods. So HMTA plays a key role in the growth of ZnO rods. The hydrolysis rate of $C_6H_{12}N_4$ is low, thus it can provide OH^- anions at a steady rate, rendering a solution with a constant concentration of OH anions. At low concentrations of $C_6H_{12}N_4$, the reaction rate of OH^- anions is low; on the other hand, the reaction rate and the growth rate of ZnO rods are high at high concentrations of $C_6H_{12}N_4$. The average diameter of the nanorod decreases with the HMTA concentration in the solution as shown in figure 3.4.

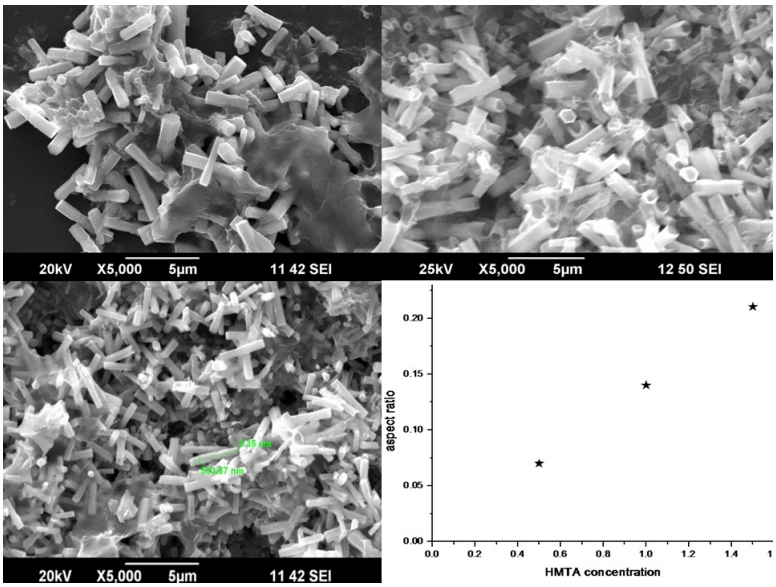

Figure 3.4: HMTA concentration dependence of ZnO nano-crystals under 80^0C,6h in $Zn(NO_3)_2$. $6H_2O$ (1mM) solutions(a)0.5 mM(b)1 mM and (c)1.5 mM and (d)HMTA concentration Vs aspect ratio

Effect of temperature

To study the effect of temperature on the ZnO DB microrod, the growth of DB microrod were performed at 70, 80 and 90^0C respectively. The corresponding scanning electron microscopic images of the rods grown at each temperature are shown in figure 3.5. Temperature is important in the growth control of ZnO nanostructures. The growth temperature has an impact on the aspect ratio of the rods. As shown in figure, the average length of the rods increases from 1.57μm to 2.88μm and average diameter decreases from 589 nm to 455.4 nm when the temperature is increased from 70 to 90^0C which was measured using digimizer which is an affordable image analysis software. In our experiment, 80^0C is the optimum temperature for obtaining high quantity nanorods. When the temperature is increased to 90^0C, the HMTA decomposes more quickly than at a low temperature, producing enough OH^- ions, resulting in the sufficient size controlled growth in ZnO with good aspect ratio compared to other two, but the alignment degree is poorer than at 80^0C. This implies that the growth rate is sensitive to temperature.

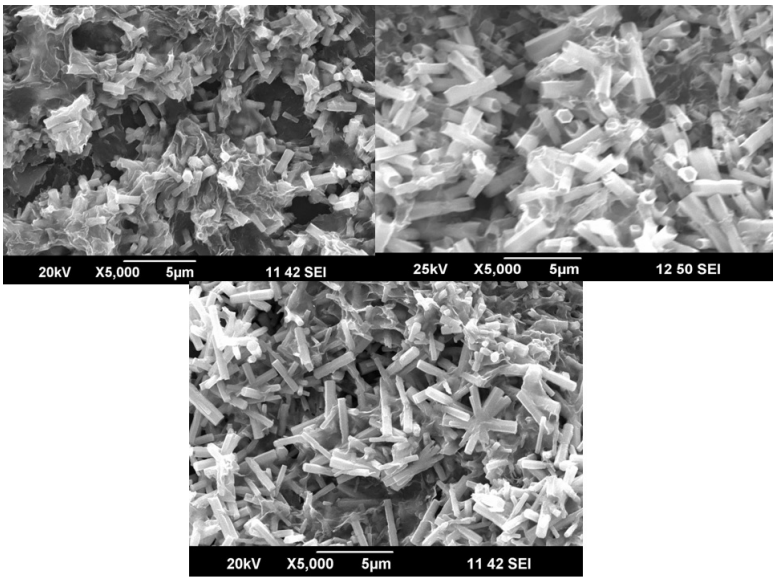

Figure 3.5: Temperature dependence of ZnO nano-crystals in Zn $(NO_3)_2$. $6H_2O$ (1 mM), HMTA (1 mM) solutions for 6h. (a) 70^0C, (b) 80^0C and (c) 90^0C

3.4.2 Absorption spectroscopy of ZnO nano/micro crystals

We have also performed optical studies to evaluate the optical qualities of ZnO structures. The ZnO crystals are characterized by optical absorption measurements recorded using a spectrophotometer (JascoV-570 UV/VIS/IR). Figure 3.6 gives the room temperature absorption spectra of the different morphologies of ZnO prepared by simple wet chemical method.

Compared with the bulk ZnO, we can see that there is a blue shift in the absorption edge. It is possible to estimate the optical band gap from the absorption spectra using the relationship of Emin et al.[15] between the absorption coefficient and the photon energy hν using equation

$$\alpha h\nu = k(h\nu - E_g)^{1/2} \tag{3.6}$$

where k is the slope of the Tauc edge called the band tail parameter, hν is the incident light energy and E_g is the optical band gap which could be calculated from $(\alpha h\nu)^2$ versus hν plot i.e.by extrapolating the linear portion of

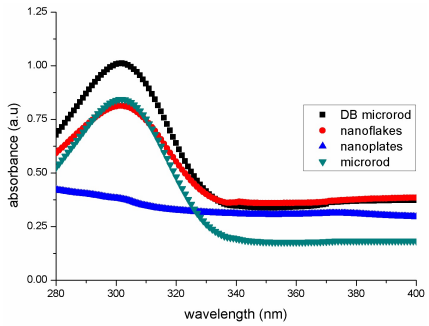

Figure 3.6: Absorption spectra of the different morphologies of ZnO

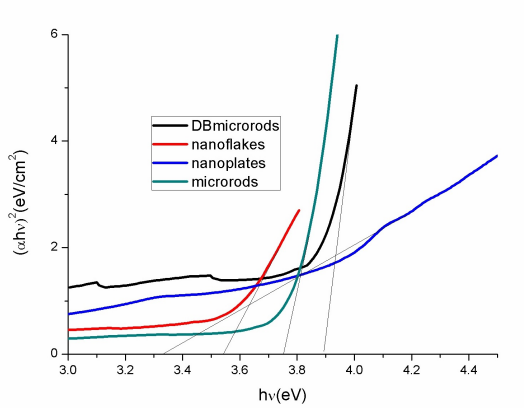

Figure 3.7: Optical band gap of the different morphologies of ZnO

the plot (i.e.Tauc extrapolation) to the energy axis gives the optical band gap value of ZnO structure. The optical band gap of ZnO structures are shown in figure 3.7.

3.4.3 Fluorescence spectroscopy

ZnO is a direct wide band gap (3.37 eV) semiconductor at room temperature, this fact, coupled with its large exciton binding energy (60 meV), makes it suitable for effective UV emission. But due to the poor crystalline quality of nanomaterials, such as high density of structural defects, impurities etc, the UV emission band which results from the recombination of excitons is liable to be

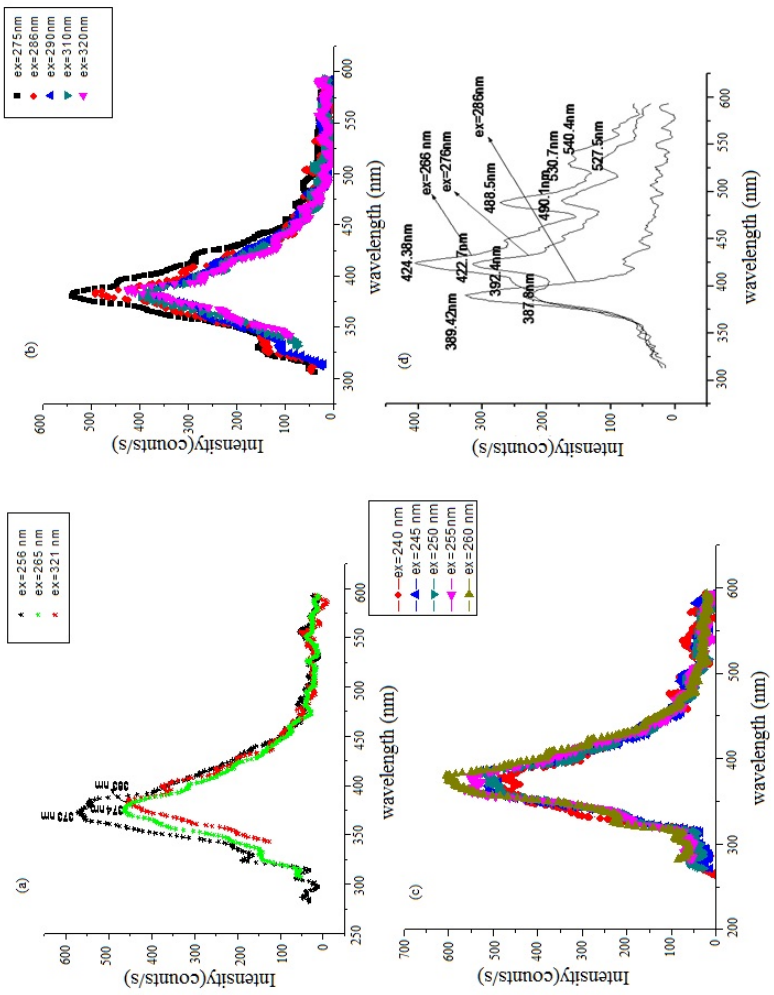

Figure 3.8: Emission spectra of ZnO nanostructures (a) DB microrod (b) nanoflakes (c) nanoplates and (d) microrod

quenched and the defect emission in the visible region is detected [16]. These deficiencies hinder the progress of ZnO in optoelectronic and lasing applications. Hence the study of photoluminescence spectra is an effective method to evaluate both ZnO defects and its optical properties. The photoluminescence of ZnO structures exhibits different features depending on their morphological variations. The fluorescence behavior of ZnO nanostructures was studied as a function of wavelength.

The DB microrods, nanoplates and nanoflakes exhibit UV peak attributed to the near band edge (NBE) emission and no defect emission is detected. The photoluminescence spectra of microrods recorded at various excitation wavelengths show striking differences in spectral features. The detailed emission spectra of ZnO structures are shown in the figure 3.8. The micro rods give out blue - green fluorescence emission for two excitation wavelengths of 266 and 276 nm and excellent UV emission at 389.42nm for an excitation wavelength of 286 nm. Green emission from ZnO microstructures centered on 530 nm is attributed to vacancies of Zn^{2+} or O^{2-} and the presence of extrinsic impurities or surface carriers. Our sample was grown at low temperature, at around 80^0C, so that Zn^{2+} vacancy can be ruled out. Therefore we assume that the emission at 530 nm is due to surface states excited along with the h_2-e_2 and h_3-e_3 exciton formation and decay [17, 18]. This also gives a series of lines at 387, 425, 490 nm in addition to the green emission. The h_1-e_1 (low energy exciton) selectively decays through emission at 387 nm because of less probability of interband transition of the electron states [19]. It is clear that crystal quality would affect the emission performance and hence the synthesized crystals with less defects exhibit enhanced UV emission intensity as well as reduced visible emission intensity.

3.5 Conclusions

- We were successful in synthesizing DB microrods,nanoflakes,nanoplates and microrods of ZnO with different ratios of polar to non-polar faces through simple, low temperature wet chemical method.
- To finely modulate the morphology of ZnO, the relationship between the morphologies and the reaction conditions were also investigated.
- It was found that the growth duration plays a crucial role in the face orientation of ZnO crystals and the precursor concentration and temperature have no obvious influence on the morphology but only affect the size slightly.

- The energy band gap of the ZnO structures is investigated from the absorption spectroscopy
- The room temperature photoluminescence of ZnO structures exhibit UV and visible emission depending on the morphology.

3.6 References

[1] Marcel Lucas, Zhong Lin Wang and Elisa Riedo "Growth direction and morphology of ZnO nanobelts revealed by combining in situ atomic force microscopy and polarized Raman spectroscopy" Phys. Rev. B 81, 045415 (2010)

[2] Yoshitake Masuda, Naoto Kinoshita and Kunihito Koumoto "Morphology control of ZnO crystalline particles in aqueous solution" Electrochim. Acta 53, 171-174 (2007)

[3] Haoquan Yan,Rongrui He,Johnny Pham and Peidong Yang "Morphologies of one dimensional ZnO nano and Microcrystals" Adv.Mater ,15, 5, 402-405 (2003)

[4] Oleg Lupan, Lee Chow, Guangyu Chai, Beatriz Roldan et al."Nano fabrication and characterization of ZnO nanorod arrays and branched microrods by aqueous solution route and rapid thermal processing" Mater. Sci. Eng.B ,145,57-66,(2007)

[5] Hui Zhang, Deren Yang, Dongshen Li, Xiangyang Ma, Shenzhong Li, and Duanlin Que "Controllable Growth of ZnO Micro crystals by a Capping-Molecule-Assisted Hydrothermal Process " Cryst. Growth Des , 5, 2, 547-550 (2005)

[6] G.Muller, J.J Metois and P.Rudolph "Crystal growth from fundamentals to technology" first ed. Elsevier (2004)

[7] Shalaka C Navale,S W Gosavi and I.S Mulla "Controlled synthesis of ZnO from nanospheres to microrods and its gas sensing studies" Talanta,75,1315-1319 (2008)

[8] Seungho Cho, Seung-Ho Jung and Kun-Hong Lee "Morphology-Controlled Growth of ZnO Nanostructures Using Microwave Irradiation: from Basic to Complex Structures" J. Phys. Chem. C,112,12769-12776 (2008)

[9] T Mahalingam, Kyung Moon Lee, Kyung ho Park et al. "Low temperature wet chemical synthesis of good optical quality vertically aligned crystalline ZnO nanorods" Nanotechnology 18, 035606 (2007)

[10] Jing-Hua Tian, JieHu, Si-SiLi, Fan Zhang Jian Shi, XinLi, Zhong-Qun Tian et al "Improved seedless hydrothermal synthesis of dense and ultra long ZnO nanowires" Nanotechnology 22, 245601 (2011)

[11] Wenquin Peng, Shengchun Qu, Guangwei Cong and Zhanguo Wang "Synthesis and structures of morphology controlled ZnO nano and micro crystals" Cryst. Growth,1518-1522 (2006)

[12] Bharati Panigrahy, M. Aslam, D. S. Misra and D. Bahadur "Polymer-mediated shape-selective synthesis of ZnO nanostructures using a single-step aqueous approach" Cryst .Eng, 11, 1920-1925 (2009)

[13] Eue Soon Jang.Jang-Hee Won, Seong-Ju hwang and Jin-Ho choy "Fine tuning of face orientation of ZnO crystals and optimize their photo catalytic activity" Adv.Mater, 18, 3309-3312(2006)

[14] Lori E. Greene, Benjamin D. Yuhas, Matt Law, David Zitoun, and Peidong Yang "Solution-Grown Zinc Oxide Nanowires" Inorg.Chem., 45, 7535-7543 (2006)

[15] Emin Bacaksiz, Serdar Aksu and Salih Yilmaz "Structural, optical and electrical properties of Al-doped ZnO microrods prepared by spray pyrolysis",Thin film solids 518, 15, 4076-4080 (2010)

[16] Min Guo, PengDiao and Shengmin Cai "Hydrothermal growth of well-aligned ZnO nanorod arrays: Dependence of morphology and alignment ordering upon preparing conditions" J. Solid State Chem., 178, 1864-1873 (2005)

[17] Chun Li Guojia Fang, Wenjie Guan and Xingzhong Zhao "Multipod ZnO 3D microstructures" Materials Letters, 61, 3310-3313 (2007)

[18] Jinping Liu, Xintang Huang, K. M. Sulieman, Fenglou Sun and Xiang He "Solution-Based Growth and Optical Properties of Self-Assembled Monocrystalline ZnO Ellipsoids" J. Phys. Chem. B, 110, 10612-10618 (2006)

[19] Litty Irimpan, Bindu Krishnan, A. Deepti, V.P.N Nampoori and P. Radhakrishnan "Excitation wavelength dependent fluorescence behaviour of nano colloids of ZnO" J.Phys D: Appl Phys., 40, 5670-5674 (2007)

Chapter 4

Nonlinear optical characterization of ZnO composites-A morphological study

4.1 Abstract:

We report a methodical study on the third order optical non linearity of anisotropic growth of ZnO crystals embedded in polymeric matrices and nanowires on the glass substrate with the use of pre-existing textured ZnO, ZnS and TiO_2 seeds employing Z-scan method with Nd: YAG laser (532 nm, 7 ns, 10 Hz). The controlled morphologies of ZnO including DB microrods, nanoflakes, nanoplates and microrods prepared by low temperature wet chemical method. The studies show that the optical non linearity of ZnO crystals is highly dependent on the structural geometry. Our study offers better insights into the third-order nonlinear optical characteristics of ZnO crystals and reveals the great potential for applications in nonlinear photonic devices.

Results of this chapter are published in

- Aparna Thankappan, Divya S, Sheenu Thomas, V.P.N. Nampoori "Optical characterization of ZnO nanoplates embedded in polymeric matrices for optical limiting applications" Optics & Laser Technology 52, 37-42 (2013)
- Aparna Thankappan ,SheenuThomas, V.P.N.Nampoori "Novel composites based on polymer micro-rods for photonic device applications" Optics &Laser Technology 58, 63-70 (2014)
- Aparna Thankappan, C.L. Linslal,S.Divya, P.V. Sabitha,Sheenu Thomas, V.P.N. Nampoori "Optical nonlinear investigations on morphology controlled growth of ZnO crystals" Optics & Laser Technology 64, 133-139 (2014)

4.2 Introduction

Fundamental science plays a vital role in the generation of future technologies. Low dimensional organic semiconductor composites possess many unusual physical, chemical and optoelectronic properties compared to their bulk counterparts, thus holding potential applications in many fields such as nonlinear optics, optical switching and single electron transistors. In recent years, the nonlinear optical properties of nanomaterials have attracted much interest due to their potential applications in nanolasers [1], optical limiting [2] and all optical switching [3] devices. Optical limiting property provided by reverse saturable absorption (RSA) in which the excited state has strong absorption compared to that of the ground state, is gaining interest over recent years due to its variety of applications in devices for protecting sensitive devices from intense optical radiations. Semiconductors are being experimented in this regard for the past few years because of their extensive applications in solid states electronics and optics. Polymers toughened with nanosized inorganic constitute a new class of materials of meticulous significance [4-6].

The use of polymer is a convenient method for the synthesis of low dimensional semiconductor structures, because the polymer matrices provide process ability, solubility and control of the morphology of nanoparticles [7]. The common approach to polymer nanocomposites includes casting of films using the mixture of nanoparticles and polymer, and another is inbuilt growth inside the solid matrix. The former mode of fabrication of films is of interest in the present study. Photonic polymers have excellent radiation stability [8,9]. As we know, ZnO is a polar crystal with hexagonal phase and high anisotropy which leads to the oriented growth along c-axis [10]. Crystal growth morphology results from the interplay of crystallographic anisotropy and growth kinetics [11]. Anisotropic tendency in the crystal growth exploring the relationship between crystal planes of solid material and their physical/chemical properties have attracted several researchers [12]. ZnO, an exceptionally important multifunctional semiconductor, has intense commercial interest in developing practical short wavelength semiconductor diode lasers for the huge market needs due to its many significant properties such as physical and chemical stability, high catalytic activity, effective antibacterial and bactericide function, intensive ultraviolet and infrared absorption [13-15], and exhibits a hexagonal structure with large band gap of 3.37 eV at room temperature and exciton binding energy of 60 meV above room temperature [16]. Therefore it is an apt candidate for ultraviolet optoelectronic applications.

Over the past few years numerous efforts have been employed in controlling the size and shape of inorganic nanocrystals to tune its properties for prospec-

tive applications such as the size, orientation and morphology, aspect ratio and even crystalline density can significantly influence various properties. So far, prismatic[17], belt like [18]flower like[19] tubular[20], tower like[21], plates [22] like ZnO have been reported using physical and chemical techniques [23]. Recent advances in nano science and nano technology have not only revealed the potential of nanoscale electronic and optoelectronic devices, target drug delivery, etc., but have also shown its potential utility as a hydrogen storage material for clean energy [24]. Therefore, development of morphology controlled synthesis of nanostructures remains a considerable challenge to answer the demand for exploring the potentials of ZnO.

In this chapter, we report a systematic study on the third order optical non linearity of controlled morphologies of ZnO nano/micro crystals which include DB microrod, nanoflakes, nanoplates and microrod structures and also investigate the nonlinear behavior of nanowires with the use of pre-existing textured ZnO, ZnS and TiO_2 seeds using an Nd: YAG laser (532 nm, 7 ns, 10 Hz). These properties are commonly defined in terms of intensity dependent nonlinear absorption coefficientα (I), which can be written in terms of linear absorption coefficient and two photon absorption coefficient β as

$$\alpha(I) = \alpha + \beta(I) \tag{4.1}$$

When SA is present this equation modifies to

$$\alpha(I) = \frac{\alpha_0}{1 + \frac{I}{I_s}} \tag{4.2}$$

The structures were characterized by scanning electron microscopy and X-ray diffraction. Depending on the pump intensity and on the absorption cross- section at the excitation wavelength, most molecules show nonlinear absorption. Therefore, it is necessary to identify their nonlinear absorption effects, and to determine their nonlinear absorption parameters, such as the saturable intensity (I_s) for saturable absorber, the TPA coefficient (β) for two-photon absorbing material. The room temperature non linear optical properties of the as-prepared ZnO significantly depend on the crystal size, orientation and morphology, aspect ratio and crystalline density.

4.3 Experimental details

4.3.1 Controlled growth of ZnO crystals

The nutrient solution was prepared from an aqueous solution of zinc nitrate hexahydrate [$Zn(NO_3)_26H_2O$] and hexamethylenetetramine (HMTA) [$(CH_2)_6N_4$]

heated at 80^0C. The synthesis procedure for the growth of ZnO crystals was described in chapter 3. To avoid sedimentation of nanocrystals, the solution was centrifuged and washed several times and finally embedded into the polyvinyl alcohol $[CH_2CH(OH)]n$ solution(15%) ,which is a water soluble polymer. Free standing films(thickness 80-90 μm) were developed (Plasto Mek,delta.0.2 kW,230 V,1 phase) which was used as samples for the nonlinear studies. The thickness of the films were measured using a Mitutoyo Micrometer (series 193). Here PVA acts as the matrix for the homogeneous distribution and immobilization. Optical properties of such crystals can be utilized in technological applications such as sensors which require large area of coating.

4.3.2 ZnO nanowires with different seeded layers

ZnO branched nanowires were grown on the glass substrate that were seeded with a thin film of nano ZnO as in the work by Greene et al [25]. ZnO seed were synthesized according to the method described by Pacholski [26]. 0.01 M zinc acetate in methanol was added drop wise to a well-stirred solution of 0.03 M NaOH in methanol maintained at 60^0C. After two hour growth, the solution was centrifuged to separate the nano of size 72 nm. Fresh methanol was infused to suspend the particles. The ZnS and TiO_2 nanoparticles were synthesized as follows.

The TiO_2 sol was prepared via sol-gel method. Titanium tetra-isopropoxide (TTIP,) was used as the precursor to prepare TiO_2 sol. A mixture of HCl and isopropyl alcohol was added to a mixture of TTIP and isopropyl alcohol under continuous magnetic agitation at room temperature. The TiO_2 sol composition was of molar ratio TTIP/isopro-panol/water =1:26.5:1.5. The [H+]/ [TTIP] molar ratio ranged from 0.02 to 1.1. The resultant TiO_2 sol was clear, yellow and stable. The as obtained nanoparticles were thermal treated at 100^0C to remove the excess moisture content. Thus amorphous TiO_2 nanoparticles of 35 nm were obtained [27].

ZnS nanocrystals are synthesized by using wet chemical precipitation at room temperature. 1M $ZnCl_2$ and 1M Na_2S in water are used as sources of Zn and S respectively and 2 ml of Tri ethanol amine (TEA) was used as capping agent and the solution was centrifuged to separate the nanoparticles. The X-ray diffraction study reveals that the size of the nanocrystals is about 2.6 nm .

The thin films are formed by dip coating the glass substrate. The nanowires were grown on the seeded substrates by placing them face down in a closed vessel containing equimolar concentration (0.025 M) of zinc nitrate hexahydrate and hexamine in de ionized water at 80^0C.

To determine third order non linear optical characteristics of ZnO crystals such as non linear absorption, the single beam Z-scan technique proposed and demonstrated by Sheik-Bahae et al[28],was employed. The transmission of a laser beam that changes near the focal point during the sample translation along the propagation path through an open-aperture (OA) and a closed-aperture (CA) was measured. A Q-switched Nd: YAG laser (Spectra Physics LAB-1760, 532 nm, 7 ns, 10Hz) was used in the Z-scan experiment to study the optical non linearity. A 20 cm converging lens was used to focus the laser beam. The radius of the beam ω_0 was calculated to be 35.4μm. The Rayleigh length, $z_0=\pi\omega_0^2/\lambda$, was estimated to be 7.4 mm, which is much greater than the thickness of the sample, and is an essential prerequisite for Z-scan experiments. The sample was fixed on a computer-controlled translation stage, so that it could be accurately moved through the focal region of the laser beam over a length of 6cm. The transmitted beam energy, reference beam energy and the ratios were measured simultaneously using an energy ratio meter (Rj7620, Laser Probe Corp.) having two identical pyroelectric detector heads (Rjp735). The detected signals were acquired, stored and processed by the computer. Optical density filters were used to vary the laser intensity at the lens focus.

4.4 Results and discussions

4.4.1 Nonlinear optical behaviour of controlled growth of ZnO crystals

Open aperture (OA)Z scan

To estimate the saturable intensity and non linear absorption coefficient, the experimental data of the samples were fitted with numerical simulations. The transmitted OA Z scan signal is given by [29]

$$T(z,S=1)=\sum_{m=0}^{\infty}\frac{[-q_0(z,0)]^m}{(m+1)^{(\frac{3}{2})}} \tag{4.3}$$

where

$$q_0(z,t)=\frac{\beta I_0(t)L_{eff}z_0^2}{z^2+z_0^2} \tag{4.4}$$

L_{eff} denotes the effective sample length, defined by

$$L_{eff}=\frac{1-exp(-\alpha l)}{\alpha} \tag{4.5}$$

with the linear absorption coefficient α, the sample thickness l and m an integer. The parameter q_0 can be obtained by fitting the experimental results

to the Eq 4.3. where Z_0 and Z are the Rayleigh range and the translated length parallel to the beam propagation, respectively. This equation can be used to fit the experimental data of the OA Z scan trace (the nonlinear absorption measurements), treating $I_0(t)$ as the position dependent intensity. The position dependence in intensity should be incorporated into the expression by considering the variation of beam size on either side of the focus. The values of n_2, calculated using Eq.(4.6),

$$n_2 = \frac{cn_0\lambda\Delta\psi_0}{40\pi 2\pi I_0 L_{eff}} \tag{4.6}$$

The imaginary part of third order susceptibility Im (χ^3) is related through the equation [30]

$$Im(\chi^3) = \frac{n_0^2 c^2 \beta}{240\pi^2\omega}(esu) \tag{4.7}$$

If excitation intensity I_0 is less than I_s, we can consider SA as a third order process and in such cases -α_0 / I_s is equivalent to nonlinear absorption coefficient β which will then give Im χ^3.

Experimentally determined nonlinear refractive index n_2 and nonlinear absorption coefficient (β) can be used in finding the absolute value of the third-order nonlinear optical susceptibility, through the relation,

$$Re(\chi^3) = \frac{n_0 n_2}{3\pi} \tag{4.8}$$

where n_0 is the linear refractive index of the film measured using Abbe refractometer, c is the velocity of light in vacuum, ω is the angular frequency of radiation used and β the nonlinear absorption coefficient. The Z-scan traces are shown in figure 4.1; fits of Eq. (4.3) to the experimental data are depicted in the figure and the measured values are tabulated in Table 4.1. The TPA coefficient (β) can be determined by analyzing the measured OA Z scan trace. Under the experimental conditions, laser beam illumination at 532 nm usually corresponds to the two-photon absorption (TPA) process because the photon energy of the 532 nm laser is within the range $E_g < 2h\nu < 2E_g$, where $h\nu$ = 2.33 eV .

Generally different processes, such as TPA,transient absorption, free carrier absorption interband absorption, photo ejection of electrons and nonlinear scattering, are reported to be operative in nonlinear absorption. The experimental data shows a slight deviation from the theoretical curve which is fitted for two photon absorption. This deviation can be attributed to two photon induced free carrier absorption which is observed in particles with larger size [31].

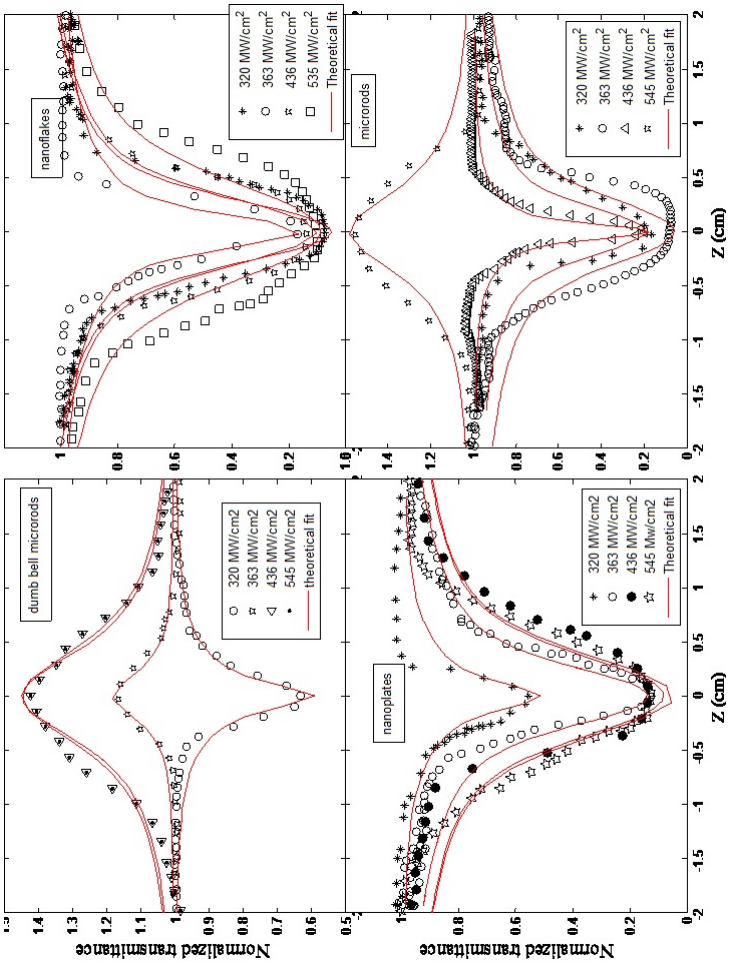

Figure 4.1: Normalized transmittance of controlled morphologies of ZnO /PVA composite film as the function of position for different input fluences in the open aperture scheme at 532 nm. The solid line shows the theoretical fit.

Table 4.1: The measured parameters of ZnO crystals in which input fluence is in MW/cm^2, β in m/GW, Im (χ^3)*10^{-9}n esu and I_s in (MW/m^2) ; β is mentioned only for the case of RSA and I_s for the case of SA. (Note: CM 1-DB microrods,CM 2-Nanoflakes,CM 3-Nanoplates and CM 4-Microrods)

	320			363			436			545		
	β	Im χ^3	I_s	β	Im χ^3	I_s	β	Im χ^3	I_s	β	Im χ^3	I_s
CM 1	6.632	0.287	—	—	—	0.051	—	—	0.243	—	—	0.242
CM 2	5.057	0.218	—	4.482	0.194	—	3.865	0.167	—	2.815	0.122	—
CM 3	6.412	0.277	—	4.913	0.212	—	4.751	0.206	—	4.919	0.213	—
CM 4	6.611	0.286	—	5.043	0.219	—	3.205	0.139	—	—	—	0.274

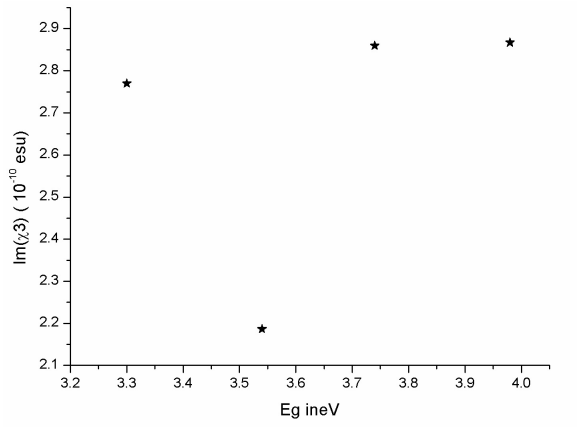

Figure 4.2: Relationship between the energy band gap and the Im(χ^3) at 320 MW/cm^2

When we plot the Im (χ^3) with corresponding band gap, we get a nonlinear curve which is shown in figure 4.2. Generally it follows an inverse relationship. Hence it can be inferred that an unusual behavior occurs in the rod structure having higher band gap [$E_{g\ DBmicrorods}$= 3.9 eV; $E_{g\ Nanoflakes}$= 3.54 eV; $E_{g\ Nanoplates}$= 3.3 eV; $E_{gMicrorods}$= 3.74 eV]

In the case of rods including both DB microrods and simple microrods, perfect switching behavior could be demonstrated by changing the pump power intensity as shown in figure 4.3.This is confirmed by measuring the transmittance of radiation by the sample. Figure 4.3 shows that transmittance of radiation is more in the case of rods as compared to plates and flakes. This can be thought that some type of confinement of radiation are more in rod shaped structures. We consider that they can both confine an externally launched light into its cavity structure formed by the hexagonal boundaries, and undergo multiple total internal reflections from the hexagonal facets, which provides an enhanced effective optical path length to confine the light and increases the communication between the excitation light and ZnO [32]. Enhancement in the optical path length increases the excited state absorption and free carrier absorption, leading to bleaching of the ground state band. The dumb bell shaped system with least defects causes switching at low power.

The nonlinear absorption coefficient calculated from the above fits shows a dependence on the input fluence and concentration. We have also studied the behavior of nanoplates by changing the concentration of sample solution

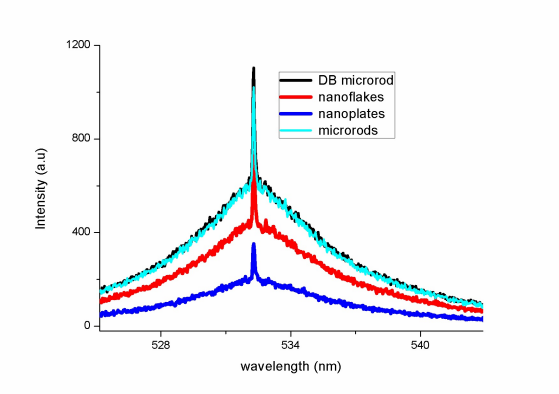

Figure 4.3: The variation of transmittance intensity with the laser input of 85μJ

1.5 m mol (C_2) and 2 m mol (C_3). There is no significant shift in the energy band gap evaluated from the optical absorption spectra. The measured values of imaginary part of the third-order susceptibility (Im χ^3) and optical limiting threshold of ZnO nanoplates/PVA at a wavelength of 532 nm for different irradiation intensities are tabulated in table 4.2.

The results of open aperture Z scan studies of samples shows that the value is decreased with the increase in concentration of nanoplates and input fluence. As given in the table, the non linear response of the nanoplates depend on both the pump power and the concentration. As the power or the concentration is increased, lowering of the non linear absorption coefficient occurs thereby diminishing the third order susceptibility, as reported by several workers [34,35], which can be due to the interplay of the non linear absorption and one photon assisted energy transfer from excited state to the nearby trapping site; and the local field enhancement through the size and structure dependent interfacial interaction between nanoplates [33].

One of the applications of reverse saturable absorption materials is in devices based on optical limiters which transmit light at a low input fluence, while they become opaque at high inputs. Reverse saturable absorption, which is generally allied with a large absorption cross section from excited state than the ground state, brings about optical limiting effects. In semiconductor materials, the optical limiting is governed by TPA as observed in this study. Semiconductor films with high TPA coefficients and strong Kerr-induced nonlinear susceptibilities are very good candidates due to their small time response as

Table 4.2: Measured values of β in m/GW, Im (χ^3)*10^{-9}in esu of ZnO nanoplates/PVA at a wavelength of 532 nm for different irradiation intensities in MW/cm^2,where 1 m mol (C1) have Eg= 3.33 eV;1.5 m mol (C2) have Eg= 3.38 eV and 2 m mol(C3) have Eg= 3.36 eV

concentration	320		360		436		545	
	β	Im χ^3	β	Im χ^3	β	Im χ^3	β	Im χ^3
C1	6.412	2.773	4.913	2.125	4.751	2.055	4.919	2.127
C2	5.443	2.354	4.853	2.099	3.85	1.665	3.239	1.401
C3	5.373	2.323		2.018	3.598	1.556	2.980	1.288

optical limiters of intense short pulse radiation [36].

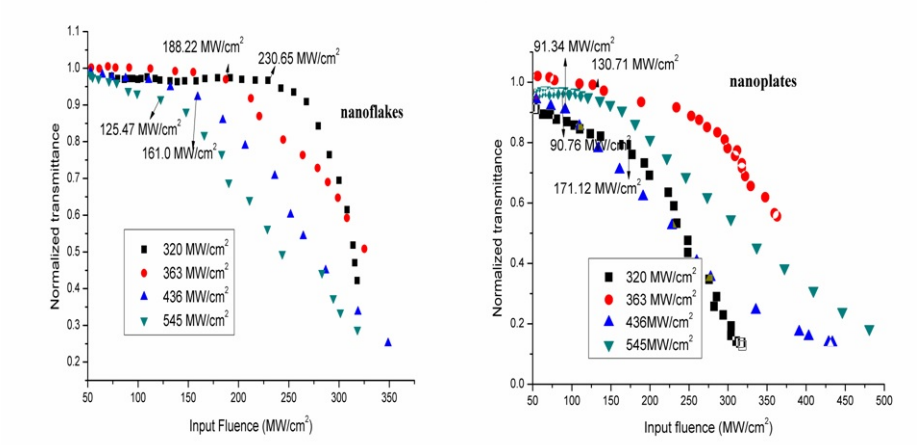

Figure 4.4: Optical limiting response of ZnO nanoplates and nanoflakes for different input fluences

As in the case of nonlinear absorption, the experimental investigation of the optical limiting in the sample was performed using OA Z scan at different input power density and concentration. Therefore these films with immobilized semiconductor nanoplates appear to be attractive candidate for optical limiting applications. Figure 4.4 represents the limiting response of nanoplates/PVA and nanoflakes/PVA, for different input fluences, the arrow in the figure indicates the approximate fluence at which the normalized transmittance begins to deviate from linearity. The limiting threshold of nanoplates/PVA at different input fluences are tabulated in table 4.3 and that of nanoflakes in table 4.4. As given in the table, the nonlinear response of the nanoplates and nanoflakes depends on both the input fluence and the concentration. The increase of the pump power and the concentration leads to the enhancement of the optical limiting performance with appreciable limiting threshold at 46.86 MW/cm^2 for C3, for higher input fluence, due to local field enhancement inside the plates and flakes. This property is desirable for the protection of sensors and human eyes from being affected by intense laser radiation. But for the C2 and C3 of nanoplates at 545 MW/cm^2, we got higher OL value than at 436 MW/cm^2.We assumed that it may due to the nonlinear scattering from the thermal induced scattering centers.

Table 4.3: Measured values of optical limiting threshold of nanoplates/ PVA for C1, C2 and C3 at a wavelength of 532 nm with different irradiation intensities.

concentration	Optical limiting threshold at		
	320 MW/cm^2	363 MW/cm^2	436 MW/cm^2
C1(Eg=3.33eV)	171.124	130.71	91.34
C2(Eg=3.38eV)	168.94	127.81	55.97
C3(Eg=3.36eV)	162.20	49.52	46.86

Table 4.4: Measured values of imaginary part of the third-order susceptibility (Im $\chi^3 10^{-10}$esu) and optical limiting threshold (OL) (MW/cm^2) of C1 (1m mol) at a wavelength of 532 nm for different irradiation intensities in MW/cm^2

	320		360		436		545	
	Im χ^3	OL	Im χ^3	OL	Im χ^3	OL	Im χ^3	OL
nanoflakes	2.382	230.65	2.022	188.22	1.759	161.0	1.388	125.47
nanoplates	2.773	171.12	2.125	130.71	2.055	91.34	2.127	90.76

Table 4.5: Measured values of nonlinear absorption coefficient β in m/GW, saturable intensity I_s in (MW/m^2), refractive index n_2 (10^{-10} in esu) and real/imaginary part of the third-order susceptibility (χ^3) in (10^{-10} esu) at a wavelength of 532 nm for different irradiation intensities(in (MW/cm^2)) for DB microrod/PVA composite.

Irradiation intensity	β	I_s	n_2	Im(χ^3)	Re (χ^3)	χ^3
320	6.631	-	-39.93	2.867	8.508	8.978
363	-	0.050	-34.32	-	7.312	-
436	-	0.243	-27.05	-	5.762	-
545	-	- 0.242	-8.77	-	1.869	-

Table 4.6: Measured values of nonlinear absorption coefficient β in m/GW, saturable intensity I_s in (MW/m^2), refractive index n_2 (10^{-10} in esu) and real/imaginary part of the third-order susceptibility (χ^3) in (10^{-10} esu) at a wavelength of 532 nm for different irradiation intensities(in (MW/cm^2)) for simple microrod/PVA composite.

Irradiation intensity	β	I_s	n_2	Im(χ^3)	Re (χ^3)	χ^3
320	6.611	-	-142.001	2.859	30.253	30.387
363	5.043	-	-26.425	-	5.629	-
436	3.205	-	-29.73	-	6.334	-
545	-	0.274	-21.07	-	4.488	-

Table 4.7: Measured values of nonlinear absorption coefficient(β in(m/GW) and saturable intensity (I_s in(MW/m^2) at a wavelength of 532 nm for different concentration and different irradiation intensities(in MW/cm^2) of DB micro-rod/PVA composite.

	320		360		436		545	
	β	I_s	β	I_s	β	I_s	β	I_s
C1	6.631	-	-	0.0501	-	0.243	-	0.242
C2	4.707	-	4.903	-	-	1.413	3.216	-
C3	5.373	-	4.651	-	4.027	-	-	0.316

Table 4.8: Measured values of nonlinear absorption coefficient(β in(m/GW) and saturable intensity (I_s in(MW/m^2) at a wavelength of 532 nm for different concentration and different irradiation intensities(in MW/cm^2) of simple microrod/PVA composite.

	320		360		436		545	
	β	I_s	β	I_s	β	I_s	β	I_s
C1	6.611	—	5.043	—	3.205	—	—	0.274
C2	4.986	—	—	0.060	3.879	—	2.765	—
C3	3.662	—	4.234	—	3.495	—	—	0.753

The obtained values at different irradiation intensities are given in table 4.5 for DB micro-rods and Table 4.6 for the simple micro-rods. The results show enhancement from the reported value for ZnO nanoparticles embedded in PMMA matrix [37]. The theory of the two photon absorption process that fits well with the experimental curve infers that TPA is the basic mechanism involved in the nonlinear absorption process, but the possibility of a higher order nonlinear process such as free carrier absorption that contributes to induced absorption cannot be ruled out. We observed that at the off resonance wavelength of 532 nm, the dumbbell micro-rods showed switching behavior from RSA to SA on increasing input fluence. Such an effect can be used for optical pulse compression, optical switching, laser pulse narrowing [38] and signal processing. The observed switchover behavior could be due to bleaching of the ground state band by laser intensity, i.e., in the case of the intraband transition, the ground-state electrons are pumped to the excited-state on increasing input fluence.

We have also studied the behavior of both dumbbell microrods and simple micro-rods by changing the concentration of sample solution to 1.5 mmol (C2: Eg=3.83 eV for DB microrods and Eg=3.77 eV for simple micro-rods) and 2 mmol (C3: Eg= 3.81 eV for DB micro-rods and Eg=3.79 eV for simple micro-rods) and the measured values are tabulated in Tables 4.7 and 4.8. As given in the table the nonlinear response of nanocrystals depends on both the irradiation intensity and concentration; therefore these films with immobilized semiconductor appear to be an attractive candidate for optical switching applications.

Closed aperture (CA) Z scan

For the CA Z scan studies we choose the morphologies of DB microrods, nanoplates and microrods. The morphology of nanoplates and nanoflakes are more or less same.

The figure from 4.5-4.7 show the CA peak -valley Z scan traces, indicate the negative nonlinear refractions due to self-defocusing. The de-focusing effect is attributed to the thermal non linearity. Self-defocusing has been observed in a variety of semiconductors and has been used to demonstrate optical limiting. To eliminate the contribution of nonlinear absorption; the CA traces were normalized by dividing them with the OA signals measured at the same intensities. The size-and structure-dependent interfacial interactions between the ZnO micro-crystals influenced the magnitude of nonlinear absorption and nonlinear scattering. The third order nonlinear refraction is attributed to the bound

electronic effect[39]due to TPA induced interband transitions; these carriers in turn block further interband transitions, giving rise to saturation of photon energies below the band gap.

The nonlinear refractive index coefficient is negative which implies that nonlinearity is of thermal origin. As irradiance intensity is increased, optical nonlinearity is reduced in the same way as Re(χ^3) and the dependence of nonlinear refractive index coefficient with irradiance intensity is nonlinear. Thermal effect at high irradiance leads to convective dynamics in the medium which reduces nonlinearity. This is also clear from the increase in the saturable intensity at higher intensities. Furthermore, the negative sign of nonlinear refraction is consistent with the optical Stark effect[40]; in addition, because of high repetition rate of laser pulse some slow nonlinearity might be involved.

For C1 the estimated average value of Im (χ^3) is 2.243*10^{-10} esu and Re (χ^3) is -9.149*10^{-10}esu and (χ^3) is 9.431*10^{-10}esu and the average nonlinear refractive index is -44*10^{-10}esu. The separation between the transmittance peak and valley in resultant Z-scan is $\approx$ Z_{pv} -1.7 Z_0, which indicates the overwhelming, effects of cubic non linearity [41,42].

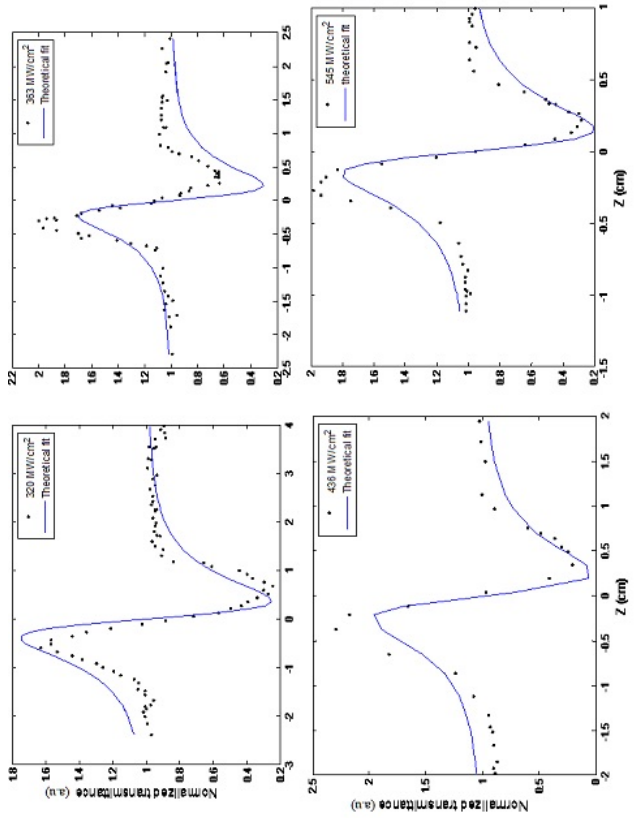

Figure 4.5: Normalized transmittance of 1 m mol ZnO nanoplates/ PVA composite film as the function of position for different input fluences in the closed aperture scheme at 532 nm. The solid line shows the theoretical fit.

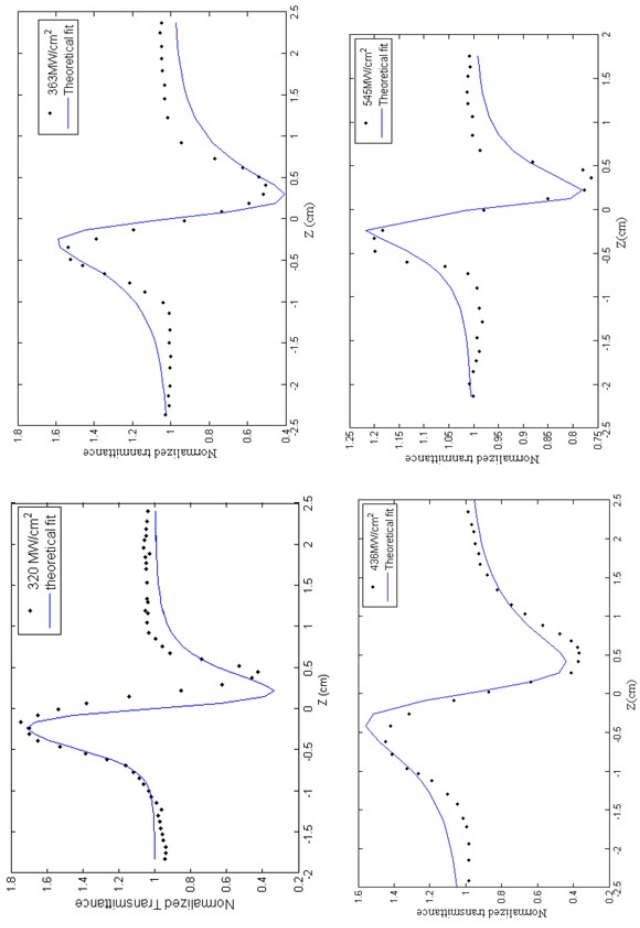

Figure 4.6: Normalized transmittance of 1 mmol ZnO DB microrods/ PVA composite film as a function of position for different input fluences in the closed aperture scheme at 532 nm. The solid line shows the theoretical fit.

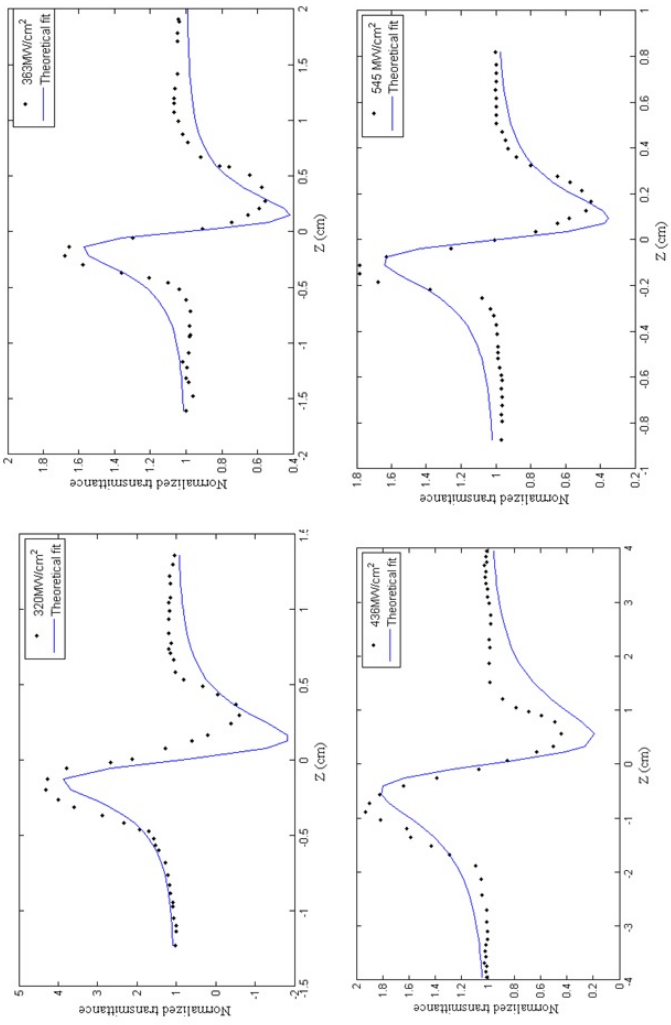

Figure 4.7: Normalized transmittance of 1 mmol ZnO simple microrods/ PVA composite film as a function of position for different input fluences in the closed aperture scheme at 532 nm. The solid line shows the theoretical fit.

4.4.2 Structural characterization of ZnO nanowires with different seeded layers

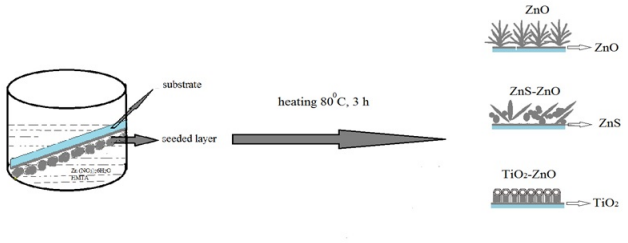

Figure 4.8: Schematic representation of tailored growth of ZnO nanostructures

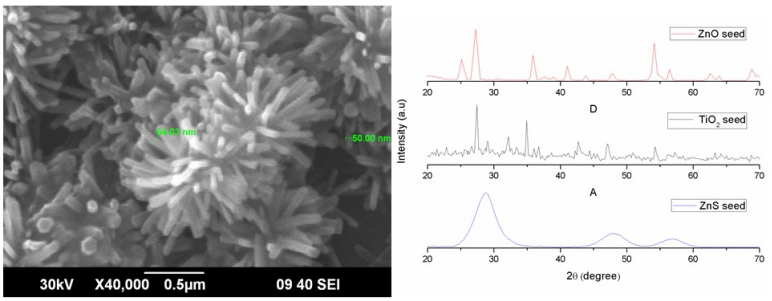

Figure 4.9: (a) SEM image of ZnO branched nanowire with ZnO seed (b) XRD pattern of various seed layers

Three kinds of crystal morphologies were obtained depending on the seeded layer. The schematic representation of the tailored growth of ZnO nanostructures is depicted in figure 4.8. We first observed the effect of same seed for the growth of nanowire; branched nanowire obtained is shown in figure 4.9. The growth of nanowires from a common nucleus may be due to the aggregation of nano ZnO-the nanowires growth along the preferential direction of the crystalline network. We repeated the same synthesis method for the nanowires with various seeded layers; the XRD pattern of seeded layers used for the synthesis is shown in figure 4.9(b). With the TiO_2 and ZnS seeds, a new morphology of nano material appears; vertical microrods (top view) and vertical nanorods. Nevertheless a small proportion of ZnS nanoparticles does

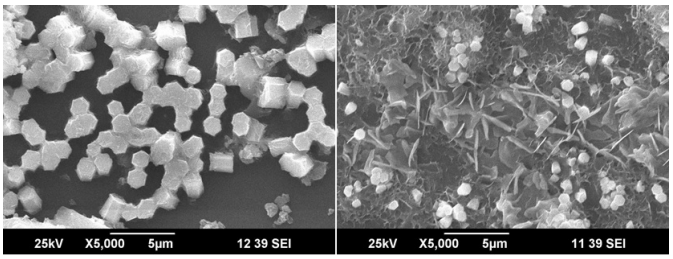

Figure 4.10: SEM image of ZnO nanostructures with TiO_2 seed and ZnS seed

not allow for the exclusive growth of nanorods. SEM image of ZnO nanostructures with TiO_2 seed and ZnS seed is shown in figure 4.10.

Introducing the nanowire into the ZnO seeds changes its band gap from 3.77 eV to 3.47 eV; for the TiO_2 seed it changes the band gap from 3.91 eV to 3.64 eV and for the ZnS seed, it changes from 3.97 eV to 3.77 eV [43] (Optical band gap was calculated from Tauc extrapolation method.).The OA Z scan studies have been carried out in the next section. But we cannot able to study the CA Z scan of these ZnO composite due to the very low transmitted intensity. The thermal nonlinearity and nonlinear scattering due to the refractive index mismatch were limits to the transmitted intensity.

4.4.3 Nonlinear optical absorption of ZnO nanowires with different seeded layers

The strength of the nonlinearity can be enhanced by using structures exhibiting quantum confinement effect. The various seeded layered nanostructure shows switching either from RSA to SA or SA to RSA is shown in figure 4.11, which is assumed to be due to the asymmetric bond between the semiconductor. The anisotropic growth from the various seed layers in growth rates of the different crystal faces of ZnO, may also affect the nonlinear absorption. The optical nonlinear parameters of nanocrystals with different seeded layers are tabulated in table 4.9. The crystallinity of the seed layer plays a crucial role in nonlinear absorption. The rod-seed interaction generates new complex resulting into new energy level. This is possible only if any of the vibrational modes of TiO_2 is coupled to the energy level structures of the seed material.This takes place comparatively at higher energy so that excited state absorption (ESA) takes place, resulting into SA. Introduction of nanowire generates energy levels so that SA further changes over to RSA by TPA/ ESA.

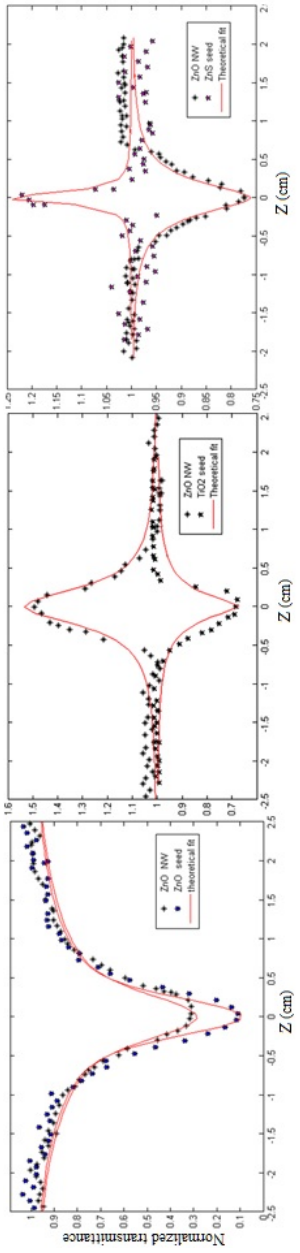

Figure 4.11: Open aperture Z scan curves showing the effect of different seeded layers on the branched nanowires with the laser input fluence of 320 MW/cm^2.

Table 4.9: The measured parameters of ZnO nanorods with various seeds in which β in m/GW, Im $(\chi^3)*10^{-9}$ in esu and I_s in (MW/m^2) ; β is mentioned only for the case of RSA and I_s for the case of SA.

	β m/GW	Im $(\chi^3)*10^{-9}$ esu	I_s in (MW/m^2)
ZnO seed	123.42	5.33	—
ZnO NW with ZnO seed	87.157	3.77	—
ZnS seed	—	—	0.011
ZnO crystal with ZnS seed	93.6	6.65	—
TiO_2 seed	127.88	9.385	—
ZnO crystal with TiO_2 seed	—	—	0.1514

4.5 Conclusion

- To summarize, the third-order optical nonlinearities and nonlinear responses of ZnO anisotropic structures synthesized by the low-temperature wet-chemical method were characterized by Z scan method with nanosecond laser.
- The optical limiting enhancements in ZnO nanoplates and nanoflakes were mostly contributed from the interfacial interaction between the structure and the local-field enhancement in addition a one photon assisted energy transfer from the excited state to the nearby trapping sites.
- The rods confine an externally launched light into its cavity structure, which provides an enhanced effective optical path length to confine the light, showing perfect switching behavior.
- The geometry of structures which is one of the crucial factors to the optical nonlinearity and our study offers better insights into the third-order nonlinear optical characteristics of ZnO crystals and reveals the great potential for applications in nonlinear photonic devices.

4.6 References

[1] Michael H. Huang, Samuel Mao, Henning Feick, Haoquan Yan, Yiying Wu, Hannes Kind, Eicke Weber,Richard Russo, "Room-Temperature Ultraviolet Nanowire Nanolasers" Science 292, 1897(2001)

[2] S. Hughes, G. Spruce, B. S. Wherrett, and T. Kobayashi "Comparison between the optical limiting behavior of chloro aluminum phthalocyanine and a cyanine dye" J. Appl. Phys. 81, 5905 (1997)

[3] Litty Irimpan, V. P. N. Nampoori, and P. Radhakrishnan"Spectral And Nonlinear Optical Characteristics Of Nanocomposites Of ZnO-CdS"J. Appl. Phys.,103, 094914 (2008)

[4] Soundararajah Q.Y, Karunaratne B.S.B, Rajapakse R.M.G, "Montmorillonite polyaniline nanocomposites:preparation,characterization and investigation of mechanical properties" Mater. Chem. Phys.,113,2, 850-855 (2009)

[5] Cai Y, Wu N, Wei Q, Zhang K, Xu Q, Gao W, et al. "Structure, surface morphology, thermal and flammability characterizations of polyamide 6/organic-modified Fe-montmorillonite nanocomposite fibers functionalized by sputter coating of silicon" Surf Coat Tech,203,3,264-70 (2008)

[6] Yeh J.M, Chen C.L, Chen Y.C, Ma C.Y, Lee K.R, Wei Y, "Enhancement of corrosion protection effect of poly (< i> o</i >-ethoxyaniline) via the formation of poly (< i> o</i>-ethoxyaniline)clay nanocomposite materials" Polymer 43, 9, 2729-2736 (2002).

[7] Wang Hongmei, Fang Pengfei, Chen Zhe, Shaojie Wang. "Synthesis and characterization of CdS/PVA nanocomposite films" Appl. Surf. Sci. ,253,8495-9 (2007)

[8] Porel Shatabdi, Singh Shashi, Sree Harsha S, Narayana Rao D, Radhakrishnan T P. "Nanoparticle-embedded polymer: in situ synthesis, free-standing films with highly monodisperse silver nanoparticles and optical limiting". Chem. Mater.,17,9-12 (2005)

[9] Hasan Tawfique, Sun Zhipei, Wang Fengqiu, Bonaccorso Francesco, Heng Tan Ping, Rozhin Aleksey G, et al. "Nanotubepolymer composites for ultrafast photonics". Adv Mater, 21,3874-99 (2009)

[10] Hui Zhang, Deren Yang, Li Dongshen, Ma Xiangyang, Shenzhong Li, Duanlin Que. "Controllable growth Of ZnO microcrystals by a capping-molecule-assisted hydrothermal process" Cryst Growth ,2, 547-50 (2005)

[11] G. Mller, J.J. Metois, P. Rudolph, (eds.), "Crystal Growth-from Fundamentals to Technology" Elsevier, Amsterdam (2004).

[12] Shalaka C, Navale SW, Gosavi IS, Mulla. "Controlled synthesis of ZnO from nanospheres to microrods and its gas sensing studies". Talanta, 75, 1315-9 (2008)

[13] Wu R, Xie CS. "Formation of tetrapod ZnO nanowhiskers and its optical properties" Mater Res Bull,39,637-45(2004)

[14] Kitano M, Shiojiri M. "Bernard convention ZnO/resins lacquer coating a new approach to electrostatic dissipative coating" Powder Technol,267-73 (1997)

[15] Yang Y, Chen HL, Zhao B, Bao XM. "Size control of ZnO nanoparticles via thermal decomposition of zinc acetate coated on organic additives" J Cryst Growth, 263:447-53 (2004)

[16] Jiang CY, Sun XW, Lo GO, Kwong DL. "Improved dye sensitized solar cells with a ZnO nanoflower photoanode". J Appl Phys Lett, 90,263501 (2007)

[17] Wang Yi, Li Meng. "Hydrothermal synthesis of single-crystalline hexagonal prism ZnO nanorods". Mater. Lett., 60,266-9(2006)

[18] lucas marcel, wang zhong lin, riedo elisa. "Growth direction and morphology of ZnO nanobelts revealed by combining in situ atomic force microscopy and polarized raman spectroscopy".Phys. Rev. B: Condens. Matter, 81045415 ,81(2010)

[19] Jiang Li, Li Guicun, Ji Qianmao, Peng Hongrui. "Morphological control offlowerlike ZnO nanostructures". Mater. Lett., 61,1964-7 (2007)

[20] Wei A, Sun XW, Xu CX, Dong ZL, Yang Y, Tan ST. "Growth mechanism of tubular ZnO formed in aqueous solution". Nanotechnology, 17,1740-4 (2006)

[21] Deng Da, Martin Scot T, Ramanathan Shriram. "Synthesis and characterization of one-dimensional flat ZnO nanotower arrays as high-efficiency adsorbents for the photocatalytic remediation of water pollutants" Nanoscale , 2, 2685, 2685-91 (2010)

[22] Yin S, Goto T, Gobo F, Huang Y F, Zhang P L, Sato T. "Synthesis of plate-like zinc oxide particles by the transcription of precursor's shape. IOP Conference Series: Materials Science and Engineering, 18,042004 (2011)

[23] Xe Yue, U Key, Wu Jin, Jianwen, Shang dejain, Zhu Ziqiang. "Synthesis,optical and field emission properties of ZnO microhairclaps" Appl. Surf. Sci., 255,6487-92 (2009)

[24] Jai Singh, Pushpendra Kumar, Hui KS, Hui KN, Ramam K, Tiwaria RS, Srivastavaa ON "Synthesis, band-gap tuning, structural and optical investigations of Mg doped ZnO Nanowires" Cryst. Eng. Comm,14:5898-904 (2012)

[25] Greene LE, Law M, Goldberger J, kim F, Johnson JC, Zhang YF, Saykally R, Yang PD " Lowtemperature waferscale production of ZnO nanowire arrays" Angew Chem Int Ed 42,3031(2003)

[26] Pacholski C, Kornowski A, Weller H. "Self assembly of ZnO: from nanodots to nanorods" Angew Chem Int Ed 2002,41,1188 (2003)

[27] S. Divya, V P N Nampoori, P Radhakrishnan, and A Mujeeb "Electronic and optical properties of TiO_2 and its polymorphs by Z-scan method" Chin. Phys. B , 23, 8 ,084203 (2014)

[28] Sheik-Bahae M, Said AA, Wei TH, Hagan DJ, Van Stryland EW " Sensitive measurement of optical nonlinearities using a single beam" J Quantum Electron 26:760 (1990)

[29] Sreekumar G, Louie Frobel PG, Muneera CI, Sathiyamoorthy K, Vijayan C, Mukherjee andrachur. "Saturable and reverse saturable absorption

and nonlinear refraction in nanoclustered Amido Black dyepolymerfilms under low power continuous wave HeNe laser light excitation" J Opt A: Pure Appl Opt 11,125204(12p) (2009)

[30] Bahae MS, Said AA, Van Stryland EW. "High-sensitivity, single-beam n_2 measurements". Opt Lett 14,955 (1989)

[31] Haripadmam PC, Kavitha MK, John Honey, Krishnan Bindu, Gopinath Pramod. "Optical limiting studies of ZnO nanotops and its polymer nanocomposite films". Appl Phys Lett, 101,071103 (2012)

[32] Aparna Thankappan, Misha Hari, Mathew S, Santhi Ani Joseph, Erni Rolf, Debajeet Bora, Artur Braun, V P N Nampoori " Synthesis of monocrystalline zinc oxide microrods by wet chemical method for light confinement applications" Physica E ,44,2118-23 (2012)

[33] Lee H W, Lee K M, Lee S, Koh K H, Park J Y, Kim K, Rotermund F."Ultrafast thirdorder optical nonlinearities of vertically-aligned ZnO nanorods" Chem. Phys. Lett 447,86-90 (2007)

[34] Smektala F, Quemard C, Couderc V, Barthelemy A. "Non-linear optical properties of chalcogenide glasses measured by Z-scan" J. Non-Cryst. Solids, 274,232 (2000)

[35] Ogusu K, Yamasaki J, Maeda S, Kitao M, Minakata M. "Linear and nonlinear optical properties of AgAsSe chalcogenide glasses for all-optical switching" Opt. Lett. 29,265(2004)

[36] Tintu R, Nampoori VPN, Radhakrishnan P, Sheenu Thomas "Preparation and optical characterization of novel GeSeSb/Pva compositefilms for optical limiting application" J. Phys. D: Appl. Phys., 44, 025101(2011)

[37] Sreeja R, John Jobina, Aneesh PM, Jayaraj MK. "Linear and nonlinear optical properties of luminescent ZnO nanoparticles embedded in PMMA matrix" Opt Commun,283, 2908-13 (2010)

[38] Band YB, Harter DJ, Bavli R. "Optical pulse compressor composed of saturable and reverse saturable absorbers" Chem. Phys. Lett. ,126,280-284 (1986)

[39] Zhang X, Fang H, Tang S, Ji W. "Determination of two-photon-generated freecarrier lifetime in semiconductors by a single-beam Z-scan technique" App.l Phys. B, 65,549-54 (1997)

[40] Wang Rongyao, Wu Xiaochun, Zou Bingsuo, Wang Li, Xie Sishen, Xu Jiren, et al. "Nonresonant optical nonlinearity of ZnO composite nanoparticles with different interfacial chemical environments" Mater. Res. Innovations ,2,49-52 (1998)

[41] Aparna Thankappan, Divya S. Sheenu Thomas, V.P.N. Nampoori "Optical characterization of ZnO nanoplates embedded in polymeric matrices for optical limiting applications" Opt Laser Technol 52, 37-42 (2013)

[42] Aparna Thankappan, Sheenu Thomas, V.P.N. Nampoori "Novel composites based on polymer micro-rods for photonic device applications" Opt Laser Technol 58, 2014, 63-70 (2014)

[43] Aparna Thankappan, C.L. Linslal,S.Divya, P.V. Sabitha,Sheenu Thomas, V.P.N. Nampoori "Optical nonlinear investigations on morphology controlled growth of ZnO crystals" Opt. Laser Technol. 64 ,133-139 (2014)

Chapter 5

Nonlinear optical characterization of betanin natural dye

5.1 Abstract:

We report on the solvent effect on the third order optical non linearity of betanin natural dye extracted from red beet root and their third order non linear optical (NLO) properties have been studied using a Q-switched Nd: YAG laser at 532 nm. The third order non linearity of these samples are dominated by non linear absorption ,which leads to strong optical limiting and their strength is influenced by the solvent used, suggesting that betanin natural dyes are promising candidate for the development of photonic non linear optic devices.

Results of this chapter are published in

- Aparna Thankappan, Sheenu Thomas, V.P.N. Nampoori "Solvent effect on the third order optical nonlinearity and optical limiting ability of betanin natural dye extracted from red beet root" Optical Materials, 35, 2332-2337 (2013)

5.2 Introduction

The need for nonlinear optical materials for applications such as phase conjugation, image processing, optical switching and optical limiting are increasingly becoming important. Recently, a large number of organic π-conjugated molecules have been investigated due to their large nonlinear optical susceptibility and the possibility of tailoring their properties which allow these materials to be used to protect optical detection elements such as human eyes and optical sensors, by controlling the fluency on the image plane below the desired level. The outcome of such studies has helped to establish certain guidelines for molecular design of the third-order nonlinear optical materials with desired properties. In general; an optical nonlinear (NLO) material for optical limiting has low loss, high nonlinearity, high damage threshold, ease of processing and a broadband spectral response. However, most of the synthesized materials require elaborated preparation procedures and safety measures, use or generation of hazardous materials, costly materials, as well as fragile or chemically unstable structures beyond certain threshold irradiance. Therefore, we suggest natural dye extracts as environment friendly, safe, and inexpensive materials, as well as having high chemical stability during optical excitations with coherent light sources. The natural dye reinforcements with the biodegradable polymers have a high potential for the design of environmentally friendly green materials for the future applications. The term green materials generally stands for substances made from sustainable or recyclable items that do not exhaust the natural resources and are also non-toxic, eco-friendly and safer alternatives for human life. These hybrid materials can provide promising applications in optics, electronics, ionics, mechanics, membranes, functional and protective coatings, catalysis, sensors and biology.

Besides anthocyanins, chlorophylls, and carotenoids, betalain are the most common pigments in the plant kingdom. These natural pigments from plants have been extensively investigated as sensitizers for the DSSC[1], in which first reported betanin DSSC study achieved efficiency of 0.67%[2]. Though the former have inherent limitations as sensitizers owing to weak absorption of green wavelengths, the absorption spectra of the latter have more favorable overlap with the solar spectrum. The betalain are water soluble and nitrogen containing pigments is relatively stable over the broad pH range from 3 to 7 [3,4,5] and have several applications in foods such as deserts, dry mixes and dairy [6-12], comprise the redpurple betacyanins, betanin (I) and betanidin (II), with maximum absorptivity at λ_{max} about 535 nm, and the yellow betaxanthins with λ_{max} near 480 nm[13-16].

The structure of betanin is shown in figure 5.1. Beetroot is one of the

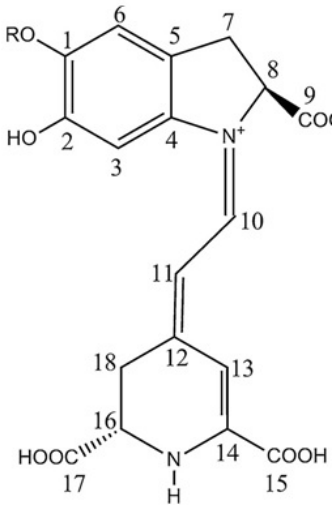

Figure 5.1: Structure of betanin pigment

richest source of betanin, the most studied betalain, was selected as a topic of the present study because of good colorant yield and the prominent peak in the visible region of the spectrum for better quantitative analysis. Unlike synthetic dyes these beetroot based natural dyes are eco-friendly and pose no environmental problems, which are very important for some sensitive applications. Determination of second and third order nonlinearities are of fundamental importance for evaluation of the properties with respect to wave-guiding structures containing betanin.

By using the Z-scan technique the optical nonlinearity of many organic materials has been explored. It is well known that the Z-scan technique, which was present by Sheik-Bahae et al.[17], has been extensively used as an effective and convenient tool for exploring the nonlinear absorption properties of various materials. In this paper we report the techniques used to prepare the natural dye extracts, optical characterizations, and determination of absorption coefficients. Also, we present here some of our findings and suggestions.

5.3 Experimental

The extracts of the red beets were obtained from fresh biological materials, pigments can be water extracted and slight acidification of the extraction medium enhances the betacyanin stability and avoids oxidation .In order to

study the effect of solvent on betanin dye, the pigments are also extracted using methanol and ethanol. The pigment extracts must be protected from direct light exposure and should be kept in cool place. The UV-VIS absorption spectra of the dye solution in different organic solvents (de ionized water, methanol, ethanol) were recorded using a UV/Vis spectrophotometer (Jasco V-570 UV/VIS/IR). Betanin dye solutions were carried out by the single beam Z scan technique. The details of which is already discussed in chapter 4.

5.4 Results and discussions

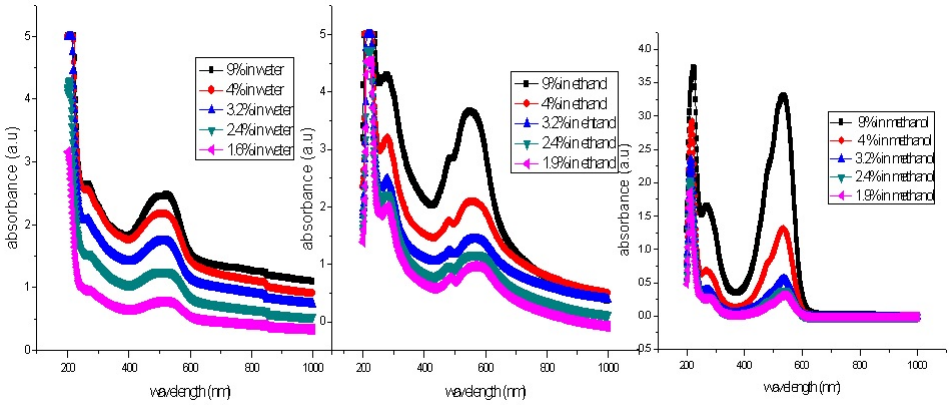

Figure 5.2: UV-VIS absorption spectra of betanin in water, ethanol and methanol

When absorption spectra of betanin are measured in solvents of different polarity(de ionized water, methanol and ethanol) at various concentrations, it is found that the positions, intensities and shapes of the absorption bands are modified by these solvents, is shown in figure 5.2 in which the visible range (520-565 nm depending on the solvent)is attributable to betanin. These changes are a result of physical intermolecular solute-solvent interactions (such as dipole-dipole, ion-dipole, hydrogen bonding, and induced dipole-dipole), which above all tend to alter the energy difference between ground state and excited state of the betanin and external solvent polarization interactions can lift internal symmetry restrictions in the solute molecule which can induce new bands. The decrease of polarity of the solvent leads to the red shift caused by the solute/solvent dispersion interactions

Optical properties of organic molecules utilized in scientific and technological applications can strongly depends on properties of the surrounding media and the interaction of the dancing molecules. For liquid solutions, solvent plays fundamental role in optical processes, and various modes of energy transfer involved in sample solution are collision between base fluid molecules, thermal diffusion in the molecules suspended in fluids, collision between the samples due to the Brownian motion, thermal interactions of dynamic or dancing samples with base fluid molecules and light induced aggregation of samples, leading to the modifications of ground state and excited states of the molecules. Such solvent effects mainly the interaction of dye molecules to the solvent surroundings which depends on the arising forces which can be determined by the charge distribution and polarizability of the solvent and solute molecules [18,19].

Figures 5.3-5.5 shows the open aperture Z-scan curve of different concentration of betanin in water, ethanol and methanol respectively. The data is analyzed using the procedures described by Sheik-Bahae et al. for a two-photon absorption (TPA) process.

As the concentration of betanin in water increases, RSA switches to SA and at the intermediate concentration RSA within SA is observed and further no energy absorption takes place. We assume the -COOH on the five membered rings to be the most acidic of the three carboxylic acid groups on Betanin. But in the case of alcohols, the H bonding is more energetic than that of water and have higher excited state absorption cross section, so as the concentration increases RSA behavior switch back to RSA after an the intermediate concentration exhibiting RSA within SA except for methanol. If the intermolecular and intra molecular H bonding interaction which takes place both in the ground state and in the excited state of the molecule is reasonably strong, it may cause a substantial change in the electronic levels of the dye molecules, and there will be a substantial change in the optical behavior of the dye molecules. The strength of the H bonding in the ground states and the excited states of the dye molecules depends on this difference in the electronic charge distribution which was clearly observed from the absorption spectra depicted in figure 5.2. This differential effect and the number density of the dye molecules in the laser beam affect the nonlinear behavior and make them interesting. In general, induced absorption can occur in betanin natural dye, due to a variety of processes such as excited state absorption, two-photon absorption, interband and intraband transitions and nonlinear scattering [20]. By light absorption the betanin pigment chromophore excites π electrons to a more energetic state (π^*), increasing reactivity or lowering activation energy for the molecule. This is attributed to the visible transition of betanin which is well-described as a HOMO$\rightarrow$ LUMO excitation from the aromatic ring to

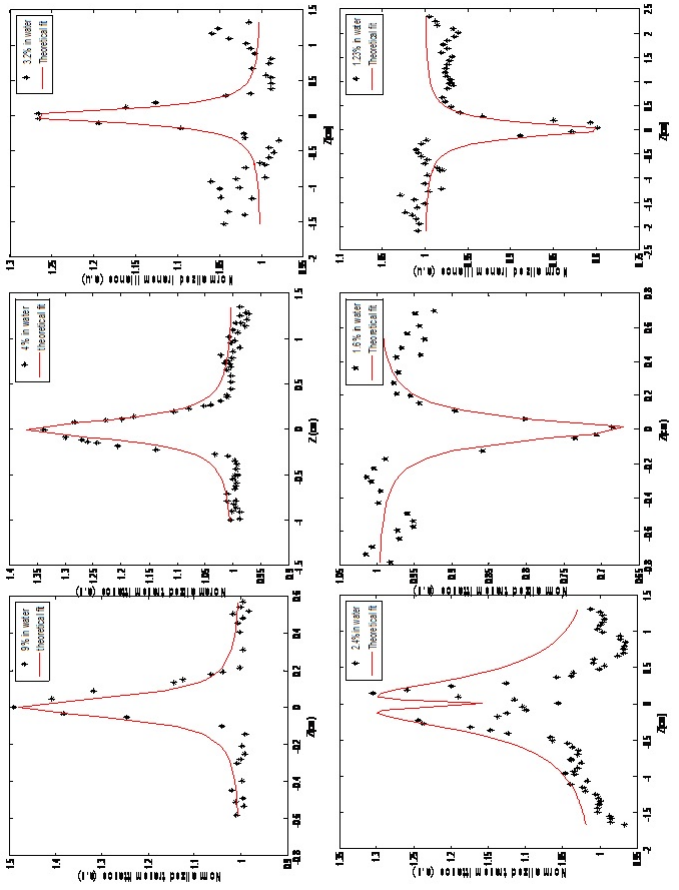

Figure 5.3: Open aperture Z scan curve of different concentration of betanin in water. The solid line shows the theoretical fit

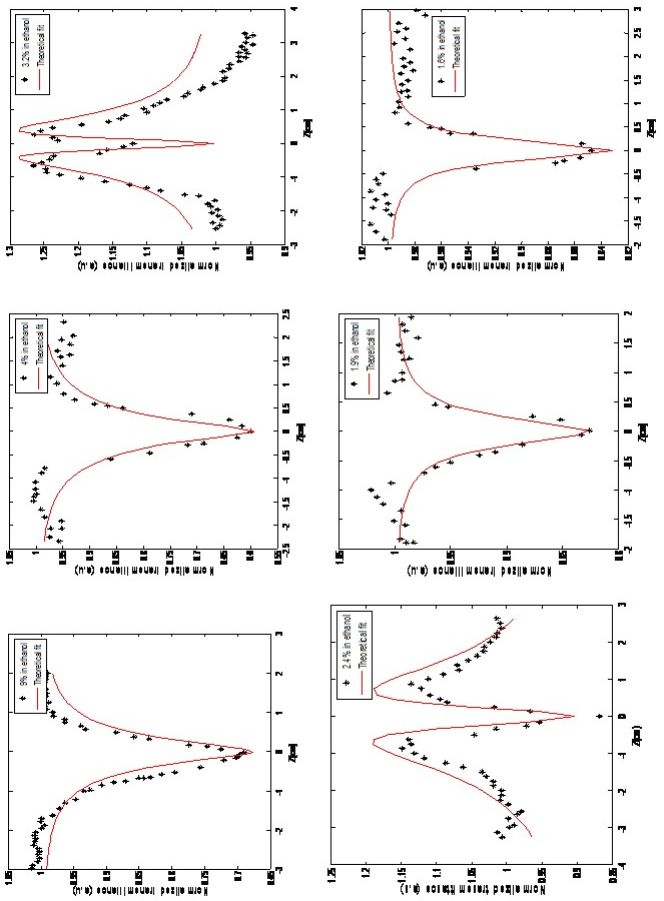

Figure 5.4: Open aperture Z scan curve of different concentration of betanin in ethanol. The solid line shows the theoretical fit

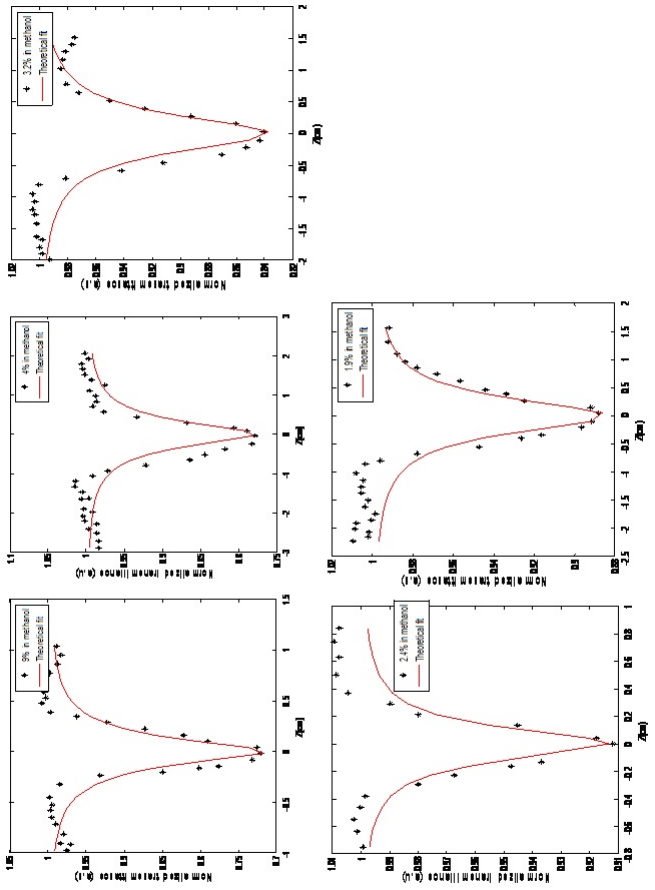

Figure 5.5: Open aperture Z scan curve of different concentration of betanin in methanol. The solid line shows the theoretical fit

Table 5.1: Polarity of solvents.

Solvent	Water(H_2O)	Ethanol(C_2H_6O)	Methanol(CH_4O)
Polarity index	9	5.2	5.0

the surrounding solvent. The betalain pigments are more extracted from the alcohol solution (yellow betaxanthins λ=480 nm) than from the water [21]. In alcohol solution such an association with -COOH group might be pronounced than water and this conjugation increases with the decreases of the polarity of the solvent. Hence the max shifts to longer wavelengths in ethanol and methanol, and the absorbance gradually increases from water to methanol. This observation suggests that the difference in energy spacing between π and π^* for the dye molecules may not be large in water and the full width half maximum (FWHM) increases with the decrease of polarity of the solvent ,which may be attributed to the interesting nonlinear behavior of betanin. From the point of view of the solvent influence, at a particular concentration, the β value increases as the solvent polarity increases, which is due to the increase of the degree of charge delocalization [22]. The decrease of polarity of the solvent also support our investigations which is indicated in table 5.1.

Thus inter molecular and intra molecular H bonding between dye and solvent molecules causes a change in the electronic distribution in the dye molecules. The observed switch over behavior could be due to the bleaching of the ground state band, i.e., in the case of the intraband transition, the ground-state electrons are pumped to the excited-state. The excited electrons are free carriers possessing a whole spectrum of energies, both kinetic and potential. Immediately after the absorption the electrons excited relax to the ground-state through electron-electron, electron-phonon and phonon-phonon interactions. Once these electrons are excited by a pulse close to absorption peak, they do not oscillate at the same frequency as that of the unexcited electrons, thus causing the ground-state band to bleach or reduce in intensity, which is almost synchronous with the primary photon absorption. Such change over in the sign of the non linearity is due to the interplay of the exciton bleaching and optical limiting mechanisms. The obtained values of the nonlinear parameters in different solvents are given in table 5.2. In the present case the irreversible damage induced by the input pulses and the presence of sucrose are supposed to play the significant role in the observed transition from SA to RSA on increasing concentration of betanin. Results of the present study provide additional mechanism for gain enhancement.

The optical limiting effects are of special interest in nonlinear optics and optoelectronics owing to their possible application for the protection of eyes and

Table 5.2: Measured values of the non linear optical parameters of betanin in different solvents at a wavelength of 532 nm for different concentration at input fluence of 436 MW/cm^2, β in(10^{-10} M/W), I_s in (MW/m ^{2}) and Im(χ^3) in (10^{-10} esu)

betanin (volume%)	water			ethanol			methanol			
	β	I_s	Im χ^3	β	I_s	Imχ^3	β	I_s	Imχ^3
9	-	0.101	-	3.091	-	0.070	3.036	-	0.069
4	-	0.160	-	3.452	-	0.078	2.215	-	0.050
3.2	-	0.089	-	-	0.177	-	1.526	-	0.034
2.4	-	0.107	-	-	0.089	-	0.0709	-	0.016
1.6	2.903	-	0.066	1.655	-	0.037	0.981	-	0.022
1.2	2.526	-	0.057	1.596	-	0.036	-	-	-

sensitive detectors against intense radiation and an important parameter in optical limiting phenomena is limiting threshold which defines the efficiency of optical limiting material[23].As shown in the Z-scan open aperture results, the betanin in deionised water, ethanol and methanol exhibited significant transmittance drop when the sample was moved to the vicinity of the focal plane. This transmittance drop is generally considered to be due to nonlinear absorption, nonlinear scattering, or combined effects. To characterize the optical limiting performance of betanin, we have directly measured the energy transmission as a function of fluence at 532 nm using 7 ns laser pulses. The results of betanin in three different solvents are shown in Figure 5.6.

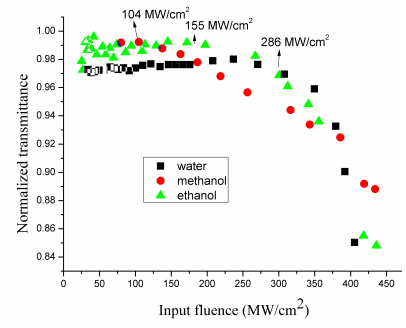

Figure 5.6: Optical limiting response of betanin in different solvents.

The deionized water, ethanol and methanol solutions exhibit significant transmittance changes as the input fluence is varied from 50 to 450 MW/cm^2, with the methanol solution showing the best result and the limiting threshold appearing to be 104 MW/cm^2. Comparing the optical limiting performance of dye molecules with their corresponding linear absorption spectra, it is observed that higher the linear absorption, better the limiting performance. Changing the solvent not only affect the linear absorption spectra, but also dramatically influence the non linear property and their optical limiting characteristics.

Figure 5.7 report CA Z-scan investigations of betanin natural dye for a fixed concentration (1.6%) in various solvents. It can be observed that the difference peak-valley transmittance as well as corresponding peak width changes with the polarity of the solvents. As illustrated in table 5.3 there is an increasing trend for the values of n_2 and χ^3 as the polarity increases. The negative sign of the CA Z-scan as well as the spatial Z-extension of the corresponding peak-valley are the indication of the dominance of the thermo-optic effect.

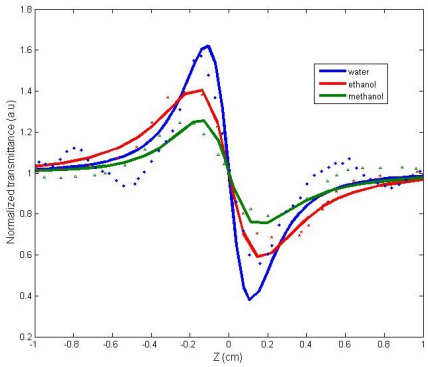

Figure 5.7: CA Z-scan measurements of the betanin natural dye in different solvents at input fluence of 436 MW/cm^2

Table 5.3: The measured parameters of betanin dye in CA Z-scan at input fluence of 436 MW/cm^2

solvent	n_2 *10^{-10}esu	Re(χ^3)*10^{-11} esu	χ^3*10^{-11} esu
water	-1.293	-2.058	2.161
ethanol	-1.047	-1.435	1.481
methanol	-0.862	-1.189	1.209

5.5 Conclusion

- In summary, our Z-scan experiments have revealed interesting features of the nonlinear absorption properties of betanin natural dye in different solvents.
- Nonlinear absorption coefficients and saturation intensity were estimated by performing numerical fitting to the experimental data.
- Both inter molecular and intra molecular H bonding has profound effect on the nonlinear optical properties of betanin.
- The solvent modified the linear absorption spectra and nonlinear behavior of betanin natural dye.
- The simultaneous occurrence of the nonlinear behavior of betanin in different surrounding media can be made use of in developing various photonic devices.
- The fact that reverse saturable absorption exists in the vicinity of the linear absorption band combined with the possible two-photon absorption

makes betanin a very promising candidate for optical limiting applications.

- The negative sign of the CA Z-scan as well as the spatial Z-extension of the corresponding peak-valley are the indication of the dominance of the thermo-optic effect.

5.6 References

[1] Angel Ramon Hernandez-Martinez , Miriam Estevez , Susana Vargas , Fracisco Quintanilla and Rogelio Rodriguez "New Dye-Sensitized Solar Cells Obtained from Extracted Bracts of Bougainvillea Glabra and Spectabilis Betalain Pigments by Different Purification Processes" Int. J. Mol. Sci.,12, 5565-5576 (2011)

[2] Cody Sandquist and Jeanne L. McHale "Improved efficiency of betanin-based dye-sensitized solar cells" J. Photochem. Photobiol., A: Chem. 221 ,90-97 (2011)

[3] Jackman, R.L. & Smith, J.L. "Anthocyanins and betalains. In: Natural food colourants" (eds. G.F. Hendry & J.D. Houghton).pp. 244-309. London: Blackie Academic & Professional.(1996)

[4] R. Castellar, J. M. Obn, M. Alacid and J. A. Fernndez-Lpez, "Color properties and stability of betacyanins from Opuntia fruits"J. Agric. Food Chem. 51, 2772-6 (2003).

[5] Pedreno MA and Escribano J. "Correlation between antiradical activity and stability of betanine from Beta vulgaris L roots under different pH, temperature and light conditions" J. Sci. Food. Agric,.81:627-631 (2001)

[6] Kimler L, R.A. Larson, L. Messenger, J.B. Moore and T.J. Mabry, "Betalamic acid, a new naturally occurring pigment" J. Chem. Soc., 21, 1329-1330 (1997)

[7] E. L. Attoe and J. H. von Elbe, "Degradation kinetics of betanin in solutions as influenced by oxygen" J.Agr. Food.Chem.30(4),708-712 (1982)

[8] Herbach K.M, M. Rohe, F.C. Stintzing and R. Carle, "Stability and color changes of thermally treated betanin, phyllocactin, and hylocerenin solutions" J. Agric. Food Chem., 54,390-398(2006).

[9] Stintzing F.C and R Carle"Betalain-emerging prospect for food scientist". Trends Food Sci. Technol., 18, 514-525 (2007)

[10] Strack D, T. Vogt and W. Schliemann "Recent advances in betalain research" Phytochem., 62: 247-269 (2003).

[11] Herbach K.M, F.C. Stintzing and R. Carle, "Thermal degradation of betacyanins in juices from purple pitaya (Hylocereus polyrhizus [Weber] Britton and Rose) monitored by high-performanceliquid chromatography-tandem mass spectrometric analyses" Eur. Food Res. Technol., 219, 377-385 (2004)

[12] K.M Herbach, F.C Stintzing and R Carle "Betalain stability and degradation structural and chromatic aspects". J. Food Sci., 71, 41-50 (2006).

[13] Dongshe Zhang , Suzanne M. Laniera, Jonathan A. Downing ,Jason L. Avent , June Lumc and Jeanne L. McHalea "Betalain pigments for dye-sensitized solar cells" J. Photochem. Photobiol., A: Chem. 195 ,72-80 (2008)

[14] Y. Z. Cai, M. Sun and H. Corke, "Characterization and application of betalain pigments from plants of the Amaranthaceae" Trends Food Sci Tech 16, 370-376(2005).

[15] Strack, D., W. Steglich, V. Wray "Betalains. In Methods in plant biochemistry"(eds P.M Dey & J.B Harborne) "Alkaloids and sulphur compounds" (ed. P.G Waterman) Academic Press London,8,UK , 421-450,(1993)

[16] Francis F. J. "Anthocyanins and betalains". In F.J Francis (Ed.), Colorants. St Paul, MN: Eagan Press, 55-66,(1999)

[17] M. Sheik-Bahae, A.A. Said, T.H. Wei, D.J. Hagan and E.W. Van Stryland "Sensitive Measurement of Optical Nonlinearities Using a Single Beam" IEEE J. Quant. Electron. 26, 760 (1990)

[18] J.R.Lakowicz: Principles of Fluorescence spectroscopy. Kluwer academic Publishers, New York (1999)

[19] Wouter Verbouwe, Lucien Viaene, Mark Van der Auweraer, Frans C. De Schryver, H. Masuhara, R.Pansu and J. Faure ," Photoinduced Intermolecular Charge Transfer in Diphenylamino-Substituted Triphenylbenzene,Biphenyl, and Fluorene" . J. Phys. Chem. A. 101, 44,8157 - 8165 (1997)

[20] Q. Shiliang, G. Yachen, J. Xiongwei, Z. Huidan, S. Yinglin, Q. Jianrong, Z. Congshan and K. Hirao, "Nonlinear absorption and optical limiting in gold-precipitated glasses induced by a femtosecond laser" , Opt. Commun. 224 , 321-327 (2003)

[21] Henriette M.C.Azeredo "Betalains: properties, sources, applications, and stability a review" Food Sci. Technol. Int., 44, 2365-2376 (2009)

[22] Paresh Chandra Ray and Jerzy Leszczynski "Two-photon absorption and first nonlinear optical properties of ionic octupolar molecules: structure-function relationships and solvent effects" J. Phys. Chem. A, 109, 6689-6696 (2005)

[23] R. Tintu, V.P.N. Nampoori, P. Radhakrishnan and Sheenu Thomas "Nanocomposite thin Films of $Ga_5Sb_{10}Ge_{25}Se_{60}$ chalcogenide glass for optical limiting applications" Opt. Mater. 33,1221-1225 (2011)

Chapter 6

Nonlinear optical characterization of bio-inspired hybrid materials

6.1 Abstract:

In this chapter, we report the intensity dependent nonlinear absorption properties of bio-inspired hybrid materials (betanin-ZnO) embedded in polymeric matrices through the Z-scan technique using an Nd: YAG laser (532 nm, 7 ns, 10 Hz).We observe a change over in the sign of nonlinearity due to the interplay of exciton bleaching and optical limiting mechanisms. Light confinement effect and ship- in-a bottle effect play crucial roles. Theoretical analysis has been performed using a model based on nonlinear absorption coefficient and saturation intensity. The results of the present study gives additional mechanism for the gain enhancement in dye doped ZnO matrix.

Result of this chapter is published in

- Aparna Thankappan,Sheenu Thomas, V. P. N. Nampoori "Effect of betanin natural dye extracted from red beet root on the non linear optical properties ZnO nanoplates embedded in polymeric matrices" Journal of Applied Physics,112, 123104 (2012)

6.2 Introduction

As we know, a great variety of low dimensional-related studies hold the attention of many researchers because of their amazing non-linear optical properties and their possible applications in many fields mainly in DSSC[1] and that they possess high nonlinear refraction (NLR) and/or nonlinear absorption (NLA). Optical materials with large coefficients of reverse saturable absorption (RSA) and nonlinear refraction can exhibit irradiance-dependent transmittance and phase shift, which co-operatively limit the throughput fluence (optical energy per unit of area) [2]. Materials with large optical nonlinearity are key elements in many areas of photonics and optical technology such as all-optical switching (optical computer) devices, three dimensional fluorescence imaging, and optical limiting.

One approach to the design of technologically important class of oxide materials is the incorporation of the natural organic molecules to modify inorganic nano/microstructures. In this instance, the inorganic oxide contributes to the enlarged functionality by the structure-function relationship of hybrids and which exhibits an interface where there is a synergistic interaction between the organic and inorganic components. These organic inorganic frameworks are particularly attractive from several perspectives such as they possess a remarkable chemical and structural diversity. It has influence on the biomineralization, hydrogen bonding, and hydrophilic-hydrophobic interactions. The ability to connect the functionalities to the material expands the scope of the science significantly. The chemistry of such nanocomposites depends mainly on their reactivity and structural relationship. Their development is especially trendy and has received a great deal of attention not only because of their potential in industrial applications but also from their fundamental point of view.

Such hybrid materials synthesized through green materials will generate increasing numbers of smart microelectronics, micro-optical and photonic components and systems and novel generations of photovoltaics. The term green materials generally stands for substances made from sustainable or recyclable items that do not exhaust the natural resources and are also non-toxic, ecofriendly and safer alternatives for human life. These hybrid materials also can provide promising applications in optics, electronics, ionics, mechanics, membranes, functional and protective coatings, catalysis, sensors and biology.

The organic-inorganic composites offer tremendous opportunities in material engineering to produce suitable materials with wonderful tailored physical properties. Sufficient attention has not been paid towards the proper utiliza-

tion of their capabilities in photonic device applications. Thus, there exists a pressing need to develop novel optical materials, for which a deep insight into the optical processes is essential. By intercalating dye molecules which exhibit strong nonlinear absorption, Canva et al. have demonstrated their usefulness for true 3D displays [3].

The present work is an attempt to design and characterize efficient optical materials embedded in a PVA matrix and the effect of betanin natural dye on their non-linear optical properties of ZnO crystals will be discussed using open aperture (OA) Z-scan technique.

6.3 Experimental method

The ZnO dumb bell microrods : PVA , ZnO nanoflakes : PVA , ZnO nanoplates and ZnO microrods : PVA were prepared for the Z-scan measurements; using aqueous solution of zinc nitrate hexahydrate ($Zn(NO_3)_26H_2O$) and hexamethylenetetramine (HMTA)($(CH_2)_6N_4$). The synthesis procedure was discussed in the previous chapter. The extracts of the red beetroot were obtained from fresh biological materials, pigments can be water extracted and slight acidification of the extraction medium enhances the betacyanin stability and avoids oxidation. The pigments extracts must be protected from direct light exposure should be kept in cool place. Dye extracts have been optically characterized by measuring maximum absorptivity at about 535 nm, using a UV/Vis spectrophotometer (Jasco V-570 UV/VIS/IR.)

To determine third order non linear optical characteristics of samples such as non linear absorption , the single beam Z-scan technique proposed and demonstrated by Sheik-Bahae et al[4],was employed. The details of which is already discussed in chapter 4. To avoid sedimentation of nanocrystals, the solution was centrifuged and washed several times and finally embedded into the polyvinyl alcohol solution and developed the free standing films of thickness around 80μm were developed (Plasto Mek, delta.0.2kW, 230V, 1 phase), which were used as samples. The transmission of a laser beam that changes near the focal point during the sample translation along the propagation path through an open-aperture (OA) was measured. A Q-switched Nd: YAG laser (Spectra Physics LAB-1760, 532 nm, 7 ns, 10Hz) was used as the light source.

6.4 Results and discussions

The linear absorption spectra of ZnO crystals in PVA, betanin doped crystals in PVA and betanin in PVA are shown in the following figures 6.1 and 6.2.

In the linear absorption spectra of betanin natural dye, the peak around 535 nm is attributable to betanin.

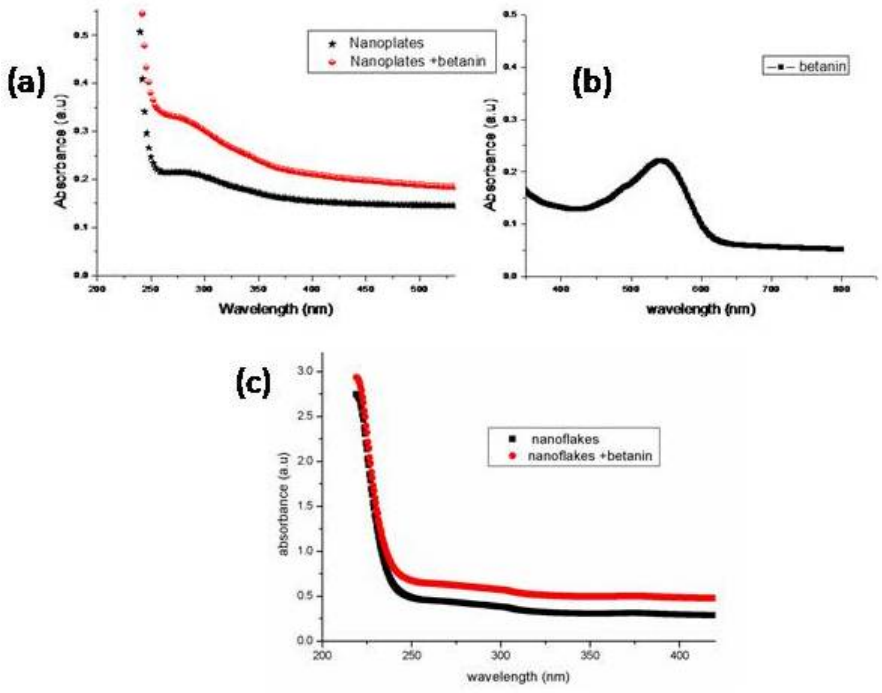

Figure 6.1: The UV-VIS absorption spectrum of the ZnO nanoplates/ PVA and dye doped nanoplates/ PVA composite film (b) corresponding of betanin/ PVA (c) that of ZnO nanoflakes/ PVA

The nonlinear absorption was measured from the normalized energy transmission using Z-scan without an aperture. Figure 6.3 shows the plot related to open aperture Z-scan experiment in betanin films at resonance wavelength of 532 nm with different input fluence. When the sample is away from the focus, the weak intensity cannot induce any nonlinearity, and have unit transmittance. As the sample is moved towards the focus, the transmittance acutely decreases with increasing light intensity to less than unity, resulting in induced absorption [5]. The data is analyzed using the procedures described by SheikBahae et al. for a two-photon absorption (TPA) process.

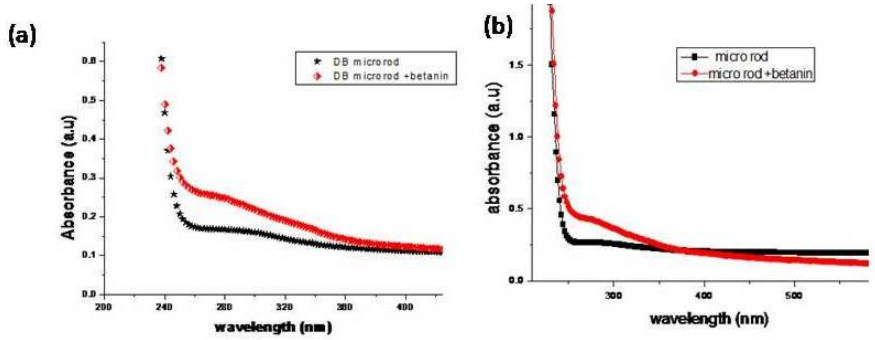

Figure 6.2: (a) The UV-VIS absorption spectrum of the ZnO DBl microrods/PVA and dye doped DBl micro rods/PVA composite film (b) that of ZnO simple microrods/PVA.

In general, induced absorption can occur in nanoclusters and in betanin natural dye, due to a variety of processes such as excited state absorption, two-photon absorption, interband and intraband transitions and nonlinear scattering.[6,7] The theory of two photon absorption process fitted well with the experimental curve, indicating that TPA is the basic mechanism for induced absorption. To estimate the role of betanin in ZnO crystals, we also performed open aperture Z-scan measurement on betanin alone and betanin doped ZnO/PVA. No obvious non linear absorption effect was found for PVA alone [8].At the resonant wavelength of 532nm, the optical non linearity increases with the input fluence. Figure 6.4 to figure 6.7 shows the combined open aperture curve for the ZnO samples /PVA sample and the effect of betanin on the ZnO/PVA.

We assume the -COOH on the five membered rings to be the most acidic of the three carboxylic acid groups on Betanin. Surprisingly, due the acid treatment the RSA behavior of the nanoplates switched to SA at input fluence of 319 MW/cm^2 and 363 MW/cm^2 and again the increase of the fluence the RSA behavior was retained[9,10]. From the non-linear optical behaviour of the controlled morphologies of ZnO, it is clear that the influence of dye diminishes at higher fluencies. The observed switch over behaviour could be due to the bleaching of the ground state band, i.e., in the case of the intraband transition, the ground-state electrons are pumped to the excited-state. Moreover, the observed switch over behaviour of ZnO rods is due to confinement structure formed by the hexagonal boundaries of the rods and due to the multi photon absorption or by the consecutive absorption of two or more photons from the organic dye species. This can be thought of, as some types of confinement of

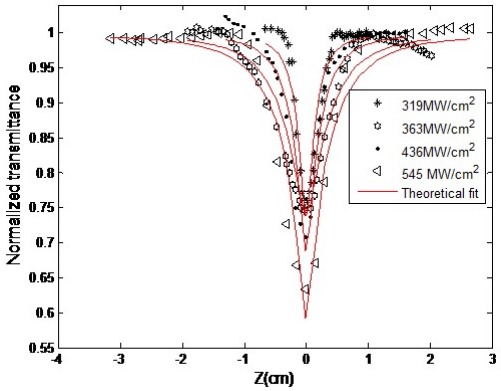

Figure 6.3: Open aperture Z scan curve of betanin/PVA composite film at different input fluences

radiation are more in rod shaped structures. We consider that they can both confine an externally launched light into its cavity structure formed by the hexagonal boundaries, and undergo multiple total internal reflections from the hexagonal facets, which provides an enhanced effective optical path length to confine the light and increases the communication between the excitation light and ZnO [11]. The proof of such confinement was depicted in the previous chapter.

The intercalation of organic component (dyes) into the matrix can dramatically influence the micro/nano structures of inorganic oxides, which providing a method for the design of technologically important novel materials and their non-linear response depends on the types of the aggregation of the individual molecules (monomers) (either J- aggregates: head-to-tail orientation or H aggregates: parallel orientation) and they coherently respond to optical excitation. In such an environment, the number of excited state deactivation pathways that are available for return to the ground state after photo excitation is substantially high as the ground state recovery is depend not only on the intrinsic properties of the individual molecules but also on their aggregates. The light induced processes of the dye molecule make a shielding effect to the semiconductor. This physical necking effect of the photoactive dye molecules will modify the physical and chemical processes of the excited states. Besides this physical necking, the dye molecules try to fit inside the internal cavities of ZnO which enhances the trapping of electrons within the cavities just like ship-in-a-bottle[12] and reveals a complex chemistry at the organic - inorganic interface. This effect is stronger in the case of one dimensional structure. The

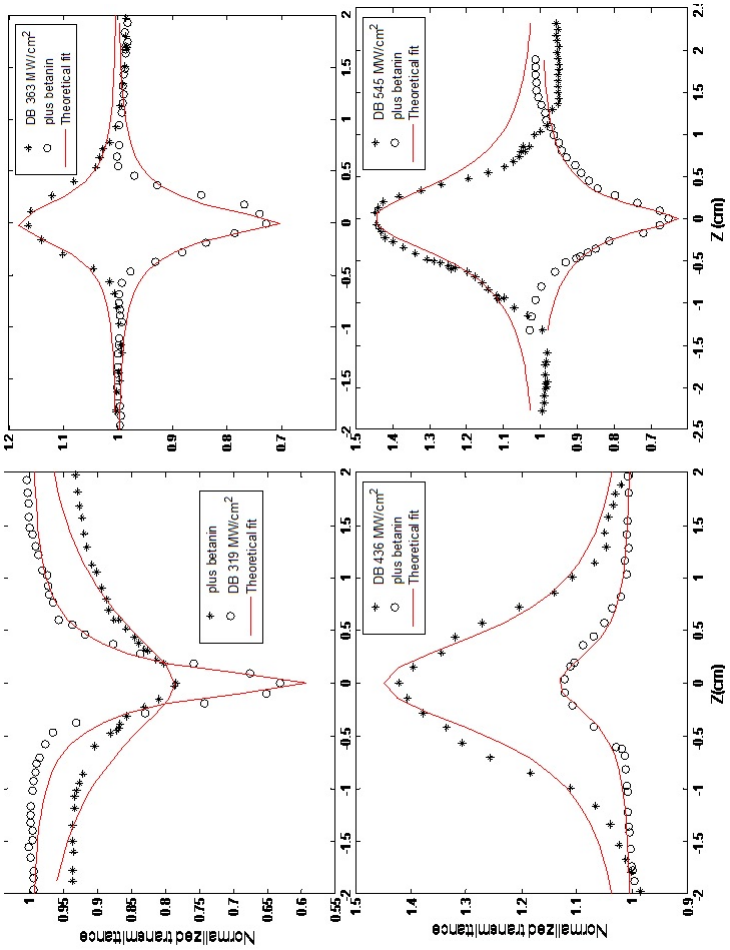

Figure 6.4: Open aperture Z scan curves showing the effect of betanin on ZnO DB microrods (a) 319 MW/cm^2, (b) 363 MW/cm^2, (c) 436 MW/cm^2, and (d) 545 MW/cm^2. The solid line shows the theoretical fit.

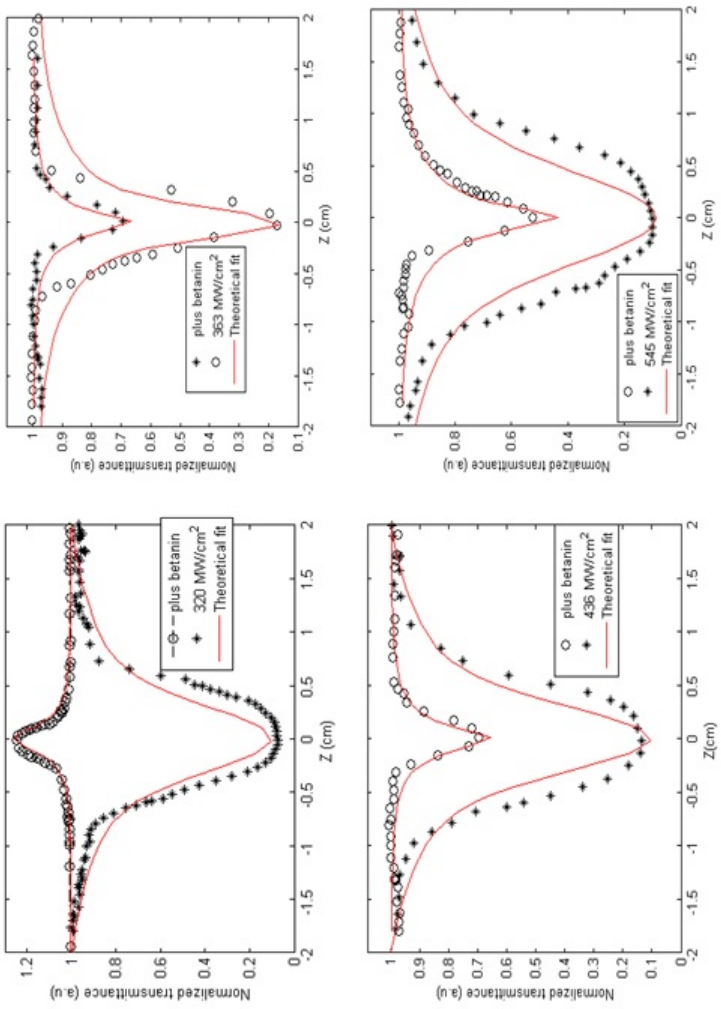

Figure 6.5: Open aperture Z scan curves showing the effect of betanin on ZnO nanoflakes (a) 319 MW/cm^2, (b) 363 MW/cm^2, (c) 436 MW/cm^2, and (d) 545 MW/cm^2.The solid line shows the theoretical fit

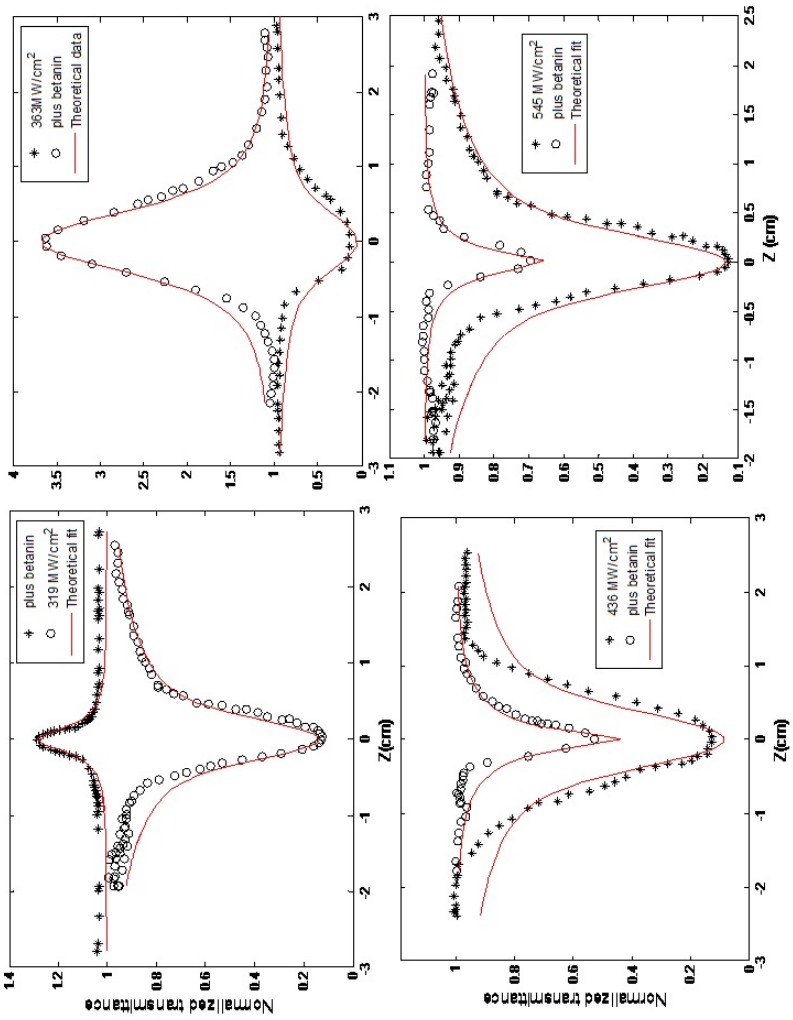

Figure 6.6: Open aperture Z scan curves showing the effect of betanin on ZnO nanoplates (a) 319MW/cm^2 (b) 363 MW/cm^2 (c) 436 MW/cm^2 and (d) 545MW/cm^2 .The solid line shows the theoretical fit

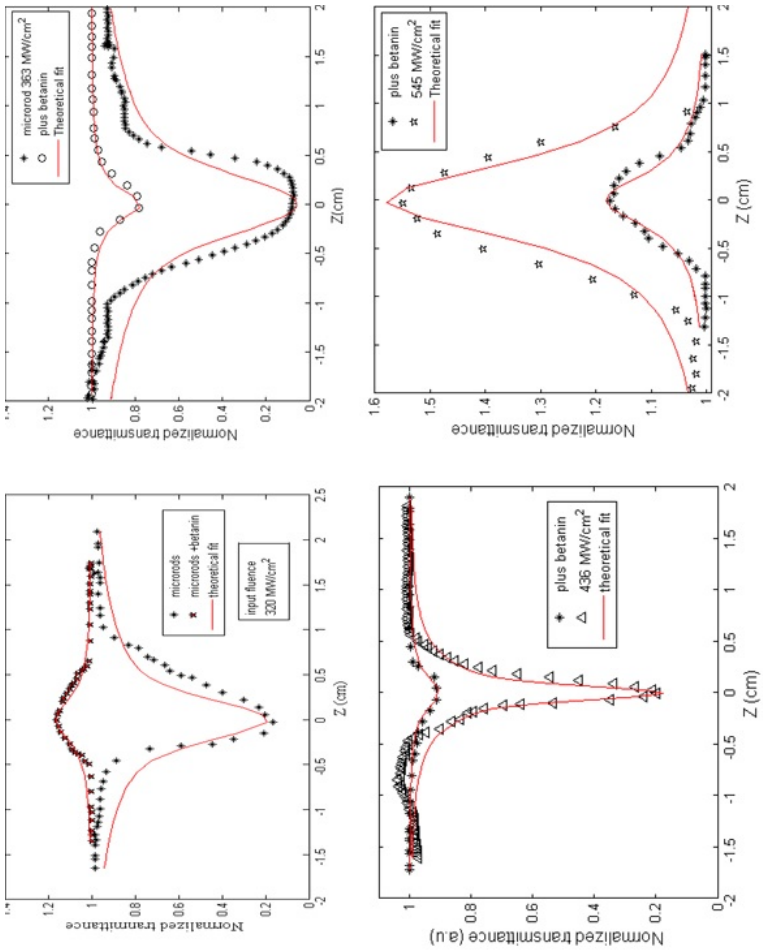

Figure 6.7: Open aperture Z scan curves showing the effect of betanin on ZnO microrods (a) 319 MW/cm^2 (b) 363 MW/cm^2 (c) 436 MW/cm^2 and (d) 545 MW/cm^2.The solid line shows the theoretical fit.

laser induced heat play another crucial role in their non-linear response. The laser induced heat causes an increase in the kinetic energy given to the dye molecules which are held together by hydrogen bonds ,making them vibrate an eventually breaking the bonds. As the temperature increases however, they no longer function properly.The schematic representation of occurred processes in the betanin-ZnO hybrids is shown in figure 6.8.

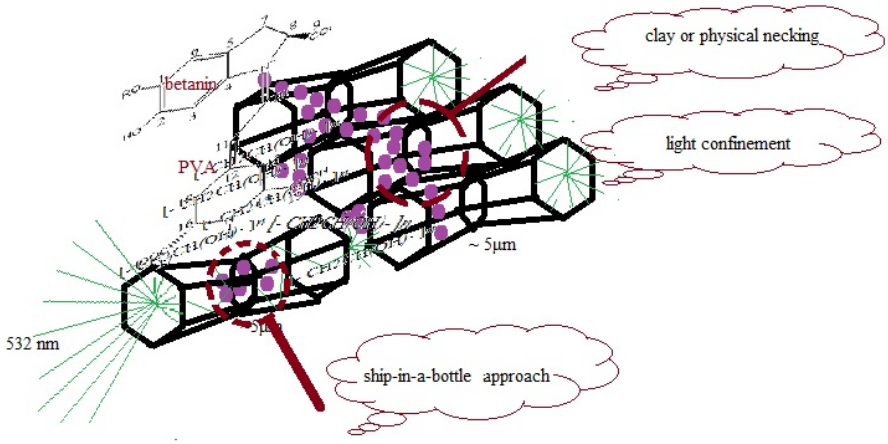

Figure 6.8: Schematic representation of the occurred processes in betanin -ZnO hybrids

Due to the high power irradiation, it is likely that irreversible photo bleaching of the dyes within the polymer matrix would result and the dyes may undergo intersystem crossing (ISC) to the long lived triplet sate, then chemically react with surrounding polymer environment. The dye degradation still occurs through the higher intensity of irradiation, but not the host matrix. The light absorption in betanin excites π electrons of the pigment chromophore to a more energetic state (π *), increasing reactivity or lowering activation energy for the molecule[13].It is possible that the presence of other compounds than the dye itself, e.g., sucrose, can affect the optical non linearity , if it is not a highly purified extract. Irreversible damage induced by the input pulses is also the another factor. The outstanding optical properties of these composite films are due to their inorganic-organic hybrid nature.

An enhancement of the gain in ZnO crystals: PVA matrix is observed on

Table 6.1: The β values of various films

	β (m/GW)
betanin	4.37±1
DB microrods	6.63
dye doped DB microrods	3.8± 0.4
nanoflakes	4.05 ±1.5
dye doped nanoflakes	2.55 ± 0.5
nanoplates	4 ±2
dye doped nanoplates	3±0.5
microrods	4.95±1.7
dye doped microrods	1.53±0.9

Table 6.2: The average value of Im (χ^3) e.s.u of various films

	average value of Im (χ^3) e.s.u
betanin/PVA	$1.891*10^{-10}$
DB/betanin/PVA microrods	$1.616*10^{-10}$
DB microrods/PVA	$2.8674*10^{-10}$
nanoflakes/betanin/PVA	$1.347 *10^{-10}$
nanoflakes/PVA	$1.887*10^{-10}$
nanoplates/betanin/PVA	$1.7027*10^{-10}$
nanoplates/PVA	$2.432 *10^{-10}$
microrods/betanin/PVA	$0.6622*10^{-10}$
microrods/PVA	$2.859 *10^{-10}$

the addition of the betanin. This is attributed to the visible transition of betanin which is well described as a HOMO→LUMO excitation from the aromatic ring to the matrix. The pump beam (532 nm) will excite both dye and crystals by one photon and two photon absorption respectively. We assume that betanin and ZnO crystals form a complex making an additional energy level which saturates the absorption at higher intensity, but on further increase of intensity the complex will absorb more leading to induced absorption. Further pump power increases, RSA will become SA and again switching back to RSA is observed. The excited dye molecules transfer their energy to the nanoplates leading to the intraband electron excitation causing ground state bleaching at input fluence up to 363 MW/cm^2 leading to saturable absorption, but further increase of intensity the behavior switches to induced absorption. The change over in the sign of the non-linearity is due to the interplay of the exciton bleach and optical limiting mechanisms. Switchover from SA to RSA on increase of the input intensity has been observed in various materials under nanosecond and picoseconds pulse excitation [14,15,16]. The estimated values of β (m/GW) and Im (χ^3) of various films are tabulated in table 6.1 and 6.2.

In the present case the irreversible damage induced by the input pulses and the presence of sucrose are supposed to play the significant role in the observed transition from SA to RSA on increase of input fluence. Therfore, the role of instantaneous two photon absorption in non linear effect observed at the intensity above 363 MW/cm^2 is significant. In figure 6.5 (a & b)the theoretical fit give the saturation intensity I_s=0.199 MW/m^2 and 1.046 MW/m^2 respectively. Results of the present study provide additional mechanism for gain enhancement.

6.5 Conclusion

- In summary, Z scan experiments have revealed interesting features of non linear absorption properties of betanin doped ZnO embedded in PVA at 532 nm excitation.
- The betanin plays the important role in the non linear optical behavior of ZnO.
- As evidenced by the structures of ZnO, the component of organic materials is not simply "clay"(i.e. physical necking) and exerts a pronounced influence on the structure. The trapping of electrons within the cavities of these composite oxide materials belies a simple "ship-in-a-bottle" approach and reveals a complex chemistry at the organic - inorganic interface.

- Due to the simultaneous occurrences of non linear processes this system can be made use of in developing various photonic devices.

6.6 References

[1] C.Y Jiang,X.W. Sun,G.O Lo and D.L Kwong " Improved dye sensitized solar cells with a ZnO nanoflower photo anode" J.appl. Phys let. 90,263501(2007)

[2] Tai-Huei Wei, Tzer-Hsiang Huang, Tzung-Tao Wu, Pei-Chang Tsai and Mu-Shih Lin "Studies of nonlinear absorption and refraction in C 60 /toluene solution" Chem. Phys. Lett. 318,53-57 (2000)

[3] Canva, M, Roger G, Cassagne F, Levy Y, Brun A, Chaput F, Boilot J.P, Rapaport A, Heerdt C, Bass M."Dye-doped sol-gel materials for two-photon absorption induced fluorescence" Opt. Mater., 18, 4,391-396 (2002)

[4] M. Sheik-Bahae, A.A. Said, T.H. Wei, D.J. Hagan and E.W. Van Stryland, "Sensitive Measurement of Optical Nonlinearities Using a Single Beam" IEEE J. Quant. Electron. 26 , 760 (1990).

[5] Misha hari, Santhi ani joseph, Nithyaja balan,Mathew S, Ravi kumar, Giridhar mishra, R. R. Yadhav, P. Radhakrishnan and V. P. N. Nampoori " Linear and nonlinear optical properties of gold nanoparticles stabilized with polyvinyl alcohol" J. Nonlinear Opt. Phys.,20, 4,467-475 (2011)

[6] Q. Shiliang, G. Yachen, J. Xiongwei, Z. Huidan, S. Yinglin, Q. Jianrong, Z. Congshan and K. Hirao, "Nonlinear absorption and optical limiting in gold-precipitated glasses induced by a femtosecond laser", Opt. Commun. 224, 321-327 (2003).

[7] Stephen E. Bialkowski "Progress toward a better understanding of signal generation in laser-excited photo thermal spectrometry of homogeneous samples" TrAC, Trends Anal. Chem.,17,8,9,(1998)

[8] B. Nithyaja,H. Misha, P. Radhakrishnan, and V. P. N. Nampoori "Effect of deoxyribonucleic acid on nonlinear optical properties of rhodamine 6g-polyvinyl alcohol solution" J. Appl. Phys., 109, 023110 (2011)

[9] Aparna Thankappan, Divya S. Sheenu Thomas and V.P.N. Nampoori "Optical characterization of ZnO nanoplates embedded in polymeric matrices for optical limiting applications" Opt Laser Technol 52,37-42(2013)

[10] Aparna Thankappan,Sheenu Thomas and V. P. N. Nampoori "Effect of betanin natural dye extracted from red beet root on the non linear optical properties ZnO nanoplates embedded in polymeric matrices" J. Appl. Phys.,112, 123104 (2012)

[11] Aparna Thankappan , Misha Hari, S. Mathew, Santhi Ani Joseph, Erni Rolf ,Debajeet Bora , Artur Braun and V.P.N. Nampoori " Synthesis of monocrystalline zinc oxide microrods by wet chemical method for light confinement applications" Physica E 44 ,2118-2123, (2012)

[12] Pamela J. Hagrman, Douglas Hagrman, and Jon Zubieta "organic- Inorganic Hybrid Materials: From Simple Coordination Polymers to Organodiamine-Templated Molybdenum Oxides" Angew. Chem. Int. Ed., 38, 2638,2684(1999)

[13] H. M. C. Azeredo "Betalains: properties, sources, applications, and stability -a review" Int. J. Food Sci. Technol.44, 2365-2376 (2009).

[14] Rao S V, Srinivas N K M N and Rao D N "Nonlinear absorption and excited state dynamics in Rhodamine B studied using Z-scan and degenerate four wave mixing techniques" Chem. Phys.Lett. 361,439-45 (2002)

[15] Gao Y, Chang Q, Ye H, Jiao W, Song Y, Wang Y and Qin "Saturable and reverse saturable absorption of a linear polymer in dimethylformamide" J Appl. Phys. B 88,2, 255-8 (2007)

[16] Srinivas N K M N, Rao S V and Rao D N "Saturable and reverse saturable absorption of Rhodamine B in methanol and water" J. Opt. Soc. Am.B 20 ,2470 (2003)

Chapter 7

ZnO crystals for dye sensitized solar cell applications

7.1 Abstract:

Performances of dye sensitized solar cells (DSSC) based on betanin natural dye with various photoanodes on transparent conducting oxide glass have been investigated. Moreover, the influences of various electrolytes have been studied. Cell efficiency of 2.99% and overall photon to current conversion efficiency of (IPCE) 20% were achieved using ZnO nanosheet (NS) electrode with iodide based electrolyte in acetonitrile (ACN) solution. To enhance solar harvesting in organic solar cells, uniform sized metal nanoparticles (NP) (gold (Au)) synthesized via microwave irradiation method were incorporated into the device consisting of ZnO NSs. Enhanced power conversion efficiency of 1.71% ZnO/Au nanocomposite was achieved compared to the 0.868% efficiency of the bare ZnO NPs DSSC with ferrocene based electrolyte. We also report heterojunction DSSC using ZnO composites synthesized through a simple facile two step solution growth method using pre-existing textured ZnO, ZnS, CdS and TiO_2 seeds and also a ZnO DSSC decorated with highly conducting and chemically stable titanium nitride (TiN) NPs.

Result of this chapter is accepted in

- Aparna Thankappan, Divya S, Anju.K. Augustine, Girijavallaban C.P, Radhakrishnan P, Sheenu Thomas, V.P.N. Nampoori "Highly efficient betanin dye based ZnO and ZnO/Au Schottky barrier DSSC" Thin solid films

7.2 Background

As the world is becoming more progressive in technology and economy, more energy is being consumed to keep up with the development and the demand on energy has boomed over the past years. The reduction of petroleum resources in this century and raising awareness of environmental change caused by the combustion of fossil fuels make nations and public reconsider the importance of exploring renewable energy sources. The results of the 2013 WEC (World Energy Council), World Energy Resources survey show that there are more energy resources in the world today than 20 years ago, or ever before. Solar energy is the most abundant permanent energy resource on earth and it is available for use in its direct (solar radiation) and indirect (wind, biomass, hydro, ocean etc.) forms. The supply of the energy from the Sun to the Earth is $3*10^{24}$ joules a year [1]. Even if only 0.1% of this energy can be converted at an efficiency of only 10%, it would be four times larger than the total worlds electricity generating capacity of about 5000GW [2]. Therefore, solar photovoltaic technology has received considerable attention as a potentially more secure sustainable energy source. The spectrum of the solar light that reaches the earth is influenced by absorption of radiation in the earths atmosphere and also by the path length of the photons through the atmosphere. Figure 7.1 shows the solar irradiance and photon flux at an air mass of 1.5 (AM1.5G) [3]. The AM1.5G spectrum corresponds to an angle between the incident solar radiation and the zenith point of the measurements of 42^0, and integrates to 1000 Wm^{-2}. The photon flux is important in determining the number of electrons that are generated, and the current produced, from a solar cell. The region between 400 and 1100 has the maximum photon density in the AM 1.5 solar spectrum. A material that can absorb sunlight between 400 and 1000 nm would be the ideal absorber. Silicon solar cells accomplish this task, because silicon's bandgap is 1.1 eV. Silicon solar cells small bandgap allows it to absorb light up to 1100 nm. While silicon-based technologies have been developed to harness solar energy efficiently; they are not yet competitive with fossil fuels mainly due to the high production costs. It is an urgent task to develop much cheaper photovoltaic devices with reasonable efficiency for widespread application of photovoltaic technology. In this context, dye sensitized solar cells (DSSCs) have emerged as an important alternative to conventional silicon solar cells.General comparison between semiconductor based solar cells and DSSC is presented in table 7.1.

By the successful combination of porous nanocrystalline TiO_2 electrodes and novel Rubipyridl complex, Grätzel and his co-workers developed a solar cell to imitate photosynthesis -the natural processes plants convert sunlight into energy, with energy conversion efficiency exceeding 7% in 1991 [4] and 10% in 1993 [5]. In order to achieve efficient light harvesting charge separation and trans-

Table 7.1: Comparison between semiconductor solar cell and DSSC

	semiconductor solar cells	DSSC
Transparency	opaque	transparent
pro-environment (material & process)	normal	great
cost	high	low
efficiency	high	normal
color	limited	various

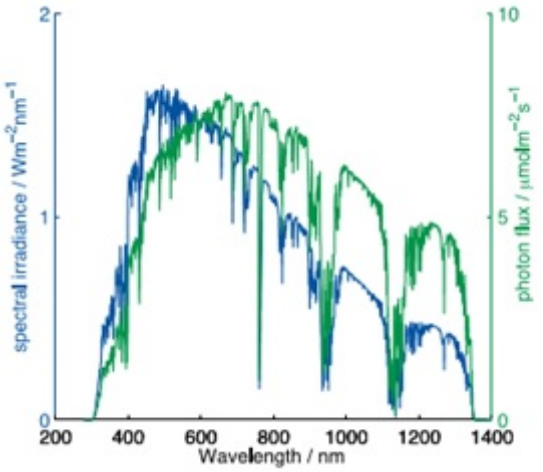

Figure 7.1: Solar irradiance and photon flux at AM1.5G illumination

port, the choice of nanostructured oxide and corresponding TCO films becomes a critical issue in cell design [6]. In DSSC, charge separation is accomplished by kinetic competition like in photosynthesis leading to photovoltaic action. The monolayer of organic dye in DSSC replaces chlorophylls (light absorbing pigments), the wide bandgap nanostructured semiconductor layer replaces oxidized dihydro-nicotinamide-adenine-dinucleotide phosphate (NADPH), and carbon dioxide acts as the electron acceptor. Besides, the electrolyte replaces the water whereas oxygen as the electron donor and oxidation product, respectively [7,8].The research activity as well as the industrial attention in this technology is growing fast.

Ruthenium- containing metalorganic complexes have been favoured in DSSCs due to their strong absorption of visible light, favourable spatial separation of HOMO (highest occupied molecular orbital) and LUMO (lowest unoccupied molecular orbital) and their ability to get repetitively oxidized and reduced without degradation[9]. The best reported devices of this class which convert solar energy to electrical energy has an efficiency of 10-11% [10-12]. Recently, the efficiency of DSSCs has improved to 12.3% by the combination of co-sensitization of porphyrin dyes and a cobalt-complex redox mediator[13]. However, synthetic dyes have offered problems as well, such as complicated synthetic routes, whereas natural dyes are more organic, or better for the environment, or safer to use, than synthetic dyes. Due to their cost efficiency, non-toxicity and environmental benefits, DSSCs based on natural dyes have

been at the center of intense research. Great efforts are directed towards increasing the efficiency by reducing the cost further and by making the price comparable to traditional energy resources.

Natural pigments from plants such as chlorophyll [14], anthocyanin [15] have been extensively examined as sensitizers for the DSSC. Betalains are a class of vegetal pigments, have favourable light absorption, existing in nature in association with various co-pigments such as the betalamic acid, indicaxathin, betanidin. These modify their light absorption properties and are capable of forming complex metal ions, possessing the requisite functional group (-COOH) to bind also to ZnO [16]. Although the betalain dyes fulfil the criteria mentioned above, they have not been suitably studied as dye sensitizers [17,18,19,20]. The betalain pigments comprise the red-purple betacyanin, betanin (I) and betanidin (II), with maximum absorptivity at λ_{max} about 535 nm, and the yellow betaxanthins with λ_{max} near 480 nm [17,21]. Within these 2 categories, many subcategories are also present [22].

7.3 Working principles of DSSC

The major charge transfer and transport processes of a DSSC are depicted in figure 7.2.[23]. Under illumination, the incoming photon is absorbed by the adsorbed dye molecules on the surface of the semiconductor which happens via the excitation between the electronic state of the molecule. Photon absorption induces an electronic transition between the HOMO and LUMO of the dye (S^0–S^*,route 1), and then the ultrafast electron injection into the conduction band of semiconductor photo-electrode (route 2) takes place on a picoseconds timescale leaving the dye molecule to an oxidized state, S^+, which means it has one less electron than earlier case. The electron transfer mechanism is strongly dependent on the electronic structure of the dye and the energy level matching between the excited state of dye (LUMO) and the conduction band of semiconductor i.e. the LUMO level is slightly above the conduction bad edge of the semiconductor and the HOMO level is slightly below the chemical potential of the redox pair in the electrolyte. There are two important back reactions in DSSC.One is recombination with the conduction band electrons with S^+(route 3) which occurs on microsecond time scale. It is noted that the reduction rate of the oxidized dye (S^+) by I^-(route 7) is also very fast, occurring on a nanosecond timescale, which can compete well with the back-reaction (route 3)to ensure the collection of photoelectrons by back-contact. The other is the recombination of conduction band electrons with I^{3+} in the electrolyte (route 4). The electron transport in the semiconductor to the back-contact (route 5) occurs on a millisecond to second timescale.

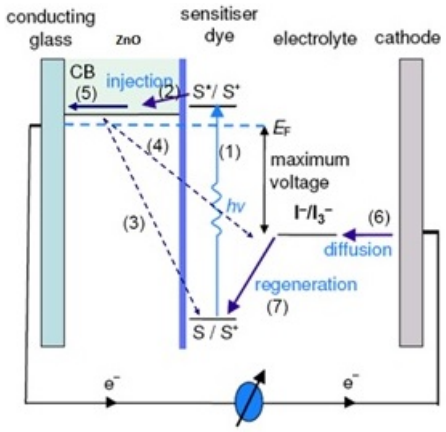

Figure 7.2: Major charge transfer and transport processes of a DSSC

The $I^-$is regenerated in turn at the CE (route 6) by the reduction of $I_3$with electrons which are transferred through TCO back contact layer by diffusion. The diffusion of electrons have been related to the series of hopping of electrons via the surface traps of different depths. These electron traps are the localized energy states lying below the conduction edge of the semiconductor and play a crucial role in the charge transport. The trapping of electrons may be the pathway for the recombination resulting in the photocurrent losses and the photovoltage losses for kinetic reasons [24].

Solar energy harvesting is a comparative fledged technology for outdoor applications. For indoor applications it is necessary to note that the efficiency of the cell is very low as of its low light luminous intensity which is less than 10 W/m^2 as compared to 100-1000 W/m^2 under outdoor conditions depending on the type of light source and distance.

7.4 Experimental details

The materials and reagents used for device fabrication was explained in chapter 2. The electrical characteristics (J-V) of the prepared solar cells were examined by using a standard solar irradiation of 1000W Xenon arc lamp as light source. The cell surface was exposed to light through a water column. The input intensity was measured using a light meter (metravi 1332). The incident light intensity in the range 4200 - 8000 Lx (6 W/m^2-12 W/m^2) was measured and then converted into W/ m^2 using the simplified relationship

1 Lx = 1.46 mW/m^2 (lx is the SI unit of lux) [25,26]. Incident monochromatic photo-to-current conversion efficiency (IPCE) measurements were carried out using small band-pass filters to create monochromatic light.

In this chapter, we focus our attention on DSSC using betanin extracts from red beets as light-absorbing material with a variety of working electrodes and is divided into five sections. The first section deals with the effect of electrolyte with different ion composition onto the bare nano ZnO based DSSC. The second section deals with performance enhancement of ZnO based dye-sensitized solar cell decorated with highly conducting and chemically stable titanium nitride (TiN)nanoparticles. This enhanced efficiency is due to the strong physical necking network formed by TiN and the electron accumulation from the interconnected TiN nanoparticles and may also be due to the partial formation of ZnO-TiO_2 composite. The third section discusses the cell performance of controlled morphologies of ZnO through single step wet chemical method. In the fourth section we discuss the use of gold (Au) NPs in a DSSC based on ZnO to improve the device performance. Here we explore the charge transfer process in a ZnO/Au nanocomposite photo electrode for DSSC application. In the last section, we compare the performances of different heterojunction DSSCs. Parameters such as sulphur doping, morphology, energy barrier were found to affect the cell performance.

7.5 Results and discussion

7.5.1 Effect of electrolyte

We have used different ion compositions as the redox electrolyte: they are

- 0.3g iodine and 1.0g potassium iodide in distilled water.
- 0.3g iodine and 1.0g potassium iodide in acetonitrile with a motivator of 0.5M 4- tert-butylpyridine (4-TBP).
- 0.05M ferrocenium hexafluorophosphate mixed with 0.1M ferrocene and 0.5M tert-butylpyridine in acetonitrile.
- 0.3g iodine 1.0g potassium iodide and 0.5M 4-TBP was dissolved into polyvinyl alcohol solution to give a homogeneous solution and was heated up to 60^0C to accelerate the polymerization. After 1hr a polymer gel electrolyte was obtained.

The solar cells with nano ZnO with different electrolytes in the presence of betanin natural dye were initially prepared in order to study the effects of electrolyte on the photovoltaic behaviour of the system. Synthesis of nano ZnO

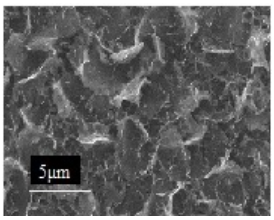

Figure 7.3: SEM image of ZnO nanostructure

were discussed in the previous chapter. The morphology of ZnO nanostructure (like nanosheets, NS) was identified by SEM (figure 7.3). The current-voltage (J-V) data for DSSC containing ZnO NS are shown in figure 7.4 and summarized in table 7.2. In this study, the cells using acetonitrile (ACN) solution have a higher efficiency of 2.99% than reported [27], and IPCE of 20% was achieved (figure 7.5). The iodide (I_2) electrolyte in ACN has shown to be the most efficient organic solvent due to its viscosity (0.34 cp, 25 C)[28] and good solubility to dissolve organic components and salts, as well as additives in the electrolytes, along with good long term stability. Because of the easy volatile and decomposing properties of the organic liquid electrolyte ,we have modified the liquid electrolyte on the addition of polymer and developed a quasi solid state DSSC. In the case of PVA based electrolyte E_{redox}-E_{HUMO} is reduced, which will affect V_{oc} and J_{sc} and the performance drops down due to the poor mobility of charge carriers as well as poor wetting ability. Its incomplete penetration into the semiconductor to regenerate the dye plays a detrimental role.

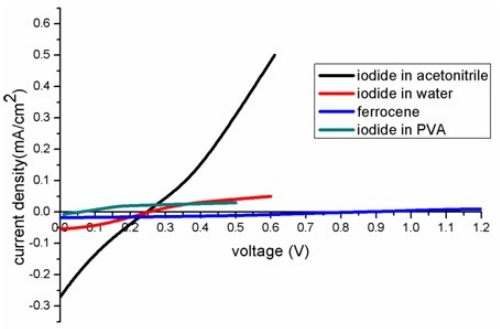

Figure 7.4: Current density against voltage characteristics of ZnO nanoparticles with different electrolytes (P_{in}=4.2 K lx)

Table 7.2: Comparison of DSSC with different electrolyte (P_{in}=4.2 K lx)

Electrolyte	Area of cell (cm^2)	J_{sc} (mA/cm^2)	Voc (V)	FF	η (%)
Ferrocene	0.52	0.02	0.84	0.35	0.87
I_2 in ACN	0.63	0.99	0.15	0.21	2.99
I_2 in water	0.56	0.05	0.25	0.33	0.48
I_2 in PVA	0.52	0.01	0.06	0.29	0.01

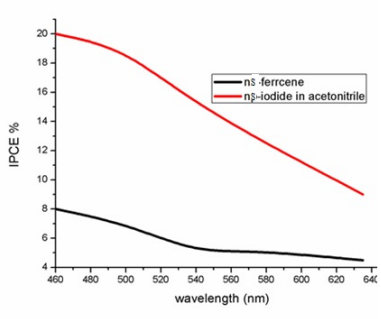

Figure 7.5: IPCE for betanin-sensitized ZnO with ferrocene based and iodide electrolyte

Even though the iodide based electrolyte showed better J_{sc} than ferrocene based electrolyte, the ferrocene based electrolyte exhibit better V_{oc} and FF which is attributed to lower charge recombination at the photo electrode. This Fe^{2+}/Fe^{3+} redox couple does not induce corrosion because it does not interact with oxygen during the fabrication process [29]. Dye degradation by ferrocene is a simple one-electron transfer reaction ($D^+ \rightarrow D + Fc$) that does not involve the cleavage or reformation of chemical bonds or the formation of high-energy intermediate radical species and has more favourable redox potential than the two electron I_3^-/I^- redox system (0.62 V)which should result in a higher open-circuit voltage(V_{oc})[30]. The nature of the resonant HOMO→LUMO transition, vibrations of the aromatic ring and conjugated framework are strongly boosted by using iodide based electrolyte in ACN. The rate of electron injection from the dye to the photo anodes was more rapid in acetonitrile than water. This is because the O atom in water/ethanol had a stronger attraction to the functional group of the dye than the N atom in acetonitrile [31]. The combined absorption spectra of different ZnO based photo anodes used in the following sections is shown in figure 7.6.

7.5.2 Enhanced performance of ZnO based DSSC decorated with Titanium nitride nanoparticles

Titanium nitride (TiN) is an extremely hard, conducting ceramic material and has different applications, and it is often used to develop electrically conducting layer for the TCO-less DSSC structure [32]. It is also known to oxidize when it is exposed to air and/or moisture [33]. Above all TiN is capable for improving the optoelectronic property and photo activity of nanostructures and

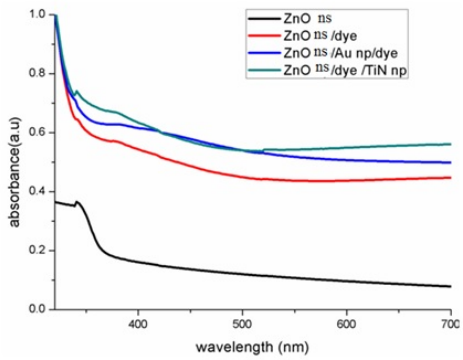

Figure 7.6: Different ZnO based photoanodes

many investigations relates the possible use of the TiN as a decorative coating as its color can approach that of gold [34,35]. By introducing TiN into ZnO, the oxidation power is certainly reduced (E_{redox} - E_v), which changes its electronic properties. It was reported that substantial amounts of oxygen vacancies exist in ZnO film, which is helpful to the creation of a filamentary conductive path with the TiN layer serving as an oxygen reservoir for the annihilation of oxygen vacancies [36]. The chances of recombination of dye with the electrolyte are limited by the presence of TiN. TiN grain boundaries provide a rapid channel for diffusing oxygen in the oxidation process. The N state induced oxygen vacancies could greatly affect its optoelectronic properties and subsequently its photo activity. Considering the features of good electrical conductivity, and chemical stability we have incorporated it into the ZnO DSSC and studied the corresponding effects on the photovoltaic with two kinds of electrolytes viz;. ferrocene and iodide based electrolyte.

TiN is a conducting ceramic material with high electrical and thermal conductivity and considerable resistance to thermal shocks [37] and have high intrinsic electro catalytic activity[38]. Commercial titanium nitride (sigma Aldrich, size 50 nm,0.025g) was dispersed into water and was thoroughly mixed. The obtained TiN NPs paste was covered onto the dye sensitized ZnO NSs. The obtained ZnO: dye: TiN photoanode was again subjected to an annealing process. The TEM image of TiN nanoparticles is shown in figure 7.7. The inter-particle connection of nanocrystalline TiN in the TiN film and the necking reaction of the small TiN particles with the relatively large ZnO particles are clearly depicted in figure 7.8(a). The possible electron transfer is also represented in figure 7.8(b). The absorption spectrum of the ITO/ZnO structure incorporated with TiN nanoparticles is characterized by a large absorbance

which is also shown in figure 7.6.

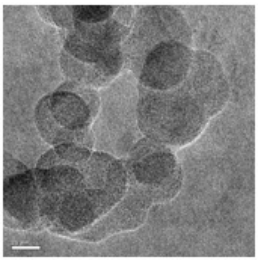

Figure 7.7: TEM image of TiN NPs

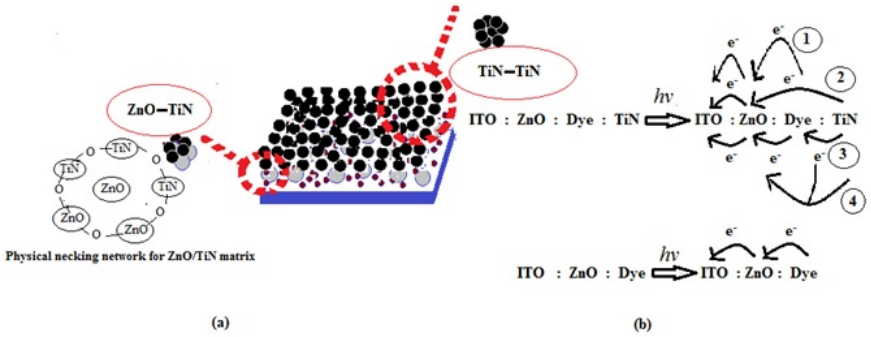

Figure 7.8: (a) Mechanism for the inter-particle connection of TiN NPs in the TiN film and TiN NPs with the other dye sensitized nano ZnO in the dye/ZnO film and (b) possible charge transport of both ZnO/Dye/TiN and ZnO/Dye photoanodes.

The current voltage (I-V) characteristics of DSSCs shows J_{sc} of 0.02 mA/cm^2, V $_{oc}$ of 0.58 V, FF=0.31and η of 0.91% [area of the cell is 0.56 cm^2, P_{in}=2.62 K lx] with ferrocene based electrolyte. The same is repeated with iodide electrolyte in acetonitrile shows J_{sc} of 0.22mA/cm^2, V_{oc} of 0.11 V, FF=0.50 and η of 3.072% [area of the cell is 0.42 cm^2].The decreased value of current density is due to the decreased surface area available for dye loading. Again the best performance was achieved in the iodide based electrolyte.

Upon irradiation on the ZnO/Dye photoanode the electrons from the LUMO band of the dye are directly transported to the conduction band (CB) of ZnO.

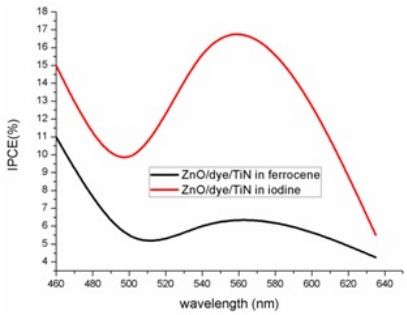

Figure 7.9: IPCE(λ) for ZnO/dye/TiN

On the other hand, in ZnO/Dye/TiN it is believed that another way of electron transfer from the electron accumulation in the TiN nanoparticle tunnelling to the ZnO and the combined electron transition from both dye and TiN to ZnO through the physical necking network thereby boosts the efficiency. Chuan-Pei Lee[39] et al. has reported that the oxide formation from the TiN nanoparticles through the annealing process i.e partial TiO_2 nanoparticles can be derived from the TiN through the thermal treatment which can generate additional possible composite of TiO_2 -ZnO providing anchorage for the additional dye adsorption .TiO_2 has similar PH value to that of dye solution [pH of TiO_2=5.5-6.5,pH of dye=5] and the formation of ion/dye complexes does not take place. The high FF is attributed to the lower value of interfacial resistance (TiN/electrolyte interface).The covering of TiN on ZnO improves the property of electron transfer resulting in 50% FF and exhibit better IPCE than the bare ZnO DSSC is shown in figure 7.9.

7.5.3 Controlled morphology

The cell performance of ZnO crystals are shown in table 7.3.During the electron transport, multiple trapping/de-trapping events indeed occur within the grain boundaries in all photoanodes and the light confinements may occur mainly in the case of microrods.

It can be seen that nanoplates and nanoflakes being 2D structures, shows higher efficiency than the 1D microrods, which may be due to the high photo catalytic activity of 2Dl structures with a high population of polar Zn[0001] faces [40].

Even though the iodide based electrolyte showed better efficiency than ferrocene electrolyte, the latter exhibits better long-term stability as it is corrosion

Table 7.3: Characterisation of DSSC based on controlled morphologies of ZnO;area of the cell in(cm^2),P_{in}(K lx),J_{sc}(mA/cm^2), V_{oc} in V and η in%

controlled morphology	Electrolyte	Area	P_{in}	J_{sc}	v_{oc}	ff	η
DB microrods	Ferrocene	0.48	2.62	0.001	0.25	0.23	0.02
	I_2 in ACN	0.81	2.62	0.003	0.39	0.25	0.09
nanoflakes	Ferrocene	1	0.8	0.01	0.02	0.34	0.07
	I_2 in ACN	1	0.8	0.01	0.05	030	0.19
nanoplates	Ferrocene	0.49	4.2	0.01	1.68	0.22	0.06
	I_2 in ACN	0.64	4.2	0.004	0.05	0.22	0.01
microrods	Ferrocene	0.64	6.2	0.001	0.72	0.17	0.02
	I_2 in ACN	0.56	4.2	0.001	0.22	0.20	0.01

free. Based on this, hereafter we evaluate the performance of DSSCs only with ferrocene electrolyte.

7.5.4 Effect of gold nanoparticles

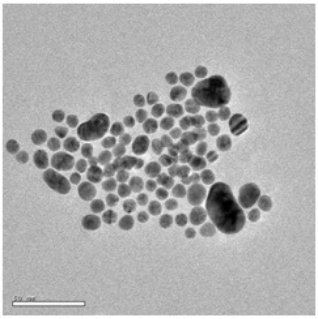

Figure 7.10: TEM image of Au NPs

Metal-doped semiconductor nanocrystallites have attracted much attention, because of their novel effects on improving their photo activity by changing its photo physical mechanism i.e. the formation of shallow charge trapping on the semiconductor surface due to the replacement of Zn^{II} by metal ions and the metal ion introducing could enhance the photocatalytic activity of ZnO in some cases. Several reports have been previously published in this

direction [41-44].

When the frequency of the incoming light is in resonance with the collective oscillations of the electron density i.e. surface plasmons, metal NPs show a strong enhancement in the local electromagnetic field. As a result, unique optical properties known as localized surface plasmon resonance (LSPR) have been observed which are depends on the size, shape, density and local dielectric environment of the NPs [45].

To enhance solar harvesting in organic solar cells, uniform sized metal nanoparticles (gold (Au) of ≈8 nm), were incorporated into the device. ZnO/Au nanocomposite photo electrodes have been prepared by wetting 1 g of ZnO with 0.5 ml of colloidal Au NPs. Microwave rapid heating, which is a simple and quick solution process, was used to synthesize the Au NPs. A 0.5mM aqueous solution of auric acid ($HAuCl_4$) and 3.8 mM aqueous solution of sodium citrate were reacted together in the presence of microwave radiations [46]. After cooling down to room temperature, products were collected, and characterised through TEM and these are shown in figure 7.10. The optical absorptions of ZnO NS on ITO, Au incorporated ZnO on ITO and betanin sensitized ITO of the same are shown in figure 7.6. The absorption spectrum of the ITO/ZnO NS structure incorporated with gold NPs is characterized by a large absorbance over the measured spectral range and a clear broad peak in the range 380-488 nm, and the observed spectral change (red shift) in this system is attributed to the plasmon resonance absorption arising from electron deficiency on the gold surface and the interfacial coupling between the Au and ZnO.

The J-V characteristics of the sandwiched cell structures with both bare ZnO and gold mixed ZnO were examined. Even though the iodide based electrolyte showed better J_{sc} than ferrocene based electrolyte, the ferrocene based electrolyte exhibit better V_{oc} and FF attributed to lower charge recombination at the photo electrode, therefore, these cells are betanin natural dye sensitized and use a ferrocene based electrolyte and an active area of 0.6 cm^2 with P_{in}= 8 K lx.

Upon illumination with simulated sunlight, the device with ZnO NP mixed with gold nanoparticles can deliver improved photocurrent was shown in figure 7.11 and power conversion efficiency improved from 0.868% to 1.71% and also exhibit IPCE of 14%,which was depicted in figure 7.12,(ferrocene based electrolyte and an active area of 0.6 cm^2 with P_{in}= 8 K lx). These changes apparently results from the enhanced visible absorption of the active layer via the high electromagnetic field strength in the vicinity of the excited surface plasmons provided by the Au NP embedded to the ZnO NS, leading to an increase

in the exciton generation. An enhancement over the visible range is related to the combined effect of betanin natural dye and the LSPR which induce more photo generated charge carriers.

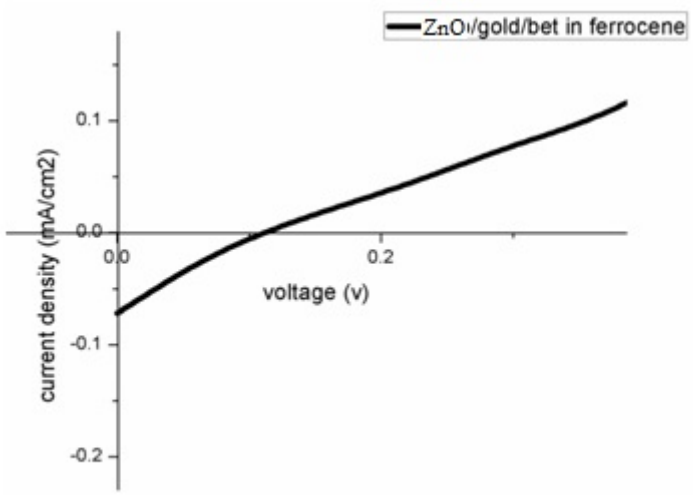

Figure 7.11: Current density against voltage characteristics of Au incorporated ZnO nanoparticles (P_{in}=8 K lx)

The formation of Schottky barrier and the possible electron transfer from the excited dye molecules to the ZnO is schematically represented in figure 7.13. Upon irradiation the electrons from the LUMO band of the dye are transported to the conduction band (CB) of ZnO through the tunnelling effect of the thin layer of gold NPs. It is further believed that another way of electron transfer from the electron accumulation in the Au nanoparticles, raising their Fermi energy level more closer to the CB of ZnO and a quick transport of electrons from Au to ZnO through the physical necking network, takes place to establish charge equilibrium in the system . The electrons transferred to nano ZnO are collected at the bottom ITO electrode thereby generating an anodic photocurrent. The Schottky barrier at the Au-ZnO interface reduces charge recombination by blocking the transfer of electrons from the ZnO conduction band to the dye and/or electrolyte thus improving the efficiency of DSSCs due

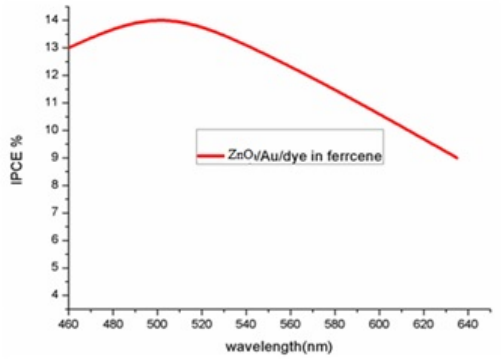

Figure 7.12: IPCE betanin sensitized ZnO/Au with ferrocene based electrolyte

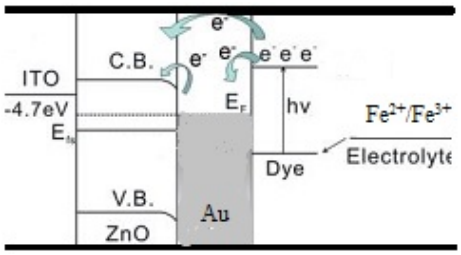

Figure 7.13: Energy level diagram and mechanism of photocurrent generation in the cell with ITO/ZnO/Au/Dye as the photo anode.

to the large work function of Au (5.1 eV) compared with the electron affinity of ZnO (4.2 eV)[47]. Normally, when the charge transport was improved the FF and J_{sc} will be improved simultaneously. But here, the FF decreased from 0.35 to 0.29 which is probably caused by an increase in the resistive loss due to the increased flux [48,49] and the charge recombination at the photo electrode coming from the Au nanoparticle agglomeration. These accumulated electrons recombine with the oxidised dye molecules or with the redox electrolytes before they can be transfer to the CB of ZnO [50,51]. The presence of carboxylic groups in the betalain presents together with the higher oxidation potential boosts the anchoring. The formation of the oxidation product, i.e. melanin like polymer of cyclo-dihydroxyphnylalanine (DOPA) along with the possible formation of indicaxanthin and the heat-induced cleavage of betanin into betalamic acid may play a crucial role in the cell performance.

To assess the stability of the assembled cell they have been wrapped in tissue and left for 1 day and for 1 month. Stability of the ZnO/Au nanoparticles with fresh ferrocene electrolyte was tested by measuring the J-V characteristics of the ZnO/Au solar cell after 24 h, only negligible changes in the cell performance were observed. But for the 1 month dated cell show the photovoltaic action with very less values of J_{sc} and V_{oc}. Although the efficiencies obtained with betanin natural dye are below the requirements for the large scale production, the results are hopeful and are suitable alternative to inorganic dyes in DSSC.

7.5.5 Performance comparison of betanin sensitized heterojunction dye-sensitized solar cells

Much effort has recently been invested to create new class of nanomaterials through surface coating such as core/shell type TiO_2/CdS nanowires[52] Cu_2S/Au nanowires [53] Zn/ZnO nanobelts [54] and through different mixing morphologies [55-57]; and to develop the dynamic and interfacial properties of DSSC [58] which could enhance the solar cell conversion efficiency. In this section, we propose a simple facile two step solution growth method to build tailored nanomaterials using pre-existing textured ZnO, ZnS, CdS and TiO_2 seeds and to construct DSSCs and compare their performance. We have synthesized nanoparticles (NPs) using different methods. The CdS NP (28 nm) were synthesized using the chemical bath deposition technique as described in literature [59]. Briefly, 1M $CdAc_2$ and 1M thiourea is dissolved in distilled water ,using triethanolamine as the capping agent. The NPs are separated from the medium by centrifugation, washed and then dried at room temperature. The synthesis procedures of other nanoparticles were discussed in previous chapter.

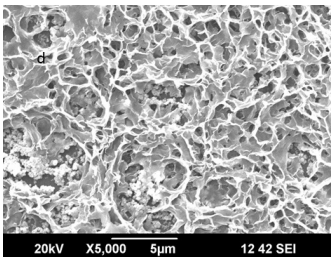

Figure 7.14: SEM images of CdS-ZnO composites

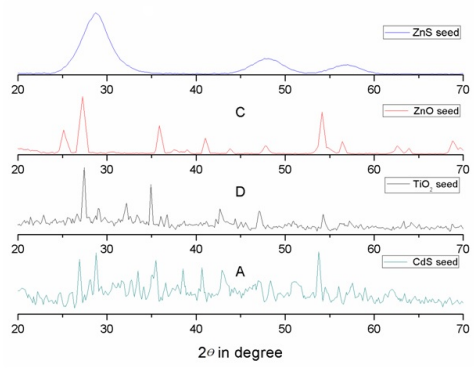

Figure 7.15: XRD pattern of different seed ZnS, ZnO, TiO_2 and CdS

The morphological features of ZnO nanostructures deposited on different pre-existing textured ZnO, ZnS, and TiO_2 seeds are identified by SEM images and were shown in chapter 4. With the TiO_2 and ZnS seed a new morphology of nanomaterial appears: vertical microrods and vertical nanorods. In addition to these structures, randomly distributed nanoplate and nanofibre structure are also observed in ZnS/ZnO composite. But with CdS nanoparticles we have obtained honey bee structure with several nanoballs ,which is shown in figure 7.14. The figure 7.15 again shows the XRD pattern of different seeds. Figure 7.16 compares the J-V characteristics of DSSCs based on different morphologies measured by using 1000W xenon arc lamp and the related physical values, such as J_{sc} ,V_{oc}, FF, and η which are summarized in table 7.4.

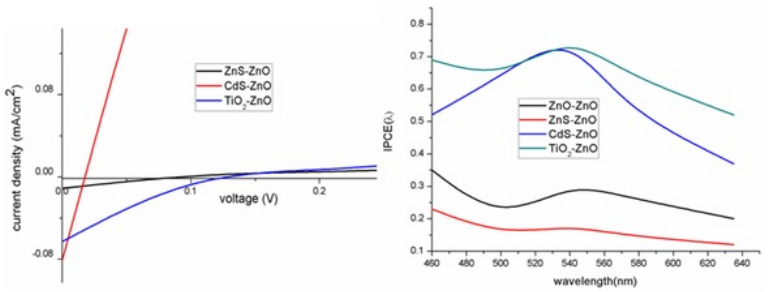

Figure 7.16: (a) Current density against voltage characteristics of different composites (b) their IPCE (λ)

Table 7.4: Comparison of DSSC based on semiconductor composites with ferrocene electrolyte

	P_{in}(K lx)	J_{sc}(mA/cm^2)	Voc(V)	FF	η(%)
ZnO-ZnO	2.62	0.06	0.07	0.46	0.48
ZnS-ZnO	0.8	0.01	0.08	0.23	0.21
CdS-ZnO	0.8	0.09	0.02	0.21	0.28
TiO_2-ZnO	0.8	0.06	0.09	0.26	1.2

The performance of cells with ZnO composites can be influenced by the dye-adsorption capability, light harvesting, sulphur doping and the existence of energy barrier. To address this issue, the dye adsorption amount of the composites was determined by using the absorption spectra of betanin sensitized composites. Hence, dye adsorption is not the only factor responsible for the final conversion efficiency. Self-seeded ZnO based DSSCs showed low efficiency compared to TiO_2-ZnO due to the formation of Zn^{2+}/dye complex by dissolving ZnO onto the -COOH group of dye,which blocks the electron injection from the dye to ZnO.

The point of zero charge of ZnO and TiO_2 are reported to be pH =8-9 [60] and pH =5.5-6.5[61,62], respectively, whereas the pH value for the dye sensitization process is approximately 5, that inactivate some dye molecules and decrease the efficiency. But for TiO_2, has similar PH value to that of dye solution, the formation of ion/dye complexes does not take place. The open circuit voltage (V_{oc}) of TiO_2-ZnO is higher than that of self-seeded ZnO branched nanowire even with a small input flux which leads to less charge recombination that reflects in higher IPCE which was shown in figure 7.15b. This reduced recombination that occurs in the TiO_2-ZnO composite is due to the existence of energy barrier formed in the TiO_2-ZnO interface (work function of ZnO=5.6 eV and that of TiO_2=4.8 eV) and due to higher electron mobility of ZnO [68]. The efficiency enhancement in TiO_2-ZnO composite is also ascribed to the enrichment of light harvesting and the reduction of electron back reaction due to direct conduction path way.

Moreover, a multi-fold enhancement of efficiency in TiO_2-ZnO composites photo anode is achieved in comparison with ZnS-ZnO composites. Due to hetero-hierarchical structure it is expected that ZnS-ZnO composite show higher photovoltaic performance, but on the contrary it shows the less efficiency, which may be due to the formation of metal-ion/dye complex, i.e. between constituents and the carboxylic group of the dye ,that hinders its dye loading ability.It is assumed that the semiconductor starts to leak electrons

before reaching the quasi-Fermi level and most of the photons do not fall into the acceptance cone of the integrating sphere and are scattered out [64] and is mainly limited to poor dye adsorption. The S atoms in the ZnS layer are able to fill with the oxygen vacancies on ZnO layer which can reduce the recombination and the tunneling of electrons from the LUMO energy levels of the betanin dyes to the conduction band the ZnO and to the ZnS is prevented by the higher band gap of ZnS. Hence the electrons are confined in the ZnO layer [65]. In the case CdS-ZnO, the trapping/detrapping events at the semiconductor-electrolyte interface such as intrinsic defect sites (oxygen defects or surface states) and at the grain boundaries of the porous of honey bee structure reduce driving force of electrons .This leads to increased scattering and it slows down the electron transport which increase the recombination with the oxidized dye molecules and/or redox species, which is obvious from the low V_{oc}.

We believe that increased photo absorption of CdS-ZnO is the main reason for the enhancement of conversion efficiency compared with ZnS-ZnO. With the absorption of sulphur atoms, the formation of new defects or surface state such as Zn-Cd-S or Cd-Zn-O in the interface region of the CdS-ZnO heterojunction improves the conductance leading to the higher photo-current [66] and higher IPCE (λ). The major problem for using CdS as a seed layer is, the trapping/detrapping events at the grain boundaries of the porous of honey bee structure reduce driving force of electrons and slows down the electron transport which can results in an increasing probability of charge recombination with the oxidized dye molecules and/or redox species, and this is obvious from the low value of V_{oc}.We suggest that great improvement in IPCE (λ) results from the sufficient light harvesting in the visible region which arise from the increased overall surface area Due to the random multiple scattering within the structure leading to photon localization that increases the probability of interaction between the dye molecules and photons. Even though we did not quantitatively measure, we could verify the higher dye adsorption as the colour of CdS-ZnO was much deeper than the other composites as seen by naked eye. The absorption and reflection of incident light by the conductive glass which could reduce the incident light power by as much as 20% [50]may also be responsible for the higher value of IPCE (λ).The higher value of IPCE (λ)suggests that betanin can inject more than one electron per photon, as betanin is capable of expending up to two electrons without being irreversibly oxidized [67].The absorbed two electrons per photon would explain how recombination could limit the maximum attainable photo voltages despite the high photo-currents obtained. The sulphur atoms can diffuse into the inner part of the ZnO,resulting in a sulphur doping effect in ZnO, this sulphur doping could be considered for the conductance enhancement. Another factor is the electron injection from the ZnO to CdS through the staggered gap (for ZnO E_g=3.37 eV

and for CdS E_g= 2.42 eV at 300K). In addition multiple scattering is responsible for the higher IPCE in CdS-ZnO which may be due to the lasing emission on the composite. We assume that the betalain derived melanin adsorbed on the TiO_2-ZnO film is very stable.

7.6 Conclusion

- Dye-sensitized solar cells with a ZnO/Au nanocomposite as the photoelectrode were successfully fabricated and their performances were compared with the bare ZnO NS DSSC and the effect of electrolyte with different ion composition onto the bare ZnO NSs has also been discussed.
    * The photochemical performance of DSSC with NS based photo anode with ferrocene based and iodide in acetonitrile solution exhibit better efficiency of 0.868% and 2.99% with a small input power of few K lx.
- In our investigation,DSSCs with the additions of TiN nanoparticles exhibited considerably higher solar to-electricity conversion efficiencies than the corresponding DSSC without these additions.
    * This enhanced efficiency is due to the strong physical necking network formed by TiN and the electron accumulation from the interconnected TiN nanoparticles.
    * The partial formation of TiO_2 through the thermal treatment of TiN may generate additional possible composite of TiO_2 -ZnO which can provide anchorage for the efficiency enhancement.
- We were compared the cell performance of controlled morphologies of ZnO.
- To enhance solar harvesting in organic solar cells, uniform sized metal nanoparticles (gold (Au) of ≈8 nm) synthesized via microwave irradiation method were incorporated into the device consisting of ZnO NSs.
    * We found that, incorporation of Au NPs led to enhanced power conversion efficiency from 0.868% to 1.71% and IPCE of 14% with ferrocene based electrolyte.
    * The formation of the Schottky barrier at the ZnO/Au interface and high optical absorption of ZnO/Au photo electrodes arising from both surface plasmon resonance of Au NPs and high dye intake are the reasons for the enhanced efficiency.

- Different heterostructures ZnS-ZnO, CdS-ZnO, TiO_2-ZnO were synthesized through a simple two step growth method and to serve as photo anode of DSSCs.
    * The DSSC with the TiO_2 - ZnO composite structure exhibited a significant increase in cell performance and IPCE compared with other composites.
    * Parameters such as sulphur doping, morphology, energy barrier were found to affect the cell performance.
    * This study provides a facile method to tailor the morphologies of nanomaterials and to prepare the nanocomposite photoanodes of solar cells, and gives some insights about the cell performance.

7.7 References

[1] Grtzel M. "Review article Photoelectrochemical cells" Nature, 414, 338-344 (2001).

[2] Survey of Energy Resources-World Energy Council 2013.

[3] http://rredc.nrel.gov/solar/spectra/am1.5.

[4] B. Oregan and M. Gratzel, "A low-cost, high-efficiency solar cell based on dye-sensitized colloidal TiO_2 films" Nature, 353, 737-740 (1991)

[5] M. K. Nazeeruddin, A. Kay, I. Rodicio, R. Humphry-Baker, E. Muller, P. Liska, N. Vlachopoulos and M. Gratzel, "Conversion of light to electricity by cis-X2-bis(2,2-bipyridyl-4,4-dicarboxylate)ruthenium(II) charge-transfer sensitizers (X= Cl-, Br-, Iod-, CN-, and SCN-) on nanocrystalline TiO_2 electrodes" J. Am. Chem. Soc.115, 6382-6390 (1993)

[6] Hanhong Chen, Aurelien Du Pasquier, GauravSaraf, JianZhong and Yicheng Lu "Dye-sensitized solar cells using ZnO nanotips and Ga-doped ZnO films" Semicond. Sci. Technol.23, 045004 (2008)

[7] Lagref J.J, Nazeeruddin M.K and Graetzel M.,"Artificial photosynthesis based on dye-sensitized nanocrystalline TiO_2solar cells", Inorg. Chim. Acta, 361, 3, 735-745.(2008)

[8] Smestad G.P. and Gratzel, M."Demonstrating Electron Transfer and Nanotechnology: A Natural Dye-Sensitized Nanocrystalline Energy Converter", J. Chem. Educ., 75, 6, 752-756 (1998).

[9] M.K. Nazeeruddin, F. De Angelis, S. Fantacci, A. Selloni, G. Viscardi, P. Liska, S. Ito, B. Takeru and M. Grtzel, "Combined experimental and DFT-TDDFT computational study of photoelectrochemical cell ruthenium sensitizers "J. Am. Chem. Soc. 127, 16835-16847 (2005)

[10] David Parlevliet and Navid Reza Moheimani "Efficient conversion of solar energy to biomass and electricity" Aquat Biosyst ,10,4,2-9 (2014)

[11] Argazzi R., Iha N.Y.M., Zabri H., Odobel F. and Bignozzi C.A. "Design of molecular dyes for application in photoelectrochemical and electrochromic devices based on nanocrystalline metal oxide semiconductors".Coord. Chem. Rev.248:1299-1316 (2004)

[12] A. S. Polo, M. K. Itokazu and N. Y. Murakami Iha,"Metal Complex Sensitizers in Dye-Sensitized Solar Cells", Coord. Chem. Rev, 248, 1343-1361 (2004).

[13] Yella A.et al. "Porphyrin-Sensitized Solar Cells with Cobalt (II/III)Based Redox Electrolyte Exceed 12 Percent Efficiency", Science 334, 629-634 (2011)

[14] Xiao-Feng Wanga, Yasushi Koyama, Osamu Kitao, Yuji Wada, ShinichSasaki, HitoshiTamiaki and Haoshen Zhou "Signicant enhancement in the power-conversion efficiency of chlorophyll co-sensitized solar cells by mimicking the principles of natural photosynthetic light-harvesting complexes" Biosens. Bioelectron., 25 ,1970-1976(2010)

[15] Hongwei Zhu , Haifeng Zeng , Venkatachalam Subramanian, Charan Masarapu, Kai-Hsuan Hung and Bingqing Wei "Anthocyanin-sensitized solar cells using carbon nanotube lms as counter electrodes" J.Nanotechnol. 19, 465204 (2008)

[16] A. Dumbrav, I. Enache, C. I. Oprea, A. Georgescu and M. A. Gru "Toward a More Efficient Utilisation of Betalainsas Pigments For Dye-Sensitized Solar Cells" Dig J Nanomater Bios,7, 339 - 351 (2012)

[17] D. Zhang, S. M. Lanier, J. A. Downing, J. L. Avent, J. Lumc and J. L. McHale, "Betalain Pigments for DyeSensitized Solar Cells", J. Photochem. Photobiol., A:Chem., 195, 1, 72-80 (2008)

[18] Zhang D., Yamamoto N., Yoshida T. and Minoura H. "Natural dye sensitized solar cells", Trans. Mater. Res. Soc. Jpn.,27,811-814 (2002).

[19] Hernandez Martinez A. R, Estevez M, Varga S, Quintanilla F and Rodriguez R "New dye-sensitized solar cells obtained from extracted brachts of bougainvillea glabra and spectabilis betalain pigments by different purification process" ,Int. J. Mol. Science 12, 5565-5576 (2011)

[20] G. Calogero, G. Di Marco, S. Cazzanti, S. Caramori, R. Argazzi, A. Di Carlo and C. A. Bignozzi, "Efficient Dye-Sensitized Solar Cells Using Red Turnip and Purple Wild Sicilian Prickly Pear Fruits" ,Int. J. Mol. Sci. 11, 254-267 (2010)

[21] Aparna Thankappan,Sheenu Thomas and V. P. N. Nampoori "Effect of betanin natural dye extracted from red beet root on the non linear optical properties ZnO nanoplates embedded in polymeric matrices" J. Appl. Phys.,112, 123104 (2012)

[22] Aparna Thankappan, Sheenu Thomas and V.P.N. Nampoori "Solvent effect on the third order optical nonlinearity and optical limiting ability of betanin natural dye extracted from red beet root" Opt. Mater., 35 , 2332-2337 (2013)

[23] A. Hagfeldt and M. Grtzel, "Light-Induced Redox Reactions in Nanocrystalline Systems"Chem. Rev., 95, 49-68 (1995)

[24] A. Hagfeldt and M. Grtzel "Molecular Photovoltaics" Acc.Chem.Res 33,5, 269-277 (2000)

[25] Ying-Wen Bai, Ta-Wei Shen and Cheng-Hung Tsai "Using Depth Image Processing and Human Skeleton Identification Methods to Reduce Uncomfortable Light from a Digital Projector" IEEE 16th International Symposium 978-1-4673-1356-8 (2012)

[26] Kalapodas et "Stereoscopic view light source, with multiple modes of operation" US. Patent May 14, US 8,439,516 B2 (2013)

[27] Cody Sandquist and Jeanne L. McHale "Improved efficiency of betanin-based dye-sensitized solar cells" J. Photochem. Photobiol., A: Chem. 221, 90-97 (2011)

[28] Hagfeldt, G. Boschloo, L. Sun, L. Kloo and H. Pettersson, "Dye-sensitized solar cells", Chem. Rev., 110(11), 6595-6663 (2010)

[29] Savas S, onmezoglu, CaferAkyurek and Seckin Akin "High-efficiency dye-sensitized solar cells using ferrocene-based electrolytes and natural photosensitizers" J. Phys. D: Appl. Phys.45,425101 (2012)

[30] Torben Daeneke ,Tae-HyukKwon ,Andrew B. Holmes, Noel W. Duffy, Udo Bach and Leone piccia "High-efficiency dye-sensitized solar cells with ferrocene-based electrolytes" Nat. Chem. 966 , 1-5(2011)

[31] NansraHeo, Yongseok Jun and Jong Hyeok Park "Dye molecules in electrolytes: new approach for suppression of dye-desorption in dye-sensitized solar cells" scientific reports 3: 1712, 01712 (2013)

[32] Beomjin Yoo,Kang-Jin Kim, Yong Hyun Kim, Kyungkon Kim, Min Jae Ko, Won Mok Kimc and Nam-Gyu Park "Titanium nitride thin film as a novel charge collector in TCO-less dye-sensitized solar cell" J Mater Chem.21, 3077(2011)

[33] Al-Abdallah MM and Said AJ. "Impedance measurement on Inconel and Monel in acidic water and methanolic media", Anti Corros Methods Mater., 42: 14-7 (1995)

[34] Min Jae Jung, Ho Young Lee, and Jeon G. Han et al. "High-rate and low-temperature synthesis of TiO_2, TiN, and TiO_2/TiN/TiO_2 thin films and study of their optical and interfacial characteristics". J.Vac. Sci. Technol. B 23:4 (2005)

[35] Straumal B, Vershinin N, Filonov K, Dimitriou R and Gust W "Masked deposition of decorative coatings on large area glass and plastic sheets". Thin Solid Films 351, 204-208 (1999)

[36] Xu N, Liu LF, Sun X, Chen C and Wang Y "Bipolar switching behaviour in TiN/ZnO/Pt. resistive non-volatile memory with fast switching and long retention" .Semicond. Sci. Technol.23: 075019 (4pp) (2008)

[37] M. Wittmer, B. Studer and H. Melchior, "Electrical characteristics of TiN contacts to N silicon"J. Appl. Phys., 52,5722 (1981)

[38] Pacholski, A. Kornowski and H. Weller," Self-assembly of ZnO: from nanodots to nanorods", Angew. Chem. Int. Ed., 41, 7, 1188-1191 (2002)

[39] Chuan Pei Lee, Lu Yin Lin, Keng-Wei Tsai, R. Vittal and Kuo-ChuanHo "Enhanced performance of dye-sensitized solar cell with thermally-treated TiN in its TiO_2 film prepared at low temperature" J. Power Sources 196(3):1632-1638 (2011)

[40] Eue Soon Jang.JangHee Won, Seong-Juhwang and Jin-Hochoy "Fine tuning of face orientation of ZnO crystals and optimize their photo catalytic activity" Adv.Mater 18, 3309-3312 (2006)

[41] Tanujjal Bora, Htet H. Kyaw, Soumik Sarkar, Samir K. Pal and Joydeep Dutta"Highly efficient ZnO/Au Schottky barrier dye-sensitized solar cells: Role of gold nanoparticles on the charge-transfer process".Beilstein J. Nanotechnol. 2: 681-690 (2011)

[42] Xianming Hou, LixiaWang, Guofang He and JingchengHao"Synthesis, optical and electrochemical properties of ZnO nanorod hybrids loaded with high-density gold nanoparticles", Cryst.Eng.Comm, 14:5158-5162 (2012)

[43] Hui Li, KaidiYuan,Yu Zhang, and John Wang "Synthesis of Au-SiO_2 Asymmetric Clusters and Their Application in ZnO Nanosheet-Based Dye-Sensitized Solar Cells "Appl. Mater. Interfaces5:5601-5608 (2013)

[44] Sixto Gimenez, Andrey L. Rogach, Andrey A. Lutich, Dieter Gross, Andreas Poeschl, Andrei S. Susha, Ivan Mora-Sero, Teresa Lana-Villarreal

and Juan Bisquert "Energy transfer versus charge separation in hybrid systems of semiconductor quantum dots and Ru-dyes as potential co-sensitizers of TiO_2-based solar cells" J. Appl. Phys.,110, 014314 (2011)

[45] Seok-Soon Kim, Seok-In Na, JangJo, Dong-Yu Kim and Yoon-Chae Nah "Plasmon enhanced performance of organic solar cells using electro deposited Ag nanoparticles" Appl. Phys. Lett., 93, 073307 (2008)

[46] Anju K. Augustine, V.P.N. Nampoori and M. Kailasnath "Rapid synthesize of gold nanoparticles by microwave irradiation method and its application as an optical limiting materia" Optik 125, 6696-6699 (2014)

[47] Tanujjal Bora, Htet H. Kyaw, SoumikSarkar, Samir K. Pal and Joy deep Dutta "Highly efficient ZnO/AuSchottky barrier dye-sensitized solar cells: Role of gold nanoparticles" Beilstein J. Nanotechnol. 2, 681-690 (2011).

[48] Y. B. Tang, Z. H. Chen, H. S. Song, C. S. Lee, H. T. Cong, H. M. Cheng, W. J. Zhang, I. Bello and S. T. Lee "Vertically Aligned p-Type Single-Crystalline GaN Nanorod Arrays on n-Type Si for Heterojunction Photovoltaic Cells",NanoLett. 8,12, 4191-4195 (2008)

[49] Beek W. J. E, Wienk M. M and Janssen R. A. J. "Hybrid solar cells from regioregular polythiophene and ZnO nanoparticles" AdV.Funct.Mater. 16(8), 1112-1116 (2006)

[50] Kamat P. V., "Quantum Dot Solar Cells. Semiconductor Nanocrystals as Light Harvestors. Centennial Feature Article " J. Phys. Chem. B, 113, 18737-18753 (2008)

[51] Haruta M. "Size- and support-dependency in the catalysis of gold " Catal. Today 36, 153-166 (1997)

[52] Cao J, Sun J. Z, Li H. Y., Hong J and Wang M. "A facile room-temperature chemical reduction method to TiO_2@CdS core/sheath heterostructure nanowires "J. Mater. Chem.,14, 1203-1206 (2004)

[53] Wen X and Yang S. "Cu_2S/Au Core/Sheath Nanowires Prepared by a Simple Redox Deposition Method" NanoLett., 2, 451 (2002).

[54] Ding Y, Kong X. Y and Wang Z. L "Interface and defect structures of Zn-ZnO core-shell heteronanobelts",J. Appl. Phys., 95, 306 (2004)

[55] C.Y. Jiang, X.W. Sun, G.Q. Lo, D.L. Kwong and J.X. Wang, "Improved dye-sensitized solar cells with a ZnO-nanoflower photoanode"Appl. Phys. Lett. 90, 263501,(2007).

[56] D.P. Singh, "Synthesis and growth of ZnO nanowires" Sci. Adv. Mater. 2, 245-272 (2010).

[57] M.S. Akhtar, K.K. Cheralathan, J.M. Chun and O.B. Yang "Composite electrolyte of heteropolyacid (HPA) and polyethylene oxide (PEO) for solid-state dye-sensitized solar cell" Electrochim. Acta 53, 6623-6628(2008)

[58] S. Ito, T. Kitamura, Y. Wada and S. Yanagida, "Facile fabrication of mesoporous TiO_2 electrodes for dye solar cells: chemical modification and repetitive coating" Sol. Energy Mater. Sol. Cells 76, 1, 3-13(2003)

[59] Rajeev R Prabhu and M Abdul Khadar "Characterization of chemically synthesized CdS nanoparticles" Pramana Indian Academy of Sciences, 65, 5 Pramana J Phy, 801-807 (2005) .

[60] Blok L. and Debruyn I P.L,"The ionic Double Layer at the ZnO/Solution Interface. I The Experimental Point of Zero Charge", J. Colloid Interface Sci., 32, 518-526 (1970).

[61] Marek Kosmulski, "The significance of the difference in the point of zero charge between rutile and anatase", Adv. Colloid Interface Sci., 99,255-264,(2002).

[62] Kallay N, Babic D and Matijevic E "Adsorption at solid/solution interfaces II. Surface charge and potential of spherical colloidal titania" Colloids Surf.19,375-386 (1986)

[63] Xue-LianYu, Jun-GuoSong, Ying-Song Fu, YangXie, XinSong, Jing Sun and Xi-Wen Du "ZnS/ZnO Heteronanostructure as Photoanode to Enhance the Conversion Efficiency of Dye-Sensitized Solar Cells" J. Phys. Chem. C,114,2380-2384 (2010)

[64] J B Baxter, A M Waker ,K van Ommering and E S Aydil "Synthesis and characterisation of ZnO nanowires and their integration into dye sensitized solar cells" Nanotechnol. 17 2006, 304-312 (2006)

[65] Jooyoung Chung, JihyunMyoung, Jisook Oh and Sangwoo Lim "Synthesis of a ZnS Shell on the ZnO Nanowire and Its Effect on the Nanowire-Based Dye-Sensitized Solar Cells" J. Phys. Chem. C,114,21360-21365 (2010)

[66] Tao Gao, Qiuhong Li and Taihong Wang "Sonochemical Synthesis, Optical Properties, and Electrical Properties of Core/Shell-Type ZnO Nanorod /CdS Nanoparticle Composites" Chem. Mater.,17,887-892 (2005)

[67] Butera D, Tesoriere L, Gaudio RD, BongiornoA,Allegra M, Pintaudi AM, Kohen R and Livrea MA "Antioxident activities of Sicilian prickly pear (Opuntia ficus indica) fruit extracts and reducing properties of its betalains : Betanin and indicaxanthin" J. Agric. Food. Chem. 50: 6895-6901 (2002).

Chapter 8

Summary and scope for future works

8.1 Abstract:

This chapter concludes the thesis by summarizing the research work and presenting the future scope based on this work.

8.2 Summary

This thesis reports on the potentiality of betanin natural dye and their composites with controlled morphologies of ZnO in the field of nanophotonics in general and in nonlinear optics and photochemical solar conversion specifically.Based on the experimental results and discussions elaborated in the chapters 3-7, a few conclusions can be drawn for this thesis work:

Very simple wet chemical methods are used to synthesize ZnO samples. The parameters that can affect the growth of ZnO were investigated in chapter 3. The optical absorption and fluorescence spectroscopy are used to characterise ZnO crystals. The as synthesized ZnO crystals have potential photonic device applications.

Polymer nano/micro composites are attracting considerable interest in polymer science research. Incorporation of different nanostructures into polymers significantly enhances their mechanical, thermal and optical properties. Bio-based materials have gained large interest as they are environmental friendly and renewable.

The nonlinear optical properties of natural dyes and natural dye based composites are becoming a subject of numerous investigations in very recent years due to their unique photonic applications. The potentialities of betanin natural dye in the field of nanophotonics and in nonlinear optics is also reported. The linear optical properties of betanin natural dyes: dye sensitized solar cells were also studied in this thesis.

The next stage in this work was to investigate the nonlinear optical properties of the ZnO composites, betanin natural dye and bio-inspired hybrid materials (betanin-ZnO). The third order nonlinearities of these samples have been characterized to assess their suitability for applications in photonics. The natural dye reinforcements with the biodegradable polymers have a high potential for the design of environmentally friendly green materials for the future applications.

The next stage in this work was to bring the knowledge gained from previous two chapters and was studied the bio-inspired hybrid materials (betanin-ZnO) for photonic applications through nonlinear optical studies. Hybrid composites present a paramount advantage for miniaturization, multifunctionalization of devices and opening a land of opportunities for applications in the field of photonics. Looking to the future, there is no doubt that these new generations of hybrid materials will open a land of promising applications in many areas: optics, electronics, energy, environment, biology, functional smart coatings, fuel and solar cells, catalysts and sensors, etc.

The final stage was to integrate the ZnO crystals into DSSC under low light conditions.

8.2.1 Major findings:

- We were successful in synthesizing ZnO crystals with different morphology through simple, low temperature wet chemical method.
- It was found that the growth duration plays a crucial role in the face orientation of ZnO crystals and the precursor concentration and temperature have no obvious influence on the morphology but only affect the size slightly.
- The room temperature photoluminescence of ZnO structures exhibit UV and visible emission depending on the morphology.
- The optical limiting enhancements in ZnO nanoplates and nanoflakes were mostly contributed from the interfacial interaction between the

structure and the local-field enhancement in addition a one photon assisted energy transfer from the excited state to the nearby trapping sites.

- The rods can confine an externally launched light into its cavity structure, which provides an enhanced effective optical path length to confine the light show perfect switching behaviour.
- The solvent modified the linear absorption spectra and nonlinear behavior of betanin natural dye.
- We observe a change over in the sign of nonlinearity due to the interplay of exciton bleaching and optical limiting mechanisms. Light confinement effect, physical necking effect and ship- in-a bottle effect play crucial roles.
- The photochemical performance of DSSC with NS based photo anode with ferrocene based and iodide in acetonitrile solution exhibit better efficiency of 0.868% and 2.99% with a small input power of few K lx.
- We found that, incorporation of Au NPs led to enhanced power conversion efficiency from 0.868% to 1.71% and IPCE of 14% with ferrocene based electrolyte.
- The DSSC with the TiO_2-ZnO composite structure exhibited a significant increase in cell performance and IPCE compared with other composites.
- In our investigation, DSSCs with the additions of TiN nanoparticles exhibited considerably higher solar to-electricity conversion efficiencies than the corresponding DSSC without these additions.

Low efficiency and low stability are the major challenges for the commercialisation of DSSCs. The factors affecting for the low efficiency and stability of DSSCs are

- poor performance of dyes in the NIR region,
- poor contact between the electrodes,
- low volatility and high viscosity of electrolytes,
- degradation of electrolyte properties due to UV absorption of light.

There are different factors to improve the performance of DSSCs. The improvement in the morphologies of semiconductor to reduce the dark current, developing low volatile and less viscous electrolytes to improve the charge transfer rate and use of additives for dyes and electrolytes that enhance their properties .These can be recommended in order to enhance the efficiency and stability of DSSC.

8.3 Scope for the further study

Based on the substantial experimental results, scientific discussion presented and conclusions drawn from this work, several potential directions for future research are highlighted below:

- The nonlinear optical properties of different natural dyes and dye mixtures
- The natural dye itself is not necessarily fluorescent. The laser induced fluorescence behaviour of dye molecules.
- The nonlinear optical behaviour of the natural dye in powder form
- The ZnO thin film sensor is a promising candidate for the sensor development and the ability to integrate with MEMS and IC based technology.
- Future results will be directed towards using various natural dyes and dye mixtures for the photonic applications including DSSC.
- The optimisation of quantum dots on ZnO can be studied for the photovoltaic applications.
- Multi hetero junction DSSC can also be studied for the photovoltaic applications.
- Temperature dependant studies on the performance of DSSC to understand the dynamics of thermal induced processes.
- Optimisation of electrolytes
- Our research focussed primarily on the natural dye incorporated ZnO composites for photonic device applications especially for DSSC, but did not determine the stability of the DSSC performance over an extended period of use. Although, DSSCs sensitised with betanin natural dye achieved better efficiency, it is unknown how long this performance will last. In order to analyze the commercialization of DSSC, the durability of the DSSC must be determined. Additional experiments should examine whether the performance of the DSSCs changes in natural sunlight.

****

APPENDIX

AIP | Journal of Applied Physics

Effect of betanin natural dye extracted from red beet root on the non linear optical properties ZnO nanoplates embedded in polymeric matrices

Aparna Thankappan, Sheenu Thomas, and V. P. N. Nampoori

Citation: J. Appl. Phys. **112**, 123104 (2012); doi: 10.1063/1.4768930
View online: http://dx.doi.org/10.1063/1.4768930
View Table of Contents: http://jap.aip.org/resource/1/JAPIAU/v112/i12
Published by the American Institute of Physics.

Effect of betanin natural dye extracted from red beet root on the non linear optical properties ZnO nanoplates embedded in polymeric matrices

Aparna Thankappan,[1,2,a)] Sheenu Thomas,[1] and V. P. N. Nampoori[1]
[1]*International School of Photonics, Cochin University of Science and Technology, Kochi, India*
[2]*Inter University Centre for Nanomaterials and Devices, Cochin University of Science and Technology, Kochi, India*

(Received 10 October 2012; accepted 12 November 2012; published online 18 December 2012)

In this article, we have investigated the effect of betanin natural dye extracted from red beetroot on nonlinear optical properties of ZnO nanoplates embedded in polymeric matrices through the *Z*-scan technique using an Nd: YAG laser (532 nm, 7 ns, 10 Hz). We observed reverse saturable absorption (RSA) at 532 nm for dye and ZnO nanoplates. A strong influence on RSA behavior of nanoplates-PVA matrix was observed by adding betanin natural dye. The influence of betanin on the nonlinear character of ZnO-PVA system leads to saturable absorption and again to RSA on increasing input fluence. Such a change over in the sign of the nonlinearity is due to the interplay of the exciton bleaching and optical limiting mechanisms, and probably due the presence of sucrose. Theoretical analysis has been performed using a model based on nonlinear absorption coefficient and saturation intensity. The result of present study gives an additional mechanism for the gain enhancement in dye doped ZnO matrix. © *2012 American Institute of Physics*. [http://dx.doi.org/10.1063/1.4768930]

I. INTRODUCTION

In recent decades, there has been great interest in engineering and synthesizing different kinds and structures of solid and liquid media that possess high nonlinear refraction (NLR) and/or nonlinear absorption (NLA).Optical materials with large coefficients of reverse saturable absorption (RSA) and nonlinear refraction can exhibit irradiance-dependent transmittance and phase shift, which cooperatively limit the throughput fluence(optical energy per unit of area).[1] Materials with large optical nonlinearity are key elements in many areas of photonics and optical technology such as all-optical switching (optical computer) devices, three dimensional fluorescence imaging, and optical limiting. However, most of the synthesized materials require elaborate preparation procedures and safety measures, use or generation of hazardous materials, costly materials, as well as fragile or chemically unstable structures beyond certain threshold irradiance. Therefore, we suggest natural dye extracts as environment friendly, safe, and inexpensive materials, as well as having high chemical stability during optical excitations with coherent light sources.

Besides anthocyanins, chlorophylls, and carotenoids, betalains are the most common pigments in the plant kingdom. These natural pigments from plants have been extensively investigated as sensitizers for the DSSC,[2] in which red beetroot pigments maximum conversion efficiency of 0.67%.[3] Though the former have inherent limitations as sensitizers owing to weak absorption of green wavelengths, the absorption spectra of the latter have more favorable overlap with the solar spectrum. The betalain pigments comprise the red-purple betacyanin, betanin (**I**), and betanidin (**II**), with maximum absorptivity at λ_{max} about 535 nm, and the yellow betaxanthins with λ_{max} near 480 nm.[4]

The structure of betanin is shown in Fig. 1. Betanin, the red-purple pigment distributed in beets, is the 5-*O*- *β*-glucoside of betanidin. Beetroot is one of the richest source of betanin, the most studied betalain, was selected as a topic of the present study because of good colorant yield and the prominent peak in the visible region of the spectrum for better quantitative analysis. Unlike synthetic dyes, these beetroot based natural dyes are eco-friendly and pose no environmental problems, which are very important for some sensitive applications. Determination of second and third order nonlinearities are of fundamental importance for evaluation of the properties with respect to wave-guiding structures containing betanin.

The basic absorption processes in dyes can be divided into linear and nonlinear absorption. Nonlinear absorption is a phenomenon defined as a nonlinear change (increase or decrease) in absorption with increasing intensity. This can be of either two types: saturable absorption (SA) and reverse saturable absorption (RSA). Depending on the pump intensity and on the absorption cross-section at the excitation wavelength, most molecules shows nonlinear absorption. With increasing intensity, if the excited states show saturation owing to their long lifetimes, the transmission will show SA characteristics. If, however, the excited state has strong absorption compared with that of the ground state, the transmission will show RSA characteristics. Therefore, it is necessary to identify their nonlinear absorption effects, and to determine their nonlinear absorption parameters, such as the saturable intensity for saturable absorber, the TPA coefficient for two-photon absorbing material. These properties are commonly defined in terms of intensity dependant

[a)]aparna.subhash@gmail.com. Telephone: 0091-484-2575848. Fax: 0091-484-2576714.

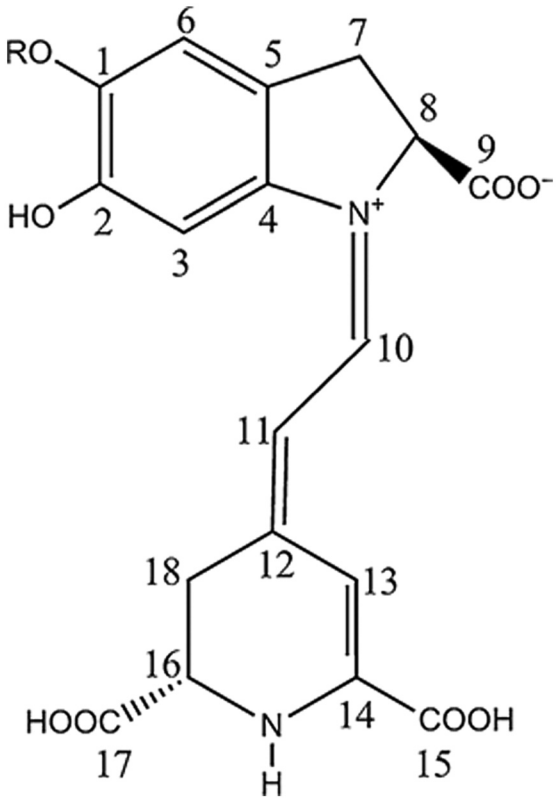

FIG. 1. Structure of betanin pigment.

nonlinear absorption coefficient $\alpha(I)$,which can be written in terms of linear absorption coefficient α and two photon absorption coefficient β as

$$\alpha(I) = \alpha + \beta I. \quad (1)$$

In this paper, we report the techniques used to prepare the betanin natural dye extracts, optical characterizations, and the effect of betanin natural dye on the optical non linearity of ZnO nanoplates will be discussed. Also, we are presenting some of our findings and suggestions. It is well known that ZnO is a promising material for these applications because of its large room temperature band gap of 3.37 eV and also the fact that the exciton binding energy of 60 meV should ensure excitonic survival well above room temperature.[5] Therefore it is a suitable candidate for ultraviolet optoelectronic applications.

II. EXPERIMENTAL METHOD

All chemicals were purchased from Merck Ltd used as received without further purification. The nutrient solution was prepared from an aqueous solution of zinc nitrate hexahydrate [Zn $(NO_3)_26H_2O$] and hexamethylenetetramine (HMTA) $[(CH_2)_6N_4]$. The hexamine solution was added to the zinc nitrate solution drop wise while stirring. Finally, the solution is kept undisturbed at 80 °C for 18 h, ZnO nanoplates ($E_g = 3.33$ eV) are formed. The size and morphology of ZnO samples were characterized by scanning electron microscopy (JEOL/EO and JSM6390). The X-ray diffraction data were collected on an AXS Bruker D% diffractometer using Cu Kα-radiation ($\lambda = 0.1541$ nm, the operating conditions were 35 m A and 40 kV at a step of 0.020 ° and step time of 29.5 s in the 2θ range from 30° to 70 °. The extracts of the red beets were obtained from fresh biological materials, pigments can be water extracted and slight acidification of the extraction medium enhances the betacyanin stability and avoids oxidation. The pigment extracts must be protected from direct light exposure should be kept in cool place. Dye extracts have been optically characterized by measuring maximum absorptivity at about 535 nm, using a UV/Vis spectrophotometer (Jasco V-570 UV/VIS/IR.)

To determine third order nonlinear optical characteristics of samples such as nonlinear absorption, the single beam z scan technique proposed and demonstrated by Sheik-Bahae *et al.*,[6] was employed. The transmission of a laser beam that changes near the focal point during the sample translation along the propagation path through an open-aperture (OA) was measured. A Q-switched Nd: YAG laser (Spectra PhysicsLAB-1760, 532 nm, 7 ns, 10 Hz) was used as the light source. A 20 cm converging lens was used to focus the laser beam. The radius of the beam ω_0 was calculated to be 35.4 μm. The Rayleigh length, $z_0 = \pi\omega_0^2/\lambda$, was estimated to be 7.4 mm, which is much greater than the thickness of the sample, and is an essential prerequisite for z-scan experiments. The sample was fixed on a computer-controlled translation stage, so that it could be accurately moved through the focal region of the laser beam over a length of 6 cm. The transmitted beam energy, reference beam energy, and the ratios were measured simultaneously using an energy ratio meter (Rj7620, Laser Probe, Corp.) having two identical pyroelectric detector heads (Rjp735). The detected signals were acquired, stored, and processed by the computer. Optical density filters were used to vary the laser intensity at the lens focus. To avoid sedimentation of nanocrystals, the solution was centrifuged and washed several times and finally embedded into the polyvinyl alcohol solution and developed the free standing films of thickness around 80 μm (Plasto Mek, delta.0.2 kW, 230 V, 1 phase), these films are used as samples.

III. RESULTS AND DISCUSSION

In order to examine the surface morphology and for measurement of the dimensions, SEM was used. Typical SEM image of ZnO nanoplates is shown in Fig. 2(a). The average thickness of the nanoplates is around 0.4 μm. It can be seen that all diffraction peaks are caused by crystalline ZnO with hexagonal wurtzite structure (space group: P63mc; a = 0.3249 nm, c = 0.5206 nm). The XRD pattern shown in Fig. 2(b) for nanoplates is found to match with that mentioned in JCPDS 36–1451, no characteristic peaks of impurity phases and no diffraction peaks except ZnO were found, which indicates that only single phase hexagonal ZnO is present. The linear absorption spectra of ZnO nanoplates, betanin, and betanin doped ZnO nanoplates free standing films is shown in Fig. 3. In the linear absorption spectra of betanin natural dye, the peak around 535 nm is attributable to betanin.

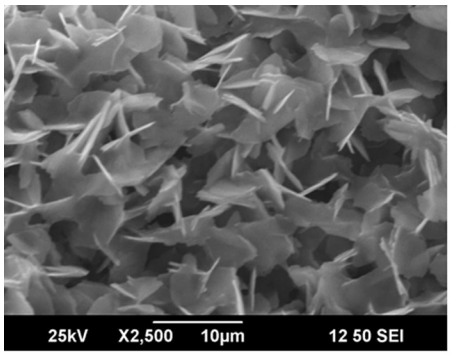

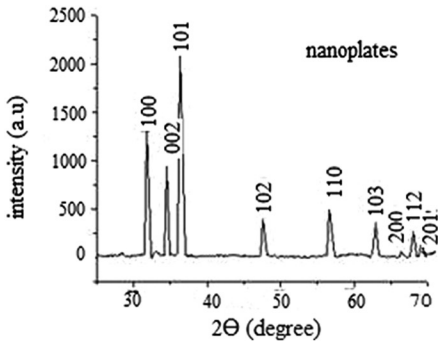

FIG. 2. (a) SEM image of ZnO nanoplates and (b) corresponding XRD pattern.

The nonlinear absorption was measured from the normalized energy transmission using Z-scan without an aperture. Fig. 4 shows the plot related to open aperture z-scan experiment in betanin films at resonance wavelength of 532 nm with different input fluence. When the sample is away from the focus, the weak intensity cannot induce any nonlinearity, and have unit transmittance. As the sample moved towards the focus, the transmittance acutely decreases with increasing light intensity to less than unity, resulting in induced absorption.[7] The data are analyzed using the procedures described by Sheik–Bahae *et al.* for a two-photon absorption (TPA) process.

The transmitted OA Z scan signal is give by

$$T(z, S = 1) = \sum_{m=0}^{\infty} \frac{[-q_0(z,0)]^m}{(m+1)^{3/2,}} \tag{2}$$

where

$$q_0(z,t) = \frac{\beta I_0(t) L_{eff} z_0^2}{z^2 + z_0^2}, \tag{3}$$

$$\mathrm{L_{eff}} = [1 - \exp(-\alpha 1)]/\alpha, \tag{4}$$

where m is an integer the parameter q_0 can be obtained by fitting the experimental results to the Eq. (2), where Z_0 and Z are the Rayleigh range and the translated length parallel to the beam propagation, respectively. I_0 denotes the intensity of the incident beam at the focal point.

Experimentally determined nonlinear absorption coefficient (β) can be used in finding the absolute value of the third-order nonlinear optical susceptibility, through the relation,

$$\mathrm{Im}\left(\chi^{(3)}\right) = \mathrm{n_0^2 c^2 \beta / 240 \pi^2 \omega (esu)}, \tag{5}$$

where n_0 is the linear refractive index of the film, c is the velocity of light in vacuum, ω is the angular frequency of radiation used, and β the nonlinear absorption coefficient. The estimated average value of Im ($\chi^{(3)}$) is 1.7027×10^{-10}esu for ZnO/betanin/PVA film, 2.432×10^{-10}esu for nanoplates/PVA and 1.891×10^{-10}esu for betanin/PVA film.

When SA is present Eq. (1) modifies to

$$\alpha(\mathrm{I}) = \alpha_0/1 + (\mathrm{I}/\mathrm{I_s}). \tag{6}$$

If excitation intensity I_0 is less than I_s, we can consider SA as a third order process and in such cases $-\alpha_0 / I_s$ is equivalent to nonlinear absorption coefficient β which will then give $\mathrm{Im}\chi^{(3)}$.

In general, induced absorption can occur in nanoclusters and in betanin natural dye, due to a variety of processes such as excited state absorption, two-photon absorption, interband and intraband transitions and nonlinear scattering.[8] The theory of two photon absorption process fitted well with the

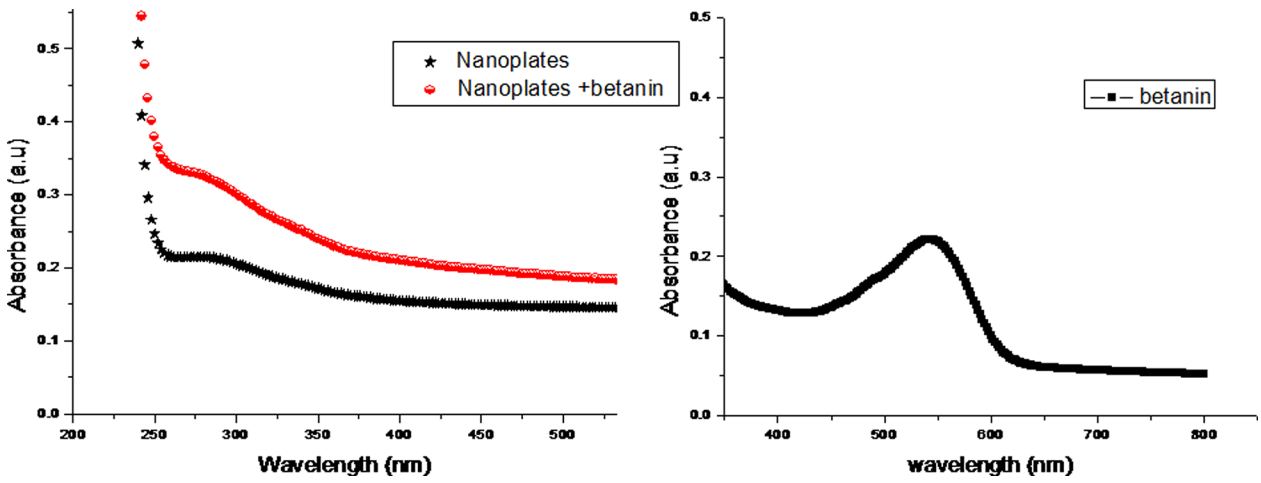

FIG. 3. (a) The UV–Vis absorption spectrum of the ZnO nanoplates/PVA and dye doped nanoplates/PVA composite film and (b) corresponding of betanin/PVA.

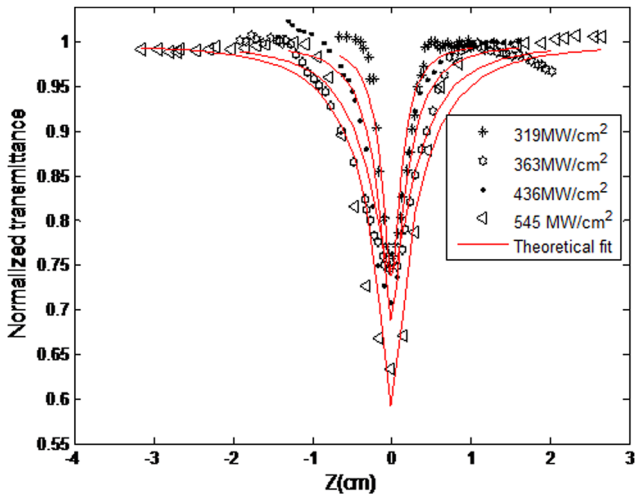

FIG. 4. Open aperture Z scan curve of betanin/PVA composite film at different input fluences.

experimental curve, indicating that TPA is the basic mechanism for induced absorption, but the possibility of the higher order nonlinear process such as free carrier absorption contributing to the induced absorption cannot be ruled out.

To estimate the role of betanin in ZnO nanoplates, we also performed open aperture Z scan measurement on betanin alone and betanin doped ZnO/PVA. No obvious nonlinear absorption effect was found for PVA alone.[9] At the resonant wavelength of 532 nm, the optical nonlinearity increases with the input fluence. Fig. 5 shows the combined open aperture curve for the ZnO /PVA sample and the effect of betanin on the ZnO/PVA. We assume the –COOH on the five membered rings to be the most acidic of the three carboxylic acid groups on Betanin. Surprisingly, due to the acid treatment the RSA behavior of the nanoplates switched to SA at input fluence of 319 MW/cm^{2}and 363 MW/cm^2 and again due to the increase of the fluence the RSA behavior was retained. The observed switch over behavior could be due to the bleaching of the ground state plasmon band, i.e., in the case of the intraband transition, the ground-state electrons are pumped to the excited-state. The excited electrons are free carriers possessing a whole spectrum of energies, both kinetic and potential, immediately after the absorption the electrons excited relax to the ground-state through electron–electron, electron–phonon, and phonon–phonon interactions. Once these electrons are excited by a pulse close to absorption peak, they do not oscillate at the same frequency as that of the unexcited electrons, thus causing the ground-state plasmon band to bleach or reduced in intensity, which is almost synchronous with the primary photon absorption.

The light absorption in betanin excites π electrons of the pigment chromophore to a more energetic state (π^*), increasing reactivity or lowering activation energy for the molecule.[10] It is possible that the presence of other compounds than the dye itself, e.g., sucrose, can affect the optical non linearity of nanoplates, if it is not highly purified extract and irreversible damage induced by the input pulses is also the another factor.

An enhancement of the gain in ZnO nanoplates-PVA matrix is observed on the addition of the betanin. This is attributed to the visible transition of betanin that is well-described as a HOMO→LUMO excitation from the aromatic ring to the matrix. The pump beam (532 nm) will excite both dye and nanoplates by one photon and two photon absorption, respectively. The excited dye molecules transfer their energy to the nanoplates leading to the intraband electron excitation causing ground state bleaching at input fluence up to 363 MW/cm^2 leading to saturable absorption, but with further increase of intensity the behavior switched to induced absorption. Such change over in the sign of the nonlinearity

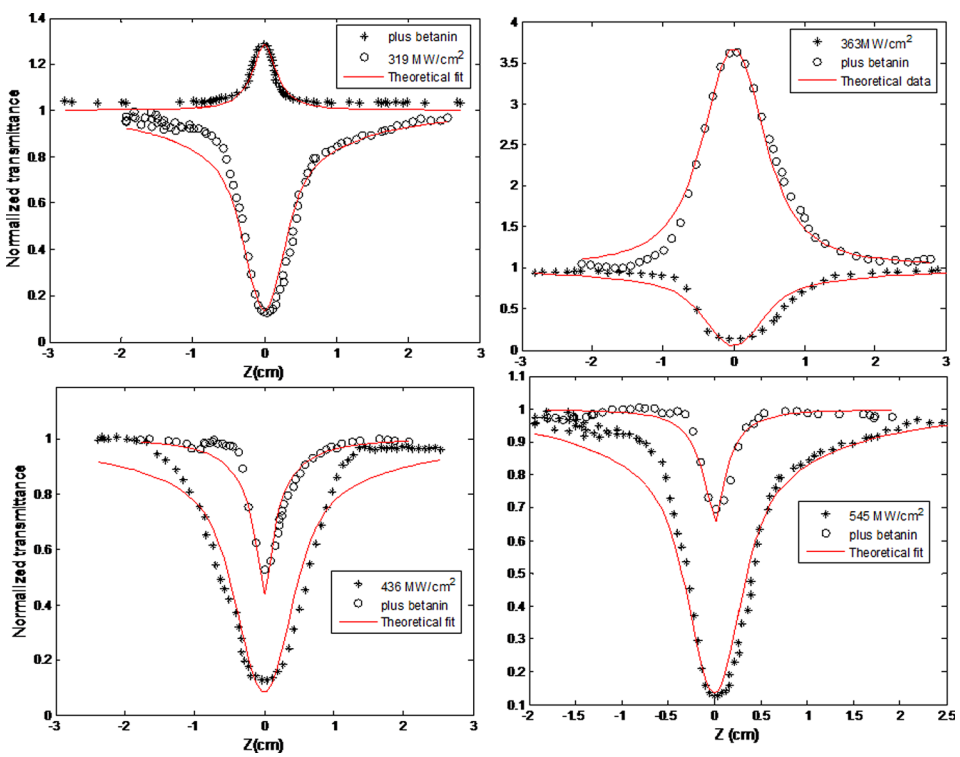

FIG. 5. Open aperture Z scan curves showing the effect of betanin on nanoplates/PVA composite film (a) 319 MW/cm^2, (b) 363 MW/cm^2, (c) 436 MW/cm^2, and (d) 545 MW/cm^2.

is due to the interplay of the exciton bleach and optical limiting mechanisms. In the present case the irreversible damage induced by the input pulses and the presence of sucrose are supposed to play the significant role in the observed transition from SA to RSA on increase of input fluence.Therfore, the role of instantaneous two photon absorption in nonlinear effect observed at the intensity above $363\,MW/cm^2$ is significant.

Switchover from SA to RSA on increase of the input intensity has been observed in various materials under nanosecond and picoseconds pulse excitation.[11–13] In Figs. 5(a) and 5(b), the theoretical fit gives the saturation intensity $I_s = 0.199\,MW/m^2$ and $1.0458\,MW/m^2$, respectively, and two photon absorption coefficient of betanin, nanoplates, and the dye doped nanoplates embedded polymer are $\beta = 4.37 \pm 1\,m/GW$, $4 \pm 2\,m/GW$, and $3 \pm 0.5\,m/GW$, respectively (I_s is estimated only for SA and β for RSA). Results of the present study provide additional mechanism for gain enhancement.

IV. CONCLUSIONS

In summary, Z scan experiments have revealed interesting features of nonlinear absorption properties of betanin doped ZnO nanoplates embedded in PVA. At 532 nm excitation, the RSA behavior was observed for both betanin and nanoplates. After doping of betanin the RSA behaviors of nanoplates switched to SA and finally to RSA depending on the input fluence.The saturation intensity and nonlinear absorption coefficient were estimated by fitting to the experimental data. The betanin plays the important role in the nonlinear behavior of nanoplates. Due to the simultaneous occurrences of nonlinear processes, this system can be made use of in developing various photonic devices.

The author AT acknowledges to IUCND for the financial support.

[1]T.-H. Wei, T.-H. Huang, T.-T. Wu, P.-C. Tsai, and M.-S. Lin, Chem. Phys. Lett. **318**, 53 (2000).
[2]M. Thambidurai, N. Muthukumarasamy, Dhayalan Velauthapillai, N. Sabari Arul, S. Agilan, and R. Balasundaraprabhu, J. Mater. Sci: Mater. Electron. **22**, 1662 (2011).
[3]C. Sandquist and J. L. McHale, J. Photochem. Photobiol., A **221**, 90 (2011).
[4]D. Zhang, S. M. Laniera, J. A. Downing, J. L. Avent, J. Lumc, J. L. McHalea, J. Photochem. Photobiol., A **195**, 72 (2008).
[5]C. Y. Jiang, X. W. Sun, G. O. Lo, and D. L. Kwong, J. Appl. Phys. Lett. **90**, 263501 (2007).
[6]M. S., Bahae, A. A. Said, T. H. Wei, D. J. Hagan, E. W. Van Stryland, IEEE J. Quant. Electron. **26**, 760 (1990).
[7]M. Hari, S. A. Joseph, N. Balan, S. Mathew, R. kumar, G. Mishra, R. R. Yadhav, P. Radhakrishnan, and V. P. N. Nampoori, J. Nonlinear Opt. Phys. Mater. **20**, 467 (2011).
[8]Q. Shiliang, G. Yachen, J. Xiongwei, Z. Huidan, S. Yinglin, Q. Jianrong, Z. Congshan, and K. Hirao, Opt. Commun. **224**, 321 (2003).
[9]B. Nithyaja, H. Misha, P. Radhakrishnan, and V. P. N. Nampoori, J. Appl. Phys. **109**, 023110 (2011).
[10]H. M. C. Azeredo, Int. J. Food Sci. Technol. **44**, 2365–2376 (2009).
[11]S. V. Rao, N. K. M. N. Srinivas, and D. N. Rao, Chem. Phys. Lett. **361**, 439–445 (2002).
[12]Y. Gao, Q. Chang, H. Ye, W. Jiao, Y. Song, Y. Wang, and J. Qin, J. Appl. Phys. B **88**, 255 (2007).
[13]N. K. M. N. Srinivas, S. V. Rao, and D. N. Rao, J. Opt. Soc. Am. B **20**, 2470 (2003).

Optics & Laser Technology 52 (2013) 37–42

Contents lists available at SciVerse ScienceDirect

Optics & Laser Technology

journal homepage: www.elsevier.com/locate/optlastec

Optical characterization of ZnO nanoplates embedded in polymeric matrices for optical limiting applications

Aparna Thankappan [a,b,*], Divya S. [a], Sheenu Thomas [a], V.P.N. Nampoori [a]

[a] International School of Photonics, Cochin University of Science and Technology, Kochi, India
[b] Inter University Centre for Nanomaterials and Devices, Cochin University of Science and Technology, Kochi, India

ARTICLE INFO

Article history:
Received 22 January 2013
Received in revised form
6 March 2013
Accepted 25 March 2013

Keywords:
ZnO
SEM
Reverse saturable absorption

ABSTRACT

We report on the optical characterization, including linear and non linear, of ZnO nanoplates embedded in PVA. Nonlinear optical characterization of these films was studied by the *Z*-scan technique using an Nd:YAG laser (532 nm, 7 ns, 10 Hz).The studies show that the material is highly nonlinear, have desirable lower optical liming threshold of 46.86 MW/cm^2 at pump power of 436 MW/cm^2 and with negative refractive index. Therefore, these films with immobilized semiconductor nanoplates appear to be attractive candidates for optical limiting applications.

1. Introduction

In recent years, wide-band-gap semiconductor compounds have attracted a great deal of attention because of the intense commercial interest in developing practical short wavelength semiconductor diode lasers for huge market needs [1]. ZnO is a promising material for these applications because of its large room temperature band gap of 3.37 eV, and also due to the fact that the exciton binding energy of 60 meV should ensure excitonic survival well above room temperature [2].Therefore, it is a suitable candidate for ultraviolet optoelectronic applications. For these reasons, a thorough understanding of recombination mechanisms and its third order optical non linearity is necessary. ZnO belongs to the space group $P6_3mc$ in the II–VI group of semiconductors. It is normally in the hexagonal (wurtzite) crystal structure, showing n-type conductivity due to intrinsic donor defects.

Because the structure of ZnO, including the morphology, aspect ratio, size, orientation, and density of crystal, has great effects on its properties and applications and is usually influenced by the preparation techniques, researchers have prepared many different-shaped ZnO nano structures in order to fit various applications. So far, prismatic [3], belt like [4], flower like [5], tubular [6], tower like [7], and plate-like [8] ZnO have been reported using physical and chemical techniques [9]. However, the assembly of nanoparticles in matrices is of the major interest in several optical and sensor applications [10], especially those requiring large area coating. The common approach to such materials includes casting of films using the mixture of nanoparticles and polymer and another is inbuilt growth inside the solid matrix. The former mode of fabrication of films is of interest in the present study. But to our knowledge, optical non linearity of free standing polymer film incorporated with plates like ZnO structure synthesized through simple wet chemical method are the first time. In this work we are focused on the third order non linear absorption and refraction properties of ZnO nanoplates.

The basic absorption processes can be divided into linear and nonlinear absorption. Nonlinear absorption is a phenomenon defined as a nonlinear change (increase or decrease) in absorption with increasing intensity. This can be of either two types: saturable absorption (SA) and reverse saturable absorption (RSA). Depending on the pump intensity and on the absorption cross-section at the excitation wavelength, most molecules shows nonlinear absorption. With increasing intensity, if the excited states show saturation owing to their long lifetimes, the transmission will show SA characteristics. If, however, the excited state has strong absorption compared with that of the ground state, the transmission will show RSA characteristics. Therefore, it is necessary to identify their nonlinear absorption effects, and to determine their nonlinear absorption parameters, such as the saturable intensity for saturable absorber, the TPA coefficient for two-photon absorbing material. These properties are commonly defined in terms of intensity dependant non linear absorption coefficient $\alpha(I)$, which can be written in terms of linear absorption coefficient α and two photon absorption coefficient β as $\alpha(I)=\alpha+\beta I$.The non linear optical response of the nanoplates/PVA film has been

* Corresponding author at: Inter University Centre for Nanomaterials and Devices, Cochin University of Science and Technology, Kochi, India.
Tel.: +91 484 2575848; fax: +91 484 2576714.
E-mail address: aparna.subhash@gmail.com (A. Thankappan).

0030-3992/$ - see front matter © 2013 Elsevier Ltd. All rights reserved.
http://dx.doi.org/10.1016/j.optlastec.2013.03.016

experimentally investigated by means of a single beam Z scan technique. The samples exhibit promisingly large non linear absorption properties characterized by reverse saturable absorption (RSA) [11–13]. This makes evaluation of non linear optical parameters straight forward. Preliminary investigations of the optical limiting capability of these films appear quite promising. Our methodology opens up a wide range of possibilities of nanoplates.

2. Experimental method

All chemicals were purchased from Merck Ltd., and used as received without further purification. The nutrient solution was prepared from an aqueous solution of zinc nitrate hexahydrate [$Zn(NO_3)_2 6H_2O$] and hexamethylenetetramine (HMTA) [$(CH_2)_6N_4$]. The hexamine solution was added to the zinc nitrate solution drop wise while stirring. Finally the solution is kept undisturbed at 80 °C for 18 h. The following reactions were involved in the crystal growth of ZnO [14].

$$(CH_2)6N_4+6H_2O \rightarrow 6CHOH+4NH_3 \quad (1)$$

$$NH_3+H_2O \leftrightarrow NH_4^+ + OH^- \quad (2)$$

$$Zn(NO_3)_2+H_2O \rightarrow Zn^{2+}+2HNO_3 \quad (3)$$

$$OH^-+Zn^{2+} \rightarrow ZnO(S)+H_2O \quad (4)$$

The reaction decomposes HMT to formaldehyde (HCHO) and ammonia (NH_3), acting as a pH buffer by slowly decomposing to provide a gradual and controlled supply of ammonia, which can form ammonium hydroxide and support OH^- [15]. Finally OH^- anions react with Zn^{2+}cations to form ZnO. To avoid sedimentation of nanocrystals, the solution was centrifuged and washed several times and finally embedded into the polyvinyl alcohol [$-CH_2CH(OH)^-$]n solution(15%) and developed the free standing films (thickness 80 μm) (Plasto Mek,delta.0.2 kW, 230 V, 1 phase),this film is used as samples for the non linear studies. The thickness of the films was measured using a Mitutoyo Micrometer (series 193). Here, PVA acts as the matrix for the homogeneous distribution and immobilization.

The size and morphology of ZnO sample was characterized by scanning electron microscopy (JEOL/EO, and JSM6390). The X-ray diffraction data were collected on an AXS Bruker D% diffractometer using CuKα-radiation (λ=0.1541 nm,the operating conditions were 35 mA and 40 kV at a step of 0.020° and step time of 29.5 s in the 2θ range from 30 to 70°. The measurement of light absorption at room temperature was carried out using a spectrophotometer (Jasco V-570 UV/VIS/IR) and the measurement of fluorescence emission was recorded using a Cary Eclipse fluorescence spectrometer (Varian).

To determine third order non linear optical characteristics of ZnO nanoplates such as non linear absorption and non linear refraction, the single beam z scan technique proposed and demonstrated by Sheik-Bahae et al. [16] was employed. The transmission of a laser beam that changes near the focal point during the sample translation along the propagation path through an open-aperture (OA) and a closed-aperture (CA) was measured. A Q-switched Nd:YAG laser (Spectra PhysicsLAB-1760, 532 nm, 7 ns, 10 Hz) was used as the light source. A 20 cm converging lens was used to focus the laser beam. The radius of the beam ω_0 was calculated to be 35.4 μm. The Rayleigh length, $z_0=\pi\omega_0^2/\lambda$, was estimated to be 7.4 mm, which is much greater than the thickness of the sample, and is an essential prerequisite for z-scan experiments. The sample was fixed on a computer-controlled translation stage, so that it could be accurately moved through the focal region of the laser beam over a length of 6 cm. The transmitted beam energy, reference beam energy and the ratios were measured simultaneously using an energy ratio meter (Rj7620, Laser Probe Corp.) having two identical pyroelectric detector heads (Rjp735). The detected signals were acquired, stored and processed by the computer. Optical density filters were used to vary the laser intensity at the lens focus. The data were analyzed using the procedure described by Bahae et al. and the non linear coefficients were obtained by fitting the experimental Z-scan plot with theoretical plots.

3. Results and discussions

In order to examine the surface morphology and for measurement of the dimensions, SEM was used. A typical SEM image of ZnO nanoplates is shown in Fig. 1(a). The average thickness of the nanoplates is around 0.4 μm. These nanoplates consist of forests of tiny crystals, millions of which would fit in a single square centimeter. It can be seen that all diffraction peaks are caused by crystalline ZnO with hexagonal wurtzite structure (space group: $P6_3mc$; a=0.3249 nm, c=0.5206 nm). The XRD pattern shown in Fig. 1(b) for nanoplates is found to match with that mentioned in JCPDS 36-1451 [17], no characteristic peaks of impurity phases and no diffraction peaks except ZnO were found, which indicates that only single phase hexagonal ZnO is present.

The average crystalline size was calculated using Scherrer's formula [18], was found to be 0.521 μm. In Fig. 1(b),the strongest detected (hkl) peaks are at 2θ values of 31.8°, 34.6°, 36.4°, 47.6°, 56.7°, and 62.9°, corresponding to the following lattice planes: (100), (002), (101),(102), and (110), respectively. The d spacing along the (101) plane is 2.468 A°.The lattice constants a and c were determined as a=0.3249 nm and c=0.5206 nm by using following equation:

$$\frac{1}{d_{hkl}^2}=\frac{4}{3}\left(\frac{h^2+hk+k^2}{a^2}\right)+\frac{l^2}{c^2} \quad (5)$$

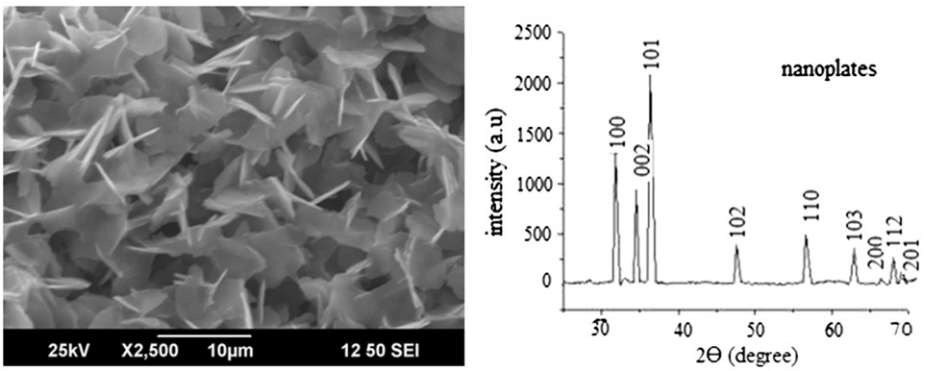

Fig. 1. (a) SEM image of ZnO nanoplates and (b) corresponding XRD pattern.

ZnO is a unique electronic and photonic semiconductor with band gap of 3.37 eV and a large exciton binding energy of 60 meV. We performed serious optical studies to evaluate the potentially optical qualities of ZnO nanoplates. The UV–vis spectrum (Fig. 2 (a)) shows a single absorption peak centered at 374 nm. The direct band gap of the same is estimated from the graph of $h\nu$ versus $(\alpha h\nu)^2$ (Fig. 2(b)) for the absorption coefficient α that is related to the band gap E_g as $(\alpha h\nu)^2 = k(h\nu - E_g)$, where k is the slope of the Tauc edge called the band tail parameter hν is the incident light energy [19]. By extrapolating the linear portion of the plot (i.e., Tauc extrapolation) to the energy axis gave the optical band gap value of 3.33 eV for ZnO nanoplates indicating excellent quality of the sample.

We further carried out the photoluminescence measurement as the function of wavelength to examine the quality of the products. As shown in Fig. 3, the spectrum of the products shows no significant changes. At room temperature, ZnO typically exhibit UV band edge emission and visible emissions. The nanoplates exhibit UV peak attributed to the near band edge (NBE) emission and no defect emission is detected. The detailed emission spectra of ZnO structure is shown in the Fig. 3. The emission for the visible light mostly caused by the defects in ZnO is very weak, indicating good quality of ZnO nanoplates. The enhanced UV emission indicates that the nanoplates possess high crystalline perfection.

The technique of open aperture (OA) and closed aperture (CA) Z scan scheme was employed to study the non linear optical properties of the nanoplates/PVA free standing film with different input fluence, and were plotted in Figs. 4 and 5. The non linear absorption and refraction were measured from the normalized energy transmission using Z-scan without an aperture and with an aperture respectively. The transmitted OA Z scan signal is give by [20]

$$T(z, S=1) = \sum_{m=0}^{\infty} \frac{[-q_0(z,0)]^m}{(m+1)^{3/2}} \tag{6}$$

where

$$q_0(z,t) = \frac{\beta I_0(t) L_{eff} z_0^z}{z^2 + z_0^2} \tag{7}$$

$$L_{eff} = \frac{[1-\exp(-\alpha 1)]}{\alpha} \tag{8}$$

where m is an integer. The parameter q_0 can be obtained by fitting the experimental results to Eq. (6), where Z_0 and Z are the Rayleigh range and the translated length parallel to the beam propagation, respectively. I_0 denotes the intensity of the incident beam at the focal point.

The values of n_2, calculated using Eq. (9), are

$$n_2 = cn_0\lambda\, \Delta\varphi_0/40\pi\, 2\pi I_0 L_{eff} \tag{9}$$

The Z scan traces are shown in Fig. 4; fits of Eq. (6) to the experimental data are depicted in the figure by solid curves. The TPA coefficient (β) can be determined by analyzing the measured

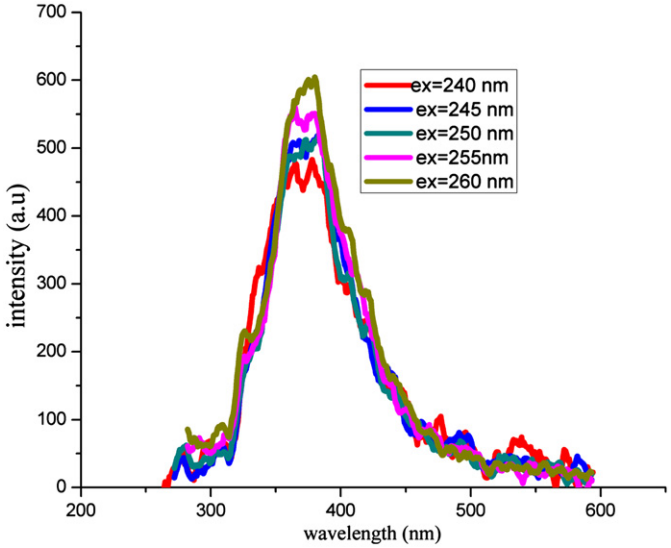

Fig. 3. Emission spectra of 1 mmol ZnO nanoplates.

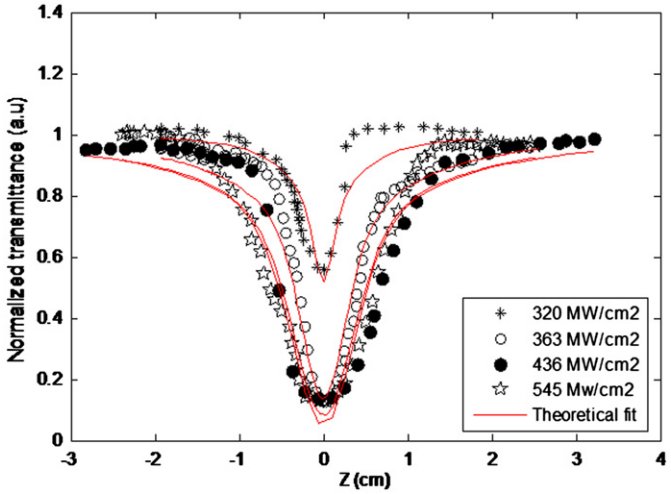

Fig. 4. Normalized transmittance of 1 mmol ZnO nanoplates/PVA composite film as the function of position for different input fluences in the open aperture scheme at 532 nm. The solid red line shows the theoretical fit. (For interpretation of the references to color in this figure legend, the reader is referred to the web version of this article.)

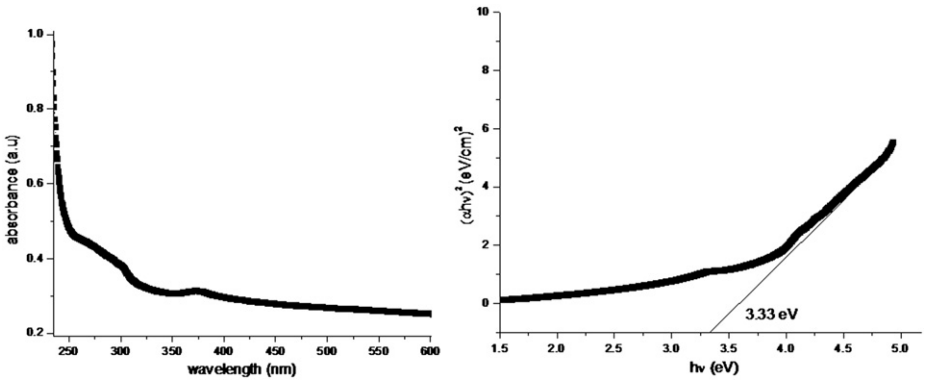

Fig. 2. (a) UV–vis absorption spectrum of the ZnO nanoplates (b) plot of $h\nu$ versus $(\alpha h\nu)^2$ for ZnO nanoplates.

OA Z scan trace. Under the experimental conditions, laser beam illumination at 532 nm usually corresponds to the two-photon absorption (TPA) process because the photon energy of the 532 nm laser is within the range $E_g < 2h\nu < 2E_g$, where $h\nu = 2.33$ eV and the optical band gap of nanoplates are 3.33 eV. Experimentally determined nonlinear refractive index n_2 and nonlinear absorption coefficient (β) can be used in finding the absolute value of the third-order nonlinear optical susceptibility, through the relation

$$\mathrm{Im}(\chi^{(3)}) = n_0^2 c^2 \beta / 240\pi^2 \omega (\mathrm{esu}) \quad (10)$$

$$\mathrm{Re}(\chi^{(3)}) = n_0 n_2 / 3\pi \quad (11)$$

where n_0 is the linear refractive index of the film, c is the velocity of light in vacuum, ω is the angular frequency of radiation used and β the non linear absorption coefficient. Z scan traces were made for four different input power densities and different concentrations of sample.

The non linear absorption coefficient calculated from the above fits shows a dependence on the input fluence and concentration. We have also studied the behavior of nanoplates by changing the concentration of sample solution 1.5 mmol (C2) and 2 mmol (C3). There is no significant shift in the energy band gap evaluated from the optical absorption spectra. The Measured values of imaginary part of the third-order susceptibility (Im χ^3) and optical limiting threshold at a wavelength of 532 nm for different irradiation intensities are tabulated in Table 1.

Generally, different processes, such as TPA, transient absorption, free carrier absorption interband absorption, photo ejection of electrons and nonlinear scattering, are reported to be operative in non linear absorption. The hence induced absorption can occur due to a variety of such processes. The experimental data shows a slight deviation from the theoretical curve which is fitted for two photon absorption. This deviation can be attributed to two photon induced free carrier absorption which is observed in particles with larger size [21].

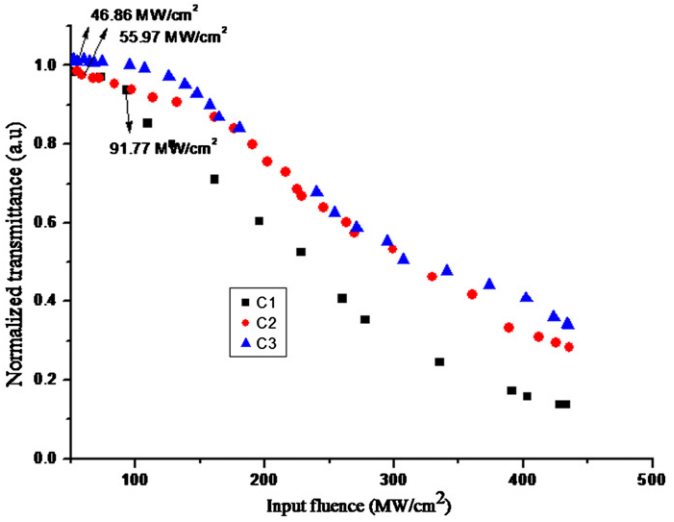

Fig. 5. Optical limiting response of ZnO nanoplates/PVA composite films for different concentrations at input fluence of 436 MW/cm^2.

The results of open aperture Z scan studies of samples shows that the β value is decreased with the increase in concentration of nanoplates and input fluence. As given in the table the non linear response of the nanoplates depend on both the pump power and the concentration. As the power or the concentration is increased, lowering of the non linear absorption co efficient occurs thereby diminishing the third order susceptibility, as reported by several workers [22,23], which can be due to the interplay of the non linear absorption and one photon assisted energy transfer from excited state to the nearby trapping site; and the local field enhancement through the size- and structure-dependent interfacial interaction between nanoplates [24].

One of the applications of reverse saturable absorption materials is in devices based on optical limiters, are devices that transmit light at a low input fluence, while they become opaque at high inputs. Reverse saturable absorption, which is generally associated with a large absorption cross section from excited state than the ground state, brings about optical limiting effects. In semiconductor materials the optical limiting is governed by TPA are observed in this study. Semiconductor films with high TPA coefficients and strong Kerr-induced nonlinear susceptibilities are very good candidates due to their small time response as optical limiters of intense short pulse radiation [25]. As in the case of non linear absorption the experimental investigation of the optical limiting in the sample was performed using OA Z scan at different input power density and concentration.Therefore these films with immobilized semiconductor nanoplates appear to be attractive candidate for optical limiting applications. Fig. 5 represents the limiting response of C1, C2, and C3 at an input power density of 436 MW cm^{-2}, the arrow in the figure indicates the approximate fluence at which the normalized transmittance begins to deviate from linearity. The limiting threshold at different input fluences are tabulated in Table 2. As given in the table, the non linear response of the nanoplates depends on both the input fluence and the concentration. The increase of the pump power and the concentration leads to the enhancement of the optical limiting performance with appreciable limiting threshold at 46.86 MW/cm^2 for C3 for higher input fluence due to local field enhancement inside the plates. This property is desirable for the protection of

Table 2
Measured values of optical limiting threshold for C1, C2 and C3 at a wavelength of 532 nm with different irradiation intensities.

Concentration	Optical limiting threshold at		
	320 MW/cm^2	363 MW/cm^2	436 MW/cm^2
C1	171.124	130.71	91.34
C2	168.94	127.81	55.97
C3	162.20	49.52	46.86

Table 1
Measured values of optical bandgap, non linear absorption coefficient (β) and imaginary part of the third-order susceptibility (Im χ^3) at a wavelength of 532 nm for different irradiation intensities.

Concentration	320 MW/cm^2		363 MW/cm^2		436 MW/cm^2		545 MW/cm^2	
	β (m/GW)	Im(χ^3) × 10^{-10} esu	β (m/GW)	Im(χ^3) × 10^{-10} esu	β (m/GW)	Im(χ^3) × 10^{-10} esu	β (m/GW)	Im(χ^3) × 10^{-10} esu
1 mmol (C1) (E_g=3.3 eV)	6.412	2.773	4.9132	2.1249	4.751	2.055	4.919	2.127
1.5 mmol (C2) (E_g=3.38 eV)	5.443	2.3539	4.853	2.099	3.85	1.665	3.239	1.401
2 mmol (C3) (E_g=3.36 eV)	5.373	2.323	4.667	2.018	3.598	1.556	2.980	1.288

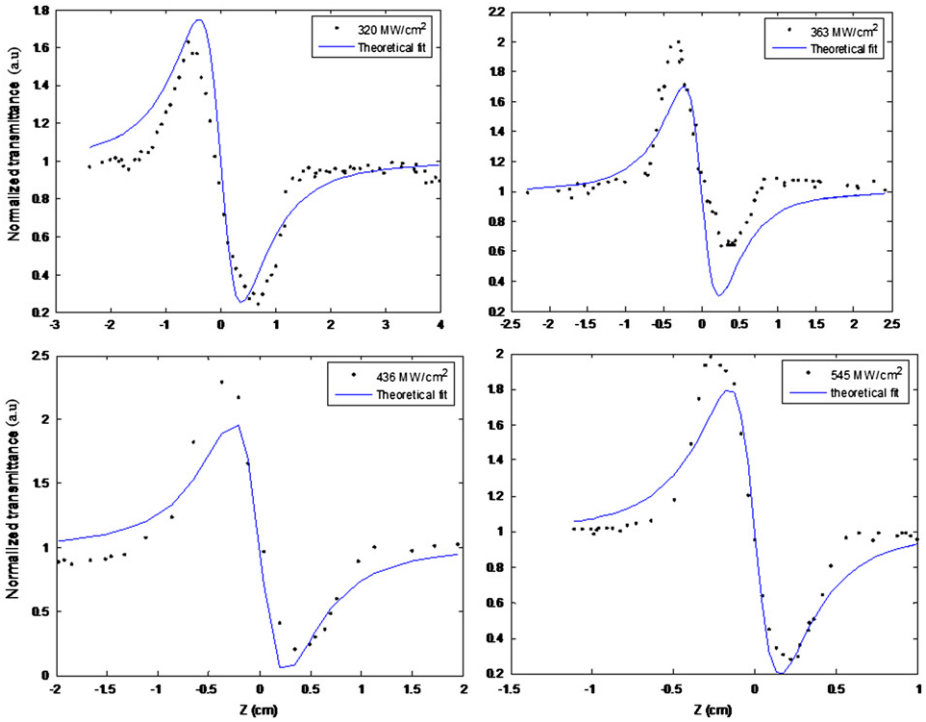

Fig. 6. Normalized transmittance of 1 mmol ZnO nanoplates/PVA composite film as the function of position for different input fluences in the closed aperture scheme at 532 nm. The solid red line shows the theoretical fit. (For interpretation of the references to color in this figure legend, the reader is referred to the web version of this article.)

sensors and human eyes from being affected by intense laser radiation.

The curves in Fig. 6 show the CA valley—peak Z scan traces, indicate the negative non linear refractions due to self defocusing. The de-focusing effect is attributed to the thermal non linearity, self-defocusing has been observed in a variety of semiconductors and has been used to demonstrate optical limiting. To eliminate the contribution of the nonlinear absorption, the CA traces were normalized by dividing with the OA signals measured at the same intensities.

For C1 the estimated average value of Im (χ^3) is 2.2432×10^{-10} esu and Re (χ^3) is -9.1488×10^{-10} esu and (χ^3) is 9.431×10^{-10} esu and the average non linear refractive index is -44×10^{-10} esu. The separation between the transmittance peak and valley in resultant Z-scan is $\sim Z_{p-v} - 1.7Z_0$, which indicates the overwhelming, effects of cubic non linearity. Furthermore, the negative sign of the nonlinear refraction is consistent with the Optical Stark effect [26].

4. Conclusion

The present studies of the ZnO nanoplates–PVA system illustrate the simple method for the fabrication of free standing semiconductor embedded polymer films. The optical energy gap was estimated using the Tauc method. We have examined the non linear absorption characteristics of ZnO/PVA film using nanosecond laser pulses, showing that they are highly nonlinear, exhibiting reverse saturable absorption, and is explained by two photon absorption. The optical limiting investigated experimentally has a desirable lower optical limiting threshold and has negative refractive index. Therefore, these films with immobilized tiny forests of semiconductor nanoplates appear to be attractive candidates for optical limiters, optoelectronic devices for the development of the non linear optical devices.

Acknowledgment

The author Aparna Thankappan acknowledges IUCND for the financial support.

References

[1] Zhigang Zang Atsushi, Nakamura Jiro Temmyo. Nitrogen doping in cuprous oxide films synthesized by radical oxidation at low temperature. Materials Letters 2013;92:188–91.
[2] Jiang CY, Sun XW, Lo GO, Kwong DL. Improved dye sensitized solar cells with a ZnO nanoflower photoanode. Journal of Applied Physics Letters 2007;90:263501.
[3] Wang Yi, Li Meng. Hydrothermal synthesis of single-crystallinehexagonalprismZnO nanorods. Materials Letters 2006;60:266–9.
[4] lucas marcel, wang zhong lin, riedo elisa. Growth direction and morphology of ZnO nanobelts revealed by combining in situ atomic force microscopy and polarized raman spectroscopy. Physical Review B 2010;81045415 2010;81.
[5] Jiang Li, Li Guicun, Ji Qianmao, Peng Hongrui. Morphological control of flower-like ZnO nanostructures. Materials Letters 2007;61:1964–7.
[6] Wei A, Sun XW, Xu CX, Dong ZL, Yang Y, Tan ST. Growth mechanism of tubular ZnO formed in aqueous solution. Nanotechnology 2006;17:1740–4.
[7] Deng Da, Martin Scot T, Ramanathan Shriram. Synthesis and characterization of one-dimensional flat ZnO nanotower arrays as high-efficiency adsorbents for the photocatalytic remediation of water pollutants. Nanoscale 2010;2(2685):2685–91.
[8] Yin S, Goto T, Gobo F, Huang Y F, Zhang P L, Sato T. Synthesis of plate-like zinc oxide particles by the transcription of precursor's shape. IOP Conference Series: Materials Science and Engineering 2011;18:042004.
[9] Xe Yue, U Key, Wu Jin, Jianwen, Shang dejain, Zhu Ziqiang. Synthesis,optical and field emission properties of ZnO microhair–claps. Applied Surface Science 2009;255:6487–92.
[10] Porel Shatabdi, Singh Shashi, Sree Harsha S, Narayana rao D, Radhakrishnan TP. Nanoparticle-embedded polymer: in situ synthesis, free-standing films with highly monodisperse silver nanoparticles and optical limiting. Chemistry of Materials 2005;17:9–12.
[11] Jin Wang Bing, Gu Hui-Tian, Wang Xiao-Wu Ni. Z-scan analytical theory for material with saturable absorption and two-photon absorption. Optics Communications 2010;283:3525–8.
[12] Nithyaja B, Yogeshwar Nath M, Amit Kumar S, Misha† H, Nampoori VPN. Linear and nonlinear optical properties of silver nanoparticles stabilized by bovine serum albumin. Journal of Nonlinear Optical Physics & Materials 2011;20(1):75–83.
[13] Cesca T, Pellegrini G, Bello V, Scian C, Mazzoldi P, Calvelli P. Nonlinear Optical Properties Of Au–Ag nanoplanets made by ion beam processing of bimetallic

nanoclusters in silica. Nuclear Instruments and Methods in Physics Research B 2010;268:3227–30.
[14] Thankappan Aparna, Hari Misha, Mathew S, Joseph Santhi Ani, Rolf Erni, Bora Debajeet. Synthesis of monocrystalline zinc oxide microrods by wet chemical method for light confinement applications. Physica E 2012;44:2118–23.
[15] Tian Jing-Hua, Hu Jie, Si-SiLi, Jian Shi Fan Zhang, Li Xin, Tian Zhong-Qun. Improved seedless hydrothermal synthesis of dense and ultra long ZnO nanowires. Nanotechnology 2011;22 245601 (9pp.).
[16] Sheik-Bahae M, Said AA, Wei TH, Hagan DJ, Van Stryland EW. Sensitive measurement of optical nonlinearities using a single beam. IEEE Journal of Quantum Electronics 1990;26:760.
[17] Cao, Bingqiang, Cai Weiping. From ZnO nanorods to nanoplates: chemical bath deposition growth and surface-related emissions. Journal of Physical Chemistry C 2008;112:680–5.
[18] Lupan Oleg, Chow Lee, Beatriz Roldan Guangyu Chai. Nanofarication and characterization of ZnO nanorod arrays and branched microrods by acqueous solution route and rapid thermal processing. Materials Science and Engineering: B 2007;145:57–66.
[19] Wood D L, Tauc J. Weak absorption tails in amorphous semiconductors. Journal of Physical Review B 1972;5:3144.
[20] Sreekumar G, Louie Frobel PG, Muneera CI, Sathiyamoorthy K, Vijayan C, Mukherjee Handrachur. Saturable and reverse saturable absorption and nonlinear refraction in nanocluste red Amido Black dye–polymer films under low power continuous wave He–Ne laser light excitation. Journal of Optics A: Pure and Applied Optics 2009;11 125204 (12 pp.).
[21] Haripadmam PC, Kavitha MK, John Honey, Krishnan Bindu, Gopinath Pramod. Optical limiting studies of ZnO nanotops and its polymer nanocomposite films. Applied Physics Letters 2012;101:071103.
[22] Smektala F, Quemard C, Couderc V, Barth´el´emy A. Non-linear optical properties of chalcogenide glasses measured by Z-scan. Journal of Non-Crystalline Solids 2000;274:232.
[23] Ogusu K, Yamasaki J, Maeda S, Kitao M, Minakata M. Linear and nonlinear optical properties of Ag–As–Se chalcogenide glasses for all-optical switching. Optics Letters 2004;29:265.
[24] Lee HW, Lee KM, Lee S, Koh KH, Park J-Y, Kim K. Ultrafast third-order optical nonlinearities of vertically-aligned ZnO nanorods. Chemical Physics Letters 2007;447:86–90.
[25] Tintu R, Nampoori VPN, Radhakrishnan P, Thomas Sheenu. Preparation and optical characterization of novel Ge–Se–Sb/PVA composite films for optical limiting application. Journal of Physics D: Applied Physics 2011;44:025101.
[26] Wang Rongyao, Wu Xiaochun, Wang Bingsuo Zou Li, Xie Sishen, Xu Jiren, Huang Wei. Nonresonant optical nonlinearity of ZnO composite nanoparticles with different interfacial chemical environments. Materials Research Innovations 1998;2:49–52.

Optics & Laser Technology 64 (2014) 133–139

Contents lists available at ScienceDirect

Optics & Laser Technology

journal homepage: www.elsevier.com/locate/optlastec

Optical nonlinear investigations on morphology controlled growth of ZnO crystals

Aparna Thankappan [a,b,*], C.L. Linslal [a], S. Divya [a], P.V. Sabitha [a], Sheenu Thomas [a], V.P.N. Nampoori [a]

[a] International School of Photonics (ISP), Cochin University of Science and Technology, India
[b] Inter University Centre for Nanomaterials and Devices (IUCND), Cochin University of Science and Technology, Kochi, India

ARTICLE INFO

Article history:
Received 10 September 2013
Received in revised form
9 February 2014
Accepted 31 March 2014
Available online 7 June 2014

Keywords:
ZnO
Z-scan
Anisotropy

ABSTRACT

We report a methodical study about the third order optical nonlinearity of anisotropic growth of ZnO crystals embedded in polymeric matrices and nanowires on the glass substrate with the use of pre-existing textured ZnO, ZnS and TiO_2 seeds using a Z-scan method with Nd:YAG laser (532 nm, 7 ns, 10 Hz). The studies show that the optical nonlinearity of ZnO crystals is highly dependent on the structural geometry and the correlation of semiconductor. Our study offers better insights into the third-order nonlinear optical characteristics of ZnO crystals and reveals great potential for applications in nonlinear photonic devices.

1. Introduction

In recent years, the nonlinear optical (NLO) properties of nanomaterials have attracted considerable interest due to their potential applications in nanolasers [1], optical limiting [2] and all optical switching [3] devices. Optical limiting property provided by reverse saturable absorption (RSA) in which the excited state has strong absorption compared with that of the ground state, is gaining interest over these years due to its variety of applications in devices for protecting sensitive devices from intense optical radiations. Semiconductors are being experimented in this regard for the past few years because of their extensive applications in solid states electronics and optics. Among these materials, ZnO is a key functional material exhibiting ultraviolet photoluminescence emission, transparent conductivity along with semiconducting, magnetic and piezoelectric properties and is a wide band gap semiconductor with band gap energy of 3.37 eV, and large exciton binding energy of 60 meV at room temperatures. It is especially attractive due to the recent developments of its applicability as a perceptive material for near UV emitters and ultrafast UV modulators [4]. A substantial amount of work has been carried out in the area of nanocomposites for photonic device applications. Until now ZnO thin films have been prepared by the number of techniques such as spray pyrolysis, pulsed laser deposition (PLD), laser molecular beam epitaxy (MBE), wet chemical method,], and metal-organic chemical vapor deposition (MOCVD) [5–7]. MOCVD and MBE can give high quality ZnO nanowire arrays, but are usually limited by the poor sample uniformity, low product yield and choices of substrate. Also, the experimental cost is usually very high, so they have been less widely adopted. Comparatively speaking, wet chemical methods are attractive for several reasons: they are low cost, less hazardous, and thus capable of easy scaling up [8,9]; growth occurs at a relatively low temperature, compatible with flexible organic substrates; there is no need for the use of metal catalysts, and thus it can be integrated with well-developed silicon technologies [10]; in addition, there are a variety of parameters that can be tuned to effectively control the morphologies and properties of the final products [11,12].

Over the past few years numerous efforts have been made in controlling the size and shape of inorganic nanocrystals to tune their properties for prospective applications as the size, orientation and morphology, aspect ratio and even crystalline density can significantly influence various properties. Recent advances in nanoscience and nanotechnology have not only revealed the potential of nanoscale electronic and optoelectronic devices, target drug delivery, etc., but have also shown their potential utility as a hydrogen storage material for clean energy [13]. Therefore, development of morphology controlled synthesis of nanostructures remains a considerable challenge to answer the demand for exploring the potentials of ZnO.

As we know, ZnO is a polar crystal with hexagonal phase and high anisotropy which leads to the oriented growth along *c*-axis [14].

* Corresponding author. Tel.: +91 484 2575848; fax: +91 484 2576714.
E-mail address: aparna.subhash@gmail.com (A. Thankappan).

http://dx.doi.org/10.1016/j.optlastec.2014.03.021
0030-3992/

Crystal growth morphology results from the interplay of crystallographic anisotropy and growth kinetics [15]. Anisotropic tendency in the crystal growth exploring the relationship between crystal planes of solid material and their physical/chemical properties has attracted the attention of several researchers [16]. We have recently published nanoplates [17,18] and betanin natural dye [19] for photonic device applications.

In this work, we report a systematic study on the third order optical nonlinearity of controlled morphologies of ZnO nano/microcrystals which include dumb bell (DB) microrod, nanoflakes, nanoplates and microrod structures and also investigate the nonlinear behavior of nanowires with the use of pre-existing textured ZnO, ZnS and TiO_2 seeds using an Nd:YAG laser (532 nm, 7 ns, 10 Hz). These properties are commonly defined in terms of intensity dependant nonlinear absorption coefficient $\alpha(I)$, which can be written in terms of linear absorption coefficient α and two photon absorption coefficient β as

$$\alpha(I) = \alpha + \beta I \quad (1)$$

When SA is present the above equation modifies to

$$\alpha(I) = \alpha_0/(1+(I/I_s)) \quad (2)$$

The structures were characterized by scanning electron microscopy and X-ray diffraction. Depending on the pump intensity and on the absorption cross-section at the excitation wavelength, most molecules shows nonlinear absorption. Therefore, it is necessary to identify their nonlinear absorption effects, and to determine their nonlinear absorption parameters, such as the saturable intensity (I_s) for saturable absorber, the TPA coefficient (β) for two-photon absorbing material. The room temperature nonlinear optical properties of the as-prepared ZnO significantly depend on the crystal size, orientation and morphology, aspect ratio and crystalline density.

2. Experimental details

2.1. Controllable growth of ZnO crystals

The ZnO crystals used for our experiments were synthesized by a low temperature wet chemical method. All chemicals purchased from Merck Ltd. were used as received without further purification. The nutrient solution was prepared from an aqueous solution of zinc nitrate hexahydrate [Zn $(NO_3)_2 6H_2O$] and hexamethylenetetramine (HMTA) [$(CH_2)_6N_4$] heated at 80 °C. The hexamine solution was added to the zinc nitrate solution dropwise while stirring. The reaction decomposes HMTA to formaldehyde (HCHO) and ammonia (NH_3), acting as a pH buffer by slowly decomposing to provide a gradual and controlled supply of ammonia, which can form ammonium hydroxide and support OH^- [20] Finally OH^- anions react with Zn^{2+}cations to form ZnO. To avoid sedimentation of crystals, the solution was centrifuged and washed several times and finally embedded into the polyvinyl alcohol solution (15%) and developed the free standing films(thickness around 90 μm) (Plasto Mek, delta.0.2 kW, 230 V,1 phase). Here PVA acts as the transparent matrix for the homogeneous distribution and immobilization. By doing so optical properties of crystals can be utilized in more technological applications mainly in sensors that require large area of coating.

2.2. Nanowire growth

ZnO branched nanowires that were seeded with a thin film of ZnO nanoparticles were grown on the glass substrate as in the work by Greene et al. [21]. ZnO seed nanoparticles were synthesized according to the method described by Pacholski [22]. 0.01 M zinc acetate in methanol was added dropwise to a well-stirred solution of 0.03 M NaOH in methanol maintained at 60 °C; after two hour growth, the solution was centrifuged to separate the nanoparticles of size 72 nm. The fresh methanol was infused to suspend the particles. The ZnS and TiO_2 nanoparticles were synthesized as follows.

The TiO_2 sol was prepared via a sol–gel method and synthesized as follows. Titanium tetra-isopropoxide (TTIP,) was used as the precursor to prepare TiO_2 sol. A mixture of HCl and isopropyl alcohol was added to a mixture of TTIP and isopropyl alcohol under continuous magnetic agitation at room temperature. The TiO_2 sol composition was of molar ratio TTIP/isopropanol/water=1:26.5:1.5. The [H+]/[TTIP] molar ratio ranged from 0.02 to 1.1. The resultant TiO_2 sol was clear, yellow and stable. The as obtained nanoparticles were thermal treated at 100 °C to remove the excess moisture content. Thus amorphous TiO_2 nanoparticles of 35 nm were obtained.

ZnS nanocrystals are synthesized by using wet chemical precipitation at room temperature. 1 M $ZnCl_2$ and 1 M Na_2S in water are used as sources of Zn and S respectively and 2 ml of Tri Ethanol Amine (TEA) is used as a capping agent; the solution was centrifuged to separate the nanoparticles. The X-ray diffraction study reveals that the size of the nanocrystals is about 2.6 nm.

The thin films are formed by dip coating the glass substrate. The nanowires were grown on the seeded substrates by placing them face down in a closed vessel containing equimolar concentration (0.025 M) of zinc nitrate hexahydrate and hexamine in deionized water at 80 °C.

The size and morphology of ZnO samples were characterized by scanning electron microscopy (JEOL/EO, and JSM6390). The X-ray diffraction data were collected on an AXS Bruker D% diffractometer using Cu Kα-radiation (λ=0.1541 nm; the operating conditions were 35 mA and 40 kV at a step of 0.020° and step time of 29.5 s in the 2θ range from 30 to 70°. To determine third order nonlinear optical characteristics of ZnO crystals such as nonlinear absorption, the single beam Z scan technique proposed and demonstrated by Sheik-Bahae et al. [23], was employed. The transmission of a laser beam that changes near the focal point during the sample translation along the propagation path through an open-aperture (OA) was measured. A Q-switched Nd:YAG laser (Spectra Physics LAB-1760, 532 nm, 7 ns, 10 Hz) was used as the light source. A 20 cm converging lens was used to focus the laser beam. The radius of the beam ω_0 was calculated to be 35.4 μm. The Rayleigh length, $z_0 = \pi\omega_0^2/\lambda$, is estimated to be 7.4 mm, which is much greater than the thickness of the sample, and is an essential prerequisite for Z-scan experiments. The sample was fixed on a computer-controlled translation stage, so that it could be accurately moved through the focal region of the laser beam over a length of 6 cm. The transmitted beam energy, reference beam energy and the ratios were measured simultaneously using an energy ratio meter (Rj 7620, Laser Probe Corp.) having two identical pyroelectric detector heads (Rjp 735). The detected signals were acquired, stored and processed by the computer. Optical density filters were used to vary the laser intensity at the lens focus.

3. Results and discussions

The morphology of the ZnO crystals synthesized with controlled growth rate at 6 h, 11 h, 18 h and 22 h is revealed by the scanning electron microscopic images shown in Fig. 1. When the reaction media was heated at 80 °C for 6 h ZnO DB microrod with an average diameter of 800 nm and length of 3 μm was formed. The ZnO DB microrods grew along the direction [0001], which are formed by co-sharing of two individual microrods, stabilized

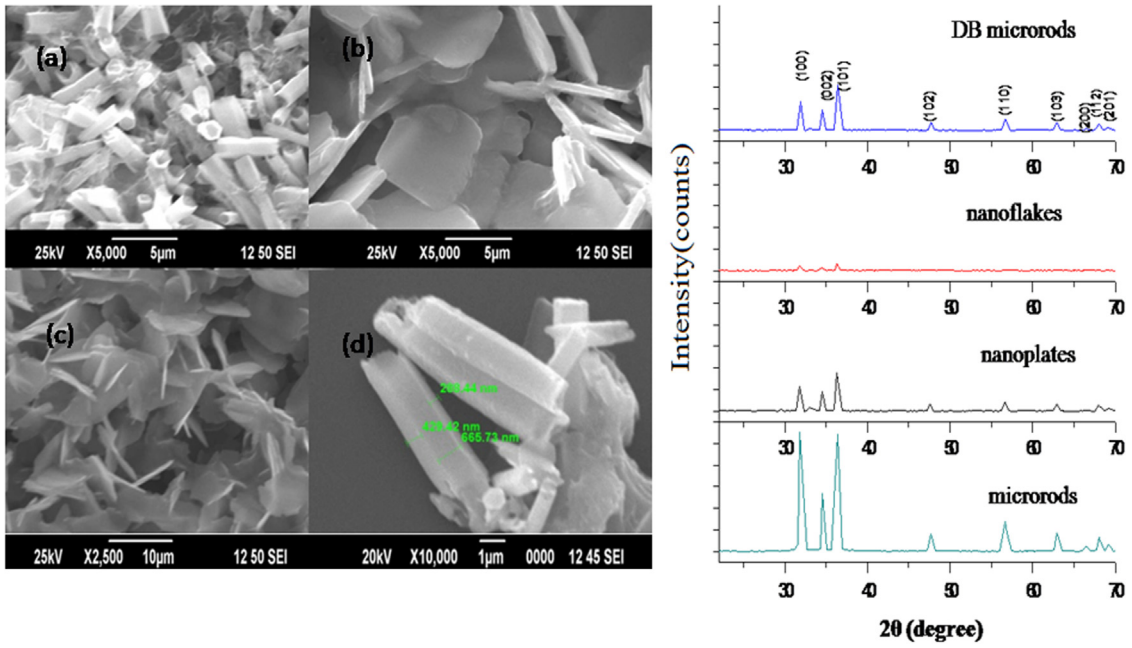

Fig. 1. SEM images of ZnO crystals (a) DB microrods (b) nanoflakes (c) nanoplates and (d) microrods and their corresponding XRD pattern.

between the Zn [0001] planes and Zn [$000\bar{1}$] faces are masked. They also have a broader size distribution than the nanoplates and nanoflakes. Wenquin et al. [24] reported the precursor concentration dependant structure morphology of ZnO nano and microcrystals. ZnO exhibits a wurzite crystal structure which is a polar molecule with [0001] polar surfaces and non-polar [$01\bar{1}0$] faces. The non-polar surfaces are electrically neutral having a low surface energy and the polar surfaces have a high surface energy, which is the main factor for the differentiation of the growth rate along both the polar and non-polar directions [25]. The length and width of the synthesized ZnO crystals would be directly affected by the growth rate in the [0001] polar face and the [0110] non-polar faces respectively. When the heating time is prolonged for 11 h, the crystal growth along [0001] direction decreases, leading to the formation of nanoflakes. The DB ZnO microrods were changed into flake shaped crystals due to the sequential dissolution of the polar O [$001\bar{1}$] and the non-polar [$01\bar{1}0$] [26].When heated for 18 h the ZnO nanoplates with uniform size are fabricated in large scale and microrods are observed for 22 h. The surface reconstruction may favor a surface orientation of a crystalline structure [27]. The ZnO microrods are assumed to be formed by stacking the nanoplates. It seems that both DB microrods and hexagonal microrods have same average diameter. Here we believe that the growth time plays a key role for anisotropic growth of well-defined ZnO morphologies. All obtained ZnO samples are of wurtzite structure (hexagonal phase, space group $P6_3mc$). Fig. 1 also displays X-ray diffraction (XRD) patterns of basic ZnO structures with different morphologies. All diffraction patterns can be indexed as pure hexagonal wurtzite ZnO structure. Because no diffraction peaks were observed from other impurities in the XRD patterns, it is concluded that pure hexagonal phase ZnO structures were synthesized through this simple wet chemical method.

Three kinds of crystal morphologies were obtained depending on the seeded layer. We first observed the effect of same seed for the growth of nanowire; obtained branched nanowire is shown in Fig. 2(a). The growth of nanowires from a common nucleus may be due to the aggregation of nanoparticles of ZnO— the nanowires growing along the preferential direction of the crystalline network. We repeat the same synthesis method for the nanowire with various seeded layers; the XRD pattern of seeded layers used for the synthesis is shown in Fig. 2(b). With the TiO_2 and ZnS seeds a new morphology of nanomaterial appears; vertical microrods (top view) and vertical nanorods. Nevertheless a small proportion of ZnS nanoparticles does not allow for the exclusive growth of nanorods. SEM image of ZnO nanostructures with TiO_2 seed and ZnS seed is shown in Fig. 3.

Introducing the nanowire into the ZnO seeds changes its band gap from 3.77 eV to 3.47 eV; for the TiO_2 seed it changes the band gap from 3.91 eV to 3.64 eV and for the ZnS seed, it changes from 3.97 eV to 3.77 eV. (Optical band gap was calculated from Tauc extrapolation method.)

To estimate the saturable intensity and nonlinear absorption coefficient, the experimental data were fitted with numerical simulations. The nonlinear absorption was measured from the normalized energy transmission using Z-scan without an aperture. The transmitted OA Z scan signal is given by [28]

$$T(z, S=1) = \sum_{m=0}^{\infty} \frac{[-q_0(z,0)]^m}{(m+1)^{3/2}} \tag{3}$$

where

$$q_0(z,t) = \frac{\beta I_0(t) L_{eff} z_0^2}{z^2 + z_0^2} \tag{4}$$

L_{eff} denotes the effective sample length defined by

$$L_{eff} = [1 - \exp(-\alpha l)]/\alpha \tag{5}$$

with the linear absorption coefficient α and the sample thickness l. Where m is an integer, the parameter q_0 can be obtained by fitting the experimental results to Eq. (3), where Z_0 and Z are the Rayleigh range and the translated length parallel to the beam propagation, respectively. This equation can be used to fit the experimental data of the open aperture Z scan trace (the nonlinear absorption measurements), treating $I_0(t)$ as the position dependent intensity. The position dependence in intensity should be incorporated into the expression by considering the variation of beam size on either side of the focus.

The imaginary part of third order susceptibility Im (χ^3) is related by the following equation [29]:

$$\mathrm{Im}(\chi^{(3)}) = n_0^2 c^2 \beta / 240\, \pi^2 \omega \ \ (\mathrm{esu}) \tag{6}$$

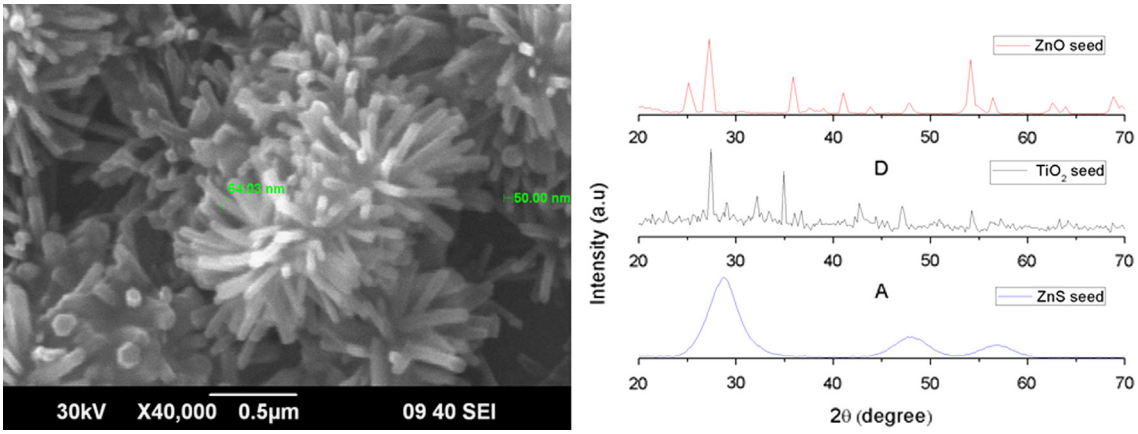

Fig. 2. SEM image of ZnO branched nanowire with ZnO seed and (b) XRD pattern of various seed layers.

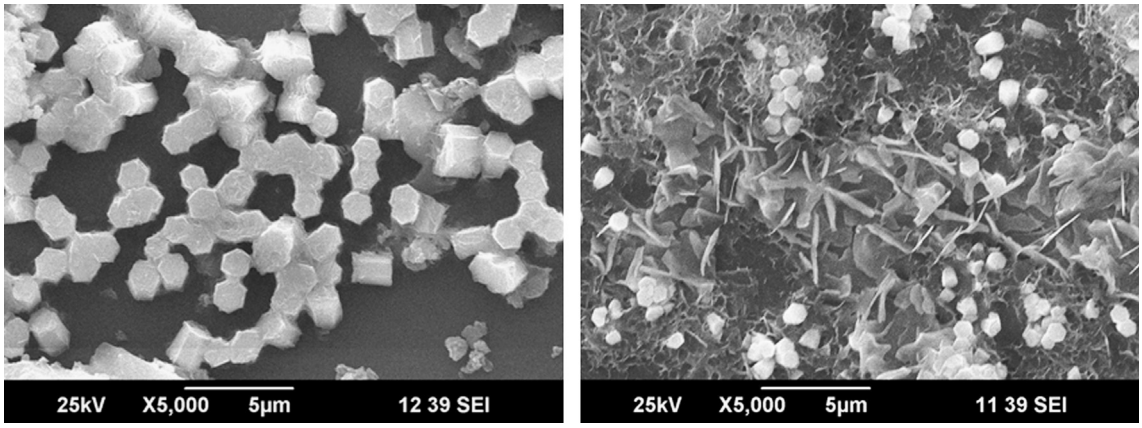

Fig. 3. SEM image of ZnO nanostructures with TiO_2 seed and ZnS seed.

where n_0 is the linear refractive index of the film measured using Abbe refractometer, c is the velocity of light in vacuum, ω is the angular frequency of radiation used and β is the nonlinear absorption coefficient.

The Z scan traces are shown in Fig. 4; fits of Eq. (3) to the experimental data are depicted in the figure by solid curves and the measured values are tabulated in Table 1.

Generally different processes, such as two photon absorption (TPA), transient absorption, free carrier absorption interband absorption, photo ejection of electrons and nonlinear scattering, are reported to be operative in nonlinear absorption. The experimental data shows a slight deviation from the theoretical curve which is fitted for two photon absorption. This deviation can be attributed to two photon induced free carrier absorption which is observed in particles with larger size [30]. As given in the table the nonlinear response of the crystals depends on the pump power and structural geometry. As the power is increased, lowering of the nonlinear absorption coefficient occurs thereby diminishing the third order susceptibility. It turned out that the local field enhancement through the size- and structure-dependent interfacial interaction among the ZnO crystals influences the magnitude of the nonlinear absorption [31]. When we plot the Im (χ^3) with corresponding band gap, we get a nonlinear curve which is shown in Fig. 4. Generally it follows an inverse relationship. Hence it can be inferred that an unusual behavior may occur in the rod structure having higher band gap [$E_{g\ DB\ microrods}=3.98$ eV; $E_{g\ Nanoflakes}=E_g=3.54$ eV; $E_{g\ Nanoplates}=3.3$ eV; $E_{g\ Microrods}=3.74$ eV].

The case of rods including both dumb bell microrods and microrods showing perfect switching behavior could be demonstrated by changing the pump power intensity as shown in Fig. 5. This is confirmed by measuring the transmittance of radiation by the sample. Fig. 6 shows that transmittance of radiation is more in the case of rods as compared to plates and flakes. This can be thought as some types of confinement of radiation are more in rod shaped structures. We consider that they can both confine an externally launched light into its cavity structure formed by the hexagonal boundaries, and undergo multiple total internal reflections from the hexagonal facets, which provides an enhanced effective optical path length to confine the light and increases the communication between the excitation light and ZnO [32].

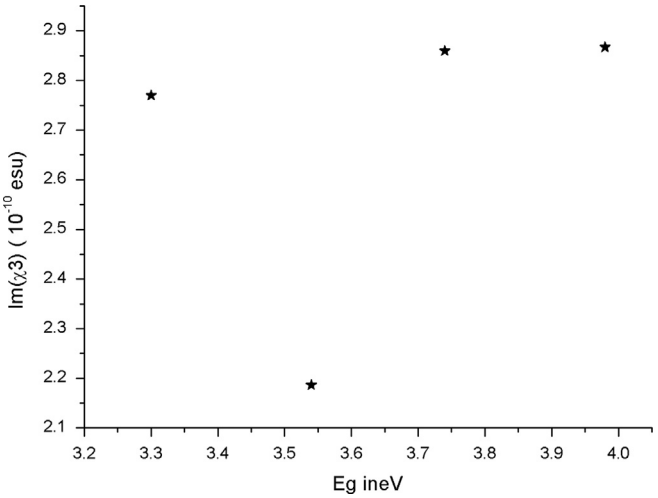

Fig. 4. Relationship between the energy band gap and the Im(χ^3) at 320 MW/cm^2.

Table 1
The measured parameters of ZnO crystals in which β is in m/GW, Im $(\chi^3)^*10^{-9}$ in esu and I_s in (MW/m^2); β is mentioned only for the case of RSA and I_s for the case of SA.

	320 MW/cm^2			363 MW/cm^2			436 MW/cm^2			545 MW/cm^2		
	β	Im(χ^3)	I_s	β	Im(χ^3)	I_s	β	Im(χ^3)	I_s	β	Im(χ^3	I_s
DB microrods	6.632	0.287	–	–	–	0.051	–	–	0.243	–	–	0.242
Nanoflakes	5.057	0.218	–	4.482	0.194	–	3.865	0.167	–	2.815	0.122	–
Nanoplates	6.412	0.277	–	4.913	0.212	–	4.751	0.206	–	4.919	0.213	–
Microrods	6.611	0.286	–	5.043	0.219	–	3.205	0.139	–	–	–	0.274

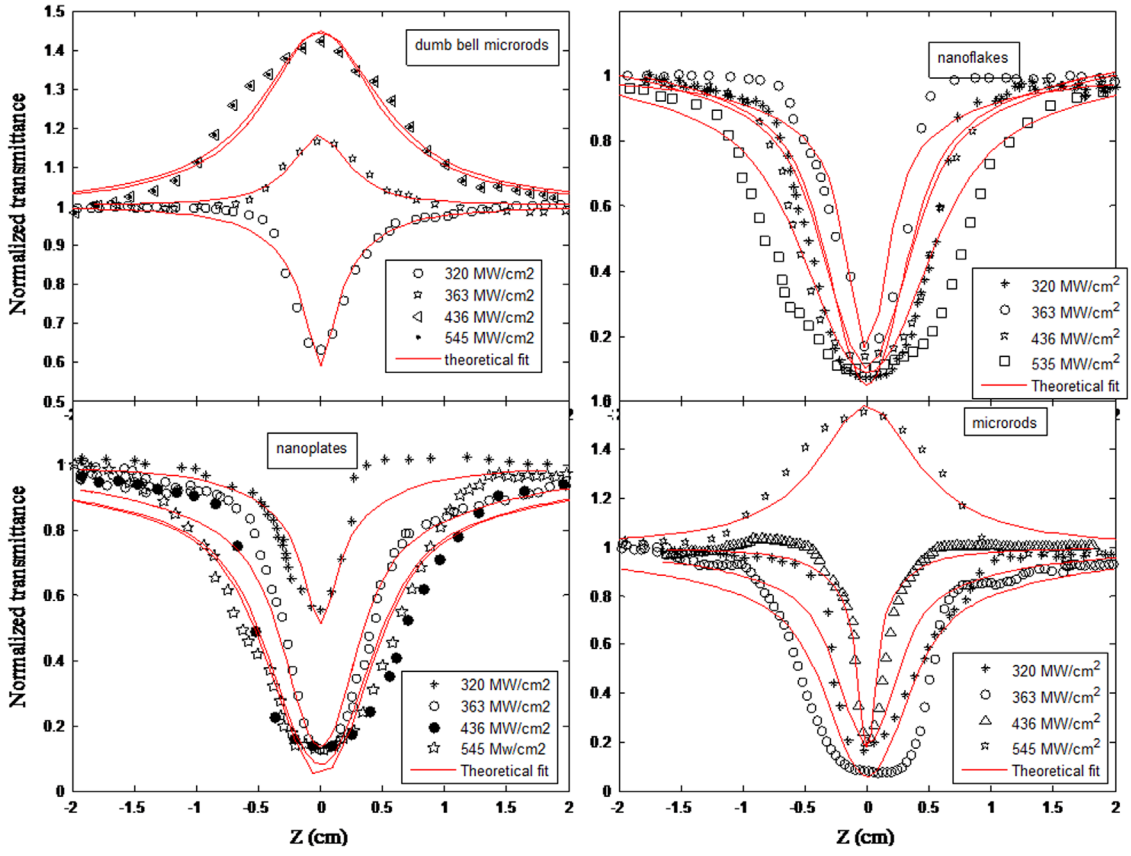

Fig. 5. Normalized transmittance of controlled morphologies of ZnO /PVA composite film as the function of position for different input fluences in the open aperture scheme at 532 nm. The solid red line shows the theoretical fit. (For interpretation of the references to color in this figure legend, the reader is referred to the web version of this article.)

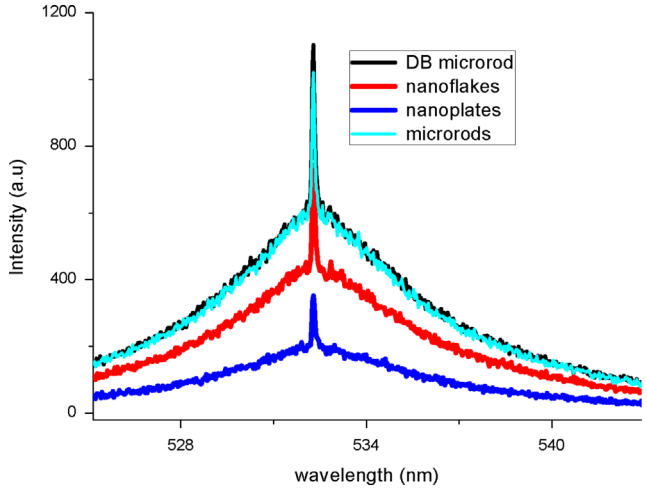

Fig. 6. The variation of transmittance intensity with the laser input of 85 μJ.

Enhancement in the optical path length increases the excited state absorption and free carrier absorption leading to bleaching of the ground state band, i.e., in the case of the intraband transition, the ground-state electrons are pumped to the excited-state on increasing the input fluence. The excited electrons are free carriers possessing a whole spectrum of energies, both kinetic and potential; immediately after the absorption the excited electrons relax to the ground-state through electron–electron, electron–phonon and phonon–phonon interactions. The dumb bell shaped system with least defects causes switching at low power.

One of the applications of reverse saturable absorption materials is in devices based on optical limiters which are devices that transmit light at a low input fluence, while they become opaque at high inputs. Reverse saturable absorption, which is generally allied with a large absorption cross section from excited state than the ground state, brings about optical limiting effects. In semiconductor materials the optical limiting is governed by TPA as observed in this study. Semiconductor films with high TPA coefficients and strong Kerr-induced nonlinear susceptibilities are very good

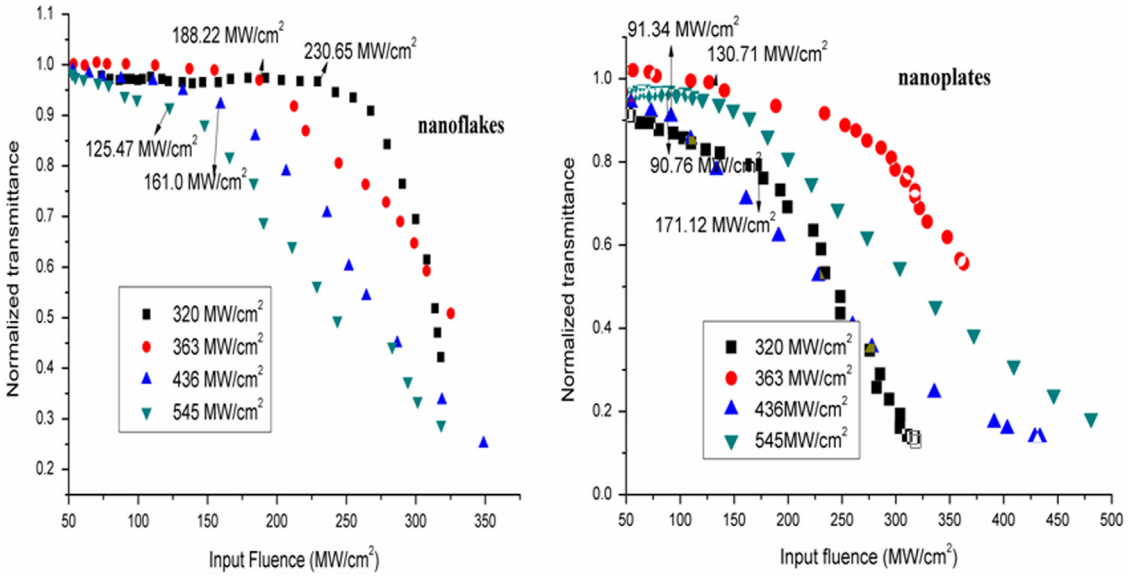

Fig. 7. Optical Limiting Response of ZnO nanoplates and nanoflakes.

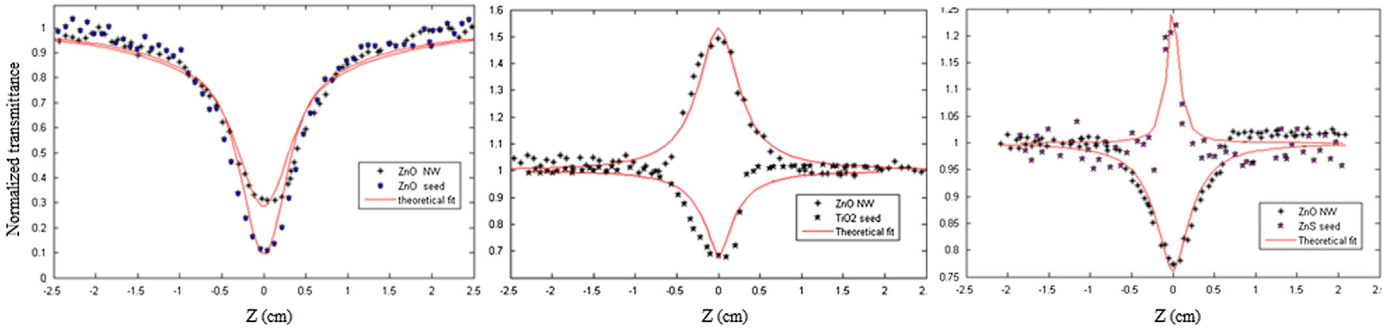

Fig. 8. Open aperture Z scan curves showing the effect of different seeded layers on the branched nanowires with the laser input fluence of 320 MW/cm^2.

Table 2
The measured parameters of ZnO nanorods with various seeds in which β in m/GW, Im (χ^3)*10^{-9} in esu and I_s in (MW/m^2); β is mentioned only for the case of RSA and I_s for the case of SA.

	β m/GW	Im(χ^3) *10^{-9} esu	I_s MW/m^2
ZnO seed	123.42	5.33	–
ZnO NW with ZnO seed	87.157	3.77	–
ZnS seed	–	–	0.011
ZnO crystal with ZnS seed	93.6	6.65	–
TiO_2 seed	127.88	9.385	–
ZnO crystal with TiO_2 seed	–	–	0.1514

candidates due to their small time response as optical limiters of intense short pulse radiation [33]. As in the case of nonlinear absorption the experimental investigation of the optical limiting in the sample was performed using OA Z scan at different input power densities. Therefore these films with immobilized semiconductor nanoplates and nanoflakes appear to be noticeable candidates for optical limiting applications. The increase of the pump power leads to the enhancement of the optical limiting due to local field enhancement inside the plates and flakes as clearly depicted in Fig. 7. This property is desirable for the protection of sensors and human eyes from being affected by intense laser radiation.

The strength of the nonlinearity can be enhanced by using structures exhibiting a quantum confinement effect. The various seeded layered nanostructure shows switching either from RSA to SA or SA to RSA as shown in Fig. 8, which is assumed to be due to the asymmetric bond between the semiconductor and the anisotropic growth results from the various seed layers in growth rates of the different crystal faces of ZnO which may also affect the nonlinear absorption. The optical nonlinear parameters of nanocrystals with different seeded layers are tabulated in Table 2. The crystallinity of the seed layer plays a crucial role in nonlinear absorption. The rod–seed interaction generates new complex resulting into new energy level. This is possible only if any of the vibrational modes of TiO_2 are coupled to the energy level structures of the seed material. This takes place comparatively at higher energy so that excited state absorption (ESA) takes place, resulting into SA. Introduction of nanowire generates energy levels so that SA further changes over to RSA either by TPA or by ESA.

4. Conclusion

To summarize, the third-order optical nonlinearities and nonlinear responses of ZnO anisotropic structures synthesized by the low-temperature wet-chemical method were characterized by Z scan method with nanosecond laser. The optical limiting enhancements in ZnO nanoplates and nanoflakes were mostly contributed from the interfacial interaction between the structure and the local-field enhancement in addition to a one photon assisted energy transfer from the excited state to the nearby trapping sites. The rods can confine an externally launched light into their cavity structure, which provides an enhanced effective

optical path length to confine the light show perfect switching behavior. i.e. the geometry of structures and the correlation of semiconductors are the crucial factors to the optical nonlinearity and our study offers better insights into the third-order nonlinear optical characteristics of ZnO crystals and reveals the great potential for applications in nonlinear photonic devices.

Acknowledgment

The author AT acknowledges IUCND for the financial support.

References

[1] Huang Michael H, Mao Samuel, Feick Henning, Yan Haoquan, Wu Yiying, Kind Hannes, Weber Eicke, Russo Richard. Room-temperature ultraviolet nanowire nanolasers. Science 2001;292:1897.
[2] Hughes S, Spruce G, Wherrett BS, Kobayashi T. Comparison between the optical limiting behavior of chloroaluminum phthalocyanine and a cyanine dye. J Appl Phys 1997;81:5905.
[3] Irimpan Litty, Nampoori VPN, Radhakrishnan P. Spectral and nonlinear optical characteristics of nanocomposites of ZnO–CdS. J Appl Phys 2008;103:094914.
[4] Petrov GI, Shcheslavskiy V, Yakovlev VV, Ozerov I, Chelnokov E, Marine W. Efficient third-harmonic generation in a thin nanocrystalline film of ZnO. Appl Phys Lett 2003;83:3993.
[5] Sofiani Z, Derkowska B, Dalasin ski P. Optical properties of ZnO and ZnO:Ce layers grown by spray pyrolysis. Opt Commun 2006;267:433–9.
[6] Kapustianyk V, Turko B, Kostruba A, et al. Influence of size effect and sputtering conditions on the crystallinity and optical properties of ZnO thin films. Opt Commun 2007;269:346–50.
[7] Alaoui Lamrani M, Addou M, Sofiani Z. Cathodoluminescent and nonlinear optical properties of undoped and erbium doped nanostructured ZnO films deposited by spray pyrolysis. Opt Commun 2007;277:196–201.
[8] Zhang H, Yang DR, Ma XY, Du N, Wu JB, Que DL. Straight and thin ZnO nanorods: Hectogram-scale synthesis at low temperature and cathodoluminescence. J Phys Chem B 2006;110:827–30.
[9] Chang PC, Lu JG. ZnO nanowire field-effect transistors. IEEE Trans Electron Devices 2008;55:2977–87.
[10] Xu S, Wei Y, Kirkham M, Liu J, Mai W, Davidovic D, Snyder RL, Wang ZL. Patterned growth of vertically aligned ZnO nanowire arrays on inorganic substrates at low temperature without catalyst. J Am Chem Soc 2008;130:14958–9.
[11] Govender K, Boyle DS, Kenway PB, O'Brien P. Understanding the factors that govern the deposition and morphology of thin films of ZnO from aqueous solution. J Mater Chem 2004;14:2575–91.
[12] Xu S, Adiga N, Ba S, Dasgupta T, Wu CFJ, Wang ZL. Optimizing and improving the growth quality of ZnO nanowire arrays guided by statistical design of experiments. ACS Nano 2009;3:1803–12.
[13] Jai Singh, Pushpendra Kumar, Hui KS, Hui KN, Ramam K, Tiwaria RS, Srivastavaa ON. Synthesis, band-gap tuning, structural and optical investigations of Mg doped ZnO Nanowires. CrystEngComm 2012;14:5898–904.
[14] Hui Zhang, Deren Yang, Li Dongshen, Ma Xiangyang, Shenzhong Li, Duanlin Que. Controllable growth Of ZnO microcrystals by a capping-molecule-assisted hydrothermal process. Cryst Growth Des 2005;5(2):547–50.
[15] Muller G, Metois J-J, Rudolph P. Crystal growth from fundamentals to technology. 1st ed., Elsevier; 2004.
[16] Shalaka C, Navale SW, Gosavi IS, Mulla. Controlled synthesis of ZnO from nanospheres to microrods and its gas sensing studies. Talanta 2008;75:1315–9.
[17] Aparna Thankappan, Divya S, Thomas Sheenu, Nampoori VPN. Optical characterization of ZnO nanoplates embedded in polymeric matrices for optical limiting applications. Opt Laser Technol 2013;52:37–42.
[18] Thankappan Aparna, Thomas Sheenu, Nampoori VPN. Effect of betanin natural dye extracted from red beet root on the nonlinear optical properties ZnO nanoplates embedded in polymeric matrices. J Appl Phys 2012;112:123104.
[19] Thankappan Aparna, Thomas Sheenu, Nampoori VPN. Solvent effect on the third order optical nonlinearity and optical limiting ability of betanin natural dye extracted from red beet root. Opt Mater 2013;35:2332–7.
[20] Tian Jing-Hua, Hu Jie, Li Si-Si, Zhang Fan, Shi Jian, Li Xin, Tian Zhong-Qun, et al. Improved seedless hydrothermal synthesis of dense and ultra long ZnO nanowires. Nanotechnology 2011;22:245601 (9p).
[21] Greene LE, Law M, Goldberger J, kim F, Johnson JC, Zhang YF, Saykally R, Yang PD. Low-temperature wafer-scale production of ZnO nanowire arrays. Angew Chem Int Ed 2003;42:3031.
[22] Pacholski C, Kornowski A, Weller H. Self-assembly of ZnO: from nanodots to nanorods. Angew Chem Int Ed 2002;41(1188):2003.
[23] Sheik-Bahae M, Said AA, Wei TH, Hagan DJ, Van Stryland EW. Sensitive measurement of optical nonlinearities using a single beam. J Quantum Electron 1990;26:760.
[24] Peng Wenquin, Qu Shengchun, Cong Guangwei, Wang Zhanguo. Synthesis and structures of morphology controlled ZnO nano and micro crystals. Cryst Growth Des 2006;6:1518–22.
[25] Panigrahy Bharati, Aslam M, Misra DS, Bahadur D. Polymer-mediated shape-selective synthesis of ZnO nanostructures using a single-step aqueous approach. CrystEngComm 20091920–5.
[26] Jang Eue Soon, Won Jung-Hee, Hwang Seong-Ju, Choy Jin-Ho. Fine tuning of face orientation of ZnO crystals and optimize their photo catalytic activity. Adv Mater 2006;18:3309–12.
[27] Zhang Lixin, Huanga Hanchen. Structural transformation Of ZnO nanostructures. Appl Phys Lett 2007;90:023115.
[28] Sreekumar G, Louie Frobel PG, Muneera CI, Sathiyamoorthy K, Vijayan C, Mukherjee andrachur. Saturable and reverse saturable absorption and nonlinear refraction in nanoclustered Amido Black dye–polymer films under low power continuous wave He–Ne laser light excitation. J Opt A: Pure Appl Opt 2009;11:125204(12p).
[29] Bahae MS, Said AA, Van Stryland EW. High-sensitivity, single-beam n_2 measurements. Opt Lett 1989;14:955.
[30] Haripadmam PC, Kavitha MK, John Honey, Krishnan Bindu, Gopinath Pramod. Optical limiting studies of ZnO nanotops and its polymer nanocomposite films. Appl Phys Lett 2012;101:071103.
[31] Lee HW, Lee KM, Lee S, Koh KH, Park J-Y, Kim K, Rotermund F. Ultrafast third-order optical nonlinearities of vertically-aligned ZnO nanorods. Chem Phys Lett 2007;447:86–90.
[32] Thankappan Aparna, Hari Misha, Mathew S, Joseph Santhi Ani, Rolf Erni, Bora Debajeet, Braun Artur, Nampoori VPN. Synthesis of monocrystalline zinc oxide microrods by wet chemical method for light confinement applications. Physica E 2012;44:2118–23.
[33] Tintu R, Nampoori VPN, Radhakrishnan P, Thomas Sheenu. Preparation and optical characterization of novel Ge–Se–Sb/Pva composite films for optical limiting application. J Phys D 2011;44:025101.

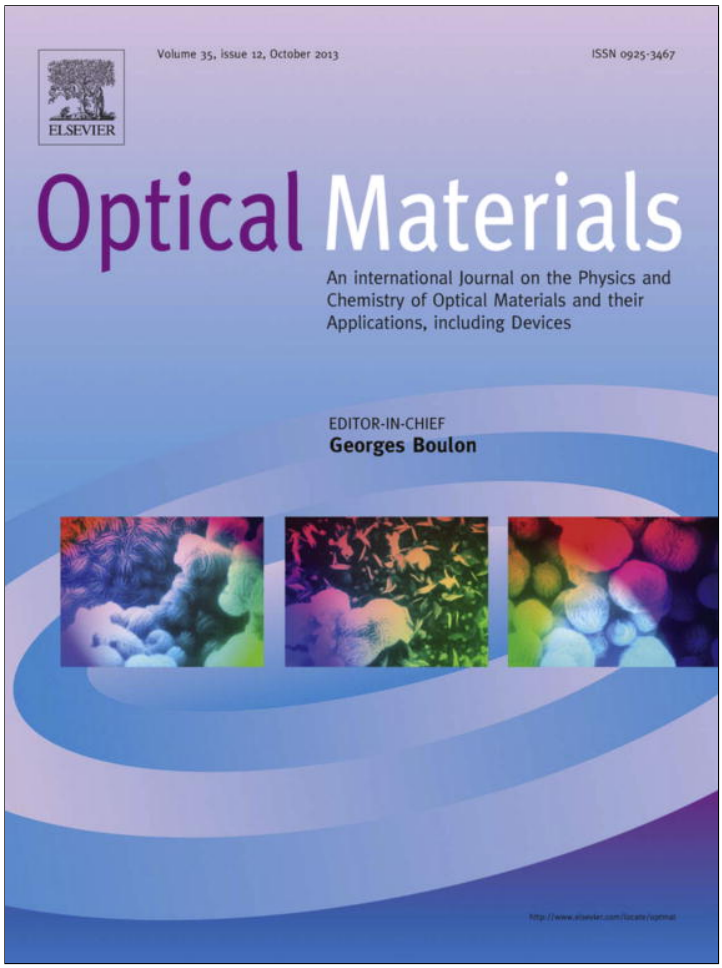

Optical Materials 35 (2013) 2332–2337

Contents lists available at SciVerse ScienceDirect

Optical Materials

journal homepage: www.elsevier.com/locate/optmat

Solvent effect on the third order optical nonlinearity and optical limiting ability of betanin natural dye extracted from red beet root

Aparna Thankappan [a,b,*], Sheenu Thomas [a], V.P.N. Nampoori [a]

[a] International School of Photonics, Cochin University of Science and Technology, Kochi, India
[b] Inter University Centre for Nanomaterials and Devices, Cochin University of Science and Technology, Kochi, India

ARTICLE INFO

Article history:
Received 17 January 2013
Received in revised form 11 June 2013
Accepted 12 June 2013
Available online 13 July 2013

Keyword:
Betanin

ABSTRACT

We report on the solvent effect on the third order optical nonlinearity of betanin natural dye extracted from red beet root and their third order nonlinear optical (NLO) properties have been studied using a Q-switched Nd:YAG laser at 532 nm. The third order nonlinearity of these samples are dominated by nonlinear absorption, which leads to strong optical limiting and their strength is influenced by the solvent used, suggesting that betanin natural dyes are promising candidate for the development of photonic nonlinear optic devices.

1. Introduction

The need for nonlinear optical materials for applications such as phase conjugation, image processing, optical switching and optical limiting are increasingly become important. Recently, a large number of organic π-conjugated molecules have been investigated due to their large nonlinear optical susceptibility and the possibility of tailoring their properties which allow these materials to be used to protect optical detection elements such as human eyes and optical sensors, by controlling the fluency on the image plane below the desired level. The outcome of such studies has helped to establish certain guidelines for molecular design of the third-order nonlinear optical materials with desired properties. In general; an optical nonlinear optical (NLO) material for optical limiting has a low loss, a high nonlinearity, high damage threshold, ease of processing and a broadband spectral response. However, most of the synthesized materials require elaborated preparation procedures and safety measures, use or generation of hazardous materials, costly materials, as well as fragile or chemically unstable structures beyond certain threshold irradiance. Therefore, we suggest natural dye extracts as environment friendly, safe, and inexpensive materials, as well as having high chemical stability during optical excitations with coherent light sources.

Besides anthocyanins, chlorophylls, and carotenoids, betalain are the most common pigments in the plant kingdom. These natural pigments from plants have been extensively investigated as sensitizers for the DSSC [1], in which red beetroot pigments maximum conversion efficiency of 0.67% [2]. Though the former have inherent limitations as sensitizers owing to weak absorption of green wavelengths, the absorption spectra of the latter have more favorable overlap with the solar spectrum. The betalain are water soluble and nitrogen containing pigments is relatively stable over the broad pH range from 3 to 7 [3] have several applications in foods such as deserts, dry mixes and dairy, comprise the red–purple betacyanins, betanin (**I**) and betanidin (**II**), with maximum absorptivity at λ_{max} about 535 nm, and the yellow betaxanthins with λ_{max} near 480 nm [4].

The structure of betanin is shown in Fig. 1. Beetroot is one of the richest source of betanin, the most studied betalain, was selected as a topic of the present study because of good colorant yield and the prominent peak in the visible region of the spectrum for better quantitative analysis. Unlike synthetic dyes these beetroot based natural dyes are eco-friendly and pose no environmental problems, which are very important for some sensitive applications. Determination of second and third order nonlinearities are of fundamental importance for evaluation of the properties with respect to wave-guiding structures containing betanin.

By using the Z-scan technique the optical nonlinearity of many organic materials has been explored. It is well known that the Z-scan technique, which was present by Sheik-Bahae et al. [5], has been extensively used as an effective and convenient tool for exploring the nonlinear absorption properties of various materials. The basic absorption processes in dyes can be divided into linear and nonlinear absorption. Nonlinear absorption is a phenomenon defined as a nonlinear change (increase or decrease) in absorption with intensity. This can be of either two types: saturable absorption (SA) and reverse saturable absorption (RSA). Depending on the pump intensity and on the absorption cross section at the excitation wavelength, most molecules show nonlinear absorption. If,

* Corresponding author Address: International School of Photonics, Cochin University of Science and Technology, Kochi, India. Tel.: +91 484 2575848; fax: +91 484 2576714.
E-mail address: aparna.subhash@gmail.com (A. Thankappan).

0925-3467/$ - see front matter © 2013 Elsevier B.V. All rights reserved.
http://dx.doi.org/10.1016/j.optmat.2013.06.032

however, the excited state has strong absorption compared with that of the ground state, the transmission will show RSA characteristics, or else SA characteristics. Therefore, it is necessary to identify their nonlinear absorption effects, and to determine their nonlinear absorption parameters, such as the saturable intensity for saturable absorber, the TPA coefficient for two-photon absorbing material. These properties are commonly defined in terms of intensity dependant nonlinear absorption coefficient $\alpha(I)$, which can be written in terms of linear absorption coefficient α and two photon absorption coefficient β as

$$\alpha(I) = \alpha + \beta I \tag{1}$$

TPA has the advantage of high transmission at low incident intensity of light with an optical frequency below the band gap frequency. In this paper we report the techniques used to prepare the natural dye extracts, optical characterizations, and determination of absorption coefficients will be discussed. Also, we are presenting some of our findings and suggestions.

2. Experimental

The extracts of the red beets were obtained from fresh biological materials, pigments can be water extracted and slight acidification of the extraction medium enhances the betacyanin stability and avoids oxidation. In order to study the effect of solvent on betanin dye, the pigments are also extracted using methanol and ethanol. The pigments extracts must be protected from direct light exposure should be kept in cool place. The UV–VIS absorption spectra of the dye solution in different organic solvents (De ionized Water, Methanol, Ethanol) were recorded using a UV/Vis spectrophotometer (Jasco V-570 UV/VIS/IR).

Betanin dye solutions were carried out by the single beam Z-scan technique. The transmission of a laser beam that changes near the focal point during the sample translation along the propagation path through an open-aperture (OA) was measured. A Q-switched Nd: YAG laser (Spectra PhysicsLAB-1760, 532 nm, 7 ns, 10 Hz) was used in the Z-scan experiment to study the optical nonlinearity. A 20 cm converging lens was used to focus the laser beam. The radius of the beam ω_0 was calculated to be 35.4 μm. The Rayleigh length, $z_0 = \pi\omega_0^2/\lambda$, was estimated to be 7.4 mm, which is much greater than the thickness of the sample, and is an essential prerequisite for Z-scan experiments. The sample was fixed on a computer-controlled translation stage, so that it could be accurately moved through the focal region of the laser beam over a length of 6 cm. The transmitted beam energy, reference beam energy and the ratios were measured simultaneously using an energy ratio meter (Rj7620, Laser Probe Corp.) having two identical pyroelectric detector heads (Rjp735). The detected signals were acquired, stored and processed by the computer. Optical density filters were used to vary the laser intensity at the lens focus.

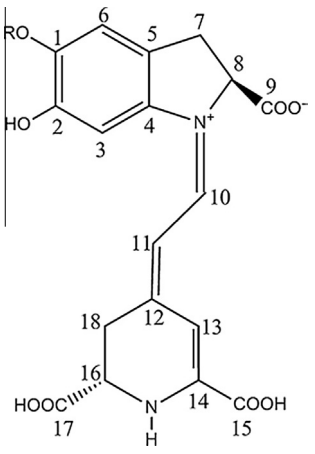

Fig. 1. Structure of betanin pigment.

3. Results and discussions

When absorption spectra of betanin are measured in solvents of different polarity(de ionized water, methanol and ethanol) at various concentrations, it is found that the positions, intensities and shapes of the absorption bands are modified by these solvents, is shown in fig. 2 in which the visible range (520–565 nm depending on the solvent)is attributable to betanin. These changes are a result of physical intermolecular solute–solvent interactions (such as dipole–dipole, ion–dipole, hydrogen bonding, and induced dipole–dipole), which above all tend to alter the energy difference between ground state and excited state of the betanin and external solvent polarization interactions can lift internal symmetry restrictions in the solute molecule can induce new bands. The decrease of polarity of the solvent leads to the red shift caused by the solute/solvent dispersion interactions.

Optical properties of organic molecules utilized in scientific and technological applications can strongly depends on properties of the surrounding media and the interaction of the dancing molecules. For liquid solutions, solvent plays fundamental role in optical processes, and various modes of energy transfer are involved in sample solution are collision between base fluid molecules, thermal diffusion in the molecules suspended in fluids, collision between the samples due to the Brownian motion, thermal interactions of dynamic or dancing samples with base fluid molecules and light induced aggregation of samples, leading to the modifications of ground state and excited states of the molecules. Such solvent effects mainly the interaction of dye molecules to the solvent surroundings which depends on the arising forces which can be determined by the charge distribution and polarizability of the solvent and solute molecules [6,7].

Figs. 3–5 show the open aperture Z-scan curve of different concentration of betanin in water, ethanol and methanol respectively. The data is analyzed using the procedures described by Sheik-Bahae et al. for a two-photon absorption (TPA) process.

The transmitted OA Z-scan signal is give by

$$T(z, S=1) = \sum_{m=0}^{\infty} \frac{[-q_0(z,0)]^m}{(m+1)^{3/2}} \tag{2}$$

where

$$q_0(z,t) = \frac{\beta I_0(t) L_{eff} z_0^2}{z^2 + z_0^2} \tag{3}$$

$$L_{eff} = [1 - \exp(-\alpha 1)]/\alpha \tag{4}$$

where m is an integer .the parameter q_0 can be obtained by fitting the experimental results to the Eq. (2).where Z_0 and Z are the Rayleigh range and the translated length parallel to the beam propagation, respectively. I_0 denotes the intensity of the incident beam at the focal point.

Experimentally determined nonlinear absorption coefficient (β) can be used in finding the absolute value of the third-order nonlinear optical susceptibility, through the relation

$$\mathrm{Im}(\chi^{(3)}) = n_0^2 c^2 \beta / 240\pi^2 \omega(esu) \tag{5}$$

where n_0 is the linear refractive index of the sample measured using Abbe refractometer, c is the velocity of light in vacuum, ω is the angular frequency of radiation used and β the nonlinear absorption coefficient. When SA is present Eq. (1) modifies to

$$\alpha(I) = \alpha_0/1 + (I/I_s) \tag{6}$$

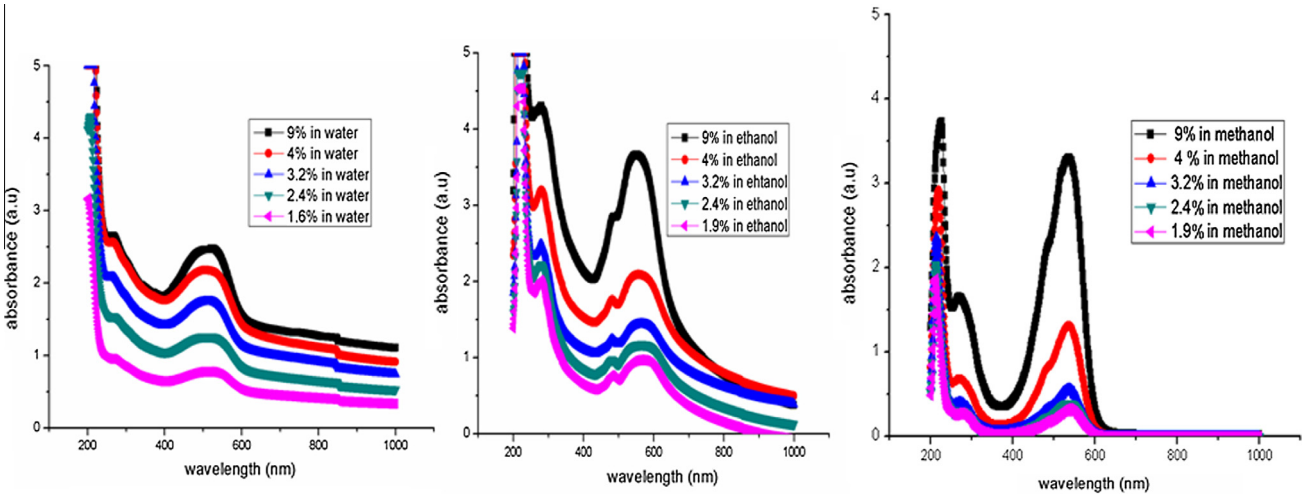

Fig. 2. UV–VIS absorption spectra of betanin in water, ethanol and methanol.

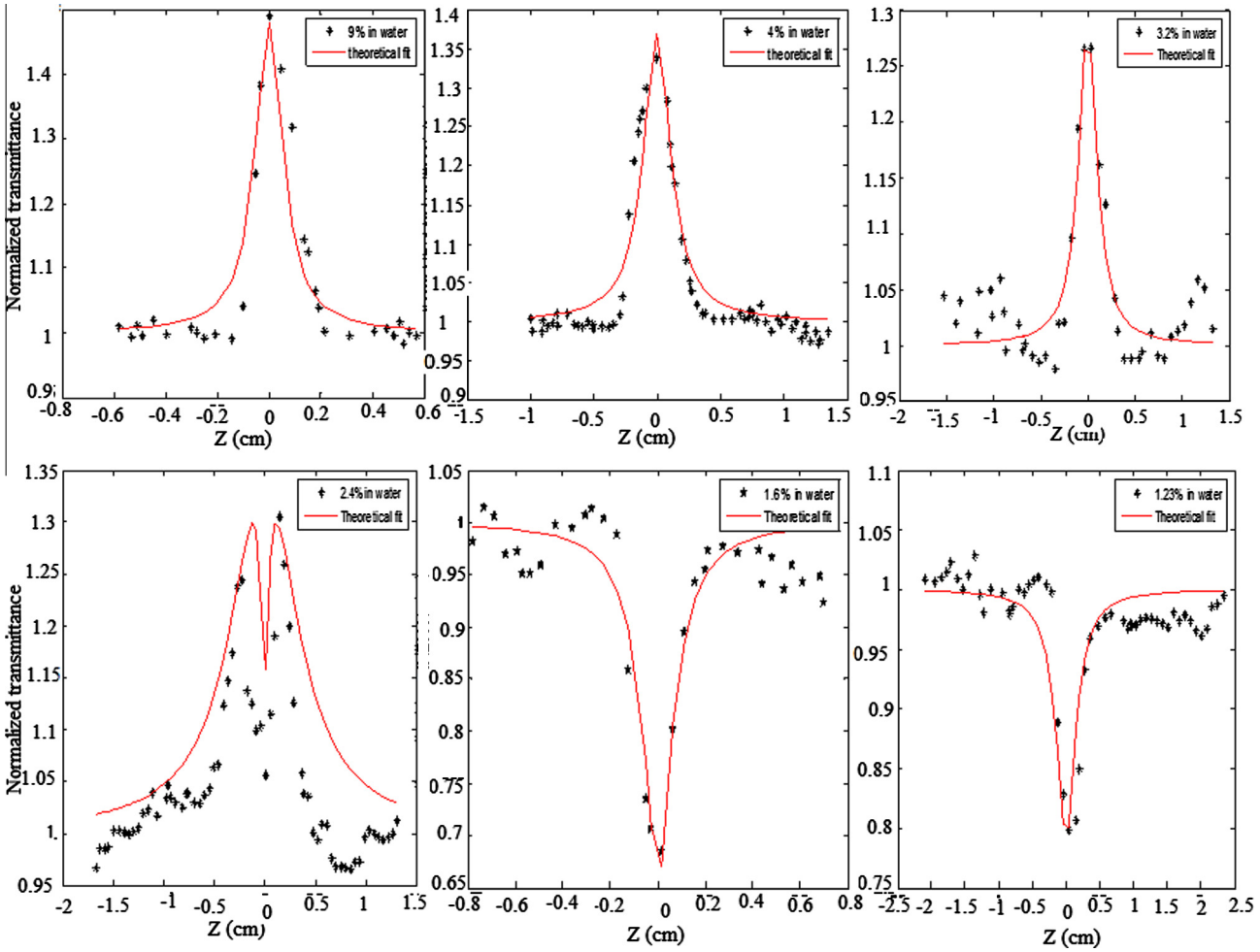

Fig. 3. Open aperture Z-scan curve of different concentration of betanin in water.

If excitation intensity I_0 is less than I_s, we can consider SA as a third order process and in such cases $-\alpha_0/I_s$ is equivalent to nonlinear absorption coefficient β which will then give $\mathrm{Im}\chi^{(3)}$.

As the concentration of betanin in water increases RSA switches to SA and at the intermediate concentration RSA within SA is observed and further no energy absorption takes place. We assume the –COOH on the five membered rings to be the most acidic of the three carboxylic acid groups on Betanin .But in the case of alcohols the H bonding is more energetic than that of water have higher excited state absorption cross section, so as the concentration increases RSA behavior switch to RSA after an the intermediate concentration exhibiting RSA within SA except for methanol. If the

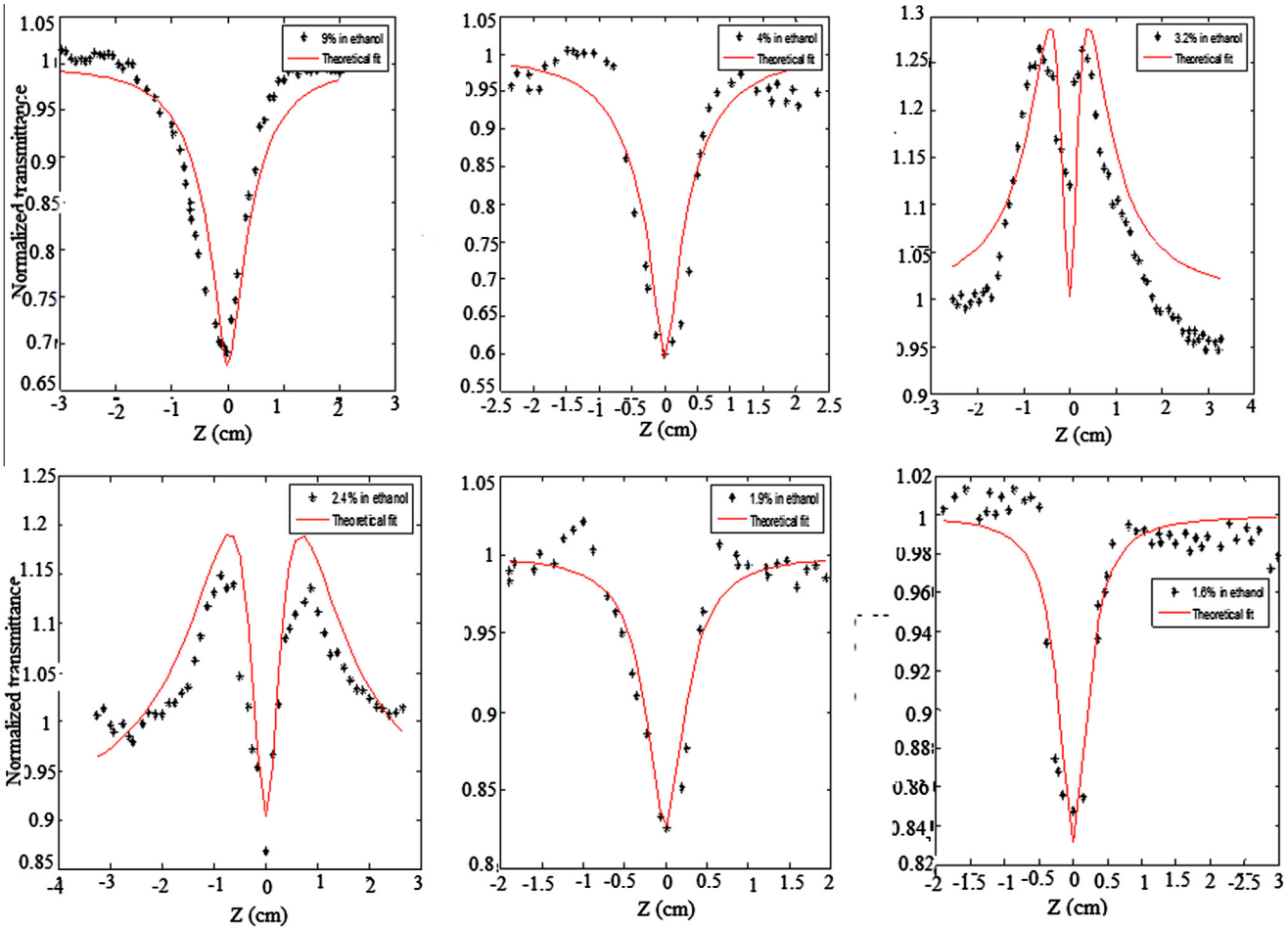

Fig. 4. Open aperture Z-scan curve of different concentration of betanin in ethanol.

intermolecular and intra molecular H bonding interaction which takes place both in the ground state and in the excited state of the molecule is reasonably strong, it may cause a substantial change in the electronic levels of the dye molecules, and there will be a substantial change in the optical behavior of the dye molecules. The strength of the H bonding in the ground states and the excited states of the dye molecules depends on this difference in the electronic charge distribution, it was clearly observed from the absorption spectra depicted in fig. 2.This differential effect and the number density of the dye molecules in the laser beam affects the nonlinear behavior and made them interesting. In general, induced absorption can occur in betanin natural dye, due to a variety of processes such as excited state absorption, two-photon absorption, interband and intraband transitions and nonlinear scattering [8]. By light absorption the betanin pigment chromophore excites π electrons to a more energetic state (π^*), increasing reactivity or lowering activation energy for the molecule. This is attributed to the visible transition of betanin is well-described as a HOMO → LUMO excitation from the aromatic ring to the surrounding solvent. The betalain pigments are more extracted from the alcohol solution (yellow betaxanthins $\lambda = 480$ nm) than from the water [9]. In alcohol solution such an association with –COOH group might be pronounced than water and this conjugation increases with the decreases of the polarity of the solvent .Hence the λ_{max} shifts to longer wavelengths in ethanol and methanol, and the absorbance gradually increases from water to methanol. This observation suggests that the difference in energy spacing between π and π^* for the dye molecules may not be large in water and the FWHM increases with the decrease of polarity of the solvent,which may attributed to the interesting nonlinear behavior of betanin. From the point of view of the solvent influence, at a particular concentration the β value increases as the solvent polarity increases which is due to the increase of the degree of charge delocalization [10]. The decrease of polarity of the solvent is also support our investigations are indicated in Table 1.

Thus inter molecular and intra molecular H bonding between dye and solvent molecules causes a change in the electronic distribution in the dye molecules. The observed switch over behavior could be due to the bleaching of the ground state band, i.e., in the case of the intraband transition, the ground-state electrons are pumped to the excited-state. The excited electrons are free carriers possessing a whole spectrum of energies, both kinetic and potential, immediately after the absorption the electrons excited relax to the ground-state through electron–electron, electron–phonon and phonon–phonon interactions. Once these electrons are excited by a pulse close to absorption peak, they do not oscillate at the same frequency as that of the unexcited electrons, thus causing the ground-state band to bleach or reduced in intensity, which is almost synchronous with the primary photon absorption. Such change over in the sign of the nonlinearity is due to the interplay of the exciton bleach and optical limiting mechanisms. The obtained values of the nonlinear parameters in different solvents are given in Table 2.

In the present case the irreversible damage induced by the input pulses and the presence of sucrose are supposed to play the

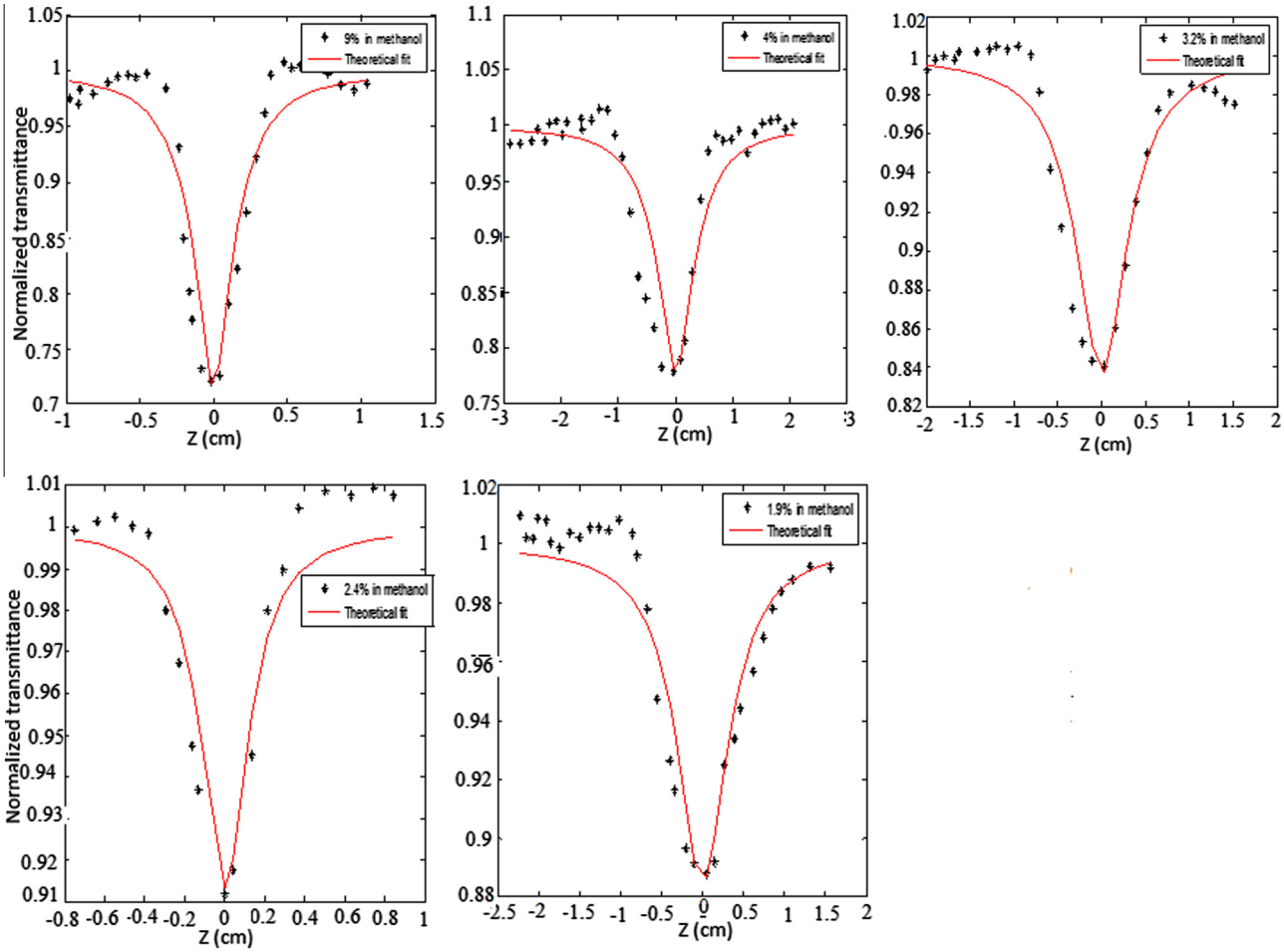

Fig. 5. Open aperture Z-scan curve of different concentration of betanin in methanol.

Table 1
Polarity of solvents.

Solvent	Water (H_2O)	Ethanol (C_2H_6O)	Methanol (CH_4O)
Polarity index	9	5.2	5.0

significant role in the observed transition from SA to RSA on increasing concentration of betanin. Results of the present study provide additional mechanism for gain enhancement.

The optical limiting effects are of special interest in nonlinear optics and optoelectronics owing to their possible application for the protection of eyes and sensitive detectors against intense radiation and an important parameter in optical limiting phenomena is limiting threshold which defines the efficiency of optical limiting material [11]. As shown in the Z-scan open aperture results, the betanin in deionised water, ethanol and methanol exhibited significant transmittance drop when the sample was moved to the vicinity of the focal plane. This transmittance drop is generally considered to be due to nonlinear absorption, nonlinear scattering, or combined effects. To characterize the optical limiting performance of betanin, we have directly measured the energy transmission as a function of fluence at 532 nm using 7 ns laser pulses. The results of betanin in three different solvents are shown in Fig. 6. The deionised water, ethanol and methanol solutions exhibit significant transmittance changes as the input fluence is varied from 50 to 450 MW/cm^2, with the methanol solution showing the best result and the limiting threshold appears to be 104 MW/cm^2.Comparing the optical limiting performance of dye molecules with their corresponding linear absorption spectra, it is observed that higher the linear absorption, better the limiting performance. Changing of the solvent not only affect the linear absorption spectra, but also dramatic influence on the nonlinear property and their optical limiting characteristics.

Table 2
Measured values of the nonlinear optical parameters of betanin in different solvents at a wavelength of 532 nm for different concentration at input fluence of 436 MW/cm^2.

Betanin concentration (Vol.%)	Water			Ethanol			Methanol		
	β (10^{-10} M/W)	I_s(MW/M^2)	Im(χ3) (10^{-10} esu)	β (10^{-10} M/W)	I_s (MW/M^2)	Im(χ3) (10^{-10} esu)	β (10^{-10} M/W)	I_s (MW/M^2)	Im(χ3) (10^{-10} esu)
9	–	0.101		3.091		0.070	3.036	–	0.069
4	–	0.160		3.452		0.078	2.215	–	0.050
3.2	–	0.089			.177		1.526	–	0.034
2.4	–	0.107			.089		.7097	–	0.016
1.6	2.903	–	0.066	1.655		0.037	.981	–	0.022
1.2	2.526	–	0.057	1.596		0.036	–	–	–

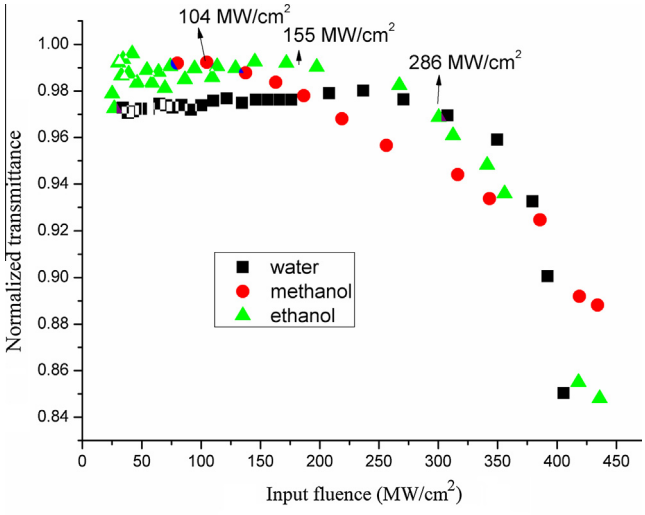

Fig. 6. Optical limiting response of betanin in different solvents.

4. Conclusion

In summary, our Z-scan experiments have revealed interesting features of the nonlinear absorption properties of betanin natural dye in different solvents. Nonlinear absorption coefficients and saturation intensity were estimated by performing numerical fitting to the experimental data. Both inter molecular and intra molecular H bonding has profound effect on the nonlinear optical properties of betanin. The solvent modified the linear absorption spectra and nonlinear behavior of betanin natural dye. The simultaneous occurrence of the nonlinear behavior of betanin in different surrounding media can be made use of in developing various photonic devices. The fact that reverse saturable absorption exists in the vicinity of the linear absorption band combined with the possible two-photon absorption makes betanin a very promising candidate for optical limiting applications.

Acknowledgement

The author AT acknowledges to IUCND for the financial support.

References

[1] Angel Ramon Hernandez-Martinez, Miriam Estevez, Susana Vargas, Fracisco Quintanilla, Rogelio Rodriguez, New dye-sensitized solar cells obtained from extracted bracts of bougainvillea glabra and spectabilis betalain pigments by different purification processes, International Journal of Molecular Sciences 12 (2011) 5565–5576.
[2] Cody Sandquist, Jeanne L. McHale, Improved efficiency of betanin-based dye-sensitized solar cells, Journal of Photochemistry and Photobiology A: Chemistry 221 (2011) 90–97.
[3] R.L. Jackman, J.L. Smith, Anthocyanins and betalains, in: G.F. Hendry, J.D. Houghton (Eds.), Natural food colourants, Blackie Academic & Professional, London, 1996, pp. 244–309.
[4] Dongshe Zhang, Suzanne M. Laniera, Jonathan A. Downing, Jason L. Avent, June Lumc, Jeanne L. McHalea, Betalain pigments for dye-sensitized solar cells, Journal of Photochemistry and Photobiology A: Chemistry 195 (2008) 72–80.
[5] M. Sheik-Bahae, A.A. Said, T.H. Wei, D.J. Hagan, E.W. Van Stryland, Sensitive measurement of optical nonlinearities using a single beam, IEEE Journal Quantum Electronics 26 (1990) 760.
[6] J.R. Lakowicz, Principles of fluorescence spectroscopy, Kluwer academic Publishers, New York, 1999.
[7] Wouter Verbouwe, Lucien Viaene, Mark Van der Auweraer, Frans C. De Schryver, H. Masuhara, R Pansu, J. Faure, Photoinduced intermolecular charge transfer in diphenylamino-substituted triphenylbenzene, biphenyl, and fluorene, Journal Physical chemistry A 101 (44) (1997) 8157–8165.
[8] Q. Shiliang, G. Yachen, J. Xiongwei, Z. Huidan, S. Yinglin, Q. Jianrong, Z. Congshan, K. Hirao, Nonlinear absorption and optical limiting in gold-precipitated glasses induced by a femtosecond laser, Optics Communications 224 (2003) 321–327.
[9] Henriette M.C. Azeredo, Betalains: properties, sources, applications, and stability – a review, International Journal of Food Science and Technology 44 (2009) 2365–2376.
[10] Paresh Chandra Ray, Jerzy Leszczynski, Two-photon absorption and first nonlinear optical properties of ionic octupolar molecules: structure-function relationships and solvent effects, Journal of Physical Chemistry A 109 (2005) 6689–6696.
[11] R. Tintu, V.P.N. Nampoori, P. Radhakrishnan, Sheenu Thomas, Nanocomposite thin films of Ga5Sb10Ge25Se60 chalcogenide glass for optical limiting applications, Optical Materials 33 (2011) 1221–1225.